NAVAL POSTGRADUATE SCHOOL
MONTEREY, CALIFORNIA

DISSERTATION

SEAWAY LEARNING AND MOTION COMPENSATION IN SHALLOW WATERS FOR SMALL AUVS

by

Jeffery Scott Riedel

June 1999

Dissertation Supervisor: **Anthony J. Healey**

Approved for public release; distribution is unlimited.

REPORT DOCUMENTATION PAGE

Form Approved
OMB No. 0704-0188

1. AGENCY USE ONLY *(leave bank)*	2. REPORT DATE	3. REPORT TYPE AND DATES COVERED
	June 1999	Ph.D. Dissertation

4. TITLE AND SUBTITLE
Seaway Learning and Motion Compensation in Shallow Waters for Small AUVs

5.FUNDING NUMBERS
N0001498WR30175

6. AUTHOR(S) Jeffery Scott Riedel

7. PERFORMING ORGANIZATION NAME(S) AND ADDRESS(ES)
Naval Postgraduate School
Monterey CA 93943-5000

8.PERFORMING ORGANIZATION REPORT NUMBER

9. SPONSORING/MONITORING AGENCY NAME(S) AND ADDRESS(ES)
Office of Naval Research (Code 32OE)
800 North Quincy Street
Arlington, VA 22217

10. SPONSORING/MONITORING AGENCY REPORT NUMBER

11. SUPPLEMENTARY NOTES
The views expressed in this thesis are those of the author and do not reflect the official policy or position of the Department of Defense or the U.S. Government.

12a. DISTRIBUTION/AVAILABILITY STATEMENT
Approved for public release; distribution is unlimited.

12b. DISTRIBUTION CODE

13. ABSTRACT *(maximum 200 words)*

The continual development of computer technology has enabled the expansion of intelligent control into the field of underwater robots, where potential uses include oceanographic research, environmental monitoring and military mine countermeasures. With the naval focus shifting to operations in the littorals, and the need to lower cost of operations, tetherless autonomous vehicles are now being proposed for use in very shallow water minefield reconnaissance. These areas are dominated by a highly energetic environment arising from waves and currents. Motion control in such an environment becomes a difficult task and is the subject of this work.

The main objective of this dissertation, is to show through modeling and simulation, and in-ocean experimental validation, that intervention tasks performed by intelligent underwater robots are improved by their ability to gather, learn and use information about their working environment. Using a new generalized approach to the modeling of underwater vehicles, which directly includes disturbance effects, a new Disturbance Compensation Controller (DCC) is proposed. The DCC, employing onboard vehicle sensors, allows the robot to learn and estimate the seaway dynamics. This self-derived knowledge is embedded in a non-linear sliding mode control law which allows significantly improved motion stabilization. The performance of the DCC has been verified in Monterey Harbor using the NPS Phoenix AUV.

14. SUBJECT TERMS	15.NUMBER OF PAGES
Disturbance Rejection, Sliding Mode Control, Seaway Learning, Autonomous Underwater Vehicles, Control Systems	265
	16. PRICE CODE

17. SECURITY CLASSIFICATION OF REPORT	18. SECURITY CLASSIFICATION OF THIS PAGE	19. SECURITY CLASSIFICATION OF ABSTRACT	20. LIMITATION OF ABSTRACT
Unclassified	Unclassified	Unclassified	UL

NSN 7540-01-280-5500

Standard Form 298 (Rev. 2-89)
Prescribed by ANSI Std. 239-18298102

Approved for public release; distribution is unlimited

SEAWAY LEARNING AND MOTION COMPENSATION IN SHALLOW WATERS FOR SMALL AUVS

Jeffery Scott Riedel
Lieutenant Commander, United States Navy
B.S., Maine Maritime Academy, 1986
M.S., Naval Postgraduate School, 1993

Submitted in partial fulfillment of the
requirements for the degree of

DOCTOR OF PHILOSOPHY IN MECHANICAL ENGINEERING

from the

NAVAL POSTGRADUATE SCHOOL
JUNE 1999

Author: _____
Jeffery S. Riedel

Approved by:

_____
Anthony J. Healey
Professor of Mechanical Engineering
Dissertation Supervisor

_____
Roberto Cristi
Associate Professor of Electrical and Computer Engineering

_____
Young S. Shin
Professor of Mechanical Engineering

_____
Fotis A. Papoulias
Associate Professor of Mechanical Engineering

_____
Edward B. Thornton
Professor of Oceanography

Approved by: _____
Terry R. McNelley, Chair, Department of Mechanical Engineering

Approved by: _____
Anthony Ciavarelli, Acting Associate Provost for Instruction

ABSTRACT

The continual development of computer technology has enabled the expansion of intelligent control into the field of underwater robots, where potential uses include oceanographic research, environmental monitoring and military mine countermeasures. With the naval focus shifting to operations in the littorals, and the need to lower cost of operations, tetherless autonomous vehicles are now being proposed for use in very shallow water minefield reconnaissance. These areas are dominated by a highly energetic environment arising from waves and currents. Motion control in such an environment becomes a difficult task and is the subject of this work.

The main objective of this dissertation, is to show through modeling and simulation, and in-ocean experimental validation, that intervention tasks performed by intelligent underwater robots are improved by their ability to gather, learn and use information about their working environment. Using a new generalized approach to the modeling of underwater vehicles, which directly includes disturbance effects, a new Disturbance Compensation Controller (DCC) is proposed. The DCC, employing onboard vehicle sensors, allows the robot to learn and estimate the seaway dynamics. This self-derived knowledge is embedded in a non-linear sliding mode control law which allows significantly improved motion stabilization. The performance of the DCC has been verified in Monterey Harbor using the NPS Phoenix AUV.

TABLE OF CONTENTS

LIST OF FIGURES

LIST OF TABLES

ACKNOWLEDGEMENTS

I would like to express my most sincere gratitude to all the members of my Doctoral Committee for their constructive guidance and suggestions during the course of this research. In particular, I wish to thank Professor Anthony Healey, my dissertation supervisor, for his time, patience, and enthusiasm, without which, this work would not have been possible. His vast knowledge, experience, and professionalism have been an inspiration.

A special thanks to Dr. David Marco for his advice, guidance, and programming pertaining to the real-time implementation of the control code in this research. Without your time and effort I would never have made it.

I would also like to recognize the financial support of the Office of Naval Research (Mr. Tom Curtin) under contract No. N0001498WR30175.

Finally, I dedicate this dissertation with love and thanks to my wife Ellen and our two beautiful children Taylor and Chelsea. Your understanding and support during the frequent trips and long hours have made you a part of this work.

I. INTRODUCTION

A. MOTIVATION

The continual development of computer technology has enabled the expansion of intelligent control into the field of remotely operated underwater vehicles. With this advent, tetherless Autonomous Underwater Vehicles (AUVs), have arrived and are expected to be self-sufficient with respect to power and control. Driven by the need to lower the cost of operations, applications associated with these vehicles are both appealing and numerous. The potential uses for these vehicles include but are not limited to: scientific (oceanography, geology, geophysics,...[Curtin 1993, Smith 1994 and Pereira 1996]), environmental (waste disposal monitoring, wetland surveillance,...[Chase 1998]), commercial (oil and gas, submerged cables, harbors,...[Hartley 1991, Butler 1998, Kato 1998]), or military (mine warfare, tactical information gathering, smart weapons,...[Honegger 1996]). During a mission, an AUV is expected to carry sensors (side scan sonar, bathymetry, bottom profiler,), track to a certain planned trajectory (traveling from point A to point B, performing the systematic exploration of a zone,...), and even make on-line decisions allowing for mission reconfiguration, [Yavani 1996, Byrnes 1996].

The payload, which the vehicle carries, can place constraints on the motion of the vehicle and mission planning. With new emphasis on naval mine countermeasures and reconnaissance in very shallow waters (VSW) [ONR 1998], a typical mission may require a vehicle to follow an unknown and profile-varying bottom at a desired altitude, while maintaining a nominal constant forward speed, and avoiding obstacles when necessary, all while operating in a highly energetic environment. Since small AUVs are sensitive to wave induced motions [An 1996], AUVs in VSW will perform better if they derive knowledge, using their onboard sensors, about their environment and operating area.

The question then is: How can environmental knowledge be obtained and used in a real-time control architecture in order to correctly and safely achieve an assigned mission? The integration of sensory data in closed-loop control of mobile robots or

vehicles has been a topic of recent research in both control architecture [Saridis 1983, Healey 1996, Marco 1996] and execution [Marco 1998] . Based on this work, two broad categories can be distinguished: 1) the behavioral approach and 2) the sensor based control approach. The first is too restrictive for general use, since it needs to specify the problem as a set of simple input/output relations for all possible situations. Among the second class, there are several methods proposed, including intelligent servo control [Marco 1996c], path following [Fryxell 1995] and collision avoidance [Williams 1990], and the task function approach [Santos 1995].

The task function approach allows a framework by which various control laws may be develop for specific mission tasks. The embedded control laws are then used based on sensor input decisions with a mission manager controlling the commands and task assignments. The goals of this research include the need to show that task assignments can be performed with less environmentally induced motions if the characteristics of the operating environment are known. This is particularly important because of the need to operate in environmentally energetic areas and because of the unpredictable nature of the VSW region.

Classically, this problem falls into the broad category of servo control disturbance rejection. This problem is well known and has a rich history of study. In principle, a high gain feedback servo is known to track commands and reject disturbances (unwanted inputs). Requirements for loop stability and sensor noise rejection are competing and the subject of optimal control formulations. It is conjectured that knowledge or direct measurement/estimation of these disturbances improves control performance. Measurement/estimation of ocean disturbances is both difficult, as well as subject to the unpredictable nature of the ocean. For all the ongoing work in the offshore oil industry, wave disturbances are still not measured and used directly for control purposes.

B. BACKGROUND

Autonomous systems for small unmanned untethered underwater vehicles have several features that separate them from traditional marine control and guidance systems. The single most important feature is that it is desirable to control a small underwater

vehicle with relatively high velocities along or about two or more axes at the same time reliably. This leads to stronger coupling, larger nonlinearities, more state equations and more unknown parameters in the vehicle's equations of motion than what would be present with surface vessels. This single most important fact makes the control of small underwater vehicles relatively difficult.

Other factors include but are not limited to:

- A small underwater vehicle may be controllable in all six degrees of freedom,
- A small underwater vehicle has a natural frequency in the same range as the environmental disturbances;
- Actuator dynamics are much faster on small underwater vehicles;
- Power for control and operations is limited by what the vehicle can carry onboard;
- Man-in-the-loop operations and human intervention for fault response are not possible, if controller problems develop;
- Small underwater vehicles, having a higher bandwidth, may compensate for the first order wave disturbances by means of feedforward and feedback control laws.

There are numerous factors that must be considered in the design of a control system that is capable of being implemented in an operating vehicle. Some of the most important items are:

- The bandwidth is limited by the control system's sampling rate, computational time delays and sensor communication delays. The time delay factor is extremely important when the control law is dependent on information from a hydro-acoustic source.
- The control system's sensitivity to noise has to be considered, because it determines how good a sensor must be and how robust the control algorithm is with respect to noisy measurements.
- The required accuracy of the system is usually a function of the commanded tasks; hence it is not meaningful to discuss this factor before a task specification is made.

- Stability is of the utmost importance. Depending on the type of system (SISO or MIMO) and the type of controller to be employed (linear or nonlinear), various techniques are available to rate these criteria.

- Requirements to handle system failures, i.e., sensor failure, actuator failure and even computer failure, must be addressed.

- Parameter variation is also an important aspect in robustness analysis of a control system. Parameter variations can be handled by a well-designed adaptive algorithm or by employing a control scheme that is robust to these variations.

The first modern DP system was first introduced by [Balchen et al., 1976], where a Kalman filter approach for solving the wave noise-filtering problem was employed. Before the employment of this system, DP systems were mainly based on PID-controllers and matching notch filters which filtered out the wave "noise" on the sensors. Kalman filter based DP systems now dominate the market and the literature [Balchen 1976, Jenssen 1980, Saelid 1983, Fung 1983, Triantafyllou 1983, Fossen 1995, and Sorensen 1996].

The Kalman filter based DP systems consist of one high and one low-frequency model where the control action is based on the low frequency model. The high frequency model is used to filter out the relatively high-frequency, first-order, wave noise that appears on the sensors.

This filtering is not necessary for small underwater vehicles, since in theory, compensation for the first order wave disturbance's is possible. For small vehicles, the DP case becomes a special case of the general control problem where desired trajectory velocities are zero. Although there exist many available DP systems for surface vessels, the *Simrad-Albatross* as one example, and even several ROV DP systems, such as the [Marquest 1991] system and the systems developed and deployed on the Norwegian Experimental Remotely Operated Vehicle (NEROV) by [Fossen and Satagun 1991], there currently are NO KNOWN AUTOMATIC DP systems for AUVs.

C. OBJECTIVES

The main objective of this research is to show through modeling, simulation and experimental validation that intervention tasks performed by intelligent underwater robots are improved by their ability to gather, learn and use information about their working environment.

Specifically this dissertation addresses the following topics:

- Generation and verification of mathematical models;
- Measurement and use of wave disturbance information for control compensation; and
- Implementation and verification of real-time embedded control processes.

D. CONTRIBUTIONS

This dissertation contains both theoretical and experimental contributions to the field of applied underwater vehicle control. The theoretical contributions are partly found in the modeling chapter (Chapter II), the disturbance rejection chapter (Chapter V), and the wave direction estimation chapter (Chapter VII). The experimental contributions (Chapter VIII) are from work carried out during operational testing of the NPS Phoenix AUV. The Phoenix and its subsystems, including system upgrades necessary to perform this research, are described in Appendix C and in [Marco 1996].

The contributions in this dissertation are described below:

- Chapter II provides a new generalized approach to the modeling of small underwater vehicles subject to shallow water wave and current effects. Using appropriate modeling formulations, as opposed to adding white or colored noise, random disturbances, or "RAO" based motions, the fluid effects are incorporated directly into the equations of motion. In addition, this formulation provides the ability to construct a generalized distributed simulation capability for the evaluation of underwater vehicle systems in shallow water. (Generally useful to U.S. Navy tactical decision making).
- It is proven through simulation (Chapter V), and verified by experimental validation (Chapter VIII), that measuring the water column velocities directly, wave induced disturbances can be substantially compensated by the vehicle

control system. This technique eliminates the need to develop and incorporate sophisticated predictive disturbance models in the control system design.

- In Chapter VII, it is shown how small underwater vehicles, using direct fluid measurements, can obtain short-term wave magnitude, directionality and current estimates, thereby providing useful information in the area of tactical oceanography. It is also shown how a general seaway direction may be obtained for use in mission planning and control.

E. DISSERTATION ORGANIZATION

This dissertation is aimed at contributions in the area of control of intelligent underwater robots. Figure 1.1 represents the general control architecture for the Phoenix AUV. Using this figure as a roadmap, the chapters and appendices consider the following:

- **Chapter II.** "Mathematical Modeling Of Underwater Vehicles" derives the complete set of nonlinear equations of motion for a small underwater vehicle subject to shallow water waves. Kinematics, Newton's laws of angular and linear momentum, general hydrodynamics and external force modeling are discussed in detail.

- **Chapter III.** "Disturbance Analysis" describes how deterministic and stochastic disturbances can be modeled for use in the vehicle control architecture. Statistical description, state space representation and autoregressive (AR) modeling are used to illustrate these ideas.

- **Chapter IV.** "Parameter Identification" describes the theoretical foundation and experimental results associated with determining the parameters and coefficients used to model the NPS Phoenix AUV in the surge direction. Comparisons between vehicle experiments and simulations show the level of certainty associated with the identified parameters.

- **Chapter V.** "Disturbance Rejection Theory" provides a survey of the classical and modern approaches to disturbance rejection and compensation. This chapter describes how a nonlinear surge controller can be applied to an underwater vehicle design. It details three specific controller designs: a LQR design, a LQR with embedded disturbance model design, and a nonlinear sliding mode controller with disturbance compensation.

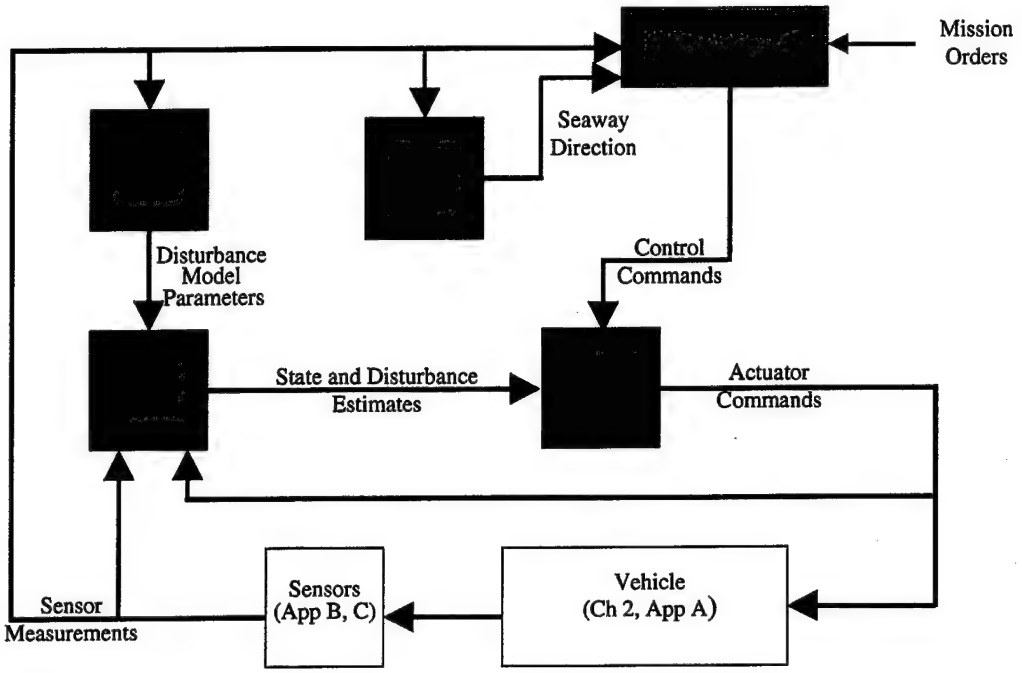

Figure 1.1 Phoenix AUV Control Architecture

- **Chapter VI.** "Disturbance Compensation Controller (DCC)" is a discussion of the design and implementation of a combined nonlinear model-based extended Kalman filter with a SMC for dynamic positioning. The state estimator is critical to the controller performance since the surge controller requires states that are not measured with existing systems and sensors. This chapter compares actual signals with estimated signals, and shows that by properly designing the filter gains, the measurement noise levels are reduced and the controller bandwidth is increased. Also, critical to the point of the dissertation, ocean fluid particle velocities, the disturbance, are estimated.

- **Chapter VII.** "Wave Directional Estimation From A Moving Platform" outlines the theory used to estimate wave directions from an AUV. It also describes the method by which a heading command, based on the dominant wave energy direction, is calculated. This heading command is used in the heading controller to properly orient the vehicle in the direction of the maximum energy, thereby reducing the drag force on the vehicle.

- **Chapter VIII.** "Experimental Results and Validation" is an analysis of the experimental missions performed during this research. It describes the real-time implementation of the various processes (filters, controllers and data acquisition code) operating in the Phoenix. The chapter shows that the Disturbance Compensation Controller (DCC) is capable of dynamic station

keeping in the presence of waves. It also displays and analyzes directional wave spectrum estimates obtained during AUVFEST '98.

- **Chapter IX.** "Conclusions and Recommendations" contains comments, conclusions and recommendations for future work.

- **Appendix A.** "Equations of Motion and Parameters for the NPS Phoenix AUV" provides the physical characteristics, the hydrodynamic coefficients and the equations of motion for the NPS Phoenix AUV.

- **Appendix B.** "Doppler Sensors" outlines the specifications and principles of operation of the SonTek® ADV and the RDI® WORKHORSE DVL.

- **Appendix C.** "The Phoenix AUV" describes in detail the vehicle more closely, including upgrades and acquisitions that allowed the Phoenix to transition from a test tank vehicle to open ocean operations.

- **Appendix D.** "AUVFEST '98" describes the NAVO sponsored underwater vehicle demonstration exercise that took place during November 1998 off the coast of Gulfport, MS.

II. MATHEMATICAL MODELING OF UNDERWATER VEHICLES

A. INTRODUCTION

The mathematical modeling of underwater vehicles can be found throughout the literature. The standard equations of motion for submarine simulation from the David Taylor Model Basin Naval Ship Research and Development Center (DTMSRDC) are described in detail by [Gertler 1967] and [Feldman 1979]. In [Kalske 1989] a survey of the motion dynamics of underwater vehicles, including ROVs and submarines, is given. A description of the linear and nonlinear motion dynamics of the University of New Hampshire Experimental Underwater Vehicle (UNH-EAVE) is found in [Humphreys 1982].

Many other papers and books have been written on this subject (see Yuh 1990, Healey 1992 and 1993, and Fossen 1994 for further examples). Each model has developed in complexity and accuracy, but each model has vehicle specific simplifications making it necessary to revisit this topic. Presently, there is no single model that combines all aspects, including environmental disturbances and their effects, into one generalized model for shallow water operations of small underwater vehicles.

Accurate modeling allows for the development of precision control. Precise control is needed for many maneuvers and tasks, such as autonomous docking and recovery, target detection, identification and localization, as well as station-keeping.

In this chapter the generalized six-degree of freedom (6DOF) equations of motion (EOM) for a small underwater vehicle operating in shallow water will be developed. As with all previous modeling work in this area, the underlying assumptions are that:

1) The vehicle behaves as a rigid body;
2) The earth's rotation is negligible as far as acceleration components of the center of mass are concerned;
3) The primary forces that act on the vehicle have inertial, gravitational, hydrostatic and hydrodynamic origins, and
4) The hydrodynamic coefficients or parameters are constant.

The chapter will begin by outlining the coordinate frames and the kinematic and dynamic relationships used in modeling a vehicle operating in free space. Next a discussion of linear wave theory and basic hydrodynamics will be presented. This discussion will set the foundation for the various force and moment expressions representing the vehicle's interaction with its fluid environment. The control forces, resulting from propellers and thrusters and from control surfaces or fins, that enable the vehicle to maneuver, will be then be detailed. With the hydrodynamic and control force and moment analysis complete, the full six degree of freedom equations of motion will be formed taking into account the necessary modifications for current and wave effects. While reduced order models representing flight control modes are detailed elsewhere, the chapter will conclude with a development and discussion of the one degree of freedom (1DOF) surge model. This model will be used in later chapters as the basis for a controller that will allow an AUV to station-keep in the presence of waves.

B. COORDINATE SYSTEMS, POSITIONAL DEFINITIONS AND KINEMATICS

For underwater vehicles that operate in three dimensional space and time, it is necessary to describe position/orientation and velocity/rotation rate of the vehicle by six independent coordinates or degrees of freedom. Typically these coordinates are chosen to correspond to the position and orientation and their time derivatives with respect to some set of mutually orthogonal coordinate axes fixed to an arbitrary origin which defines a reference frame. Likewise, the forces/moments acting on or produced by the vehicle can be referenced to a set of coordinate axes. In this dissertation, standard notation, [SNAME 1950], is used to describe the aforementioned 6 DOF quantities and is summarized in Table 2.1.

Note that by convention for underwater vehicles, the positive x-direction is taken as forward, the positive y-direction is taken to the right, the positive z-direction is taken as down, and the right hand rule applies for angles. It is convenient to group the linear and angular body fixed velocities into a vector quantity $\boldsymbol{x}$, where $\boldsymbol{x} = [u, v, w, p, q, r]^T$, and the global positions and Euler angles as a vector quantity $\boldsymbol{z}$, where

$z = [X, Y, Z, \phi, \theta, \psi]^T$. The externally applied forces and moments are grouped into a vector quantity f, where $f = [X_f, Y_f, Z_f, K_f, M_f, N_f]^T$.

DOF	Motions	Forces and Moments	Linear and Angular Velocities	Positions and Euler Angles
1	surge	X_f	u	X
2	sway	Y_f	v	Y
3	heave	Z_f	w	Z
4	roll	K_f	p	ϕ
5	pitch	M_f	q	θ
6	yaw	N_f	r	ψ

Table 2.1 Standard Underwater Vehicle Notation

1. Reference Frames

As discussed earlier and outlined in Table 2.1, to properly describe or model the motion of a rigid body three independent positions and angles are required, and for convenience, three orthogonal coordinate frames are used. First, a global frame *OXYZ*, as shown in Figure 2.1, is defined with origin *O*, and a set of axes aligned with directions North, East and Down. This produces a right-hand reference frame with unit vectors ***I***, ***J***, and ***K***. Ignoring the earth's rotation rate in comparison to the angular rates produced by the vehicle's motion, it can be said that the *OXYZ* coordinate frame is an inertial reference frame in which Newton's Laws of Motion will be valid. A vehicle's position in this global frame will have the vector components, $\boldsymbol{r}_{O'} = [X\boldsymbol{I} + Y\boldsymbol{J} + Z\boldsymbol{K}]$.

Secondly, a body fixed frame of reference $O'xyz$, with the origin O', and unit vectors ***i***, ***j***, ***k***, located on the vehicle centerline, moving and rotating with the vehicle is defined. The origin O', will be the point about which all vehicle body force will be computed in later sections of this chapter. The vehicle's center of gravity (mass), *CG*, and center of buoyancy, *CB*, do not generally lie at the origin of the body fixed frame, nor

are they collocated. The positional vectors of the *CG* and *CB* relative to the origin of the body fixed frame are ρ_G and ρ_B, respectively, and can be represented in component form as $[x_G i + y_G j + z_G k]$ and $[x_B i + y_B j + z_B k]$. The location of the center of mass (gravity) is important because Newton's Laws of Motion simplify when forces and moments on a body are applied to its center of mass. The center of buoyancy is determined by the shape of the submerged portion of the body, while the center of gravity is determined by the distribution of the weight.

Lastly, a fluid frame is defined with origin O_f. This frame is aligned parallel to the global reference frame but moves with the local fluid particles. Defining the fluid reference frame in this manner simplifies the hydrodynamic force modeling which will be discussed in later sections.

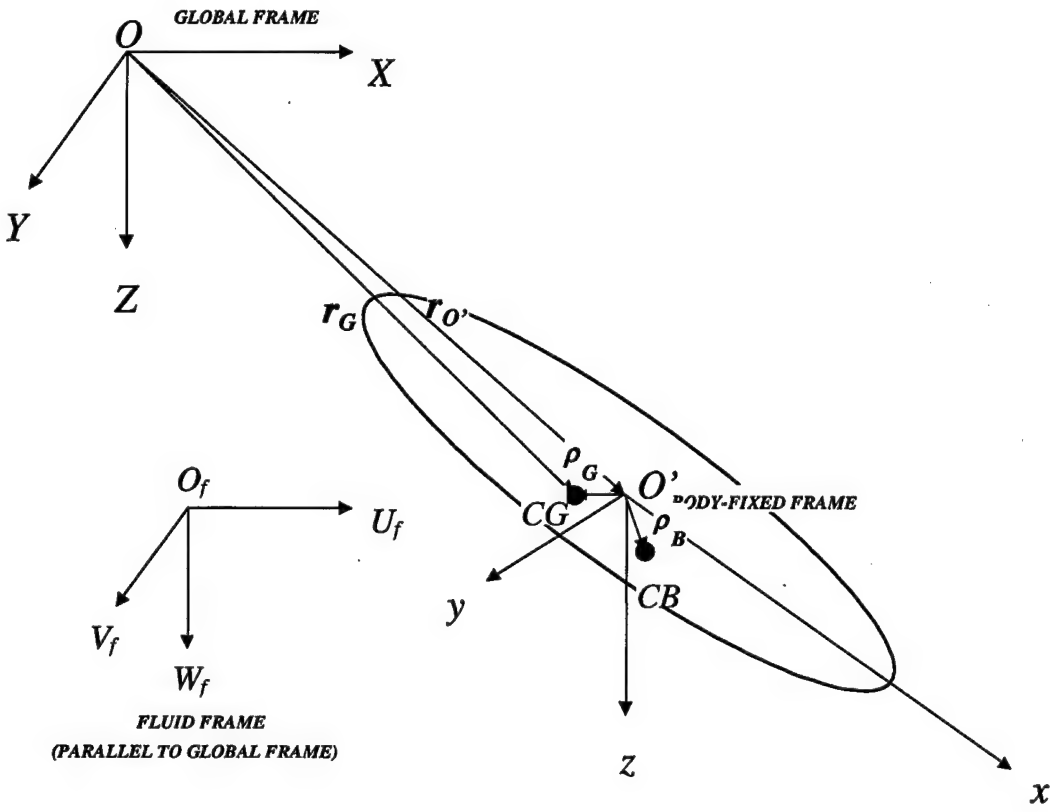

Figure 2.1 Coordinate Frames and Axes Convention

2. Euler Angles

The transformation from one Cartesian coordinate system to another can be performed by means of three successive rotations in sequence. While there are several different methods to describe the attitude of a vehicle in the global reference frame, the most common method uses so-called Euler angles. This method uniquely defines the angular orientation of the vehicle reference frame relative to the global reference frame. There are several Euler angle conventions to describe these three successive rotations, see [Craig 1989] for a complete list. However, for the purpose of this dissertation, the so called "roll, pitch, yaw,'' "X-Y-Z fixed angle" or "Tait-Bryant" convention will be used. One concern that may arise with the use of Euler angles is that a singularity exists when the elevation reaches 90 degrees. This limitation which can sometimes, although rarely, cause trouble in flight simulations and control computations may be overcome by the use of quaternions [Craig 1989], which introduce four rather than three variables to describe angular position.

For the "roll, pitch, yaw" convention, a forward transformation is performed by beginning with a vector quantity originally referenced in the global reference frame. Then, through a sequence of three rotations it is transformed into a frame that is assumed to be parallel to and moving with the vehicle body coordinate frame. To start the transformation, begin by defining an azimuth rotation ψ, as a positive rotation about the global Z-axis. Next define a subsequent rotation θ, (positive up) about the new Y-axis, followed by a positive rotation ϕ, about the new X-axis. The triple rotational transformation in terms of these three angles, is then sufficient to describe the angular orientation of the vehicle at any time.

It follows that any position vector, $\boldsymbol{r}_o$, in an original global reference frame given by $\boldsymbol{r}_o = [X_o, Y_o, Z_o]$, will have different coordinates in a rotated frame when an azimuth rotation by angle ψ, is made about the global Z-axis.

If the new position is defined by $\boldsymbol{r}_1 = [X_1, Y_1, Z_1]$, it can be seen that there is a relation between the vector's coordinates in the new reference frame with those that it had in the old reference frame. It follows that,

$$X_1 = X_o \cos\psi + Y_o \sin\psi \tag{2.1}$$

$$Y_1 = -X_o \sin\psi + Y_o \cos\psi, \tag{2.2}$$

with $Z_1=Z_o$. This relation can be expressed in matrix form by the rotation matrix operation,

$$\boldsymbol{r_1} = [\boldsymbol{T}_{\psi,Z}]\boldsymbol{r_o}; \tag{2.3}$$

where the rotation matrix $\boldsymbol{T}_{\psi,Z}$, represents an orthogonal transformation. Multiplication of this rotation matrix with any vector, $\boldsymbol{r_o}$, will produce the components of the same vector in the rotated coordinate frame. Continuing with the series of rotations results in a combined total rotational transformation,

$$\boldsymbol{T_1}(\phi,\theta,\psi) = \boldsymbol{T}(\phi)\,\boldsymbol{T}(\theta)\,\boldsymbol{T}(\psi). \tag{2.4}$$

In expanded notation Equation 2.4 takes the form

$$\boldsymbol{T_1}(\phi,\theta,\psi) = \begin{bmatrix} c\psi c\theta & s\psi c\theta & -s\theta \\ c\psi s\theta s\phi - s\psi c\phi & s\psi s\theta s\phi + c\psi c\phi & c\theta s\phi \\ c\psi s\theta c\phi + s\psi s\phi & s\psi s\theta c\phi - c\psi s\phi & c\theta c\phi \end{bmatrix},$$

where c and s are abbreviations for *cos* and *sin*. It can be said that any positional vector in an original reference frame may be expressed in a rotated frame with coordinates given by the operation,

$$\boldsymbol{r}_{ijk} = \boldsymbol{T_1}(\phi,\theta,\psi)\,\boldsymbol{r}_{IJK}. \tag{2.5}$$

3. Kinematics

Kinematics deal with the relationships of motion quantities regardless of the forces induced by their prescribed motions. Description of a body's position both translational and rotational, will need to be related to velocities, both translational and rotational, prior to extending the analysis to accelerations. The connection between translational velocity and the rate of change of translational position is straight forward.

Define a global velocity as,

$$\dot{\boldsymbol{r}} = \begin{bmatrix} \dot{X} \\ \dot{Y} \\ \dot{Z} \end{bmatrix}. \tag{2.6}$$

This vector will have components that are different when seen in a body fixed frame. Selecting the linear components of the body fixed velocity vector, $v = [u, v, w]^T$, these components, in global quantities are found, using the forward transformation defined in Equation 2.5, to be

$$\begin{bmatrix} u \\ v \\ w \end{bmatrix} = \boldsymbol{T}_1(\phi,\theta,\psi) \begin{bmatrix} \dot{X} \\ \dot{Y} \\ \dot{Z} \end{bmatrix}. \tag{2.7}$$

It is a simple reverse coordinate transformation from body fixed to global coordinates to see that,

$$\begin{bmatrix} \dot{X} \\ \dot{Y} \\ \dot{Z} \end{bmatrix} = \boldsymbol{T}_1^{-1}(\phi,\theta,\psi) \begin{bmatrix} u \\ v \\ w \end{bmatrix}, \tag{2.8}$$

where $\boldsymbol{T}_1^{-1}(\phi,\theta,\psi)$ is the transpose of Equation 2.4, since $\boldsymbol{T}_1(\phi,\theta,\psi)$ is orthogonal. This shows that the progression of a vehicle in the global frame clearly depends on its local velocity components and its attitude.

The connection between angular attitude and angular velocity is not quite so obvious. At first sight, it is tempting to define the instantaneous angular velocity of the vehicle simply as the rate of change of its angular position defined by the Euler angles. This is erroneous however, because the rotation θ, was defined as a rotation about the intermediate frame after a rotation ψ, had been made. It should be noted that the order of multiplication in Equation 2.4 must be followed since the rotations do not commute, i.e., $\boldsymbol{T}(\phi,\theta,\psi) \neq \boldsymbol{T}(\theta,\psi,\phi)$. Since the rotation do not commute, the set cannot form a vector space and therefore the derivatives cannot represent the body's angular velocity.

Vehicle inertial angular rates are defined in terms of components that have angular velocities about the global axes. It is necessary to relate both Euler angles and their rates of change, to angular velocity components about the global axes and to their components lying along the body fixed axes in any attitude. The prime reason for this is that it is difficult to construct physical sensors to measure rates of change of Euler angles. (Rate gyros in common use today are easily constructed to measure the components of

the inertial angular velocity of a vehicle that lie along the vehicle's body axes.) It follows that the instantaneous angular velocity of the vehicle can be related to the instantaneous rate of change of angular orientation only after considerations of the intermediate transformations used. In other words, if $\boldsymbol{\alpha}$ is defined as the angular attitude vector, $\boldsymbol{\alpha} = [\phi, \theta, \psi]^T$, and the inertial components of the vehicle angular rate lying along the body axes are defined as $\boldsymbol{\omega} = [p,q,r]^T$, then $\dot{\boldsymbol{\alpha}} = f(\boldsymbol{\alpha}, \boldsymbol{\omega})$.

The details of the nonlinear functional relations involved are provided by viewing the rate of change of the rotation ψ, as a vector quantity lying along the original *Z*-axis. The rate of change of the angle θ, is viewed as a vector quantity lying along the *Y*-axis of the first intermediate frame, and the rate of change of the angle ϕ, is viewed as a vector lying along the *X*-axis of the final (body fixed) frame. Each of these component rates of change of angular position has component parts that project onto the final frame and it is the sum total of all the components that give the total angular velocity as seen in the final frame of reference. Using the required transformations for the rate components from each Euler angle,

$$\begin{bmatrix} p \\ q \\ r \end{bmatrix} = \sum \boldsymbol{T}(\phi)\boldsymbol{T}(\theta)\boldsymbol{T}(\psi) \begin{bmatrix} 0 \\ 0 \\ \dot{\psi} \end{bmatrix} + \sum \boldsymbol{T}(\phi)\boldsymbol{T}(\theta) \begin{bmatrix} 0 \\ \dot{\theta} \\ 0 \end{bmatrix} + \boldsymbol{T}(\phi) \begin{bmatrix} \dot{\phi} \\ 0 \\ 0 \end{bmatrix} = \boldsymbol{T}_2(\phi,\theta,\psi) \begin{bmatrix} \dot{\phi} \\ \dot{\theta} \\ \dot{\psi} \end{bmatrix}, \qquad (2.9)$$

the body rates are obtained with the result,

$$\begin{bmatrix} p \\ q \\ r \end{bmatrix} = \begin{bmatrix} -\dot{\psi}\sin\theta + \dot{\phi} \\ \dot{\psi}\sin\theta + \dot{\theta}\cos\phi \\ \dot{\psi}\cos\theta\cos\phi - \dot{\theta}\sin\phi \end{bmatrix} = \begin{bmatrix} 1 & 0 & -\sin\theta \\ 0 & \cos\theta & \sin\theta \\ 0 & -\sin\phi & \cos\theta\cos\phi \end{bmatrix} \begin{bmatrix} \dot{\phi} \\ \dot{\theta} \\ \dot{\psi} \end{bmatrix}. \qquad (2.10)$$

Inverting Equation 2.10 yields a solution for the rates of change of the Euler angles in terms of the body fixed components of the angular velocity vector,

$$\begin{bmatrix} \dot{\phi} \\ \dot{\theta} \\ \dot{\psi} \end{bmatrix} = \begin{bmatrix} p + q\sin\phi\tan\theta + r\cos\phi\tan\theta \\ q\cos\phi - r\sin\phi \\ (q\sin\phi + r\cos\phi)/\cos\theta \end{bmatrix} = \begin{bmatrix} 1 & \sin\phi\tan\theta & \cos\phi\tan\theta \\ 0 & \cos\phi & -\sin\phi \\ 0 & -\sin\phi/\cos\theta & \cos\phi/\cos\theta \end{bmatrix} \begin{bmatrix} p \\ q \\ r \end{bmatrix}. \qquad (2.11)$$

Notice that for small angular rotations, as expected,

$$\dot{\phi} = p;$$
$$\dot{\theta} = q;$$
$$\dot{\psi} = r,$$

as expected. As a note, it should be pointed out that unlike the transformation matrix T_1, T_2 is not orthogonal, therefore, $T_2^{-1} \neq T_2^T$.

At this point the kinematic relationships between velocities, as seen in the body fixed frame, and the rates of change of global positions and Euler angles have been defined. The resulting set of differential equations forms a consistent set in that given a set of vehicle velocity data versus time, its position and attitude may be computed. Expending and combining equations 2.8 and 2.11, this set of differential equations is summarized here;

$$\begin{bmatrix} \dot{X} \\ \dot{Y} \\ \dot{Z} \\ \dot{\phi} \\ \dot{\theta} \\ \dot{\psi} \end{bmatrix} = \begin{bmatrix} u\cos\theta\sin\psi + v(-\cos\phi\sin\psi + \sin\phi\sin\theta\cos\psi) + w(\sin\phi\sin\psi + \cos\phi\sin\theta\cos\psi \\ u\cos\theta\sin\psi + v(\cos\phi\cos\psi + \sin\phi\sin\theta\sin\psi) + w(-\sin\phi\cos\psi + \cos\phi\sin\theta\sin\psi) \\ -u\sin\theta + v\sin\phi\cos\theta + w\cos\phi\cos\theta \\ p + q\sin\phi\tan\theta + r\cos\phi\tan\theta \\ q\cos\phi - r\sin\phi \\ (q\sin\phi + r\cos\phi)/\cos\theta \end{bmatrix}.$$

In vector-matrix form, this set of equations can be expressed as;

$$\dot{z} = \begin{bmatrix} T_1^{-1} & 0 \\ 0 & T_2^{-1} \end{bmatrix} x$$

C. NEWTON'S SECOND LAW

Since the motion of the vehicle is composed of both translational and rotational components, it is necessary to retain the distinction between the vehicle or body fixed frame and the global or inertial frame. This is particularly important because the dominant forces that act on a submerged body depend on the local motion of the vehicle relative to the fluid particles, not on the global velocities. Returning to Figure 2.1, the global position, velocity and acceleration vectors of the vehicle's center of gravity is defined as $r_G = r_O + \rho_G$, $\frac{dr_G}{dt}$ and $\frac{d^2 r_G}{dt^2}$ respectively. Since the center of mass lies in a

body that is both translating and rotating, the total time derivative of r_G comes from two parts. The first part is from the time derivative as if the body fixed frame was not rotating, while the second part is due to the rotation of the body fixed frame. A detailed explanation of this can be found in [Greenwood 1988].

For a general vector r, in a frame rotating at an angular velocity ω, the total derivative is given as

$$\frac{dr}{dt} = \dot{r} + \omega \times r, \tag{2.12}$$

where the first right hand side term is a rate of growth part and the second right hand side term is a rate of transport part. Using this logic, the velocity of the vehicle's center of mass is given by

$$\frac{dr_G}{dt} = \dot{r}_{O'} + \omega \times \rho_G = v_{O'} + \omega \times \rho_G. \tag{2.13}$$

The inertial velocity of the origin of the body fixed frame is expressed as $v_{O'}$ and may be written in either global or body fixed coordinates, therefore;

$$v_{O'} = \dot{r}_{O'} = [\frac{dX}{dt} I + \frac{dY}{dt} J + \frac{dZ}{dt} K] = [ui + vj + wk]. \tag{2.14}$$

1. Translational Equations of Motion

With the coordinate frames defined, Newton's second law of motion, $f_{Trans} = \frac{d}{dt}(mv_G)$, may be used to formulate a translational model of the system. The global acceleration of the center of mass is derived by differentiating the velocity vector, $\dot{r}_G$, realizing that the center of mass lies in a rotating reference frame. Considering the total differential, the global acceleration of the center of mass becomes,

$$\ddot{r}_G = v_{O'} + \dot{\omega} \times \rho_G + \omega \times \omega \times \rho_G + \omega \times v_{O'}. \tag{2.15}$$

The translational equation of motion is found by equating the product of this acceleration and the vehicle mass, to the net sum of all forces acting on the vehicle in three translational degrees of freedom (*X, Y, Z*). One important factor to recognize is that the equation of motion derived in this manner is a vector equation with the components expressed in the body fixed frame with unit vectors i, j and k. As discussed earlier, this

has been deliberately done because the dominant forces acting on a submerged body in motion are developed in relation to the shape of the vehicle and are more conveniently expressed in relation to the body axes. Applying Newton's second law results in the vector equation,

$$\mathbf{f}_{Trans} = m\{\dot{\mathbf{v}}_{O'} + \dot{\omega}\times\rho_G + \omega\times\omega\times\rho_G + \omega\times\mathbf{v}_{O'}\}. \tag{2.16}$$

2. Rotational Equations of Motion

To develop the rotational equations of motion, the sum of applied moments about the vehicle's center of mass is equated to the rate of change of angular momentum of the vehicle about its center of mass. In the practical case of marine vehicles, however, the statement just made is modified slightly because it is much more difficult to assess the vehicle's mass moments of inertia about its center of gravity (*CG*), as the *CG* changes with loading. It becomes simpler to evaluate the mass moments of inertia about the body fixed frame which tends to lie along the vehicle's axes of symmetry. The inertia tensor required to be computed is,

$$\boldsymbol{I}_{o'} = \begin{bmatrix} I_{xx} & I_{xy} & I_{xz} \\ I_{yx} & I_{yy} & I_{yz} \\ I_{zx} & I_{zy} & I_{zz} \end{bmatrix}, \tag{2.17}$$

where,

$I_{xx} = \sum_{i=1}^{N} dm_i(y^2 + z^2)$ and $I_{xy} = I_{yx} = -\sum_{i=1}^{N} dm_i(xy)$, for example.

The angular momentum of the body is given by,

$$\boldsymbol{h}_{o'} = \boldsymbol{I}_{o'}\boldsymbol{\omega}. \tag{2.18}$$

The total applied rotational moments about the vehicle's reference frame origin is given by,

$$\boldsymbol{m}_{o'} = \dot{\boldsymbol{h}}_{o'} + \rho_G \times (m\dot{\boldsymbol{v}}_G). \tag{2.19}$$

Differentiating Equation 2.18, the rate of change of angular momentum is found to be,

$$\dot{\boldsymbol{h}}_{o'} = \boldsymbol{I}_{o'}\dot{\boldsymbol{\omega}} + \boldsymbol{\omega}\times\boldsymbol{h}_{o'}, \tag{2.20}$$

and the acceleration of the global position vector $\boldsymbol{r}_{o'}$, is given by,

$$\ddot{\boldsymbol{r}}_{o'} = \dot{\boldsymbol{v}}_{o'} + \boldsymbol{\omega} \times \boldsymbol{v}_{o'}. \tag{2.21}$$

Substituting equations 2.20 and 2.21 into Equation 2.19, the rotational equation of motion in vector form is given by,

$$\boldsymbol{m}_{rot} = \boldsymbol{I}_o \dot{\boldsymbol{\omega}} + \boldsymbol{\omega} \times (\boldsymbol{I}_o \boldsymbol{\omega}) + m\{\boldsymbol{\rho}_G \times \dot{\boldsymbol{v}}_{o'} + \boldsymbol{\rho}_G \times \boldsymbol{\omega} \times \boldsymbol{v}_{o'}\}. \tag{2.22}$$

(Again, for a more detailed discussion, the reader is referred to [Greenwood 1988]).

3. Equations of Motion in Free Space

At this point, there are three translational equations obtained from Equation 2.16, three rotational equations obtained from Equation 2.22, and six unknown velocities ($\boldsymbol{v}$ and $\boldsymbol{\omega}$). This set of equation written in long form is;

$$m[\dot{u} - vr + wq - x_G(q^2 + r^2) + y_G(pq - \dot{r}) + z_G(pr + \dot{q})] = X_f, \tag{2.23}$$

$$m[\dot{v} + ur - wp + x_G(pq + \dot{r}) - y_G(p^2 + r^2) + z_G(qr - \dot{p})] = Y_f, \tag{2.24}$$

$$m[\dot{w} - uq + vp + x_G(pr - \dot{q}) + y_G(qr + \dot{p}) - z_G(p^2 + q^2)] = Z_f, \tag{2.25}$$

$$\begin{aligned} &I_x \dot{p} + (I_z - I_y)qr + I_{xy}(pr - \dot{q}) - I_{yz}(q^2 - r^2) - I_{xz}(pq + \dot{r}) + \\ &m[y_G(\dot{w} - uq + vp) - z_G(\dot{v} + ur - wp)] = K_f \end{aligned}, \tag{2.26}$$

$$\begin{aligned} &I_y \dot{q} + (I_x - I_z)pr - I_{xy}(qr + \dot{p}) + I_{yz}(pq - \dot{r}) + I_{xz}(p^2 - r^2) - \\ &m[x_G(\dot{w} - uq + vp) - z_G(\dot{u} - vr + wq)] = M_f \end{aligned}, \tag{2.27}$$

and

$$\begin{aligned} &I_z \dot{r} + (I_y - I_x)pq - I_{xy}(p^2 - q^2) - I_{yz}(pr + \dot{q}) + I_{xz}(qr - \dot{p}) + \\ &m[x_G(\dot{v} + ur - wp) - y_G(\dot{u} - vr + wq)] = N_f \end{aligned}. \tag{2.28}$$

These preceding six equations are the most general form of Newton's laws for rigid body motion used today. They consist of a constant mass and inertia tensor, and are formulated in the body fixed frame. This set of equations can be simplified depending on the location of the local axes. If the axes are selected to coincide with the vehicle's principal axis of inertia, then the terms including the product of inertia become zero. This simplification is possible only if the *xy*-, *xz*-, and *yz*-planes are planes of symmetry. This is typically not the case. (Practically, most designs are only symmetric about the *xz*-plane. Further simplifications can be made, including locating the origin of the body

fixed frame at the vehicle's center of gravity, however, these assumptions are not physically realizable.)

The previous nonlinear system, equations 2.23-2.28, can be written in a compact vector form. Using the vector $\boldsymbol{x}$ the state vector of body fixed velocities, and defining $\boldsymbol{M_{RB}}$ as a rigid body mass matrix including translational and rotational inertial elements,

$$\boldsymbol{M}_{RB} = \begin{bmatrix} m & 0 & 0 & 0 & mz_G & -my_G \\ 0 & m & 0 & -mz_G & 0 & mx_G \\ 0 & 0 & m & my_G & -mx_G & 0 \\ 0 & -mz_G & my_G & I_{xx} & I_{xy} & I_{xz} \\ mz_G & 0 & -mx_G & I_{yx} & I_{yy} & I_{yz} \\ -my_G & mx_G & 0 & I_{zx} & I_{zy} & I_{zz} \end{bmatrix},$$

and $\boldsymbol{C_{RB}(x)}$ as a state dependent matrix containing the rigid body coriolis and centrifugal terms,

$$\boldsymbol{C}_{RB}(\boldsymbol{x}) = \begin{bmatrix} 0 & -mr & mq & m(y_Gq+z_Gr) & -mx_Gq & -mx_Gr \\ mr & 0 & -mp & -my_Gp & m(z_Gr+x_Gp) & -my_Gr \\ -mq & mp & 0 & -mz_Gp & -mz_Gq & m(x_Gp+y_Gq) \\ -m(y_Gq+z_Gr) & my_Gp & mz_Gp & 0 & -I_{yz}q-I_{xz}p+I_zr & I_{yz}r+I_{xy}p-I_yq \\ mx_Gq & -m(z_Gr+x_Gp) & mz_Gq & I_{yz}q+I_{xz}p-I_zr & 0 & -I_{zz}r-I_{xy}q+I_xp \\ mx_Gr & my_Gr & -m(x_Gp+y_Gq) & -I_{yz}r-I_{xy}p+I_yq & I_{zz}r+I_{xy}q-I_xp & 0 \end{bmatrix},$$

the equations of motion can be written in vector form as,

$$\boldsymbol{M}_{RB}\dot{\boldsymbol{x}} + \boldsymbol{C}_{RB}(\boldsymbol{x})\boldsymbol{x} = \boldsymbol{f}\,. \tag{2.29}$$

The right hand term in Equation 2.29 is the vector of external forces and moments outlined in Table 2.1. These forces and moments come from hydrostatic and hydrodynamic forces due to gravity, radiation and excitation, viscous damping (lift and drag), and control inputs. The origin of these forces and their application to the developed equations of motion will be discussed in detail in following sections.

D. RESTORING FORCES AND MOMENTS

In hydrodynamic terminology, the gravitational and buoyant forces are called restoring forces. The weight, *W*, and buoyant, *B*, forces that act at the centers of gravity and buoyancy must be defined from static analyses. For submerged bodies the weight and buoyancy force vectors do not change with vehicle attitude. Assuming that weight

and buoyancy are fixed in relation to the body fixed frame, then the gravitational and buoyant forces may be expressed as, $f_W = 0I + 0J + WK$, and $f_B = 0I + 0J - BK$. Since the weight and buoyancy terms in the applied forces act in the global vertical direction, they must be transformed into components in the vehicle fixed frame before they can be added into the equations of motion. Returning to Equation 2.4, it can be seen that the components acting along the vertical vehicle fixed frame are the third column of the transformation matrix. Therefore, the net vertical force components become,

$$f_g = (W - B)\begin{bmatrix} -\sin\theta \\ \cos\theta\sin\phi \\ \cos\theta\cos\phi \end{bmatrix}. \tag{2.30}$$

The weight portion of the vertical force acts at the center of gravity of the vehicle, while the buoyancy portion of the vertical force acts at the center of buoyancy. Because these forces act in locations away from the body center they create a moment about the body center given by,

$$m_g = W\rho_G \times \begin{bmatrix} -\sin\theta \\ \cos\theta\sin\phi \\ \cos\theta\cos\phi \end{bmatrix} - B\rho_B \times \begin{bmatrix} -\sin\theta \\ \cos\theta\sin\phi \\ \cos\theta\cos\phi \end{bmatrix}. \tag{2.31}$$

This moment will be non-zero even if W and B are equal, since ρ_G and ρ_B are usually not collocated. For static stability it is necessary to locate the center of gravity below the center of buoyancy. The total vertical force vector can be written as,

$$f_G = \begin{bmatrix} f_g \\ m_g \end{bmatrix} = \begin{bmatrix} -(W-B)\sin\theta \\ (W-B)\cos\theta\sin\phi \\ (W-B)\cos\theta\cos\phi \\ (y_G W - y_B B)\cos\theta\cos\phi - (z_G W - z_B B)\cos\theta\sin\phi \\ -(x_G W - x_B B)\cos\theta\cos\phi - (z_G W - z_B B)\sin\theta \\ (x_G W - x_B B)\cos\theta\sin\phi + (y_G W - y_B B)\sin\theta \end{bmatrix} = -F(z), \tag{2.32}$$

and is added to the right hand side of the equations of motion.

E. WAVE THEORY AND HYDRODYNAMICS

1. Linear Wave Theory

The simplest free surface wave formation, which nevertheless has great practical significance, is the plane progressive wave system where the water column is modeled as an inviscid, irrotational fluid in a gravity field. This motion is two dimensional, (x, z), sinusoidal in time with angular frequency ω, and propagates with a phase velocity c_p such that to an observer moving with this speed the wave appears to be stationary. A Cartesian coordinate system is adopted, see Figure 2.2, with $z = 0$, the plane of the undisturbed free surface (still water level) and the z-axis positive upwards. The vertical elevation of any point on the free surface may be defined by a function $z = \eta(x,t)$. With these requirements, the free surface elevation must be of the general form

$$\eta(x,t) = A\cos(kx - \omega t), \tag{2.33}$$

where the positive x-axis is chosen to coincide with the direction of wave propagation. Here, A is the wave amplitude, and the parameter

$$k = \frac{\omega}{c_p}, \tag{2.34}$$

is the wavenumber, the number of waves per unit distance along the x-axis. Clearly, the wavenumber can also be written as,

$$k = \frac{2\pi}{L}, \tag{2.35}$$

where the wavelength L, is the distance between successive points on the wave with the same phase, see Figure 2.2. The solution of this problem is expressed in terms of a two dimensional velocity potential, which must satisfy Laplace's equation

$$\nabla^2\phi = 0, \tag{2.36}$$

and appropriate boundary conditions. Furthermore, the velocity potential, ϕ, must yield the wave elevation given by Equation 2.33 from

$$\eta = -\frac{1}{g}\frac{\partial\phi}{\partial t}, \quad at \quad z = 0. \tag{2.37}$$

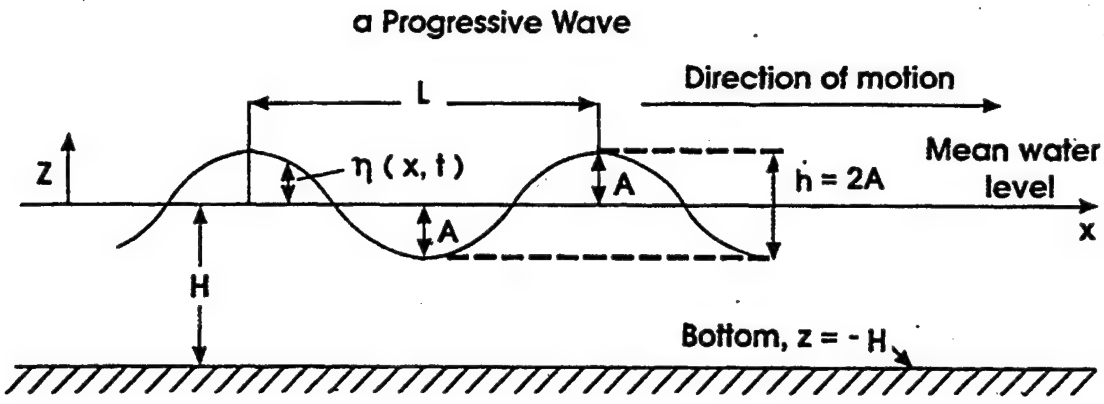

Figure 2.2 Monochromatic Progressive Surface Gravity Wave [Rahman 1994]

Equation 2.37 is the linearized dynamic boundary condition on the free surface and is an expression of the fact, through Bernoulli's equation, that the pressure on the free surface must be the same as the ambient atmospheric pressure. An appropriate boundary condition on the sea bottom is

$$\frac{\partial \phi}{\partial z} = 0, \quad at \quad z = -H, \tag{2.38}$$

i.e., the bottom at depth H is a rigid impermeable plane. Finally, the free surface boundary condition is

$$\frac{\partial^2 \phi}{\partial t^2} + g\frac{\partial \phi}{\partial z} = 0, \quad at \quad z = 0. \tag{2.39}$$

Equation 2.39 is a combined dynamic and kinematic surface boundary condition. The dynamic condition was discussed earlier, while the kinematic condition simply states,

$$\frac{\partial \eta}{\partial t} = \frac{\partial \phi}{\partial z}, \tag{2.40}$$

that the vertical velocities of the free surface and fluid particles are the same. Combining equations 2.37 and 2.40, Equation 2.39 is obtained, ignoring the small departures of the free surface η from the horizontal orientation of $z = 0$.

From the requirements of the problem, it is clear that the velocity potential ϕ must be sinusoidal in the same sense as Equation 2.30; therefore a solution of the form

$$\phi(x,z,t)=\sin(kx-\omega t)F(z), \tag{2.41}$$

is attempted. Substituting Equation 2.41 into Equation 2.36, *F(z)* must satisfy the ordinary differential equation

$$\frac{d^2F(z)}{dt^2}-k^2F(z)=0, \tag{2.42}$$

throughout the domain of the fluid. The solution to Equation 2.42 satisfying the bottom boundary condition is

$$F(z)=A\cosh(k(z+H)). \tag{2.43}$$

Substitution of equations 2.41 and 2.43 into the surface boundary condition, Equation 2.37, yields an important relationship between the wavenumber k and the frequency ω,

$$\omega^2=gk\tanh(kH), \tag{2.44}$$

which is called the dispersion relationship. The surface elevation η follows from Equation 2.37 as,

$$\eta(x,t)=a\cos(kx-\omega t), \tag{2.45}$$

with the amplitude a, given by

$$a=\frac{\omega A}{g}\cosh(kH). \tag{2.46}$$

Substitution of equations 2.43 and 2.46 into the velocity potential function, Equation 2.41, yields

$$\phi(x,z,t)=\frac{ag}{\omega}\frac{\cosh(k(z+H))}{\cosh(kH)}\sin(kx-\omega t). \tag{2.47}$$

An underlying assumption associated with potential flow theory and Laplace's Equation, is that the velocity field can be expressed as the gradient of a velocity potential function. This allows the expressions for the velocities in the x and z direction to be given as

$$\begin{aligned} u&=\frac{\partial\phi}{\partial x}\\ w&=\frac{\partial\phi}{\partial z} \end{aligned} \tag{2.48}$$

Using Equation 2.48, and the linearized form of the Bernoulli's equation,

$$p = -\rho \frac{\partial \phi}{\partial t} - \rho g z , \tag{2.49}$$

the expressions for the fluid velocity and pressure fields are

$$\begin{aligned} u &= a \frac{gk}{\omega} \frac{\cosh(k(z+H))}{\cosh(kH)} \cos(kx - \omega t) \\ w &= a \frac{gk}{\omega} \frac{\sinh(k(z+H))}{\cosh(kH)} \sin(kx - \omega t) \\ p &= \rho g a \frac{\cosh(k(z+H))}{\cosh(kH)} \cos(kx - \omega t) - \rho g z \end{aligned} \tag{2.50}$$

It can be seen from Equation 2.50 that the trajectories of the fluid particles are elliptical.

There are several simplifications that may be made to the above-derived expressions for the cases of shallow (long waves) and deep (short waves) water. The shallow and deep water ranges correspond to $H/L < \pi/10$ and $H/L > \pi$, respectively. Over these ranges approximate expressions may be substituted for the hyperbolic functions that have been encountered. Table 2.2 summarizes these results. Figure 2.3 depicts the comparison of water particle velocity between long and short waves. The key points that should be observed are that shallow water waves are non-dispersive, i.e., the vertical component of the wave particle velocity is linear in depth, and that the classification of shallow water depends on the ratio of water depth to wavelength.

As an example, consider a one-meter high, monochromatic wave with a ten-second period (0.1 Hz), propagating in water six meters deep. The deep water and shallow water wavelengths are 156 meters and 76.7 meters, respectively. The ratios of water depth to wavelength are 0.038, for the deep water case, and 0.078, for the shallow water case. Referring to Table 2.2, it can be seen that neither the deep water nor shallow water simplifications may be used. In fact, the water depth must be reduced to 2.45 meters before the shallow water equations are valid. Conversely, if the water depth remains at 6 meters, then the wave period must become greater than 15.6 seconds or the wave frequency less than 0.064 Hz. This indicates that only low frequency waves typically qualify as shallow water (non-dispersive) waves which becomes an important consideration in the proper modeling of the wave induced disturbances.

	Deep water (short) waves, $H/L>1/2$, $kH>\pi$	Intermediate depth waves, $1/20 \leq H/L \leq 1/2$, $\pi/10 < kH < \pi$	Shallow water (long) waves, $H/L < 1/20$, $kH < \pi/10$
In all cases, $\theta=kx-\omega t$			
Profile, η	$\eta = A\cos\theta$	$\eta = A\cos\theta$	$\eta = A\cos\theta$
Wave velocity, C	$C=\frac{g}{\omega}$	$C=\frac{g}{\omega}\tanh(kH)$	$C=\sqrt{gH}$
Wavelength, L	$L=\frac{gT^2}{2\pi}$	$L=\frac{gT^2}{2\pi}\tanh(\frac{2\pi H}{L})$	$L=T\sqrt{gH}$
Velocity potential, ϕ	$\phi=\frac{A\omega}{k}e^{kz}\sin\theta$	$\phi=\frac{A\omega}{k}\frac{\cosh(k(z+H))}{\cosh(kH)}\sin\theta$	$\phi=\frac{AgT}{2\pi}\sin\theta$
Particle velocity, u	$u=A\omega e^{kz}\cos\theta$	$u=A\omega\frac{\cosh(k(z+H))}{\cosh(kH)}\cos\theta$	$u=\frac{A\omega}{kH}\cos\theta$
Particle velocity, w	$w=-A\omega e^{kz}\sin\theta$	$w=A\omega\frac{\sinh(k(z+H))}{\cosh(kH)}\sin\theta$	$w=-A\omega(1+\frac{z}{H})\sin\theta$
Pressure, p	$p=\rho g(\eta e^{kz}-z)$	$p=\rho g(\eta\frac{\cosh(k(z+H))}{\cosh(kH)}-z)$	$p=\rho g(\eta-z)$

Table 2.2 Summary Of Small Amplitude Linear Wave Equations

As a side note, it should be pointed out that the wave height has no bearing in determining whether a wave is classified as long or short. The wave height is significant in order to determine the subsurface water particle velocities, and when the wave breaks.

The plane progressive wave described so far is a single, discrete wave system, with a prescribed monochromatic component of frequency ω and wavenumber k, moving in the positive x-direction. More general wave motions, which are not monochromatic,

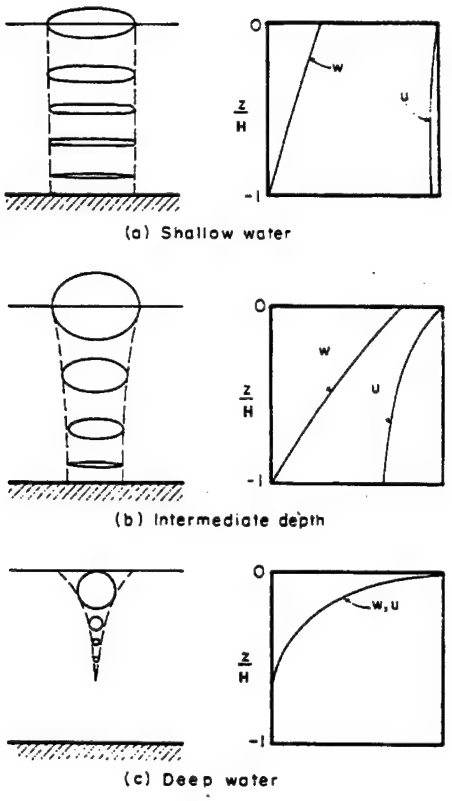

Figure 2.3 Particle Orbits And Variation Of Particle Velocity Amplitude With Depth [Sarpkaya 1981]

can be obtained by superimposing plane waves of different frequencies and wavenumbers. The elevation of the sea surface $\eta(t)$ can thus be described as the superposition of an infinite number of sinusoids of the form:

$$\eta(t) = \sum_{n=1}^{\infty} a_n \cos(k_n x - \omega_n t + \phi_n) = \sum_{n=1}^{\infty} \eta_n . \tag{2.51}$$

The equations for the horizontal and vertical velocities, and the dynamic pressure are,

$$u(t) = \sum_{n=1}^{\infty} \left[\frac{\omega_n \cosh k_n (H+z)}{\sinh k_n H} \right] \eta_n ; \tag{2.52}$$

$$w(t) = \sum_{n=1}^{\infty} \left[\frac{\omega_n \sinh k_n (H+z)}{\sinh k_n H} \right] \eta_n ; \tag{2.53}$$

$$p(t) = \rho g \sum_{n=1}^{\infty} \left[\frac{\omega_n \cosh k_n (H+z)}{\cosh k_n H} \right] \eta_n - \rho g z ; \tag{2.54}$$

respectively, where the parameters/variables in equations 2.51-2.54 are identical to those in the monochromatic case.

2. Hydrodynamics

[Newman 1977] has shown that the total velocity potential ϕ, may be written as $\phi = \phi_W + \phi_D + \phi_R$, the linear sum of three components. These three components come from wave, diffraction and radiation potentials where,

- ϕ_W is the incident regular wave velocity potential;
- ϕ_D is the diffraction potential caused by reflection when the vehicle is considered restrained from motion; and
- ϕ_R is the radiation potentials in 6 DOF caused by forcing the vehicle to oscillate with wave excitation frequency, when there are no incident waves present.

Linear wave theory implies that the wave induced forces and moments acting on a vehicle come from the superposition of the radiation induced forces and moments and the excitation forces and moments.

Radiation induced forces and moments act on the vehicle when the vehicle is forced to oscillate with the wave excitation frequency without incident waves present. The forces due to wave radiation are classified as restoring, added mass and potential damping forces.

Excitation forces and moments act on the vehicle when the vehicle is restrained from motion and incident waves are present. These forces and moments caused by wave excitation are classified as Froude-Kriloff (*FK*) and diffraction forces. The *FK* forces and moments are found by integrating the pressure distribution over the vehicle cause by the undisturbed wave field, while the diffraction forces and moments are determined by the pressure distribution created when the waves are reflected from the vehicle.

As a general summary, the unforced equations of motion for any stationary body in waves, can be given as

$$(\mathbf{M}_{RB} + \mathbf{A}(\omega))\ddot{\eta} + \mathbf{B}(\omega)\dot{\eta} + \mathbf{C}\eta - (\mathbf{M}_{FK} + \mathbf{A}(\omega))\ddot{\eta}_f - \mathbf{B}(\omega)\dot{\eta}_f - \mathbf{C}\eta_f = 0, \quad (2.55)$$

where η is a vector of linear and angular displacements. Stationary in this sense implies that the vehicle is non-maneuvering and that its only motion is that caused by the body's

interaction with the waves. As seen, the added mass and damping matrices, $A(\omega)$ and $B(\omega)$ respectively, are functions of the incident wave frequency. However, if the vehicle is moving with some forward velocity U, the wave frequency, ω, is not the frequency encountered by the vehicle. The encounter frequency, ω_e, can be expressed as

$$\omega_e = \omega + kU\cos\beta . \tag{2.56}$$

In this equation, which is based on the Doppler effect, β is the heading angle between the vehicle and the wave propagation direction and k is the wavenumber. More detailed information on the Doppler effect maybe found in Appendix B.

As a simplification, if the body is small in comparison to the wavelength, it is totally submerged and neutrally buoyant with homogeneous mass distribution, then Equation 2.55 can be simplified to yield

$$(\mathbf{M}_{RB} + \mathbf{A}(\omega_e))\ddot{\eta}_r + \mathbf{B}(\omega_e)\dot{\eta}_r + \mathbf{C}\eta_r = 0, \tag{2.57}$$

where $\dot{\eta}_r = \dot{\eta} - \dot{\eta}_f$, is the relative velocity of the fluid over the vehicle. It is necessary to point out that the above equation was based on the assumption of inviscid flow. Due to this fact, viscous damping terms (skin friction and drag), must be taken into account for a vehicle operating in a real fluid, to complete the model.

In 1950, Morison developed an expression for the horizontal force on a cylindrical pile subjected to waves. His work showed that the elemental force dF on a vertical strip of a cylinder dz, may be written as

$$dF = \rho\frac{\pi D^2}{4}dzC_M\dot{u}_f + \frac{1}{2}\rho C_D D dz u_f|u_f| . \tag{2.58}$$

In this expression, coined "*Morison's equation*", D is the characteristic diameter, $\dot{u}_f$ and u_f are the horizontal component of the undisturbed fluid acceleration and velocity, respectively, and C_M and C_D are mass and drag coefficients which may be determined experimentally. This equation has two parts, the first term representing an inertia force proportional to the accelerating fluid acting on the pile (a mass force), and the second term, a nonlinear drag term proportional to the sign squared fluid velocity (a drag force).

In practice, Morison's equation can only be applied to small volume bodies. By small volume bodies, it is meant that the characteristic cross sectional dimension of the

body is small relative to the wavelength [Morison 1950]. For vertical piles, small volume applies only if $L>5D$, where D is the pile diameter, refer to Figure 2.4. As shown, for small vehicles operating in shallow water, inertia and drag forces are dominant, where as reflection and diffraction effects can be considered unimportant.

It is known that the ratios of wavelength and wave height to the characteristic diameter are key parameters in predicting the load regime of waves acting on a structure [Faltinsen 1990]. These regimes are also depicted in Figure 2.4.

For a stationary object in a simple harmonic flow, the total force can be expressed as

$$F_T = F_D \sin \omega t \left| \sin \omega t \right| + F_I \cos \omega t , \tag{2.59}$$

where F_D and F_I represent the maxima of the drag and inertia force components, respectively. [Dean 1984] divided the flow force regimes into two areas; one where the inertially derived component dominated the total force, and one where both drag and inertial effects are important. This expression is represented as

$$\left| F_T \right| = \begin{Bmatrix} F_I ; & 2F_D \le F_I \\ F_D + \dfrac{F_I^2}{4F_D} ; & 2F_D > F_I \end{Bmatrix} . \tag{2.60}$$

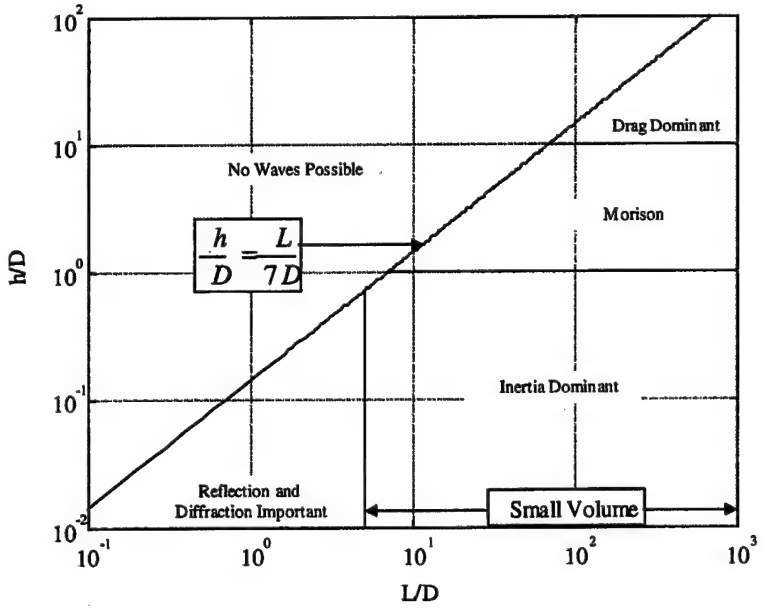

Figure 2.4 Load Regimes

The significance of the above expression is that the maximum force on the body is not affected by additional drag force until the amplitude of the drag is at least one half that of the inertia force. For oscillating flows, such as those caused by waves, while even small amounts of drag may be important when considering the shape of the load function on a stationary body, the peak amplitude of the force is only affected when the drag component is greater than one-half the inertia force. Extensive experimental verification of Morison's approach to force modeling, and the evaluation of the frequency dependent nature of the drag and added mass coefficients was given by [Sarpkaya 1975].

When the wave field causes motion of the water particles at the vehicle's operating depth to be of the order of one diameter or less, it is expected that the predominant hydrodynamic force on the AUV due to the wave disturbance would be inertial in nature. Since the AUV operates below the surface, it is not the wave height to vehicle diameter ratio that is of concern, but more appropriately the double amplitude of the water particle motion at the vehicle operating depth compared to the vehicle characteristic length of interest. While this analogy is approximate in nature, it does provide a means to predict which hydrodynamic forces may be of concern when estimating the total load on a vehicle. These above concepts may be used to estimate the dominant forces acting on an underwater vehicle subject to waves, and therefore assist in the sizing of the propulsion system.

F. HYDRODYNAMIC FORCES AND MOMENTS

Hydrodynamic forces and moments are the result of body/fluid interactions. The forces and moments on the body arise from the modification to the pressure distribution summed around the surface area of the body. This modification to the pressure field can only arise from relative velocity and acceleration between the body and fluid. Therefore, for the purposes of this discussion it is necessary to re-define the body fixed velocity vector $\boldsymbol{x}$, in terms of a relative body fixed velocity vector $\boldsymbol{x}_r$, where $\boldsymbol{x}_r = [u_r, v_r, w_r, p, q, r]^T$. Also at this time it is convenient to define a globally based fluid velocity vector $\boldsymbol{U}_f$, where $\boldsymbol{U}_f = [U_f, V_f, W_f, 0, 0, 0]^T$. Since it is assumed that the fluid

velocity is irrotational, no changes to the angular rate terms are necessary in the body fixed velocity vector, and no angular rates are present in the fluid velocity vector.

1. Radiation Induced Forces and Moments

a) Added Mass

Like the rigid body kinematics, it is desirable to separate the added mass terms into terms which belong to an added mass matrix $\boldsymbol{M}_{AM}$ and a matrix of Coriolis and centrifugal terms $\boldsymbol{C}_{AM}(\boldsymbol{x})$. For underwater vehicles this implies that the added mass forces and moments can be written as:

$$\boldsymbol{f}_{AM} = -\boldsymbol{M}_{AM}\dot{\boldsymbol{x}}_r - \boldsymbol{C}_{AM}(\boldsymbol{x}_r)\boldsymbol{x}_r \tag{2.61}$$

where $\boldsymbol{f}_{AM}=[X_A, Y_A, Z_A, K_A, M_A, N_A]^T=[f_A,\ m_A]^T$ is the total added mass force and moment vector.

The added mass terms represent the inertial reaction of fluid particles surrounding the submerged body that are accelerated with it. Any motion of the vehicle induces a motion in the otherwise stationary fluid. In order to allow the vehicle to pass through the fluid, the fluid must move aside and then close behind the vehicle. As a consequence, the fluid passage possesses kinetic energy that it would lack if the vehicle was not in motion.

[Lamb 1932] gives the following expression for the fluid kinetic energy, E_k, which may be expressed in a quadratic form of the body axis velocity vector components;

$$E_k = -\frac{1}{2}\rho\int_S \phi\frac{\partial\phi}{\partial n}dS = \frac{1}{2}\boldsymbol{x}_r^{\,T}\boldsymbol{M}_{AM}\boldsymbol{x}_r. \tag{2.61}$$

In Equation 2.61, $\boldsymbol{M}_{AM}$ is a 6x6 added mass matrix. For a rigid body moving in an ideal fluid the added mass matrix is symmetrical, i.e., $\boldsymbol{M}_{AM} = \boldsymbol{M}_{AM}^{\,T}$. In a real fluid these 36 elements may all be distinct. [Wendel 1956] has shown that the numerical values of added mass in a real fluid are usually in good agreement with those obtained from ideal theory. For a body possessing vertical plane symmetry only, and applying $\boldsymbol{M}_{AM} = \boldsymbol{M}_{AM}^{\,T}$, the added mass matrix is written as

$$M_{AM} = -\begin{bmatrix} X_{\dot{u}} & 0 & X_{\dot{w}} & 0 & X_{\dot{q}} & 0 \\ 0 & Y_{\dot{v}} & 0 & Y_{\dot{p}} & 0 & Y_{\dot{r}} \\ X_{\dot{w}} & 0 & Z_{\dot{w}} & 0 & Z_{\dot{q}} & 0 \\ 0 & Y_{\dot{p}} & 0 & K_{\dot{p}} & 0 & K_{\dot{r}} \\ X_{\dot{q}} & 0 & Z_{\dot{q}} & 0 & M_{\dot{q}} & 0 \\ 0 & Y_{\dot{r}} & 0 & K_{\dot{r}} & 0 & N_{\dot{r}} \end{bmatrix},$$

The notation of [SNAME 1950] is used in this expression. This notation indicates the degree of freedom on which the hydrodynamic added mass force acts, as well as the cause of the force. As an example, $Y_{\dot{u}}\dot{u}$ is a force acting along the body fixed y-axis due to an acceleration $\dot{u}$ in the x-direction, and can be thought of mathematically as $Y_{\dot{u}} = \frac{\partial Y}{\partial \dot{u}}$. This definition implies that the hydrodynamic derivatives corresponding to the diagonal of the added mass matrix will all be negative.

The added mass terms are obtained from potential theory. This theory assumes an inviscid fluid, no circulation and that the body is completed submerged in an unbounded fluid. The last assumption is violated at the seabed, near underwater objects and at the surface. [Milne-Thomson 1968] has shown that the expressions for the force and moments resulting from added mass effects can be found by applying Kirchhoff's equations,

$$\begin{aligned} \frac{d}{dt}\left(\frac{\partial E_k}{\partial \boldsymbol{u}}\right) + \boldsymbol{\omega} \times \frac{\partial E_k}{\partial \boldsymbol{u}} &= -\boldsymbol{f}_A \\ \frac{d}{dt}\left(\frac{\partial E_k}{\partial \boldsymbol{\omega}}\right) + \boldsymbol{\omega} \times \frac{\partial E_k}{\partial \boldsymbol{\omega}} + \boldsymbol{u} \times \frac{\partial E_k}{\partial \boldsymbol{u}} &= -\boldsymbol{m}_A \end{aligned}, \tag{2.63}$$

in vector form. Expanding Equation 2.63, the expression for the added mass terms associated with the x-direction is

$$\begin{aligned} X_A = {} & X_{\dot{u}}\dot{u} + X_{\dot{w}}(\dot{w} + uq) + X_{\dot{q}}\dot{q} + Z_{\dot{w}}wq + Z_{\dot{q}}q^2 \\ & - Y_{\dot{v}}vr - Y_{\dot{p}}rp - Y_{\dot{r}}r^2 \end{aligned}. \tag{2.64}$$

(Derivation of the added mass terms associated with the other degrees of freedom is left to the reader.) Many of the added mass derivatives contained in the general form are either zero or mutually related to another term when the body has various symmetries. A

more detailed discussion of added mass terms applied to an underwater vehicle, is found in [Humphreys 1978].

Extracting the added mass derivatives corresponding to the velocity coupling terms from 2.63 yields;

$$C_A(x)=\begin{bmatrix} 0 & 0 & 0 & 0 & C_{15} & C_{16} \\ 0 & 0 & 0 & C_{24} & 0 & C_{26} \\ 0 & 0 & 0 & C_{34} & C_{35} & 0 \\ 0 & -C_{24}- & C_{34} & 0 & C_{45} & C_{46} \\ -C_{15} & 0 & -C_{35} & -C_{45} & 0 & C_{56} \\ -C_{16} & -C_{26} & 0 & -C_{46} & -C_{56} & 0 \end{bmatrix},$$

where,

$$\begin{aligned} C_{15} &= -X_{\dot{w}}u - Z_{\dot{w}}w - Z_{\dot{q}}q & C_{35} &= X_{\dot{u}}u + X_{\dot{w}}w + X_{\dot{q}}q \\ C_{16} &= Y_{\dot{v}}v + Y_{\dot{p}}p + Y_{\dot{r}}r & C_{45} &= -Y_{\dot{r}}v - K_{\dot{r}}p - N_{\dot{r}}r \\ C_{24} &= X_{\dot{w}}u + Z_{\dot{w}}w + Z_{\dot{q}}q & C_{46} &= X_{\dot{q}}u + Z_{\dot{q}}w + M_{\dot{q}}q\,. \\ C_{26} &= -X_{\dot{u}}u - X_{\dot{w}}w - X_{\dot{q}}q & C_{56} &= -Y_{\dot{p}}v - K_{\dot{p}}p - N_{\dot{r}}r \\ C_{34} &= -Y_{\dot{v}}v - Y_{\dot{p}}p - Y_{\dot{r}}r \end{aligned}$$

b) Wave Radiation or Potential Damping

The contribution from the potential damping terms compared to other dissipative terms like viscous damping terms are usually negligible for underwater vehicles operating at great depth. Nevertheless, underwater vehicles operating in shallow water near to the free surface should consider potential damping effects, especially, those underwater vehicles that tend to have a non-streamlined body, i.e., vehicles build with sensor and equipment mounted in such a manner that the equipment causes the vehicle not be streamlined. The linear potential damping can be modeled as

$$f_d = -D_d x_r\,. \tag{2.65}$$

The linear damping matrix D_d is a positive definite matrix of linear damping coefficients. These linear damping terms are small when compared to the viscous forces, and therefore are often included in the viscous drag forces.

2. Excitation Forces

When applying potential theory, the fluid motion was assumed to be irrotational. This implies that only the linear velocity components, U_f, of the fluid are considered when determining the excitation forces. In linear theory, the wave induced forces and moments acting on a vehicle are considered to be the sum of the radiation induced forces and moments and the excitation forces and moments. For nonlinear theory, this is not the case. The forces and moments due to radiation and diffraction are nonlinear functions of the relative velocity and acceleration between the vehicle and the fluid.

a) Froude-Kriloff Forces

The Froude-Kriloff force and moment vector can be expressed as

$$f_{FK} = M_{FK}\dot{u}_f, \tag{2.66}$$

where M_{FK} can be interpreted as the Froude-Kriloff (FK) mass matrix and $\dot{u}_f$ is the fluid acceleration expressed in body fixed coordinates. Coriolis and centrifugal terms will not appear in the general expression for the FK forces and moments since it was assumed that the rotational fluid motion was zero. This mass matrix can be determined by computing the mass of the fluid displaced by the vehicle and substituting this value into the rigid body mass matrix in place of the vehicle mass. Also, it should be recognized that this excitation force acts at the center of buoyancy not the center of gravity. The mass and the moments and products of inertia for the FK mass matrix are

$$\overline{m} = \rho\nabla = B/g,\ \bar{I}_{xx} = \sum_{i=1}^{N} d\overline{m}_i(y^2+z^2) \text{ and } \bar{I}_{xy} = \bar{I}_{yx} = -\sum_{i=1}^{N} d\overline{m}_i(xy).$$

Substituting these values into the rigid body mass matrix yields the FK mass matrix, for a small volume completely submerged body.

$$M_{FK} = \begin{bmatrix} \overline{m} & 0 & 0 & 0 & \overline{m}z_B & -\overline{m}y_B \\ 0 & \overline{m} & 0 & -\overline{m}z_B & 0 & \overline{m}x_B \\ 0 & 0 & \overline{m} & \overline{m}y_B & -\overline{m}x_B & 0 \\ 0 & -\overline{m}z_B & \overline{m}y_B & \bar{I}_{xx} & \bar{I}_{xy} & \bar{I}_{xz} \\ \overline{m}z_B & 0 & -\overline{m}x_B & \bar{I}_{yx} & \bar{I}_{yy} & \bar{I}_{yz} \\ -\overline{m}y_B & \overline{m}x_B & 0 & \bar{I}_{zx} & \bar{I}_{zy} & \bar{I}_{zz} \end{bmatrix}$$

[Sarpkaya 1981] and [Newman 1977] have shown that the body fixed inertia force to which a symmetric body moving in an unsteady flow field is subject, may be written as

$$f = \rho\nabla(I + C_A)\left[\frac{\partial u_f}{\partial t} + \frac{\partial u_f}{\partial x}(u_f - u)\right] - \rho\nabla C_A \dot{u}. \qquad (2.67)$$

In this equation, it is important to note the presence of a buoyancy-like force that is proportional to the displaced volume of the body as well as the presence of some convective terms . The terms that include the displaced volume, when grouped together, represent the added mass and Froude-Kriloff forces. The convective terms represent the forces from the spacial changes of the unsteady flow field over the body, and for large bodies, may be significant. [Silvestre 1998b] has shown that by comparing the force contribution of the convective terms to the total inertia force exerted on a rigid body subject to wave disturbances, that the forces due to the convective terms are small and for all practical purposes may be neglected.

3. Viscous Damping Forces and Moments

a) Drag Force

The drag effects on an underwater vehicles are mainly caused by

- Linear skin friction due to laminar boundary layers;
- Quadratic skin friction due to turbulent boundary layers; and
- Quadratic drag due to vortex shedding (Morison's equation).

The viscous damping forces and moments will be functions of the relative fluid motion. In the range of Reynolds numbers in which underwater vehicles typically operate, flow is turbulent, therefore the drag force is approximated by the square law resistance arising from Morison's equation. Referring to Equation 2.55, the quadratic drag force in the x-direction can be expressed as

$$f = \frac{1}{2}\rho C_D A u_r |u_r| \qquad (2.68)$$

where A is the projected cross-sectional area, C_D is the drag-coefficient based on the representative area, ρ is the fluid density and u_r is the relative longitudinal velocity.

A generalization of Morison's equation could be to use a truncated second order Taylor series expansion to describe the viscous damping in 6 DOF. This suggests that the viscous damping forces could be written as

$$\boldsymbol{f}_v = -\boldsymbol{D}_l \boldsymbol{x}_r - \boldsymbol{D}_q(\boldsymbol{x}_r) - higer\ order\ terms\ . \tag{2.69}$$

This expression is a combination of linear and quadratic drag components. The linear portion $\boldsymbol{D}_l \boldsymbol{x}_r$, can be modeled as a positive definite matrix of linear damping coefficients multiplied by the body fixed relative velocity vector, while the quadratic portion $\boldsymbol{D}_q(\boldsymbol{x}_r)$, is a nonlinear matrix incorporating the contributions due to skin drag and vortex shedding.

It is quite complicated to determine the hydrodynamic coefficients associated with the quadratic portion, especially for high angles of attack. However, a simple, but fairly accurate method of modeling these viscous drag forces is to include the linear drag components associated with the diagonal of $\boldsymbol{D}_l \boldsymbol{x}_r$, and to use a cross flow integral to account for the $\boldsymbol{D}_q(\boldsymbol{x}_r)$ terms. The general cross flow drag expression for a body of revolution in the *y*-direction (sway) is given by

$$Y_{drag} = -\frac{1}{2}\rho \int_{-l/2}^{l/2} [C_{D_Y} D(x)(v + xr)^2 + C_{D_Z} D(x)(w - xq)^2] \frac{(v + xr)}{U_{cf}(x)} dx\ . \tag{2.70}$$

In this expression, the minus sign is present because the drag force opposes the motion, and the cross flow velocity is given by

$$U_{cf}(x) = [(v + xr)^2 + (w - xq)^2]^{1/2}\ . \tag{2.71}$$

Equation 2.70 is valid for a vehicle that has a hull form consistent with a body of revolution, however, for underwater vehicle's with different shapes this equation must be modified. As an example, consider the box shape hull form of the NPS Phoenix AUV [Marco 1996]. The cross flow drag expression in the sway direction for this shape vehicle becomes

$$Y_{drag} = -\frac{1}{2}\rho \int_{-l/2}^{l/2} C_{D_Y} h(x)(v + xr)|(v + xr)| dx\ . \tag{2.72}$$

As depicted in Figure 2.5, this expression reflects the drag force over the entire range of angles of attack.

b) Lift Forces

Lift is a force acting on a body in a direction perpendicular to that of the flow of the fluid. As relative motion is created between the underwater vehicle and its fluid environment, the vehicle body experiences lift forces similar to those experienced by an airfoil. The expression for the lift generated by an airfoil is given as

$$f = -\frac{1}{2}\rho V^2 A \frac{dC_L}{d\alpha}\left(\frac{v_r}{u_r}\right), \tag{2.73}$$

where A is the projected cross-sectional area, C_L is the lift-coefficient, α is the local angle of attack, ρ is the fluid density, and u_r and v_r are the relative velocity components in the body fixed x and y directions. See [Hoerner 1975] for further detail.

The lift forces can be modeled as a state dependent matrix multiplied by the respective relative velocity and is given by

$$\boldsymbol{f}_L = -\boldsymbol{D}_L(\boldsymbol{x}_r)\boldsymbol{x}_r. \tag{2.74}$$

The parameters/coefficients used in this matrix, like the drag coefficients are difficult to predict and vary with the shape of the body and the angle of attack of the fluid. As with the drag forces, determination of these constant coefficients is typically done using a 3-D CFD solver, with the constant coefficients validated over a range of angles of attack.

G. CONTROL FORCES

Small underwater vehicles are usually maneuvered with thrusters and control surfaces. Thrusters are effective only at low forward vehicle speed due to the fact that the action of the thrust is a nonlinear function of the relative velocity of the vehicle. However, control surfaces are effectively used in maintaining heading as well as trim and depth changing maneuvers. The reason for this is that the force generating capacity of the control surfaces is dependent on the speed of the vehicle (the lift force is proportional to the square of the velocity). The control forces and moments can be described by

$$\boldsymbol{f}_C = \boldsymbol{B}(\boldsymbol{x}_r, \boldsymbol{u}_{control})\boldsymbol{u}_{control} \tag{2.75}$$

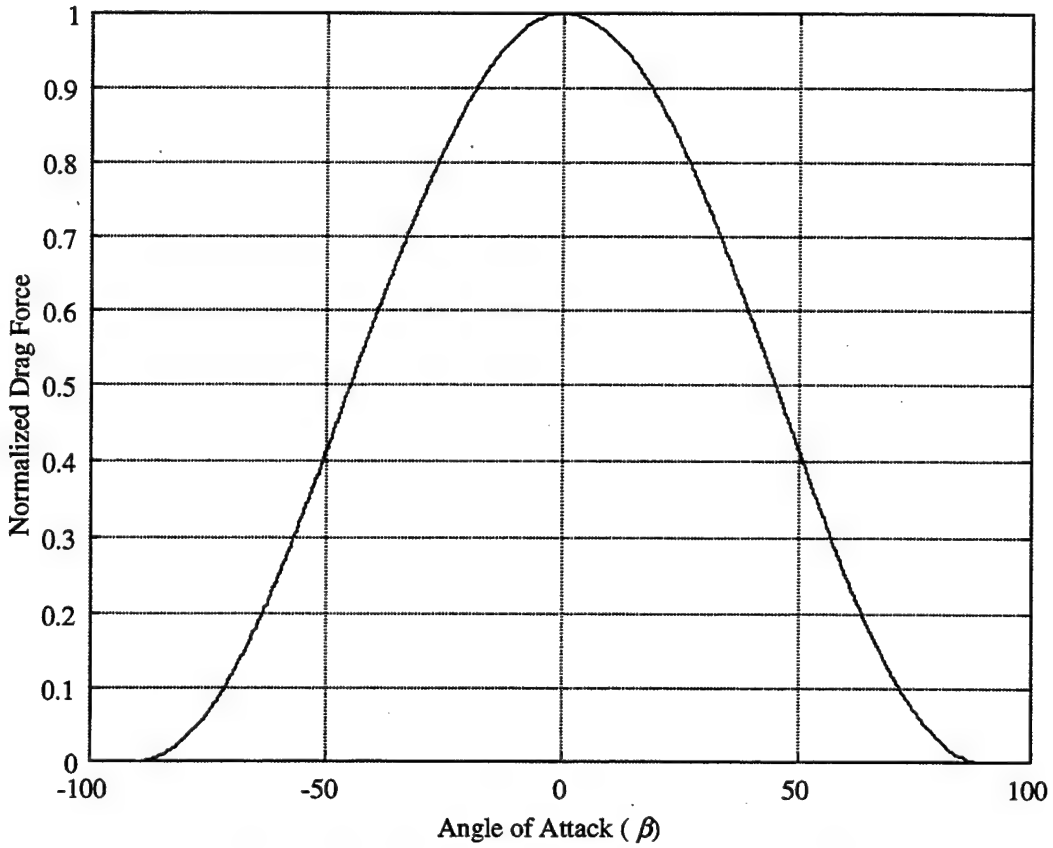

Figure 2.5 Normalized Drag Force vs. Angle of Attack

where $u_{control}$ is an input vector and $B(x_r, u_{control})$ is a state dependent input matrix. This input matrix contains the necessary coefficients to model the forces developed by the control actuators. The total force/moment vector f_C, is the sum of the propulsion force vector, f_p, due to thrusters and propellers, and the actuator force vector, f_δ, due to fin and rudder deflection.

1. Propulsion Forces

The derivation of a steady-state hydrodynamic model for propellers operating in an incompressible fluid can be found in many introductory fluid texts see [Lewis 1988, Newman 1977 and White 1986] for examples. These models are based on large open propellers. The use of small thrusters for control of underwater vehicles is an area of current research. This is because the vehicles are small, require fast response and are required to conduct dynamic positioning maneuvers. [Yoeger 1991] developed a lumped

parameter model that improved on the popular notion that for a given unit the thrust and input torque are related to the square of the propeller rotational rate and the angle of advance. He also showed that by accounting for thruster dynamics, improvements in position control could be obtained. Yoeger's work introduced the concept that fluid momentum considerations resulted in a time lag in the thrust response to a step input. Although his work improved the modeling of thrusters, it left room for significant improvements.

[Healey et al., 1995], improved on Yoeger's work by providing a generic thruster model that considered propeller thrust and torque as a mapping linked to lift/drag force variations caused by changes in the local angle of attack of the propeller blade. They also were able to associate the lags and overshoots in the thrust response to lags in the development of the local angle of attack and dynamic development of the blade pressure distributions. Research by [Whitcomb 1995] and [Bachmayer 1998] has provided further experimental validation that the four-quadrant model proposed by Healey is valid for small ducted thrusters.

The model proposed by the researchers in the above paragraph can be best expressed as a first order differential equation of the form

$$\dot{F} = \frac{-1}{\tau} F + \frac{\gamma}{\tau} u_r |n| + \frac{\beta}{\tau} n|n|, \tag{2.76}$$

where F is the propulsive force imparted to the vehicle. The parameter τ is the time constant associated with the force lag, the second term containing γ, is a thrust reduction cause by the change in local angle of attack as the propeller advances through the water and the last term containing β, is the thrust to rotation rate mapping. In standard propeller design terms, the parameter γ can be related to J, while β can be related to K_T.

Referring to Figure 2.6, it can be seen that the thrust coefficient K_T is a function of the propeller speed of advance J. The value of the non-dimensional thrust coefficient at a zero speed of advance is associated with the bollard pull condition. This relates the thrust to the rotational rate of the propeller as

$$T = K_T \rho D^4 n|n|, \tag{2.77}$$

where D is the diameter of the propeller and n is the rotational rate.

For any other operating condition, it can be seen that the thrust coefficient is reduced as the propeller moves through the fluid with some speed of advance. The thrust for this operating condition is given by

$$T = K_T \rho D^4 n|n| + \gamma_o J \rho D^4 n|n|, \tag{2.78}$$

where γ_o is the slope of the K_T curve at the particular operating condition of interest (negative over the entire curve), and J is the non-dimensional speed of advance. Substituting the expression for J, shown in Figure 2.6, the parameters β and γ from Equation 2.76 can be related to the parameters in Equation 2.78 as

$$\begin{aligned} \beta &= K_T \rho D^4 \\ \gamma &= \gamma_o \rho D^3 \end{aligned} \tag{2.79}$$

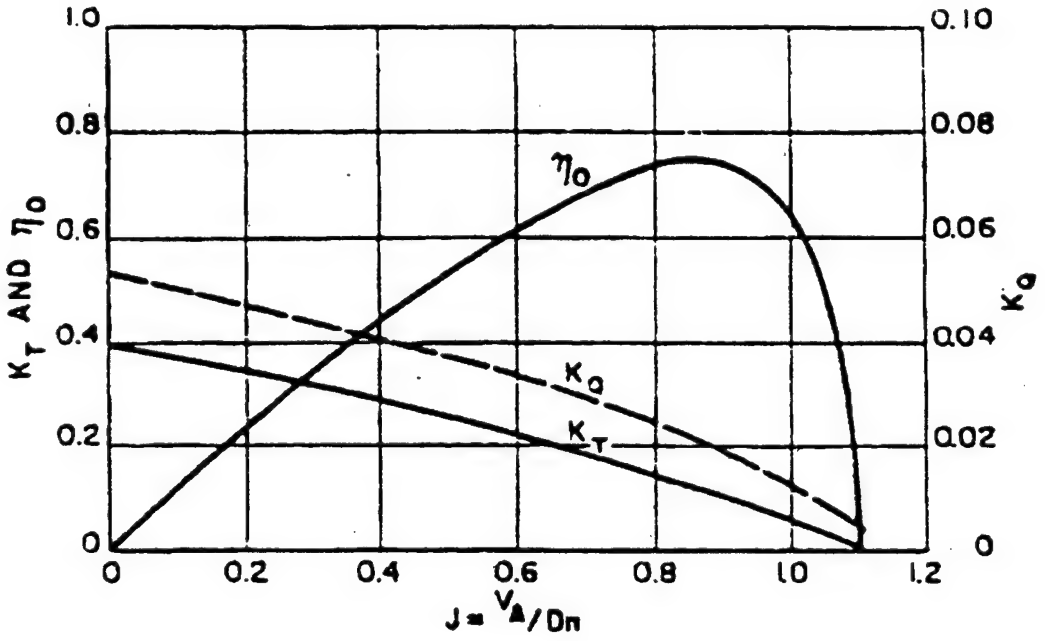

Figure 2.6 Thrust and Torque Coefficients versus Angle of Attack [Lewis 1988]

The force/moment vector caused by the propulsion forces due to the set of thrusters and main propellers for the NPS Phoenix AUV is,

$$f_p = \begin{bmatrix} F_{ls} + F_{rs} \\ F_{blt} + F_{slt} \\ F_{bvt} + F_{svt} \\ 0 \\ -x_{bvt}F_{bvt} + x_{svt}F_{svt} \\ x_{blt}F_{blt} - x_{slt}F_{slt} + y_{ls}F_{ls} - y_{rs}F_{rs} \end{bmatrix}, \tag{2.80}$$

where the x and y distances are all positive values measured from their respective plane of origin.

2. Actuator Forces

Control of a small AUV at anything other than slow speed must be accomplished by using control surfaces since the effect of non-propulsion thrusters decreases as the forward speed of the vehicle increases. These control surfaces are comprised of fins/planes and rudders. The forces and moments exerted by these actuators are derived from airfoil theory and are composed of lift and drag components. With the exception of the longitudinal direction, the force/moment applied to the vehicle is directly proportional to the amount of angular deflection of the control surface. In the longitudinal direction the force exerted by a deflection of a surface amounts to an additional drag force on the vehicle. The vector of forces and moments caused by these surfaces is

$$f_\delta = \begin{bmatrix} [(X_{q\delta_{sp}}\delta_{sp} + X_{q\delta_{bp}}\delta_{bp})uq + (X_{r\delta_{br}}\delta_{br} + X_{r\delta_{sr}}\delta_{sr})ur + X_{v\delta_s}\delta_s uv + \dots \\ (X_{w\delta_s}\delta_s + X_{w\delta_b}\delta_b)uw + (X_{\delta_r\delta_r}(\delta_{sr}^2 + \delta_{br}^2) + X_{\delta_{sp}\delta_{sp}}\delta_{sp}^2 + X_{\delta_{bp}\delta_{bp}}\delta_{bp}^2)u|u|] \\ (Y_{\delta_{sr}}\delta_{sr} + Y_{\delta_{br}}\delta_{br})u|u| \\ (Z_{\delta_{sp}}\delta_{sp} + Z_{\delta_{bp}}\delta_{bp})u|u| \\ 0 \\ (M_{\delta_{sp}}\delta_{sp} + M_{\delta_{bp}}\delta_{bp})u|u| \\ (N_{\delta_{sr}}\delta_{sr} + N_{\delta_{br}}\delta_{br})u|u| \end{bmatrix}. \tag{2.81}$$

The modeling represented in Equation 2.81 is for a vehicle equipped with a standard fin arrangement. By this it is meant that each pair of control surfaces, stern planes, bow planes or rudders, move together and are not independently controlled. If the vehicle is equipped with either an X-brace configuration[Humphreys 1994], or the actuators in a standard configuration are allowed to be moved independently, then the

modeling of these control forces will change. Specifically, there will be the ability to actively control roll and there will be some level of redundancy for each of the other control modes. For a detailed description of the origin of these control forces, the reader is referred to [Hoerner 1965, Hoerner 1975 and Lewis 1988].

H. 6DOF EQUATIONS OF MOTION

1. No Fluid Motion

Using Equation 2.29, and substituting the external forces discussed in the previous sections, the 6DOF EOM can be written as

$$\boldsymbol{M}_{RB}\dot{\boldsymbol{x}}+\boldsymbol{C}_{RB}(\boldsymbol{x})\boldsymbol{x}=\boldsymbol{f}_G+\boldsymbol{f}_{AM}+\boldsymbol{f}_d+\boldsymbol{f}_{FK}+\boldsymbol{f}_v+\boldsymbol{f}_L+\boldsymbol{f}_C. \tag{2.82}$$

Expanding Equation 2.82 by substituting the appropriate expressions for the force/moment vectors, and recognizing that without fluid motion $\boldsymbol{x} = \boldsymbol{x}_r$ and $\boldsymbol{u}_f = \boldsymbol{0}$, the following equation is obtained

$$\begin{aligned}&\boldsymbol{M}_{RB}\dot{\boldsymbol{x}}+\boldsymbol{C}_{RB}(\boldsymbol{x})\boldsymbol{x}+\boldsymbol{F}(z)+\boldsymbol{M}_{AM}\dot{\boldsymbol{x}}+\boldsymbol{C}_{Am}(\boldsymbol{x})\boldsymbol{x}+\\&\boldsymbol{D}_d\boldsymbol{x}+\boldsymbol{D}_l\boldsymbol{x}+\boldsymbol{D}_q(\boldsymbol{x})+\boldsymbol{D}_L(\boldsymbol{x})\boldsymbol{x}=\boldsymbol{B}(\boldsymbol{x},\boldsymbol{u}_{control})\boldsymbol{u}_{control}\end{aligned}. \tag{2.83}$$

As seen, Equation 2.83 contains a mixture of coordinates; both body fixed and global. To use a system of equations expressed in this form for simulation studies or control system development, this system must be augmented with the relationships between the various coordinate frames. The link between the global and body fixed coordinates is accomplished by augmenting Equation 2.83 with equations 2.8 and 2.11. This system is represented by

$$\begin{aligned}&[\boldsymbol{M}_{RB}+\boldsymbol{M}_{AM}]\dot{\boldsymbol{x}}+[\boldsymbol{C}_{RB}(\boldsymbol{x})+\boldsymbol{C}_{Am}(\boldsymbol{x})]\boldsymbol{x}+\\&[\boldsymbol{D}_d+\boldsymbol{D}_l+\boldsymbol{D}_L(\boldsymbol{x})]\boldsymbol{x}+\boldsymbol{D}_q(\boldsymbol{x})+\boldsymbol{F}(z)=\boldsymbol{B}(\boldsymbol{x},\boldsymbol{u}_{control})\boldsymbol{u}_{control}\\&\dot{z}=\boldsymbol{g}(\boldsymbol{x},z)\end{aligned} \tag{2.84}$$

2. Modifications To Account For Fluid Motion

In the case where fluid motion is present, Equation 2.83 is represented as

$$\begin{aligned}&\boldsymbol{M}_{RB}\dot{\boldsymbol{x}}+\boldsymbol{C}_{RB}(\boldsymbol{x})\boldsymbol{x}+\boldsymbol{F}(z)+\boldsymbol{M}_{AM}\dot{\boldsymbol{x}}_r+\boldsymbol{C}_{Am}(\boldsymbol{x}_r)\boldsymbol{x}_r+\boldsymbol{D}_d\boldsymbol{x}_r\\&-\boldsymbol{M}_{FK}\dot{\boldsymbol{u}}_f+\boldsymbol{D}_l\boldsymbol{x}_r+\boldsymbol{D}_q(\boldsymbol{x}_r)+\boldsymbol{D}_L(\boldsymbol{x}_r)\boldsymbol{x}_r=\boldsymbol{B}(\boldsymbol{x}_r,\boldsymbol{u}_{control})\boldsymbol{u}_{control}\end{aligned}. \tag{2.85}$$

This equation, as was Equation 2.83, is a mixture of various coordinate frame variables; body fixed, body fixed relative, global and fluid. To solve this system of equations, the equations must be expressed in variables that can be related to each other. Since, for this case, the vehicle is considered to be in an unsteady fluid referenced to the global frame (refer to Figure 2.1), the logical choice for variables is body fixed relative x_r, and global, z.

Remembering that relative velocity is defined as $x_r = x - u_f$, and that the body fixed fluid velocity can be expressed as

$$u_f = \begin{bmatrix} T_1 & 0 \\ 0 & T_2 \end{bmatrix} U_f = TU_f, \tag{2.86}$$

Equation 2.85 can be modified so that it is expressed in body fixed relative and global variables. Manipulating Equation 2.85 results in

$$\begin{aligned} &[M_{RB} + M_{AM}]\dot{x}_r + [C_{RB}(x_r) + C_{Am}(x_r)]x_r + [D_d + D_v(x_r) + D_L(x_r)]x_r + F(z) \\ &= -M_{RB}\frac{d(TU_f)}{dt} - C_{RB}(u_f)TU_f + M_{FK}\frac{d(TU_f)}{dt} + B(x_r, u_{control})u_{control} \end{aligned} \tag{2.87}$$

Looking at Equation 2.87 and recalling that the fluid was defined as irrotational, it can be seen that the $C_{RB}(u_f)$ term on the right hand side of the equation is zero. The other two terms, on the right hand side, containing the rigid body mass matrix M_{RB}, and the Froude-Kriloff mass matrix M_{FK}, are excitation forces resulting from the fluid motion.

As seen in Equation 2.87, the Froude-Kriloff excitation forces and moments are functions of the weight and buoyancy mismatch (*W-B*), the fluid velocities and fluid accelerations, expressed in body fixed values. For a neutrally buoyant vehicle, where *W=B*, the wave excitation forces do not present themselves in the translational equations of motion, however, they still provide excitation moments to the rotational equations. The reason behind this is because the fluid components (acceleration and velocity) act at the vehicle center of buoyancy, while the body inertial acceleration reaction force acts at the vehicle's center of mass.

At this point the 6DOF EOM representing the vehicle dynamics has been modified to account for a moving fluid by representing the body fixed velocities in

relative terms, Equation 2.87. However, as with the system of equations for the case of no fluid motion, the system in Equation 2.87 must be augmented to provide the necessary link between the global and body fixed velocities. In order to account for the fluid motion, either wave induced or steady current, Equation 2.8 is modified and is represented as

$$\begin{bmatrix} \dot{X} \\ \dot{Y} \\ \dot{Z} \end{bmatrix} = \boldsymbol{T}_1^{-1}(\phi,\theta,\psi) \begin{bmatrix} u_r \\ v_r \\ w_r \end{bmatrix} + \begin{bmatrix} U_f \\ V_f \\ W_f \end{bmatrix}, \tag{2.88}$$

where the fluid velocity is represented in the global frame. Combining equations 2.87, 2.88 and 2.11 into a system of equations results in the necessary equations to describe the motion of a small underwater vehicle subject to shallow water waves.

It was shown earlier in this chapter that the total time derivative is composed of a rate of growth term and a rate of transport term. In the case of the time derivative of the rotation transformation matrix $\boldsymbol{T}$, since there is no translation, the time derivative can be expressed solely as $\boldsymbol{\omega}\times\boldsymbol{T}$. [Healey 1992a] and [Fossen 1994] have shown that the cross-product operation ($\boldsymbol{\omega}\times$), can be represented as a matrix by defining the screw symmetric matrix,

$$\boldsymbol{S}(\boldsymbol{\omega}) = \begin{bmatrix} 0 & -r & q \\ r & 0 & -p \\ -q & p & 0 \end{bmatrix}. \tag{2.89}$$

The elements of $\boldsymbol{S}(\boldsymbol{\omega})$ are based on the consideration that both vector-matrix quantities in the cross-product operation are represented in the same coordinate frame. In the case where $\boldsymbol{T}$ is the transformation matrix from global to body fixed coordinates, the expression for the rotation matrix time derivative is

$$\dot{\boldsymbol{T}} = \begin{bmatrix} \boldsymbol{S}^T(\boldsymbol{\omega})\boldsymbol{T}_1 & \boldsymbol{0} \\ \boldsymbol{0} & \dot{\boldsymbol{T}}_2 \end{bmatrix}. \tag{2.90}$$

$\boldsymbol{S}^T(\boldsymbol{\omega})$ is the transpose of the matrix represented in Equation 2.89 since $\boldsymbol{T}$ is not in the same coordinate frame as $\boldsymbol{\omega}$. Using Equation 2.90, and the fact that the coriolis matrix, $\boldsymbol{C}_{RB}(\boldsymbol{u}_f)$, is null, the vehicle dynamics equations expressed in matrix form are

$$[M_{RB} + M_{AM}]\dot{x}_r + [C_{RB}(x_r) + C_{Am}(x_r)]x_r + [D_d + D_v(x_r) + D_L(x_r)]x_r + F(z)$$
$$= [M_{FK} - M_{RB}][\dot{T}U_f + T\dot{U}_f] + B(x_r, u_{control})u_{control} \tag{2.91}$$

The complete expanded 6DOF EOM, including physical parameters for the NPS Phoenix AUV, are outlined in Appendix A.

I. DEVELOPMENT OF LONGITUDINAL SURGE MODEL

Restricting the motion of the vehicle to surge only, the significant motions/quantities that must be incorporated to effectively model the vehicle in the longitudinal direction are, the surge velocity u_r, and the global position X. This restriction simplifies the twelve previously developed equations to a system of two non-linear equations of motion. Based on the NPS PHOENIX AUV equations of motion, see Appendix A, this reduced set which models longitudinal surge motion is,

$$\begin{aligned}(m - X_{\dot{u}})\dot{u}_r + X_{u|u|}u_r|u_r| + \left(\frac{W-B}{g}\right)\dot{U}_f &= F_{prop} \\ \dot{X} &= u_r + U_f\end{aligned} \tag{2.92}$$

This set of equations, with a slight modification, is also valid for modeling relative motion. By representing all variables in body fixed quantities, the set of equations for relative positioning is,

$$\begin{aligned}(m - X_{\dot{u}})\dot{u}_r + X_{u|u|}u_r|u_r| + \left(\frac{W-B}{g}\right)\dot{u}_f &= F_{prop}, \\ \dot{x} &= u_r + u_f\end{aligned} \tag{2.93}$$

where the position x, is measured relative to the vehicle fixed frame.

The purpose of this longitudinal surge model is to allow for the development of a surge controller that will allow a vehicle to hold position in the presence of waves. To complete this model, the propulsion system dynamics must be included. Therefore, the system given in Equation 2.93 must be augmented with Equation 2.76. Augmenting Equation 2.93 with the propeller force equation, and assuming a neutrally buoyant vehicle, the set of equations to be used as the basis of the longitudinal surge controller becomes,

$$\begin{aligned} \dot{x} &= u_r + u_f \\ \dot{u}_r &= \alpha u_r |u_r| + F \\ \dot{F} &= \frac{-1}{\tau} F + \frac{\gamma}{\tau} u_r |n| + \frac{\beta}{\tau} n|n| \end{aligned} \quad , \tag{2.94}$$

where the parameters α, β, γ and τ must be determined through system identification. The process by which these parameters are determined will be presented in Chapter IV. Note, it should be pointed out, that in the form used in Equation 2.94, F becomes a generalized force with units the same as an acceleration rather than a direct thrust value.

J. SUMMARY

This chapter has presented the kinematic and dynamic relationships used in modeling a small underwater vehicle operating in a shallow water wave environment. It discussed the various external forces and moments that act on an AUV. The chapter concluded with the development of the one degree of freedom (1DOF) surge model that will be used as basis for a controller that will allow an AUV to station-keep in the presence of waves.

III. DISTURBANCE ANALYSIS

A. INTRODUCTION

In general, the disturbances that act on an underwater vehicle can be placed in three categories and described as follows:

- Additive disturbances are external forces and moments which act additively on the vehicle. By including their effects, the total description of the vehicle model is extended by additional states (e.g., current, waves, and wind).
- Multiplicative disturbances affect the dynamics of the system (e.g., the depth of the water, load conditions, trim, and speed changes). These disturbances can be regarded as time variant.
- Measurement disturbances are due to incorrect measurements (e.g., noise on the vehicle's sensors).

For this dissertation, only the additive disturbances will be taken into account. From the class of disturbances causing additive effects on an underwater vehicle in shallow water, only waves and current will be considered since they are most dominant. The ability to control a vehicle is known to be significantly affected by its environment. Since the modeling of external disturbances, especially waves, is rather complicated, many attempts to design control systems have suffered.

A general assumption that is used in the modeling of AUVs is that forces and moments, which are added to the "calm sea" model, can model environmental induced disturbances. This procedure was outlined in the previous chapter. This method, using the principle of superposition, is a good approximation for most marine control applications; however, it should be noted that for large general maneuvers it is not expected to be valid.

This chapter will begin with a discussion of the stochastic nature of sea waves, including a description of several empirical relationships that can be used to represent the spectral content of a wave field. This will be followed by an overview of state space representations and recursive modeling of wave disturbances with specific application to control design. Finally, a methodology for the use of empirically derived spectral

relationships as well as measured wave elevation time series in distributed simulations will be outlined.

B. STATISTICAL DESCRIPTION OF SEA WAVES

The proper characterization of the real sea surface is difficult to obtain. With respect to the design of a control system, it is sufficient to assume a simplified description of the sea by considering only unidirectional linear waves. Based on this assumption, and on the superposition principle, simplified models can be determined. Concerning the modeling of waves, there exist two typical approaches: regular waves and irregular waves.

Regular waves can be represented as a simple two-dimensional, sinusoidal wave train over an infinite water surface with infinite depth. This interpretation is based on the empirical observation, that the motions generated by waves have strong periodic components, see [Kallstrom 1979] for details. The characterization of the sea level as a train of regular waves, is however, an approximation, which is not necessarily accurate.

Irregular waves allow the stochastic nature of waves to be taken into account. According to this method, the sea level can be modeled as either a superposition of a large number of regular waves of different amplitudes, frequencies, phase angles and directions of propagation, or as a narrow band stochastic process. In the case where the sea level is regarded as a stochastic process, the spectral and probability density description should be available, thus the model for the variation of the wave elevation can be determined from its spectral density function. The irregular waves are considered probabilistically with respect to amplitude and wavelength. Since the origin of waves is usually due mainly to the wind, the frequency and the steady state amplitude of the waves depend on the mean value of the wind speed. In this and the following sections, the stochastic characteristics of waves are considered.

The wave elevation of a long-crested irregular sea propagating in the positive x-direction can be written as the sum of a large number of wave components represented by,

$$\eta(x,t) = \sum_{i=1}^{N} A_i \sin(k_i x - \omega_i t + \phi_i) \tag{3.1}$$

where, A_i is the wave amplitude, ω_i is the wave frequency, ϕ_i is a random phase angle and

$$k_i = \frac{2\pi}{L_i} \tag{3.2}$$

is the wave number, with L_i as the wavelength. The wave amplitude can be expressed as a wave spectrum $S(\omega)$, by

$$A_i^2 = 2S(\omega_i)\Delta\omega \tag{3.3}$$

where, $\Delta\omega$ is a constant difference between successive frequencies. The instantaneous wave elevation has a Gaussian distribution with a zero-mean and a variance σ^2 defined as

$$\sigma^2 = \int_0^\infty S(\omega)d\omega . \tag{3.4}$$

1. Wave Spectral Densities

Several formulations of wave spectral densities have been proposed. The four spectra commonly encountered in practice are:

- The Amplitude Spectrum. In this spectrum, the ordinates of the spectral density are proportional to the amplitude squared of the component waves. The area under the spectrum curve, S_A, is proportional to twice the average energy of the record.

- The Energy Spectrum. The ordinates of the spectral density are proportional to half the amplitude squared of the component waves. The area under the spectrum curve, S_E, is proportional to the average energy of the record and equals $S_A/2$.

- The Height Spectrum. The ordinates of the spectral density are proportional to the height squared of the component waves. The area under the spectrum curve, S_H, equals $4S_A$.

- The Double Height Spectrum. The ordinates of the spectral density are proportional to twice the height squared of the component waves. The area under the spectrum curve, S_{2H}, is therefore equal to $8S_A$.

Graphical representations of these spectra are shown schematically in Figure 3.1.

2. Statistical Description of Wave Amplitudes

The probability density function of wave amplitudes with a narrow band spectrum can be expressed by the Rayleigh distribution,

$$p(r) = \frac{2r}{\bar{r}^2} e^{-r^2/\bar{r}^2} \tag{3.5}$$

where $p(r)dr$ is the probability that a wave amplitude (r) lies between r and $r+dr$, and $\bar{r}^2$ is the mean square value of the wave amplitudes in the record, [Longuet-Higgins 1953]. It has been shown through the use of histograms that actual wave amplitudes closely follow this theoretical distribution, therefore, with the use of Equation 3.5, some quantitative statistical results may be formed.

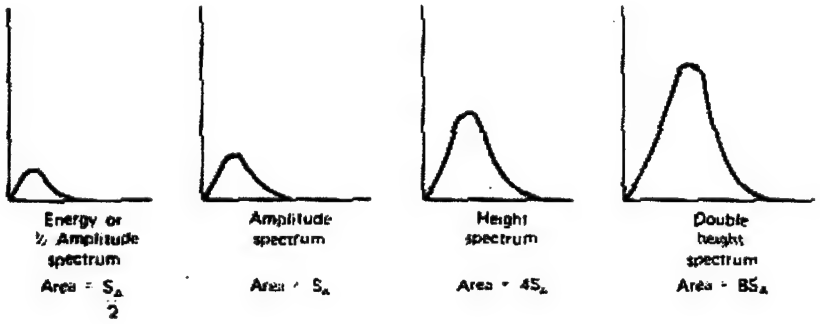

Figure 3.1 Wave Spectral Density Comparisons [Berteaux 1976]

a) Most Probable Wave Amplitude

The most probable wave amplitude is the value of r for which

$$\frac{d}{dr} p(r) = 0 . \tag{3.6}$$

Differentiating the probability density function, Equation 3.5, and equating it to zero as indicated in Equation 3.6, yields an expression for the most probable wave amplitude r_m, as

$$r_m = 0.707\sqrt{\bar{r}^2} \tag{3.7}$$

where $\sqrt{\bar{r}^2}$ is the root mean square value of the wave amplitudes in the record.

b) Mean Amplitude

The fraction f $(0 \le f \le 1)$ of wave amplitudes larger than a given amplitude r_o is represented by

$$f = \int_{r_o}^{\infty} p(r)dr . \tag{3.8}$$

The average of the f highest amplitudes can be found from the integration

$$\bar{r}_f = \frac{1}{f}\int_{r_o}^{\infty} rp(r)dr . \tag{3.9}$$

The mean amplitude of all the waves in the record is then obtained when $f = 1$ and $r_o = 0$ and is given by the first moment

$$\bar{r} = \int_{0}^{\infty} rp(r)dr . \tag{3.10}$$

Table 3.1 shows the integration results for several values of f.

Fraction of Largest Amplitudes Considered	Mean Values $(\bar{r}_f / \sqrt{\bar{r}^2})$
0.01	2.359
0.1	1.800
0.333	1.416
0.5	1.256
1.0	0.886

Table 3.1 Wave Amplitude Means

c) Maximum Expected Wave Amplitude

The expectation of the largest amplitude in a sample of N waves is found from the first moment of the probability distribution of the maximum amplitudes, r_{max}. Results obtained from this computation are summarized in Table 3.2.

3. Empirical Formulation of Sea Spectra

Several empirical formulas, based on the analysis of many wave records have been proposed to express the spectral density of the energy spectrum as a function of the wave frequency. The two most general cases use either wind speed, or significant wave height and significant wave period in the empirical formulas. The significant wave height and significant wave period, for most ocean engineering applications, is defined as the mean of the one-third highest waves and the mean of the wave periods associated with the one-third highest waves, respectively.

Number of Waves N	Maximum Wave Amplitudes $(r_{max}/\sqrt{\overline{r^2}})$
50	2.12
100	2.28
500	2.61
1,000	2.78
10,000	3.13
100,000	3.47

Table 3.2 Expected Maximum Amplitudes [Longuet-Higgins 1953]

In the first case, the spectral density $S(\omega)$ is of the form

$$S(\omega) = \frac{A}{\omega^5} e^{-(B/V^4\omega^4)}, \tag{3.5}$$

where A and B are empirical constants, and V is the speed of the wind.

In the second case $S(\omega)$ is given by

$$S(\omega) = \frac{AH_s^2}{T_s^4\omega^5} e^{-(B/T_s^4\omega^4)}, \tag{3.6}$$

where A and B are again empirical constants, T_s is the significant period and H_s the significant wave height. Table 3.3 presents a useful compilation of wave heights and

wave periods as a function of sea states and wind speed that may be used in the following formulas.

Sea State	Wind Velocity (kts)	Wave Height (feet)			Wave Period (sec)		
		Average	Significant	$H_{1/10}$	T_z	T_{max}	$T_{1/3}$
0	0	0	0	0	-	-	-
	2	0.05	0.08	0.10	≤ 1.2	0.7	0.5
1	5	0.18	0.29	0.37	0.4-2.8	2.0	1.4
	8.5	0.6	1.0	1.2	0.8-5.0	3.4	2.4
2	10	0.88	1.4	1.8	1.0-6.0	4	2.9
	12	1.4	2.2	2.8	1.0-7.0	4.8	3.4
	13.5	1.8	2.9	3.7	1.4-7.6	5.4	3.9
3	14	2.0	3.3	4.2	1.5-7.8	5.6	4.0
	16	2.9	4.6	5.8	2.0-8.8	6.5	4.6
4	18	3.8	6.1	7.8	2.5-10.0	7.2	5.1
	19	4.3	6.9	8.7	2.8-10.6	7.7	5.4
5	20	5.0	8.0	10	3.0-11.1	8.1	5.7
	22	6.4	10	13	3.4-12.2	8.9	6.3
	24	7.9	12	16	3.7-13.5	9.7	6.8
6	24.5	8.2	13	17	3.8-13.6	9.9	7.0
	26	9.6	15	20	4.0-14.5	10.5	7.4
	28	11	18	23	4.5-15.5	11.3	7.9

Table 3.3 Sea State and Wave Parameter Comparison [Berteaux 1976]

a) Pierson-Moskowitz (PM) Formula

A frequently used one parameter description of $S(\omega)$ for a fully developed sea, resulting from extended wind with unlimited fetch, is the PM spectrum. Using

Equation 3.5 as a basis, the single parameter used to describe the spectrum is the wind velocity V, with the empirical constants A and B having the values $0.0081g^2$ and $0.74g^4$, respectively. The units associated with the gravitational constant g, and the wind velocity V must be the same for dimensional consistency.

b) International Towing Tank Conference (ITTC) Formula

Using statistical properties the relationship between the one-third significant wave height, $H_{1/3}$, and the wind speed, V, for the PM spectrum is

$$H_{1/3} = 0.2092\frac{V^2}{g}, \tag{3.7}$$

therefore, the formula for the PM spectrum with the significant wave height as the single parameter is

$$S(\omega) = \frac{A}{\omega^5} e^{-(B/H_{1/3}^2\omega^4)}. \tag{3.8}$$

In this form, the empirical constants A and B have the values $0.0081g^{\,2}$ and $0.0324g^{\,2}$, and the resulting one-parameter expression that uses significant wave height is referred to as the ITTC formula.

Since this one-parameter formula describes a fully developed sea resulting from conditions that are rarely encountered (extended wind with unlimited fetch), the PM spectrum should be viewed as an asymptotic form. To overcome the limitations associated with the one-parameter spectral family, a two-parameter family, given by Equation 3.6, can be used.

c) Bretschneider Formula

The Bretschneider spectrum is a general form, and represents experimental data very well. The formula for the Bretschneider spectrum is

$$S(\omega) = \frac{4200H_s^2}{T_s^4\omega^5} e^{-1050/(T_s^4\omega^4)}, \tag{3.9}$$

where H_s and T_s are the significant wave height and significant wave period, respectively. This expression can be used to represent developing, fully developed and decaying seas depending on the value of T_s chosen, [Lewis 1989].

d) International Ship Structure Congress (ISSC) Formula

The ISSC spectrum is similar in form to the Bretschneider spectrum, with the exception that it is based on a mean frequency corresponding to the spectrum's center of area. This spectrum is represented by

$$S(\omega) = \frac{171 H_s^2}{\overline{T}^4 \omega^5} e^{-686/(\overline{T}^4 \omega^4)}, \tag{3.10}$$

where H_s and $\overline{T}$ are the significant wave height and mean wave period, respectively. A comparison of the ITTC, ISSC and Bretschneider spectrum for a sea state 3 condition is shown in Figure 3.2.

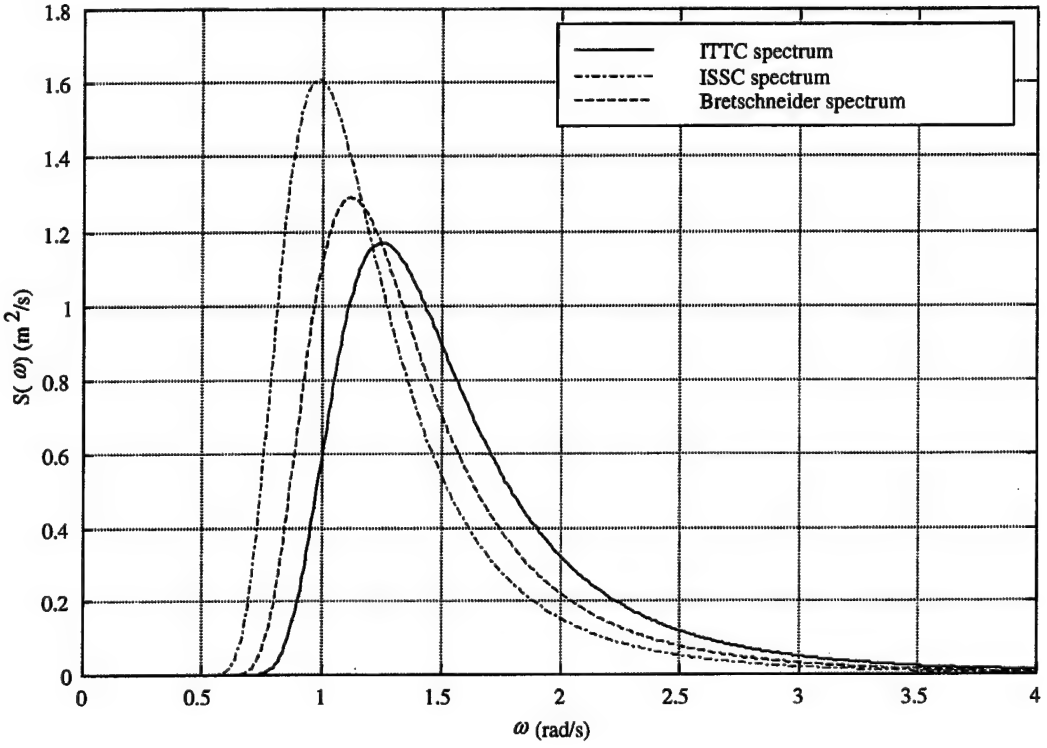

Figure 3.2 Comparison of Empirical Spectra

e) Other Spectral Representations

There are many other empirical relationships that have been used to model spectral characteristics of the sea, where each model is useful for a given area or sea condition that has specific characteristics. Examples of these are the Joint North Sea

Wave Project (JONSWAP) spectrum [Hasselmann 1973], the Ochi Six-Parameter Wave spectrum [Ochi 1076], the Wallops spectrum [Huang 1981] and the Generalized spectrum [Liu 1983]. The Wallops spectrum and the Generalized spectrum with variable exponents are adaptable for both deep and shallow water applications.

It is common to use the recommended sea spectra from the ITTC and ISSC in ocean engineering design. For open sea conditions, the PM spectrum is recommended, and for fetch limited conditions either the Bretschneider, Ochi or JONSWAP spectrum is available.

C. LINEAR REPRESENTATION OF SEA WAVES

1. Spectral Approximations

To properly estimate and cancel the wave induced disturbances acting on an underwater vehicle, some type of disturbance model is necessary. The necessity arises from the need to either embed the disturbance model in the vehicle's controller, or to use the disturbance model in a state estimator. It is known that a linear, Gauss-Markov stochastic process may be generated by sending white noise through an appropriate transfer function, where white noise is to mean a random process whose power spectral density is constant over the whole spectrum. Therefore, a linear approximation to the spectral representations in the previous sections can be obtained by sending a random white-noise signal through a second order filter, [Spanos 1981]. This process can be written as

$$y(s) = h(s)q(s), \tag{3.11}$$

with the linear approximation to the desired spectrum represented as

$$\Phi_{yy}(\omega) = \left|h(j\omega)\right|^2 \Phi_{qq} = \left\|h(j\omega)\right\|^2. \tag{3.12}$$

In Equation 3.11, $y(s)$ is the wave amplitude, $q(s)$ is a white noise source with power spectrum

$$\Phi_{qq} = 1.0 \tag{3.13}$$

and $h(s)$ is a second order transfer function of the form

$$h(s) = \frac{2k(s/\omega_o)}{1+2\zeta(s/\omega_o)+(s/\omega_o)^2}. \tag{3.14}$$

Using equations 3.11-3.14 and substituting $s = j\omega$, the approximate power spectrum can be given by

$$\Phi_{yy}(\omega) = |h(j\omega)|^2 \Phi_{qq}(\omega) = \frac{4k^2(\omega/\omega_o)^2}{(1-(\omega/\omega_o)^2)^2 + 4\zeta^2(\omega/\omega_o)^2}. \tag{3.15}$$

The power spectrum of this filter, $\Phi_{yy}(\omega)$, has zero energy for zero frequency and the maximum value of $\Phi_{yy}(\omega)$ occurs at $\omega \approx \omega_o$ for small values of ζ. This is desirable considering the shapes of the spectra displayed in Figure 3.2. The parameters ζ and k in Equation 3.15, are found by minimizing the performance index

$$J = \int_0^\infty (\Phi_{yy}(j\omega) - S(\omega))^2 d\omega. \tag{3.16}$$

2. State Space Formulation

A linear state space model can be derived from equations 3.11 and 3.14. By defining the states as

$$\begin{aligned} x_1 &= \int_0^t y(\tau)d\tau \\ x_2 &= y \end{aligned}, \tag{3.17}$$

the system states can be represented by the set of equations

$$\begin{aligned} \begin{bmatrix} \dot{x}_1 \\ \dot{x}_2 \end{bmatrix} &= \begin{bmatrix} 0 & 1 \\ -\omega_o^2 & -2\zeta\omega_o \end{bmatrix} \begin{bmatrix} x_1 \\ x_2 \end{bmatrix} + \begin{bmatrix} 0 \\ 2k\omega_o \end{bmatrix} q \\ y &= \begin{bmatrix} 0 & 1 \end{bmatrix} \begin{bmatrix} x_1 \\ x_2 \end{bmatrix} \end{aligned}. \tag{3.18}$$

The transfer function in Equation 3.14, is useful for representing the sea surface elevation, but it cannot be used to generate the wave velocity. This is seen by taking the limit

$$\lim_{s\to\infty} sy(s), \tag{3.19}$$

as s tends to infinity. The result of this calculation is a constant, $2k\omega_o$, that cannot represent the oscillatory wave velocity. [Saelid 1983] has shown that using the proper transfer function

$$\frac{\dot{y}}{q} = \frac{2\zeta\sigma(s/\omega_o)s}{(1+2\zeta(s/\omega_o)+(s/\omega_o)^2)^2} \tag{3.20}$$

can solve this problem and [Riedel 1997] has demonstrated through the use of linear prediction theory that an eighth-order transfer function of the form

$$\frac{u_f}{q} = \left[\frac{2\zeta\sigma(s/\omega_o)s}{1+2\zeta(s/\omega_o)+(s/\omega_o)^2}\right]^4, \tag{3.21}$$

allows extremely accurate matching of the target spectrum enabling fluid velocity prediction as much as one period ahead.

Based on Equation 3.20, a generalized transfer function may be written in the form

$$\frac{u_f}{q} = \frac{ks^2}{(a+bs+s^2)^2} \tag{3.22}$$

which implies

$$(s^4+2bs^3+(2a+b^2)s^2+2abs+a^2)u_f(s) = kq(s). \tag{3.23}$$

[Astrom 1989] has shown that the parameters a, b and k, representing a PM spectrum based on sea state 3 conditions, can be found using Equation 3.16 to be $a = k = 1$ and $b = 2$. In this form, Equation 3.23 becomes an all-pole filter thus avoiding the problem of base period repetition of wave records, [Riedel 1997].

3. Spectral Modifications for a Moving Vehicle

The spectrum that the vehicle "sees" while moving through a wave field with some forward velocity is not the same as that which a still vehicle would encounter. The actual spectrum that the vehicle encounters is a function of the vehicle's forward speed U and its heading angle relative to the propagation direction of the sea waves, β. The definition of the encounter angle β is given by

$$\beta = \pi - (\gamma - \psi), \tag{3.24}$$

where γ is the direction from which the waves are propagating referenced to the inertial reference frame, and ψ is the heading angle of the vehicle [Lewis 1988b], see Figure 3.3. The frequency modification that must occur to the disturbance spectrum is represented by

the Doppler equation, (Equation 2.56), given in the previous chapter. The Doppler equation, in an alternate more useful form is

$$\omega_e \approx \omega - \frac{\omega^2}{g} U \cos\beta . \tag{3.25}$$

Depending on the encounter angle, specific terms have been given to the orientation of the sea with reference to the vehicle, this is shown in Figure 3.4. As an example, consider the case where the encounter angle is zero, namely the vehicle is moving in the direction of wave propagation, this is referred to as a "following sea". In this case, as equation 3.25 indicates, the frequency of encounter, ω_e, is less than the actual wave frequency. For this case, it is interesting to note that the encounter frequency can be negative for large values of forward velocity U.

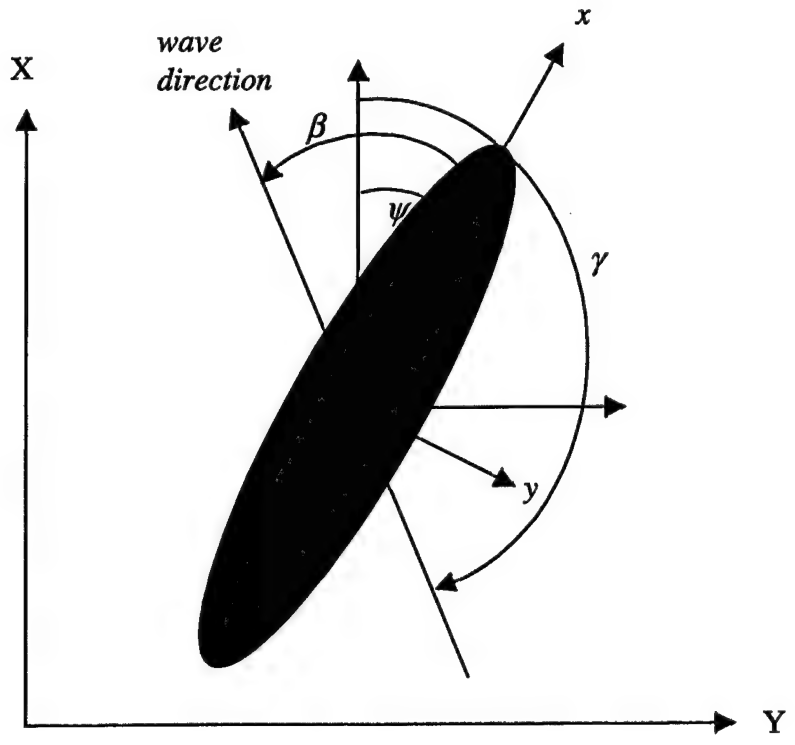

Figure 3.3 Incident Wave Directions

The methods for spectral approximation and state space realization of sea waves presented in this section are useful in simulation studies when the target spectrum is known, including the frequency shift. However, if the target spectrum is not known,

which is typically the case with a deployed vehicle, alternate techniques must be used. The following section presents one such technique which will allow a vehicle to estimate the encounter spectrum on-line.

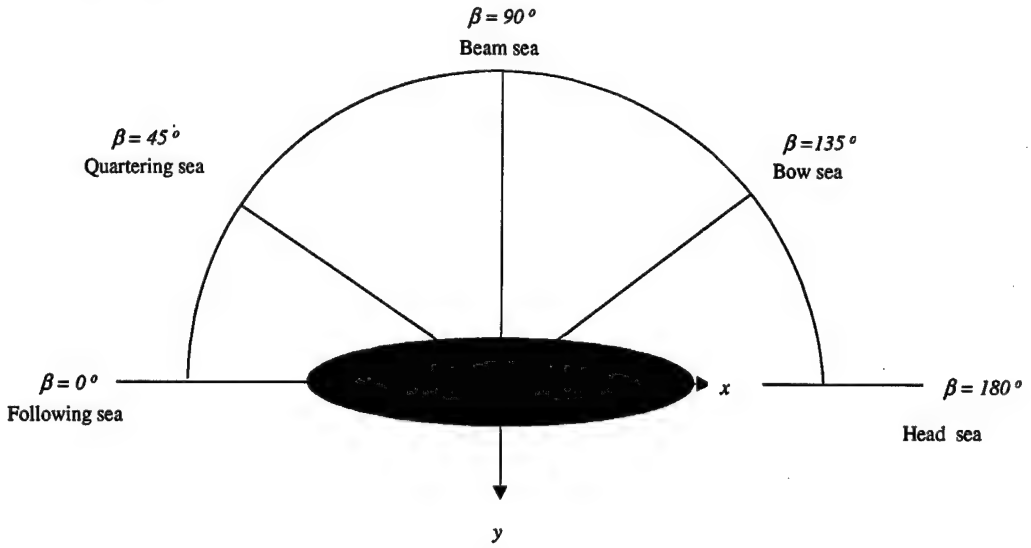

Figure 3.4 Encounter Angle

D. WAVE MODELING USING RECURSIVE METHODS

A typical experiment in system identification consists in recording a set of input/output data and fitting a parametric model. In discrete time, the attempt is to fit a Linear Difference Equation (LDE) model of the form

$$y(t) + a_1 y(t-1) + \ldots + a_n y(t-n) = b_1 u(t-1) + \ldots + b_n u(t-n) + \varepsilon(t), \qquad (3.26)$$

with $t : [0, \infty]$ denoting the integer discrete time index, and $\varepsilon(t)$ an error term which accounts for the fact that the data never matches the model exactly. The problem is to estimate the parameter vector

$$\theta = [a_1, \ldots, a_n, b_1, \ldots, b_n]^T \qquad (3.27)$$

from a set of data. This section will present the general procedure to estimate the parameters associated with a discrete linear model.

Equation 3.26 may be written in regression form as

$$y(t) = \phi(t-1)^T \theta + \varepsilon(t) \qquad (3.28)$$

with

$$\phi(t-1) = [-y(t-1),\ldots,-y(t-n),u(t-1),\ldots,u(t-n)]^T \qquad (3.29)$$

being a sliding window of input and output data. Now the problem is to determine a technique to compute an estimate of the parameter vector θ on the basis of the data set $Z = \{u(0),\ldots,u(N),y(0),\ldots,y(N)\}$, if it is assumed that N data points are collected.

If the problem is cast in a probabilistic framework, a probability density for the data set Z given the model θ can be written as

$$P(Z|\theta) = \Pr(\varepsilon(0),\ldots,\varepsilon(N)) \qquad (3.30)$$

with $\varepsilon(t) = y(t) - \phi^T(t-1)\theta$. If we assume the disturbance term sequence to be Gaussian and white, then the density on the right hand side becomes

$$\Pr(\varepsilon(0),\ldots,\varepsilon(N)) = \prod_{t=0}^{N} \Pr(\varepsilon(t)) \qquad (3.31)$$

with

$$\Pr(\varepsilon) = \frac{1}{2\pi\sigma} e^{-\frac{\varepsilon^2}{2\sigma^2}}. \qquad (3.32)$$

As a consequence it can be seen that

$$\Pr(Z|\theta) = Ce^{-\frac{1}{2\sigma^2}\sum\left|y(t)-\phi^T(t-1)\theta\right|^2}. \qquad (3.33)$$

Minimizing the summation in the exponential can maximize this probability. So if the estimate of the parameters is defined as the vector that minimizes the probability, as

$$\hat{\theta} = \arg\min_{\theta} \Pr(Z|\theta) \qquad (3.34)$$

then it can be computed as a least squares solution

$$\hat{\theta} = \arg\min_{\theta} \sum_{t=1}^{M} \left|y(t) - \phi^T(t)\theta\right|^2. \qquad (3.35)$$

The solution can be obtained using standard techniques, by writing $\hat{\theta}$ as the least squares solution of the system of equations

$$\begin{bmatrix} y(1) \\ y(2) \\ \vdots \\ y(M) \end{bmatrix} = \begin{bmatrix} \phi(1)^T \\ \phi(2)^T \\ \vdots \\ \phi(M)^T \end{bmatrix} \theta \tag{3.36}$$

or, compactly

$$y = \Phi\theta . \tag{3.37}$$

The solution given by the pseudoinverse becomes

$$\hat{\theta} = (\Phi^T\Phi)^{-1}\Phi^T y \tag{3.38}$$

which can be written as

$$\hat{\theta} = \left[\frac{1}{M}\sum_{t=1}^{M}\phi(t)\phi(t)^T\right]^{-1}\left[\frac{1}{M}\sum_{t=1}^{M}\phi(t)y(t)\right]. \tag{3.39}$$

This is true provided the error sequence $e(t)$ is white and Gaussian. If the error is not white, then the estimate of the parameter vector θ is biased.

Now that we have set the foundation, the problem that arises is how do we estimate the parameters associated with a transfer function that will properly represent a model of the seaway in a recursive fashion. If $\hat{\theta}(t)$ is the estimate of the parameters at time t, the goal is to compute the successive estimate $\hat{\theta}(t+1)$ by updating $\hat{\theta}(t)$ using the latest observations. It turns out that this problem can be put in a very nice framework that makes use of the considerations on the Kalman Filter. More on this approach will be discussed in Chapter IV.

The auto-regressive (AR) model, with numerator equal to one, can be written as

$$y(t) = \phi(t-1)^T\theta + e(t) \tag{3.40}$$

with $e(t)$ a white noise sequence. If it is assumed that θ is constant, Equation 3.40 can be written in state space form, where the state is the parameter vector itself, as

$$\begin{aligned} \theta(t+1) &= \theta(t) \\ y(t) &= \phi(t-1)^T\theta(t) + e(t) \end{aligned} \tag{3.41}$$

This form is just a particular case of the stochastic state space model with **A** being the identity matrix, **B=0** and **C=**$\phi(t)^T$. Since this is a stochastic process, the Kalman Filter approach for the estimation of $\theta(t)$ is used, which leads to

$$\hat{\theta}(t+1) = \hat{\theta}(t) + \frac{\overline{P}(t)\phi(t-1)}{\lambda^2 + \phi(t-1)^T \overline{P}(t)\phi(t-1)}(y(t) - \hat{\theta}(t)^T \phi(t-1))$$
$$\overline{P}(t+1) = \overline{P}(t) - \frac{\overline{P}(t)\phi(t-1)\phi(t-1)^T \overline{P}(t)}{\lambda^2 + \phi(t-1)^T \overline{P}(t)\phi(t-1)} \quad , \qquad (3.42)$$

with $\lambda^2 = \mathrm{E}\left\{|e(t)|^2\right\}$. Clearly, the parameter λ is never known, and the need to know it can be eliminated by proper normalization. Dividing the numerator and denominator of Equation 3.42 by λ^2 the following algorithm is obtained;

$$\hat{\theta}(t+1) = \hat{\theta}(t) + \frac{P(t)\phi(t-1)}{1 + \phi(t-1)^T P(t)\phi(t-1)}(y(t) - \hat{\theta}(t)^T \phi(t-1))$$
$$P(t+1) = P(t) - \frac{P(t)\phi(t-1)\phi(t-1)^T P(t)}{1 + \phi(t-1)^T P(t)\phi(t-1)} \quad , \qquad (3.43)$$

which can be easily verified by setting $P(t) = \overline{P}(t)/\lambda^2$. This algorithm is called the Recursive Least Squares (RLS) algorithm, [Ljung 1987].

Using the above developed RLS algorithm the parameters of an AR model of the form

$$w(t) + d_1 w(t-1) + \ldots + d_N w(t-N) = e(t)\,, \qquad (3.44)$$

with *w(t)* representing the sea surface elevation due to wave action, and *e(t)*, a zero mean, white noise otherwise know as the innovation, may be developed. The main advantage of the AR model is the fact that the parameter estimation is a linear operation. In fact, if the numerator pertinent to the noise term is not one, then the error state model, Equation 3.41, is not white and we cannot apply Kalman Filtering techniques directly. In the general case, the problem is nonlinear in the parameters and the Extended Kalman Filter must be applied.

The problem that now arises is to determine the order (*N*) of the model to properly reflect the actual frequency spectrum of the time series *w(t)* while keeping the complexity of the model at a minimum. By computing the covariance of the innovation as the order

of the model is increased it can be shown that there is a value to which the covariance converges. Using surface wave elevation data obtained in Monterey Bay, from a Waverider measurement buoy, an Auto Regressive model of various orders was determined and the covariance of the innovation compared. The results of this analysis are shown is Figure 3.5.

As can be seen, the covariance begins to flatten out around an eighth order model. This would have one believe that the correct order model to choose would be an eighth order model. However, as shown in Figure 3.6, an eighth order model fails to accurately reflect the actual spectrum. As the order of the model is increased, the error in the matching of the actual spectrum decreases, however, not until a 100^{th} order AR model is computed, is the desired spectrum actually realized, see Figure 3.7. The issues associated with using a model order this high include parameter corruption due to noise causing inaccurate identification.

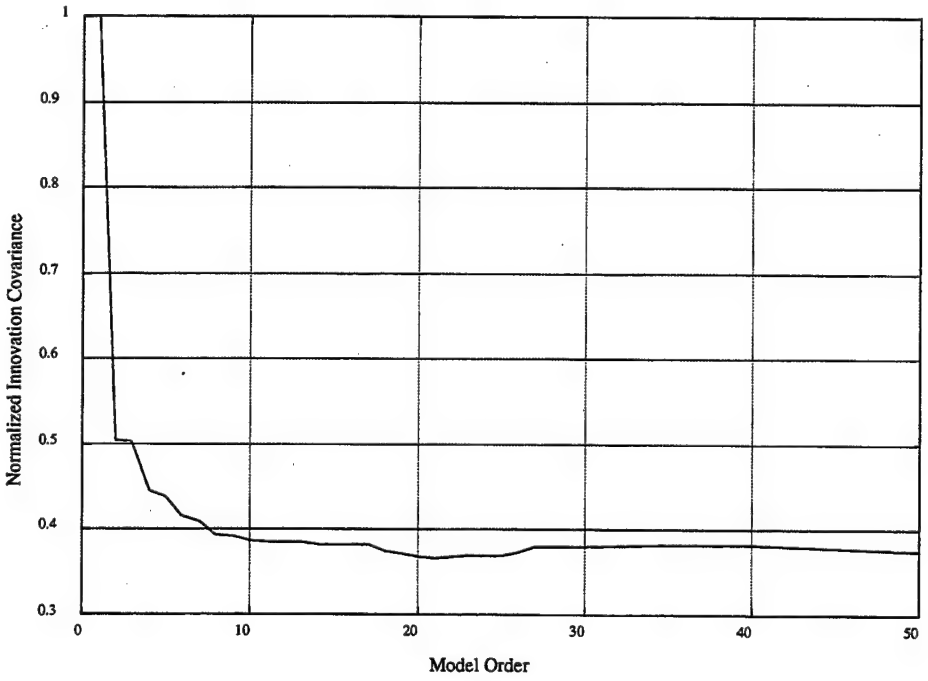

Figure 3.5 Comparison Of Innovation Covariance To AR Model Order

There are those that will argue that the energy associated with the low and high frequency modes is minimal, and that proper modeling of those modes is not important. However, as was discussed in Chapter II, it is the low frequency modes of the wave train

that are considered shallow water, non-dispersive waves. It is these modes that will have the most effect on the submerged vehicle trying to maintain station.

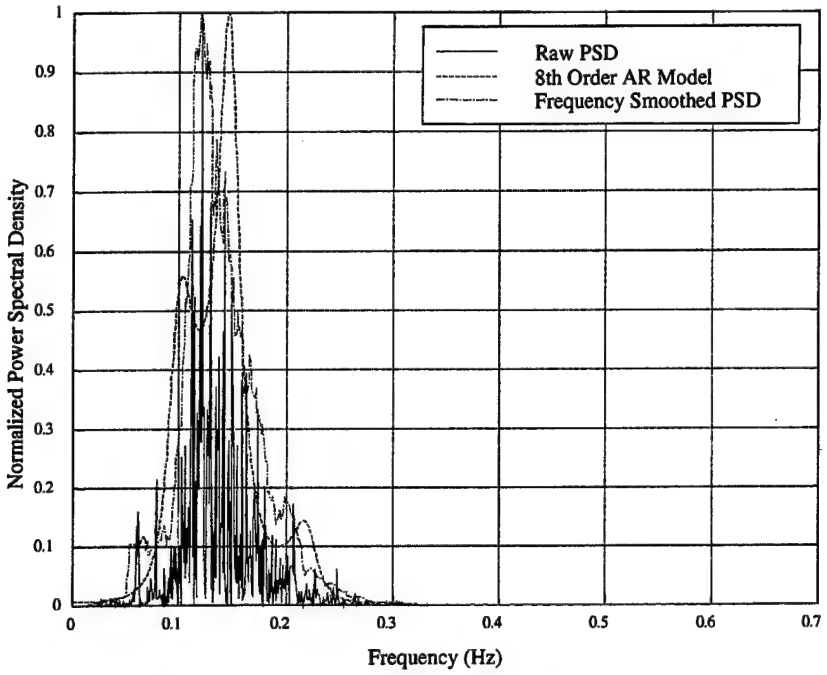

Figure 3.6 8th Order AR Model – Fit to Monterey Bay Data

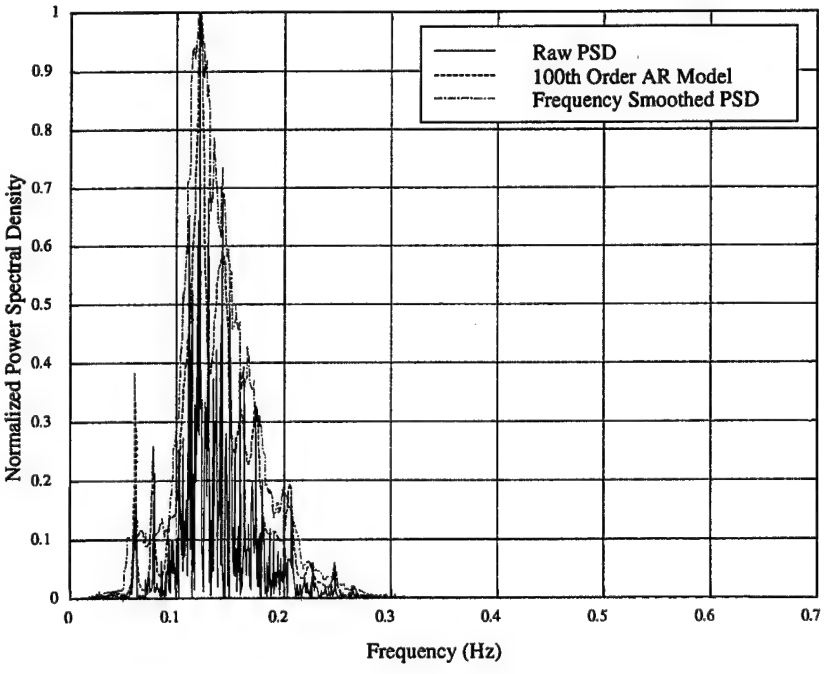

Figure 3.7 100th Order AR Model– Fit to Monterey Bay Data

Therefore, as in any design, trade-offs must be made based on analysis, as to how accurate the wave disturbance model must be compared to the resulting controller complexity.

Using a model order much greater than that of an eighth order approximation creates difficulties in real-time embedded processes currently used on small underwater vehicles. However, using a stable, reduced order disturbance model in an estimator where measurements are available to correct the model errors provides a very good means of tracking and compensating for the disturbance, [Riedel 1998a]. Further information regarding the estimation and accuracy of these models will be discussed in Chapter V.

E. APPLICATION TO DISTRIBUTED SIMULATIONS

This section will present a method by which realistic wave data as well as empirical relationships may be implemented into a distributed simulation. The purpose of this approach is to further the development of simulation capabilities for control system design, multiple vehicle coordination as well as mission planning.

The simplest method of obtaining information about wave disturbances in a particular operating area is from a wave buoy. However, to use this information to simulate the disturbance forces and moments acting on a submerged vehicle, it is necessary to transform the wave elevation record into a water particle velocity record at the vehicle operating depth. There are two approaches to this problem. The first uses spectral analysis while the second uses Fourier analysis.

Using the spectral analysis approach, the procedure is to first compute the power spectral density, $\Phi_{\eta\eta}(\omega)$, of the surface elevation, then modify the PSD by the appropriate depth related transfer function, $|H(\omega, Z)|^2$, and finally convert the new spectral density back to the time domain for replications of the subsurface water particle velocities. Although the resulting time series reflects the proper magnitude of the water particle velocities, the disadvantage to this method is that the phase information is lost, and the resulting subsurface velocity time series do not accurately reflect the motion caused by

the surface elevation times series. It is critical to ensure that the phase relationship between the horizontal and vertical wave induced velocities and accelerations are correct in order to provide realistic vehicle motion in simulation since, as Chapter II outlined, the 6DOF EOM are coupled.

Through the use of the Fourier analysis method, the shortcomings of the spectral analysis are overcome and the disturbance phase relationship is maintained. In this method, a FFT of the surface wave record is taken, then the Fourier coefficients are multiplied by the appropriate value of the modifier for each frequency component. Once this has been completed, an inverse FFT is performed. The resulting disturbance records now reflect both the proper amplitude and phase relations. Figures 3.8-3.11 depict this Fourier analysis translation procedure for a wave elevation time series recorded in Monterey Bay, CA.

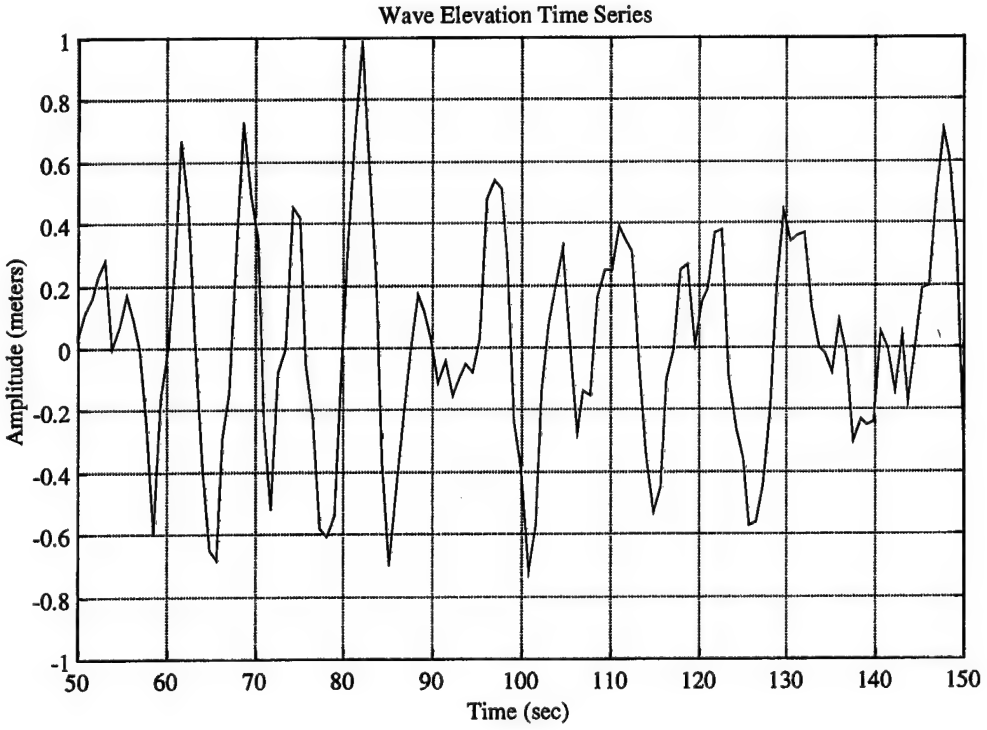

Figure 3.8 Wave Elevation Time Series, Monterey Bay April 1998

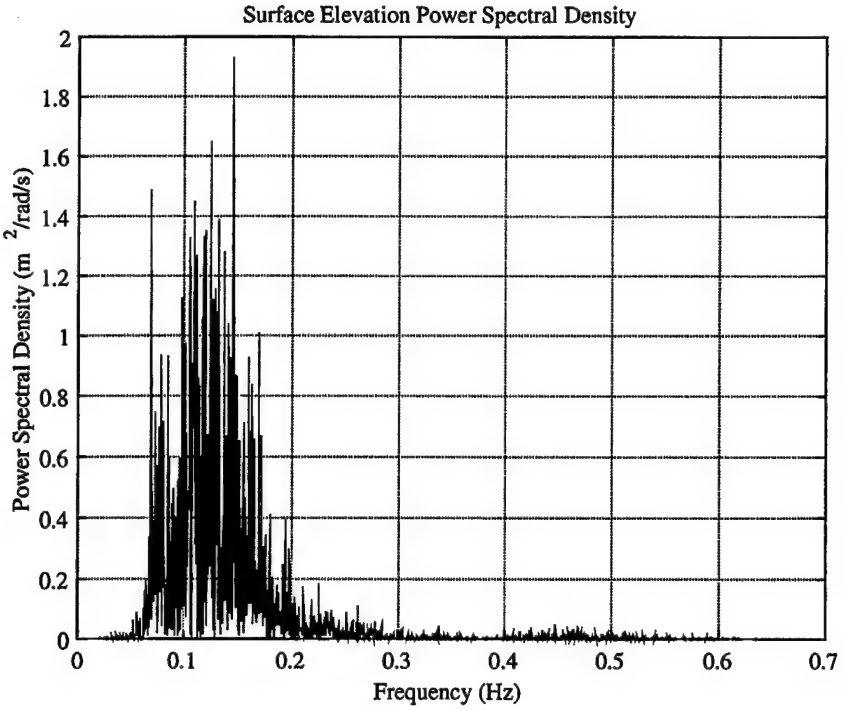

Figure 3.9 Surface Elevation PSD, $\Phi_{\eta\eta}(f)$

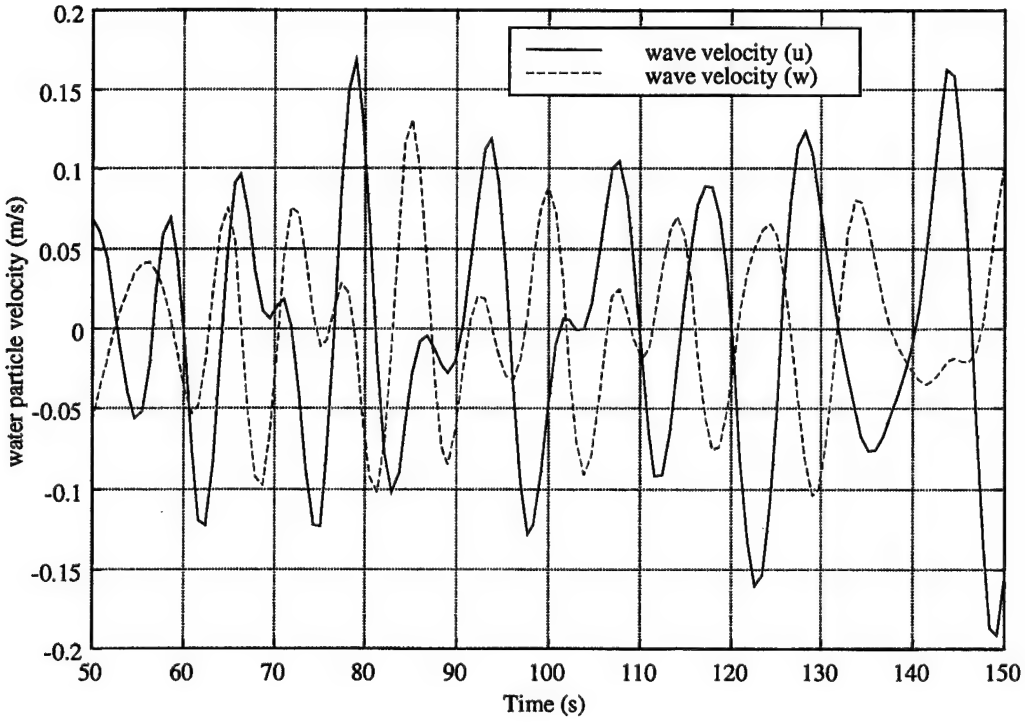

Figure 3.10 Sub-surface Water Particle Velocity Series, (H=45 m, Z=22.5 m)

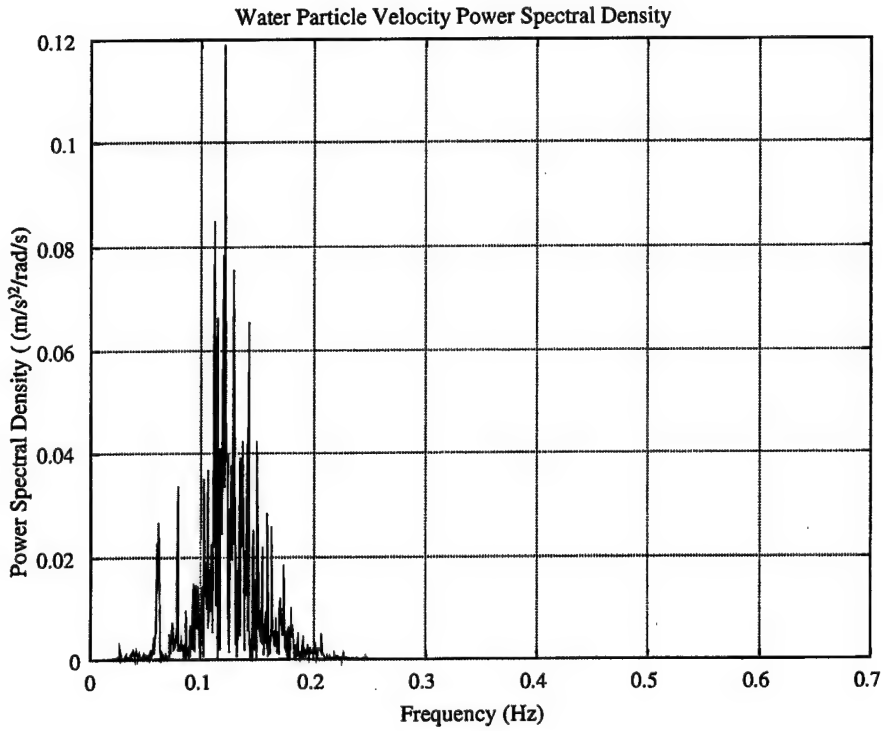

Figure 3.11 Horizontal Water Particle Velocity PSD, $\Phi_{uu}(f)$, (H=45 m, Z=22.5 m)

The elevation data, displayed in Figure 3.8, was recorded by a Waverider® buoy in 45 meters (150 feet) of water. The resulting velocity record, Figure 3.10, is from a transformation of the elevation record for an operating depth of 22.8 meters (75 feet). Referring to the PSD of the transformed velocity record, Figure 3.11, it is interesting to note that in addition to the dominate peak frequency at 0.12 Hz , there are two additional lower frequency components at 0.05 Hz and 0.07 Hz. Recalling comments made with respect to shallow water waves in Chapter II, for this water depth only the frequency component less than 0.05 Hz may be treated as shallow water waves.

To accurately reflect, in simulation, the wave field approximated by any of the empirical relationships discussed in Section B, Equation 3.3 as well as the relationships given in Table 2.2 are used. The stochastic nature of the sea waves is introduced in the simulation by including a random phase angle in the oscillatory θ term given in Table 2.2. The proper velocity amplitudes for this wave field are determined by using the vehicle's depth in the exponential modifier. The correct phasing, with respect to the

vehicle, is obtained by using the vehicle's global position, X, in the θ term associated with the water particle velocities. As a note, this approach models first order wave processes, however, to adequately represent the nonlinear second order wave effects, the $\Delta\omega$ in Equation 3.3 is often varied to provide frequency bands of equal energy.

F. SUMMARY

This chapter has presented a detailed discussion of wave disturbances. It has described the statistical nature of the sea and presented several empirical relationships that may be used for approximating the spectral properties of the ocean. Methodologies for identifying and employing state space models of the sea, in control applications, have been highlighted. Approaches for using wave information, from empirical relationships or real data, in distributed simulations has been discussed.

IV. PARAMETER ESTIMATION

A. INTRODUCTION

As shown in Chapter II, accurate modeling of underwater vehicles has lead to the development of complicated equations of motion. Apart from the non-linearities inherent with underwater vehicle motion, the forces and moments acting on the submerged body are typically determined by a combination of theoretical and experimental results. [Healey 1992 and 1993] has suggested the use of three, independent, decoupled, equations of motion sets, which model speed, steering and diving control. The use of these simpler models, which describe only particular vehicle dynamics, is useful in control law design.

Recent interest in underwater vehicle maneuvering and control in shallow water has generated the need for a greater understanding of vehicle dynamics in this regime. Specifically, improved vehicle models foster the development of sophisticated control architectures, which produce the high degree of autonomy necessary to allow vehicles to maintain acceptable performance in an ocean environment. Critical to the solution, since dynamic positioning of an underwater implies a nonlinear response, is the use of an adequate input-output mapping of the vehicle dynamics.

In this chapter, a method for identifying the decoupled longitudinal surge motion dynamic parameters is presented. The identification is based on post-process Kalman filtering of data obtained from in-water vehicle experiments. Identification of the parameters associated with the surge equations of motion is performed, and a comparison between experimental data from in water measurements with the Phoenix AUV, and simulated results is conducted. Lastly, the nonlinear function that relates the commanded propeller speed to the required propulsion motor voltage is determined. This function is critical in the implementation of a real-time surge controller that will allow a vehicle to maintain position while disturbed by waves.

B. ESTIMATION METHODOLOGY

Parameter estimation has been called a "can of worms" by Astrom [Astrom 1983], in which he refers to the difficulty of making theoretically sound methodology work with real data. With this said, many different techniques have been employed in the area of system identification or parameter estimation, see [Lung 1987, Gelb 1968 and Astrom 1989] for examples, to attack this daunting task. In this work, a recursive Kalman filter approach was chosen since this technique is suitable for real-time implementation. The Kalman filter method is similar to weighted least squares algorithms [Ljung 1987], and allows for the incorporation of system and measurement errors.

In the Kalman filter algorithm, it is assumed that the parameter model is based on a nominally constant parameters set, where the state vector is the parameter vector $\boldsymbol{\theta}$, and the dynamics are described in discrete time by

$$\begin{aligned} \boldsymbol{\theta}(k+1) &= \boldsymbol{\theta}(k) + \boldsymbol{\Gamma w} \\ z(k+1) &= \boldsymbol{h}(k)\boldsymbol{\theta}(k) + \boldsymbol{v} \end{aligned} \quad . \tag{4.1}$$

The system noise, $\boldsymbol{w}$, and the measurement noise, $\boldsymbol{v}$, are considered to be zero-mean, white noise sequences with associated covariance matrices $\boldsymbol{Q}$ and $\boldsymbol{R}$, respectively. The recursive Kalman filter estimation equations as given by [Gelb 1974] are

$$\begin{aligned} \hat{\boldsymbol{\theta}}_{k/k-1} &= \boldsymbol{\Phi}_{k/k-1}\hat{\boldsymbol{\theta}}_{k-1/k-1} \\ \boldsymbol{P}_{k/k-1} &= \boldsymbol{\Phi}_{k/k-1}\boldsymbol{P}_{k-1/k-1}\boldsymbol{\Phi}^{T}_{k/k-1} + \boldsymbol{\Gamma}_{k/k-1}\boldsymbol{Q}\boldsymbol{\Gamma}^{T}_{k/k-1} \\ \boldsymbol{K}_k &= \boldsymbol{P}_{k/k-1}\boldsymbol{h}_k^T[\boldsymbol{h}_k\boldsymbol{P}_{k/k-1}\boldsymbol{h}_k^T + \boldsymbol{R}]^{-1} \\ \hat{\boldsymbol{\theta}}_{k/k} &= \hat{\boldsymbol{\theta}}_{k/k-1} + \boldsymbol{K}_k[z_k - \boldsymbol{h}_k\hat{\boldsymbol{\theta}}_{k/k-1}] \\ \boldsymbol{P}_{k/k} &= [\boldsymbol{I} - \boldsymbol{K}_k\boldsymbol{h}_k]\boldsymbol{P}_{k/k-1} \end{aligned} \quad , \tag{4.2}$$

where $\boldsymbol{K}$ is a time varying optimal gain that produces a least squares solution for the parameter estimate, and $\boldsymbol{P}$ is the parameter estimation error covariance. These expressions are equivalent to the formulation by [Ljung 1987], where the "forgetting factor" λ, is related to the noise covariance $\boldsymbol{R}$. This recursive algorithm is expressed as

$$\hat{\boldsymbol{\theta}}(t) = \hat{\boldsymbol{\theta}}(t-1) + \boldsymbol{L}(t)\boldsymbol{\varepsilon}(t)$$
$$\boldsymbol{\varepsilon}(t) = [z(t) - \boldsymbol{h}(t)\hat{\boldsymbol{\theta}}(t-1)]$$
$$\boldsymbol{L}(t) = \boldsymbol{P}(t)\boldsymbol{\Phi}(t) = \boldsymbol{P}(t-1)\boldsymbol{\Phi}(t)\left[\lambda(t)\boldsymbol{I} + \boldsymbol{\Phi}^T(t)\boldsymbol{P}(t-1)\boldsymbol{\Phi}(t)\right]^{-1}, \qquad (4.3)$$
$$\boldsymbol{P}(t) = \frac{1}{\lambda(t)}\left[\boldsymbol{P}(t-1) - \frac{\boldsymbol{P}(t-1)\boldsymbol{\Phi}(t)\boldsymbol{\Phi}^T(t)\boldsymbol{P}(t-1)}{\lambda(t)\boldsymbol{I} + \boldsymbol{\Phi}^T(t)\boldsymbol{P}(t-1)\boldsymbol{\Phi}(t)}\right]$$

where the standard Recursive Least Squares (RLS) algorithm is obtained for the special case of $\lambda \equiv 1$.

C. PARAMETER IDENTIFICATION MODEL

The surge model developed in Chapter II is in continuous time, however, real-time control and estimation is done in discrete time, therefore the set of equations given by Equation 2.91 must be converted to a digital form. To produce a digital set of equations, a standard Euler discretization can be used. Assuming a sampling period T, the discrete system of equations, disregarding the kinematic relation, for the surge model becomes

$$u_r(k+1) = (\alpha u_r(k)|u_r(k)| + F(k))T^{-1} + u_r(k)$$
$$F(k+1) = (\frac{-1}{\tau}F(k) + \frac{\gamma}{\tau}u_r(k)|n(k)| + \frac{\beta}{\tau}n(k)|n(k)|)T^{-1} + F(k) \qquad (4.4)$$

The model presented in Equation 4.4 contains four unknown parameters, α, β, γ and τ, that must be determined by experimental means. To properly identify the dynamic parameters associated with this mode, the model must be expressed in terms of the measurement variables only. The measured input-output data channels that are available for this identification are the relative longitudinal velocity, $u_r(t)$, and the propeller revolutions, $n(t)$. Since the propeller thrust value F, cannot be measured, the two first-order equations must be combined into a second-order equation containing only these two measured variables. Defining the change of variables

$$b=\frac{1}{\tau}$$
$$c=\frac{\gamma}{\tau}\,, \tag{4.5}$$
$$d=\frac{\beta}{\tau}$$

and combining the two first-order equations in Equation 4.4, a second-order discrete model in u_r can be formed,

$$\begin{aligned} u_r(k+2) = {} & 2u_r(k+1)-u_r(k) \\ & +T\alpha\left[u_r(k+1)\left|u_r(k+1)\right|-u_r(k)\left|u_r(k)\right|\right] \\ & +Tb\left[u_r(k)-u_r(k+1)\right]+T^2b\alpha\left[u_r(k)\left|u_r(k)\right|\right] \\ & +T^2c\left[u_r(k)\left|n(k)\right|\right]+T^2d\left[n(k)\left|n(k)\right|\right] \end{aligned} \tag{4.6}$$

Unfortunately, the model in Equation 4.6 is nonlinear in parameters making it difficult to apply standard system identification techniques. However, the nonlinear model can be transformed to be linear in its parameters and variables, thereby allowing the use of well established estimation tools, by defining an additional change of variables as,

$$\begin{aligned} C_1 &= T\alpha & h_1 &= u_r(k+1)\left|u_r(k+1)\right|-u_r(k)\left|u_r(k)\right| \\ C_2 &= Tb & h_2 &= u_r(k)-u_r(k+1) \\ C_3 &= T^2b\alpha & h_3 &= u_r(k)\left|u_r(k)\right| \\ C_4 &= T^2c & h_4 &= u_r(k)\left|n(k)\right| \\ C_5 &= T^2d & h_5 &= n(k)\left|n(k)\right| \end{aligned}\,, \tag{4.7}$$

and

$$\begin{aligned} z &= u_r(k+2)-2u_r(k+1)+u_r(k) \\ \boldsymbol{h} &= \begin{bmatrix} h_1 & h_2 & h_3 & h_4 & h_5 \end{bmatrix} \\ \boldsymbol{\theta} &= \begin{bmatrix} C_1 & C_2 & C_3 & C_4 & C_5 \end{bmatrix}^T \end{aligned}\,. \tag{4.8}$$

With these definitions, the model can now be written in matrix notation as

$$z=\boldsymbol{h}\boldsymbol{\theta}\,. \tag{4.9}$$

The parameter vector, $\boldsymbol{\theta}$, contains five coefficients where only four parameters are of interest. The additional coefficient, C_3, is a result of the nonlinearity associated with the

original model represented by Equation 4.9. The parameter vector, θ, will be estimated in a least squares sense using Equation 4.9, and in this case, one extra degree of freedom is present which may cause a slight decrease in the accuracy of the other parameters.

In theory, the additional coefficient defines an implicit relationship between the other parameters of the model; in reality however, this additional coefficient lumps together any modeling errors and therefore it is not constrained thereby allowing convergence of the parameters in a least squares sense. The model parameters α, β, γ and τ, are therefore determined from the four coefficients C_1, C_5, C_4 and C_2, respectively.

D. SYSTEM IDENTIFCATION

1. Input Signal Design

Prior to estimating the parameters associated with the surge model, data must be obtained for use in the estimation filter. This data must contain measured control input and response output variables from a ''persistent'' excitation. It is a well-documented theorem that to ensure a unique, unbiased, least squares estimate, the system or plant must be persistently excited, [Astrom 1989]. In addition, the system identification should take place using open loop control, if possible, so that controller dynamics do not effect the results, [Ljung 1987].

Since the purpose of this piece of work is to determine the parameters of the surge dynamics model that will be the basis for a surge controller, the input data must persistently excite the vehicle over the expected frequency range of the surge velocity disturbance. For shallow water applications, the period of the surge disturbance that an underwater vehicle may encounter can range from approximately 4 to 40 seconds. It is necessary therefore, that the propeller revolution input to the vehicle, for identification purposes, also contains this frequency content. By selecting a square wave of various periods the control input was designed that contained the desired frequency components. A portion of the time series used for the control input is shown in Figure 4.1, and the frequency content of this input signal is depicted in Figure 4.2.

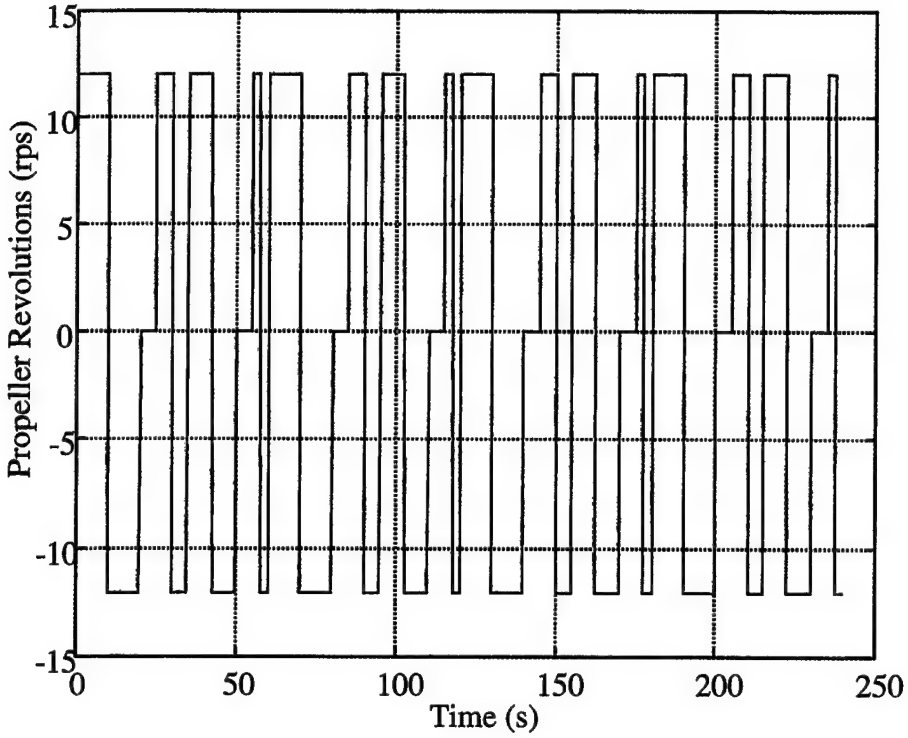

Figure 4.1 Control Input Time Series

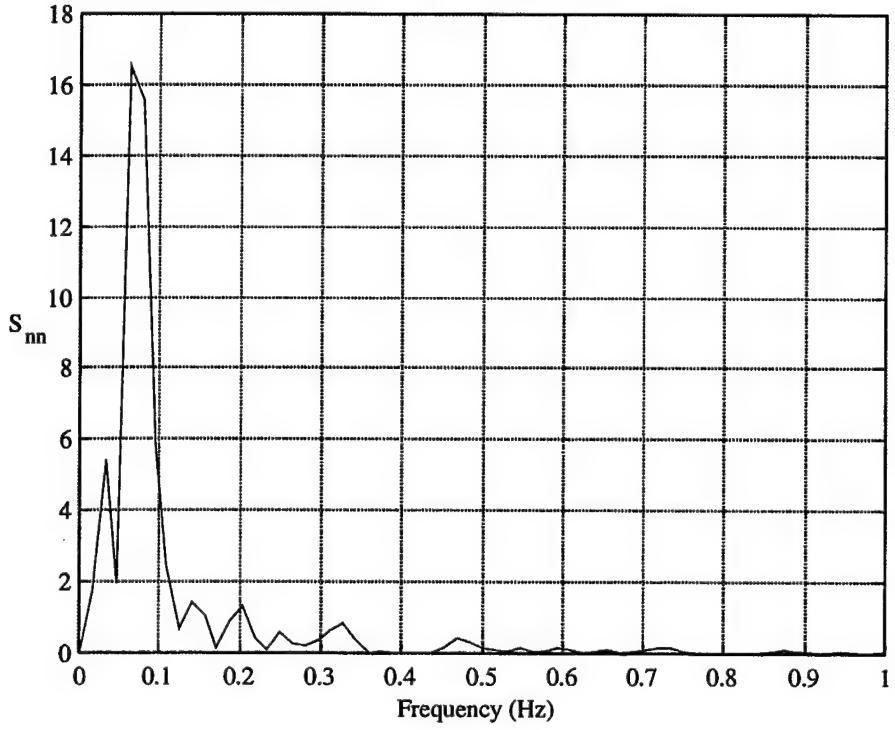

Figure 4.2 Control Input Frequency Content

As seen in Figure 4.2, the frequency components of this input signal range from 0.02 Hz to 0.35 Hz. The dominant frequency was designed to be around 0.05 Hz to 0.08 Hz,or a 12.5 to 20 second period. The purpose of designing the input signal in this manner is to ensure that the parameters were weighted in the range of the dominant surge period. With the input signal properly designed the system identification data runs can proceed. Note that considering the input to be $n(t)$ or $n(t)|n(t)|$ makes no difference in the spectral content of the input signal.

2. Data Collection

A series of four in-water experiments were conducted in the Monterey Harbor Basin on March 5, 1999. The Phoenix vehicle was placed under active control in both heading and depth through the use of control surfaces, and the propeller RPMs were commanded through the use of an input file representing the input signal shown in Figure 4.1. During these runs Phoenix carried its standard sensor suite, which includes a SonTek® ADV and a RDI® Navigator DVL. These sensors were used to measure the vehicle's response to the control input. Information concerning each of these sensors may be found in Appendix B. A sample of the measured input and output data obtained during run three is depicted in Figure 4.3.

The input-output response shown in Figure 4.3 indicates that the vehicle is less efficient when operating astern. This is evident by observing that the magnitude of the astern velocity is significantly less than that of the forward velocity, for the same propeller revolutions. This decrease in efficiency is an issue that must be addressed during the estimation process.

An additional item observed during data analysis is that the voltage required by the propulsion motors to obtain the same revolutions is different. The reason for the difference is attributed to the starboard propulsion train having to overcome a greater amount of friction. This friction is caused by misalignment that resulted from structural damage that was incurred by Phoenix early in its operating life. The voltage difference is shown in Figure 4.4. To account for the differences in propeller revolutions, an average input was used during the system identification. The speed from the two shafts was

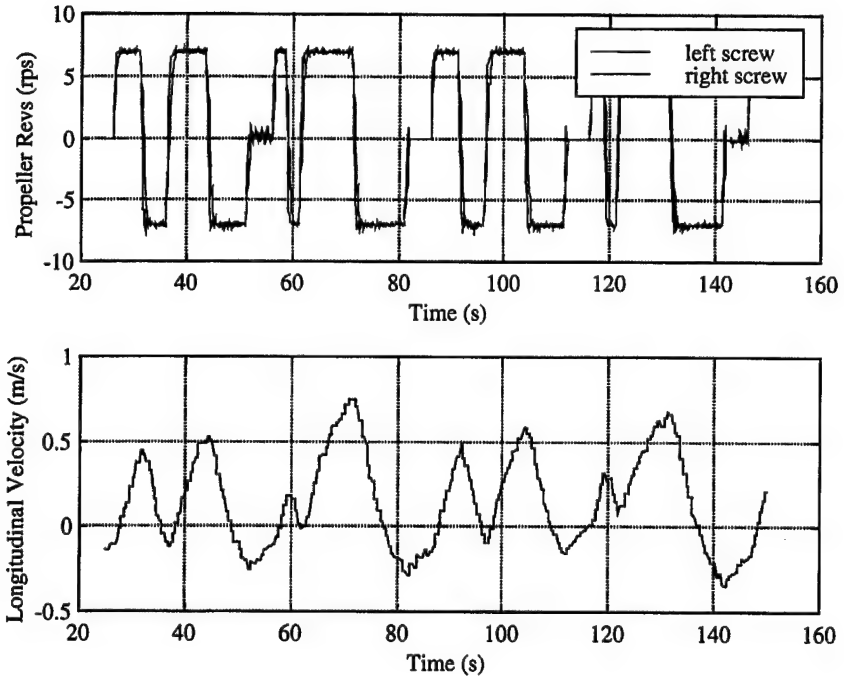

Figure 4.3 Example of Measured Data, Propeller Revolutions, n, And Ground Velocity, u_g, From The RDI

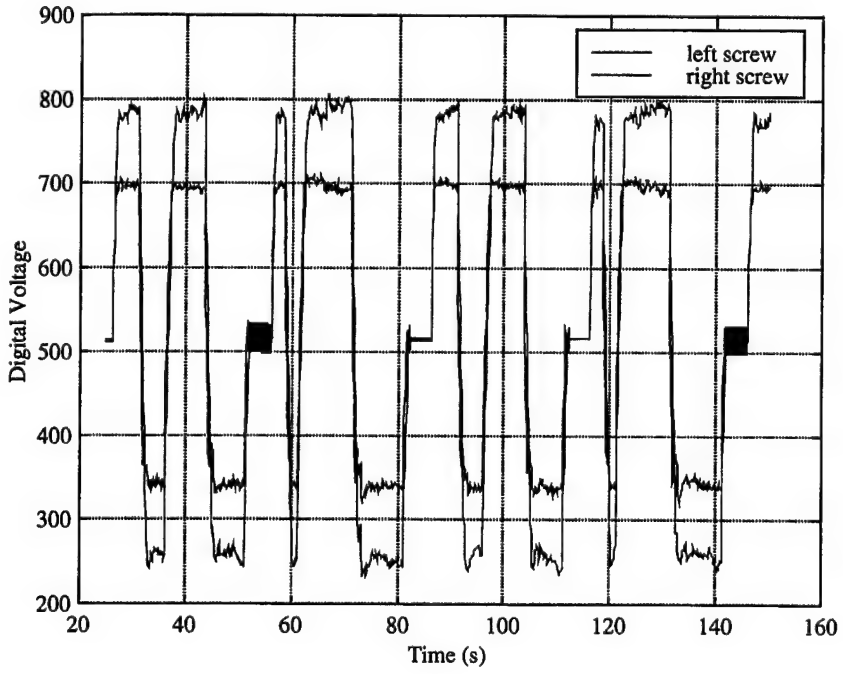

Figure 4.4 Digital Voltage to Propulsion Motors

averaged, and the vehicle was treated as having a single input. The parameter β is then determined for the assumed single shaft system, with the recognition to the fact that the actual parameter for each shaft on the vehicle will be $\beta/2$.

Since the output of the digital controller is a commanded voltage, this voltage mismatch can be accounted for in the controller software. To ensure that the propellers produce approximately equal thrust, the function that maps the commanded revolutions from the controller to delivered voltage to the motors must be determined. Once this function is found, it can be coded into the vehicle control computer thereby ensuring the propeller mismatch is minimized. Another way of ensuring that the shaft speeds are the same is to "close the loop" around propeller speed. However, this solution adds additional system dynamics making the controller formulation more difficult. The methods used to determine this mapping will be discussed later in this chapter in Section E.

3. Parameter Identification Results

In the application of the parameter estimator, the measurement noise covariance, v, was set to 0.01, a constant scalar. The values of the diagonal elements, q_{ii}, of the model noise covariance matrix, $\boldsymbol{Q}$, were chosen to match the bandwidth of the input signal. With this choice, a tradeoff between convergence, stability and precision of the estimates is made. The following results are presented for one of the many data runs and selected values of q_{ii} that produced the "best" results in parameter estimation. The term "best" is a subjective measure based on a balance between the whiteness of the residuals, the values of the parameters compared to parameters previously identified and a comparison between measured data and simulated results. The final results of the selected parameters from the estimation process are shown in Table 4.1, including statistics on the estimation error and the residual e.

The evolution of the parameter estimates and the diagonal elements of the covariance matrix, $\boldsymbol{P}$, associated with these parameters is shown in Figures 4.5 and 4.6, respectively. Referring to Figure 4.5, it can be seen that the parameters do converge, but exhibit some slight fluctuations. The noise observed in the evolution of the covariance

Parameter (units)	Lower Bounds	Estimate	Upper Bounds	Uncertainty
α (m^{-1})	-2.8606	-2.5412	-2.2218	12 %
β ($m \cdot rev^{-2}$)	0.028	0.0359	0.0438	22 %
γ (rev^{-1})	-0.2891	-0.1796	-0.07	61 %
τ (s)	3.0854	3.0997	3.1197	0.5 %
μ_e		0.007		
σ_e		0.0255		

Table 4.1 Parameter Estimation Values and Residual Statistics

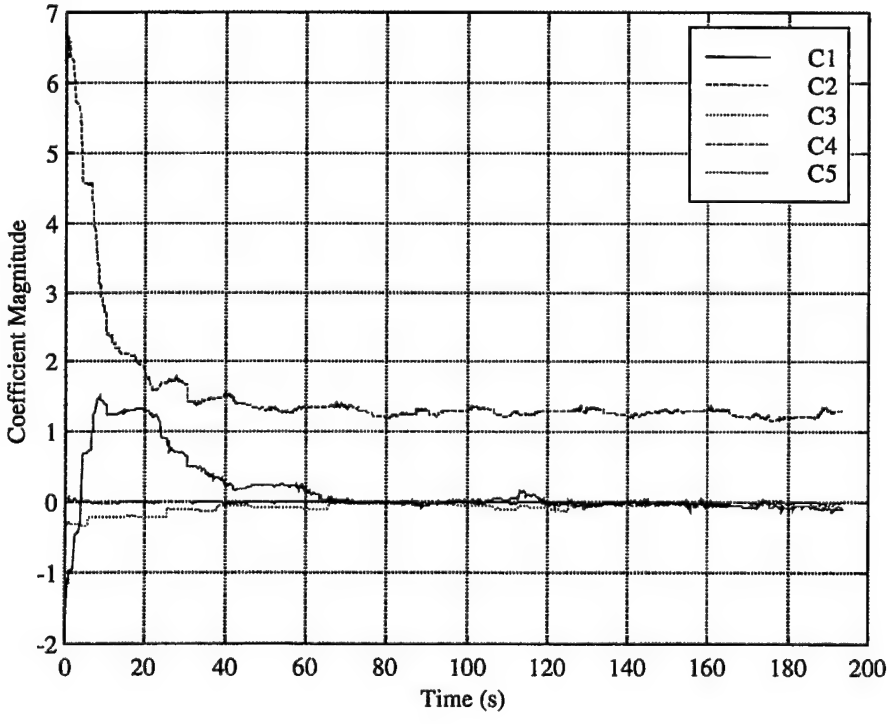

Figure 4.5 Parameter Evolution

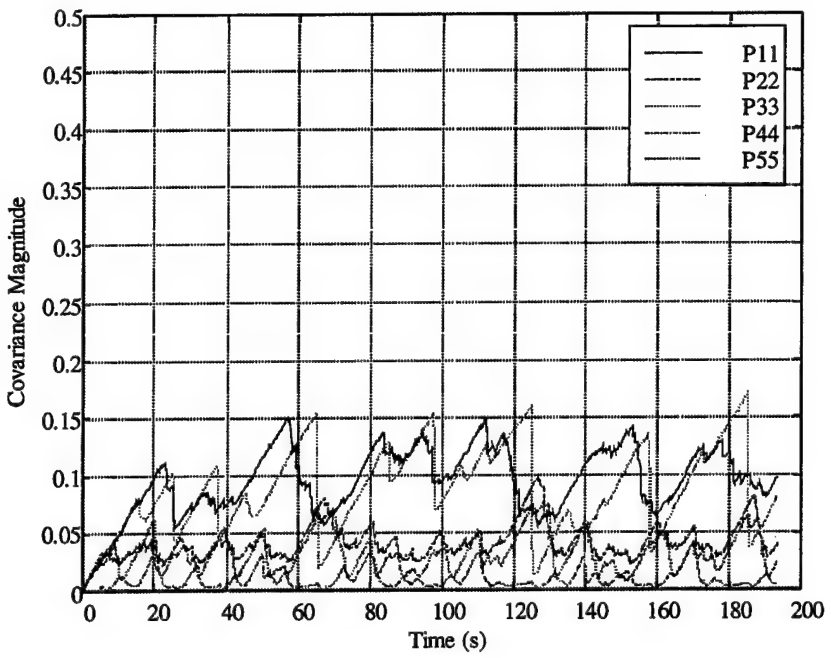

Figure 4.6 Covariance Evolution

matrix, Figure 4.6, is caused by the rather large values of the diagonal elements of $\boldsymbol{Q}$, $q_{ii} = 5.0$. The large values needed for these were necessitated by the additional degree of freedom in the filter, the uncertainty associated with the thrust reduction term and the large bandwidth of the input signal.

The performance of the filter can be determined by computing the autocorrelation of the residuals. The autocorrelation provides a measure of how the value of a random variable at a time t, will influence its value at some future time, $t+\tau$. If the filter is properly tuned, the residuals should be white. For the residuals to be classified as white, there will be ideally zero correlation at any time shift τ, and the time series will be highly correlated at $\tau = 0$. Figure 4.7 indicates that the residuals are not white, but exhibit some correlation. The non-whiteness of the residuals indicates the lack of modeling capability. Since Kalman filter theory assumes that any measurement noise has a Gaussian distribution, the measurement noise model is corrupted by unmodeled, colored noise. This corruption of the measurement model caused the residuals also to display colored noise properties. Also, since the reduction in propeller efficiency when the vehicle

operates astern is not known, additional modeling errors are introduced which effects filter performance.

Despite the issues associated with the non-whiteness of the filter residuals, apparent satisfactory parameter identification was obtained. The parameter estimation was deemed satisfactory by comparing the measured vehicle response to simulated response results. Using the identified parameters, listed in Table 4.1, and the measured propeller input shown, in Figure 4.3, a simulation was conducted with the results presented in Figure 4.8.

The response traces shown in Figure 4.8 indicate that the identified parameter set provides a reasonable predictive response. Recalling that the parameters are estimated in a least squares sense, the errors between the two traces are acceptable. The two responses are not lagged indicating good agreement in the propulsion system time constant and vehicle drag coefficient. The error in response amplitude is attributed to the uncertainty associated with the identification of the β and γ parameters.

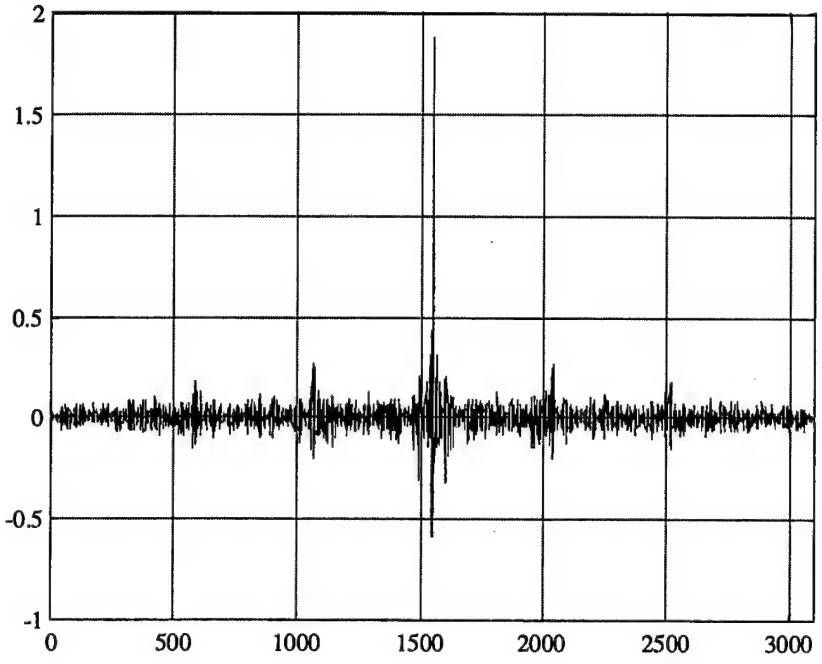

Figure 4.7 Autocorrelation of Estimation Filter Residuals

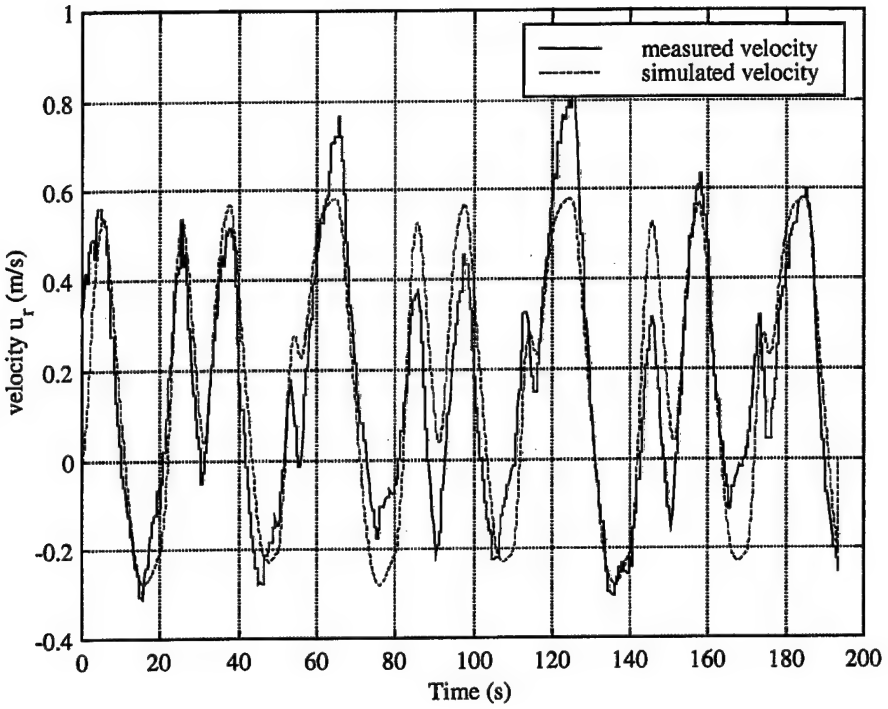

Figure 4.8 Comparison of Measured and Simulated Vehicle Response.

The uncertainty in each parameter may be estimated by using the magnitude of the covariance matrix diagonal corresponding to the estimated parameter. The calculated uncertainty for each of the parameters, based on the covariance levels, is shown in Table 4.1. Although the level of uncertainty with these parameters may seem excessive, it is not too different from the "standard" level of uncertainty associated with underwater vehicle parameter estimates, which typically is around ±40 %. It is this variability in parameters, as well as other items, that produces the need for robust control law design, which will be discussed in the following chapter.

E. PROPULSION SYSTEM BALANCING

As outlined earlier in this chapter, the required propulsion motor voltage to produce a desired propeller revolution is different for each shaft. Under position control, this difference if not accounted for could cause unsatisfactory results since for position control the loop is closed around position error and not propulsion shaft speed.

In the control system architecture of the Phoenix AUV, the shaft speed is controlled by a motor voltage command which originates from the execution level computer. The particular control law that has been implemented in the vehicle calculates this voltage; therefore, the relationship that maps desired shaft revolutions to voltage must be determined.

By fitting a curve to an overlay of data obtained during the four, system identification runs, the relationship between propeller "revs" and motor voltage for each shaft can be determined. Using the MATLAB® **polyfit** algorithm it was determined that a third order polynomial adequately mapped the two input-output relationships. The nonlinear functions for these relationships are,

$$\begin{aligned} V_{right} &= 0.022607 n_{com}^3 + 0.000194 n_{com}^2 + 0.832982 n_{com} \\ V_{left} &= 0.022356 n_{com}^3 - 0.009507 n_{com}^2 + 0.345086 n_{com} \end{aligned}, \qquad (4.9)$$

with the graphical results of the "goodness of fit" shown in Figure 4.9.

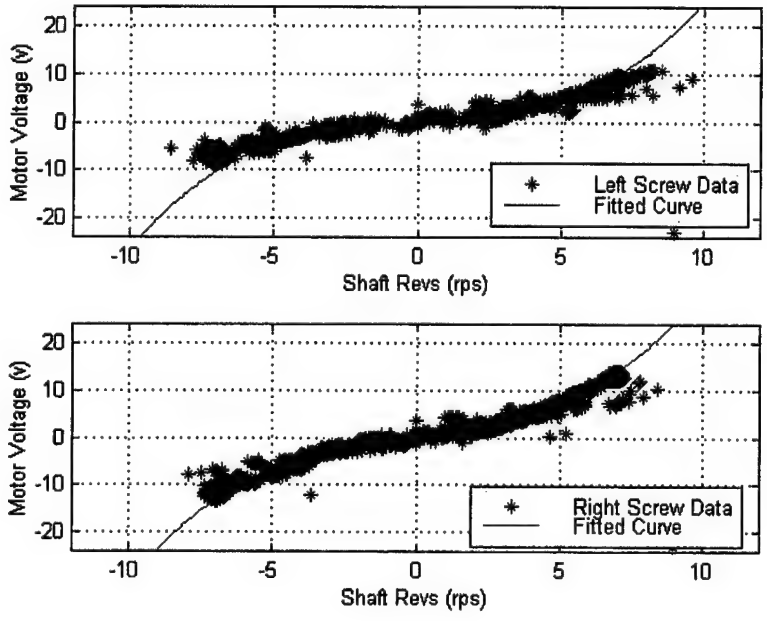

Figure 4.9 Nonlinear Shaft Revolution to Motor Voltage Function

As a note, the polynomial curves in Figure 4.9, indicate that the starboard shaft will produce approximately 8.5 rps for an applied voltage of 24 volts, while the port shaft

produces almost 10 rps for the same applied voltage. Although there is no data displayed in Figure 4.9 to validate this curve at high speed, the shaft revolution values estimated by these curves have been observed during full power trials.

F. SUMMARY

This chapter has presented the work performed to identify the parameters associated with the longitudinal dynamics of the NPS Phoenix AUV from open water experiments. The results show the necessity of a non-linear dynamics model and of the need to include a force lag and a thrust reduction term in the propulsion model. The results obtained are satisfactory although the filter residuals appear to be non-white due to limited modeling capabilities. Regardless of the level of whiteness, it must be stressed that the simple model identified is very useful for control law development.

One interesting point observed during the estimation process was that taking $\boldsymbol{Q}$ as a diagonal matrix with equal values produced better results in the sense that the residuals were minimized and the filter produces stable parameter evolution. This reflected a priori, equal certainty in each initial parameter estimate. Moreover, the interrelationships between the parameters implied a uniform characterization of the modeling noise in the filter. The tuning of the estimation filter proved to be an important step towards obtaining a good model.

Finally, the methodology presented here can be extended to other types of vehicle motions and represents a basis for the development of models and identification techniques that can be applied to other coupled or decoupled motion models.

V. DISTURBANCE REJECTION THEORY

A. INTRODUCTION

Many different techniques have been applied to the disturbance rejection problem in the past. For years, passive techniques employing improved electro-mechanical design were used. With current advancements in the computing industry, adaptive methods have become a popular means of active control. Recent research in the area of nonlinear control has shown that Variable Structure or Sliding Mode Control provides a very robust method of disturbance compensation.

This chapter will begin with an overview of disturbance rejection theory developed to date. This will provide the reader a foundation from which to see the extensions made here in regards to the development of disturbance rejection techniques for small underwater vehicles.

Next, a series of three case studies will be presented. These case studies will demonstrate the major approaches available in the design of disturbance rejection compensators, including the effect that the spectral content of the input disturbance has on controller performance.

Lastly, the results of a simulation study, for the design of a station keeping controller that will be used on the NPS Phoenix AUV, will be discussed.

B. OVERVIEW OF CLASSICAL CONTROL TECHNIQUES

The most intuitive and oldest means of eliminating the effects of a disturbance is to attempt to attenuate the disturbance at the source. This often translates to corrective measures in the system. For example, modifying the electronics in a sensor so that the noise is reduced, is one common application of this technique. Other examples are reducing friction forces in a servo by using better bearings, or moving a sensor to a position where the disturbances are smaller. Although this method of reduction at the source is beautiful in its simplicity, it is often impossible to achieve.

1. Feedback Control

If the disturbances cannot be rejected at the source, feedback control can be used. For this method, the manner in which the disturbance enters the system must be known, and the system must be both controllable and observable. In this way, the effects of the disturbance can be mitigated by using local feedback.

The classical control problem, Figure 5.1, simply stated, is, given a plant model G_p, design a controller, G_c, such that the closed loop system

1. is stable and exhibits some level of robustness against plant parameter variations;
2. accurately tracks the reference input signal, r; and
3. rejects the disturbance d, and noise v.

The solution to this problem is accomplished, in general, by selecting a controller such that a high loop gain is obtained over the frequency range of the input disturbance, while obtaining a low loop gain over the range of the frequencies associated with the measurement noise.

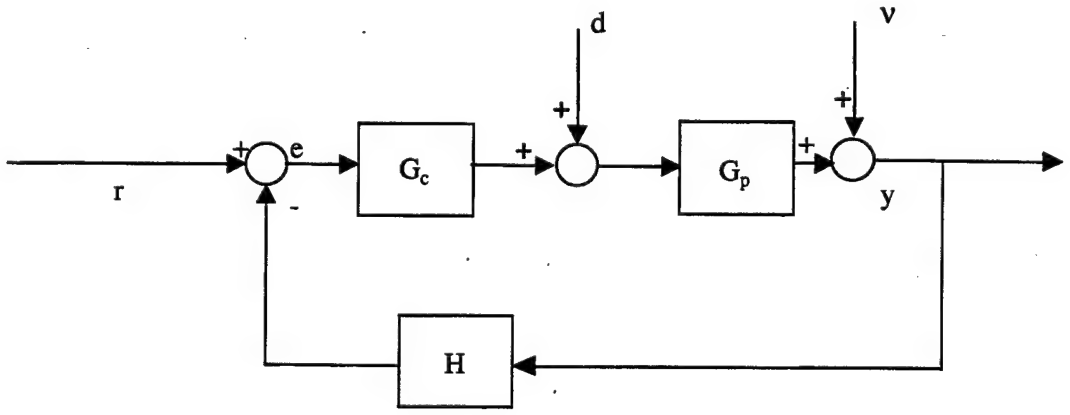

Figure 5.1 Block Diagram of a Feedback Controller

A proper design can be obtained by simultaneously solving the two performance criterion,

$$\frac{\|e\|}{\|d\|} < \gamma_1 \quad , \qquad (5.1)$$
$$\frac{\|e\|}{\|v\|} < \gamma_2$$

over the range of frequencies of interest. This approach is typically referred to as "loop-shaping," and any of the standard control design techniques can be used to accomplish this goal, [Ogata 1990].

To eliminate any step or bias error (or to follow a step input), an integrator is added to the system The integrator directly changes the system's sensitivity to disturbances, specifically targeting bias disturbances. Integral control, in application, needs to be managed carefully using anti-windup methods. This compensation technique does not specifically reject the disturbance, but acts to alter the resulting dynamics of the system when a disturbance is present.

2. Feedforward of Directly Measured Disturbance

If a disturbance can be measured or estimated, feedforward control is a useful method of canceling its effects on the system response. Unlike feedback control, this method is advantageous in that it is implemented by approximately compensating for disturbances before they are sensed. In feedforward control, a signal from a measurable disturbance maybe used to generate an appropriate control force to counteract or mitigate the effects of the disturbance. It minimizes the magnitude of the output for the disturbance input without the use of error integration.

Feedforward control alone can minimize transient errors but there are no guarantees of its accuracy due to its open-loop nature. Thus, feedforward alone is unrealistic for most applications with unsuitable open-loop dynamics. For this reason, feedback control is often used together with feedforward control to compensate for the latter's inaccuracies in minimizing the error. This approach is shown in Figure 5.2.

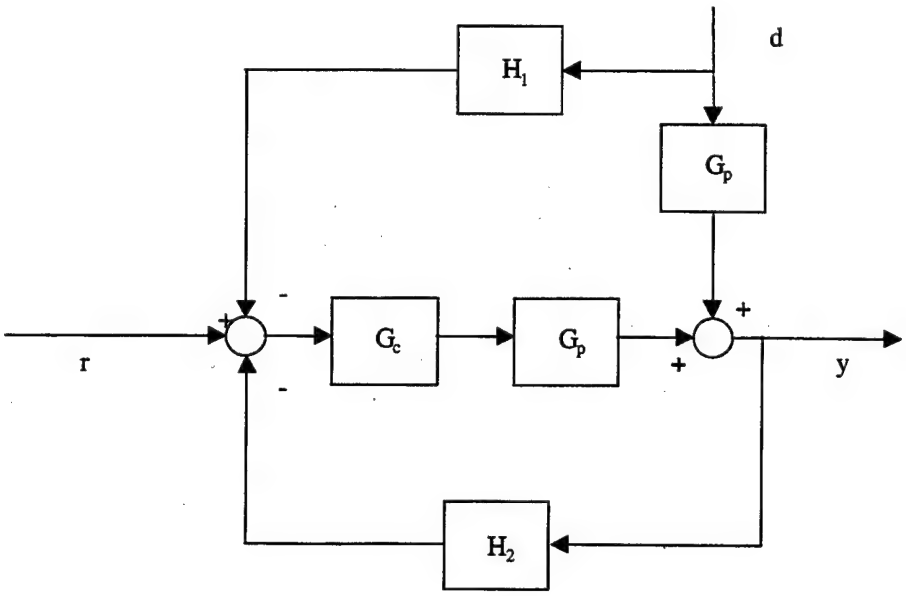

Figure 5.2 Feedforward-Feedback Controller Block Diagram

C. MODEL BASED CONTROL

The state-space representation of a linear system may be defined by the following set of equations:

$$\begin{aligned} \dot{x}(t) &= Ax(t) + Bu(t) \\ y(t) &= Cx(t) + Du(t) \end{aligned}, \tag{5.2}$$

where A, B, C and D are determined from the differential equations describing a system. A block diagram depicting this system is shown in Figure 5.3.

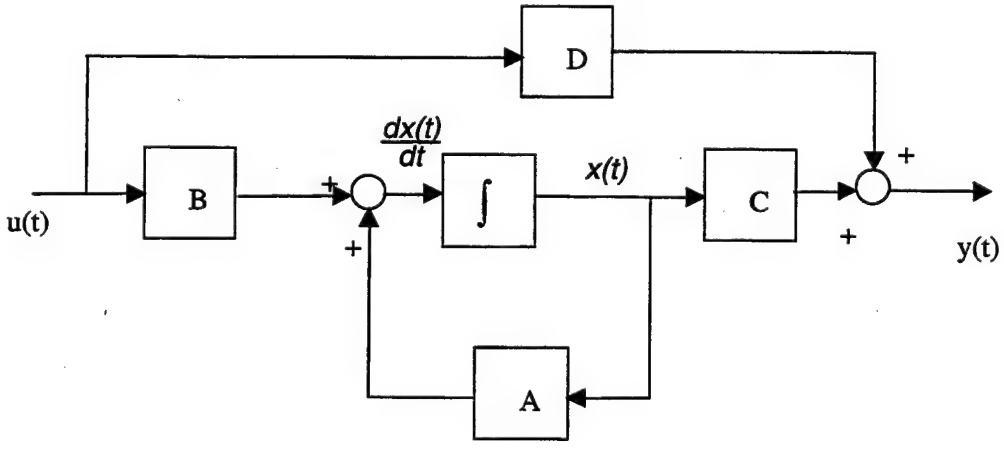

Figure 5.3 Block Diagram of State-Space System

1. Linear Quadratic Regulator Control

Performance indexes are a way of obtaining desirable output regulation without requiring excessive input signals. One of the most common and useful is the LQR performance index defined by

$$J_{LQR} = \boldsymbol{x}^T \boldsymbol{M}\boldsymbol{x} + \int_0^{t_f} \left(\boldsymbol{x}^T \boldsymbol{Q}\boldsymbol{x} + \boldsymbol{u}^T \boldsymbol{R}\boldsymbol{u}\right) d\tau \tag{5.3}$$

where $\boldsymbol{M}$ and $\boldsymbol{Q}$ are real, symmetric positive semi-definite matrices and $\boldsymbol{R}$ is a real, symmetric positive definite matrix. $\boldsymbol{M}$ is called the terminal penalty matrix, $\boldsymbol{Q}$ is the state weighting matrix, and $\boldsymbol{R}$ is the control weighting matrix.

Using a performance index of this form, subject to the system dynamics given in Equation 5.2, a linear state feedback (LSF) control law of the form

$$u(t) = Kx(t) \tag{5.4}$$

was found to be optimal for minimizing J_{LQR}. This control law results in the block diagram depicted in Figure 5.4.

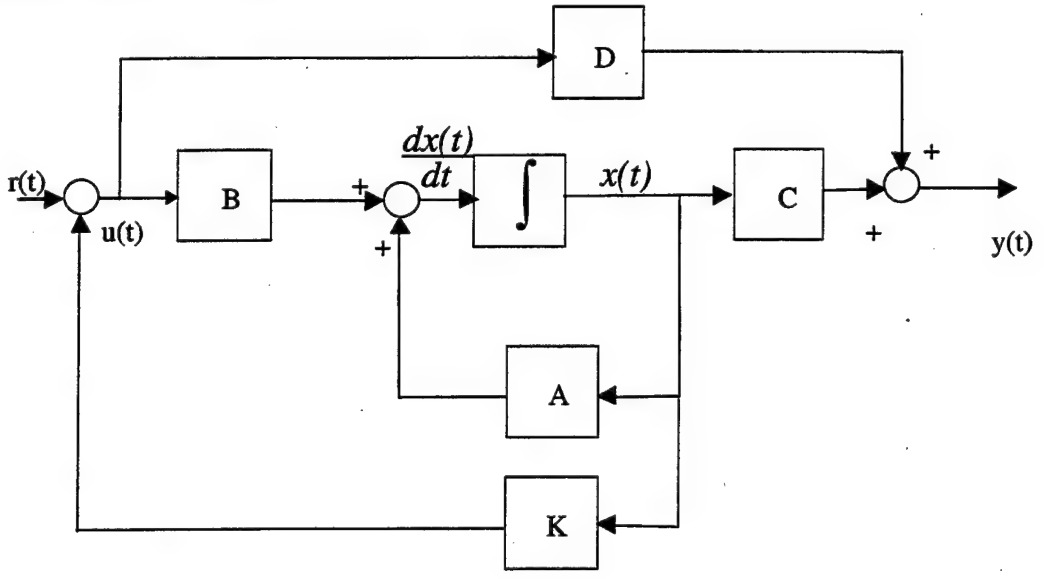

Figure 5.4 Block Diagram of Closed-Loop State-Space System with LSF

If a unique positive definite solution to the steady-state matrix Riccati equation,

$$\boldsymbol{Q} - \boldsymbol{P}\boldsymbol{B}\boldsymbol{R}^{-1}\boldsymbol{B}^T\boldsymbol{P} + \boldsymbol{P}\boldsymbol{A} + \boldsymbol{A}^T\boldsymbol{P} = \boldsymbol{0}\,, \tag{5.5}$$

represented by $\boldsymbol{P}$, existed, then the LSF control law in Equation 5.4 results in the minimization of J_{LQR}. The minimization of J_{LQR} implies a desire to minimize both excessive output excursions and the control effort required to prevent such excursions. The adjustable weights $\boldsymbol{M}$, $\boldsymbol{Q}$, and $\boldsymbol{R}$ can be used to obtain an appropriate compromise between these two conflicting goals. The optimal control for this problem then becomes

$$u(t) = -\boldsymbol{R}^{-1}\boldsymbol{B}^{T}\boldsymbol{P}\boldsymbol{x}(t). \tag{5.6}$$

Use of LQR control results in the optimal gain K and optimal pole positions. This method works for time-invariant or time-varying systems and is just as easy for MIMO systems as for SISO systems. Like the classical control methods previously discussed however, this control method is a feedback approach which attempts to tailor the system response while not specifically rejecting a disturbance. However, if the state dynamics matrix is augmented, to include the internal states of the disturbance signal, the disturbance can be rejected.

2. LQR Control with Disturbance Feedforward

Given the state-space equation of the system,

$$\dot{\boldsymbol{x}} = \boldsymbol{A}\boldsymbol{x} + \boldsymbol{B}\boldsymbol{u} + \boldsymbol{F}_{d}\boldsymbol{d} \tag{5.7}$$

if $\boldsymbol{B}$ and $\boldsymbol{F}$ are collinear, then the system can be rewritten as

$$\dot{\boldsymbol{x}} = \boldsymbol{A}\boldsymbol{x} + \boldsymbol{B}(\boldsymbol{u} + \alpha\boldsymbol{d}), \tag{5.8}$$

and the control law can be written in the form

$$u = -\boldsymbol{K}\boldsymbol{x} - \alpha\boldsymbol{d}, \tag{5.9}$$

as long as the disturbance is measurable.

However, if $\boldsymbol{B}$ and $\boldsymbol{F}$ are not collinear, then direct feedforward cannot be used and a disturbance estimator must be employed. With this approach, the state space system must be augmented with a disturbance model, and a controller designed based on this augmented system. With a design of this form, the LQR controller can account for the effects of the unwanted input. This can be done only when some assumptions about the form of the disturbance model can be made.

The disturbance state z, with internal dynamics $\boldsymbol{A}_{d}$, may be represented by

$$\dot{\boldsymbol{z}} = \boldsymbol{A}_{d}\boldsymbol{z}, \tag{5.10}$$

where

$$\boldsymbol{d} = \boldsymbol{C}_d \boldsymbol{z}. \tag{5.11}$$

Augmenting the system states, x, with the disturbance states, z, yields the following state space equation

$$\begin{bmatrix} \dot{\boldsymbol{x}}(t) \\ \dot{\boldsymbol{z}}(t) \end{bmatrix} = \begin{bmatrix} \boldsymbol{A} & \boldsymbol{F}_d \boldsymbol{C}_d \\ \boldsymbol{0} & \boldsymbol{A}_d \end{bmatrix} \begin{bmatrix} \boldsymbol{x}(t) \\ \boldsymbol{z}(t) \end{bmatrix} + \begin{bmatrix} \boldsymbol{B} \\ \boldsymbol{0} \end{bmatrix} \boldsymbol{u}(t), \tag{5.12}$$

which may be expressed compactly as

$$\dot{\boldsymbol{x}}_a(t) = \boldsymbol{A}_a \boldsymbol{x}_a(t) + \boldsymbol{B}_a \boldsymbol{u}(t) + \boldsymbol{w};\ \boldsymbol{u} = -\boldsymbol{K}_1 \boldsymbol{x} - \boldsymbol{K}_2 \boldsymbol{z}, \tag{5.13}$$

with $\boldsymbol{K}_1$ and $\boldsymbol{K}_2$ representing the feedback and feedforward gains, respectively.

With the disturbance dynamics included in the state dynamics matrix, the cost function, J_{LQR}, is minimized to determine a new set of gains based on the augmented system. A disturbance state estimator is necessary to provide the internal disturbance states and the LQR controller uses these estimated states in the state feedback loop. Figure 5.5 depicts this system. Note, that the augmentation of the states has no effect on the dynamics of the disturbance estimator since it is uncontrollable from $u(t)$. The disturbance state estimation is driven by measurements from the output or disturbance as available. With the formulation shown in Equation 5.13 the effects of the disturbance can be reduced, and in theory cancelled if a perfect disturbance model is available.

To this point, the control methods discussed have been based on linear or linearized systems. The ability to use these tools for the design of controllers that will be used on nonlinear systems is some what limited. In general, the linear systems may not very robust to model mismatch which can result in system instabilities, although, robustness measures can be implemented into the design process by H_2/H_∞ and LMI techniques, [Silvestre 1998a,b].

3. Nonlinear Methods

In nonlinear control, the concept of feedback plays a fundamental role in controller design, as it does in linear control. However, the importance of feedforward is much more marked than in linear control. Feedforward is used to cancel the effects of known disturbances and provide anticipatory corrections in tracking behavior. Very

often, it is impossible to control a nonlinear system without feedforward compensation. Note that a model of the plant is always required for feedforward compensation, although this model need not be very accurate.

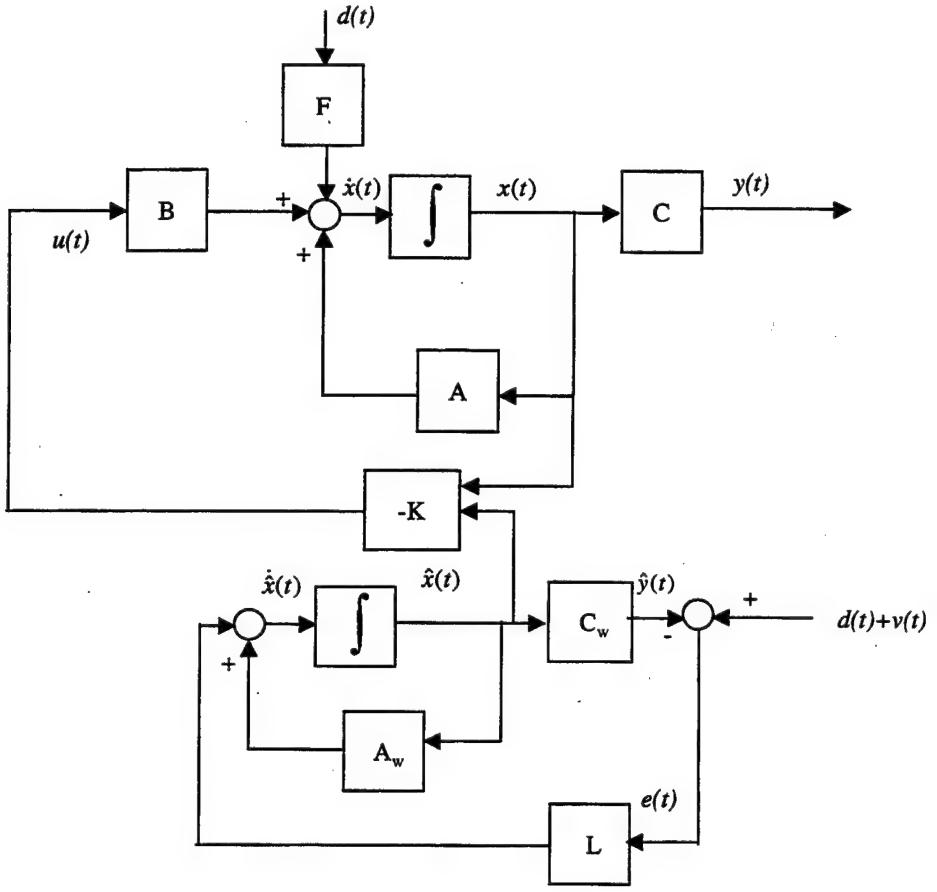

Figure 5.5 Block Diagram of Closed-Loop State-Space System with LSF and Estimated Disturbance Feedforward

There is no general method for the design of nonlinear controllers. What is available to the designer is a collection of tools that are applicable to particular classes of nonlinear control problems. These nonlinear design tools can be placed in one of five categories: Trial-and-error, Feedback/Input Linearization, Adaptive Control, Robust or Sliding Mode Control and Gain-scheduling. Unlike the linear control discussion, the sections that follow will briefly discuss some of the salient points of these techniques. For further detailed information on each of these design tools, the reader is referred to [Slotine and Li 1991].

Trial-and-error can be used to develop controllers. This method is similar in approach to linear lead-lag compensator design using Bode plots. The goal is to use analysis tools, (i.e., phase plane, describing function, Lyapunov analysis), to assist in the search for a control solution that can be qualified by analysis and simulation. Experience plays a major role in this technique, which, for complex system typically fails.

Feedback linearization deals with techniques for transforming complex models into equivalent models of a simpler form, [Slotine and Li 1991]. In this nonlinear design methodology, the idea is to first transform the nonlinear system into a full or partially linear system. Once this has been done, then any of the linear design tools may be used to develop the necessary control system. Two draw backs of this method are that it typically requires full state feedback and it is not very robust to parametric uncertainty or disturbances. These draw backs can be overcome by the use of either robust or adaptive control methods.

For uncertain or time varying systems adaptive control is very useful. Current adaptive control design applies mainly to systems that have well known dynamics, but unknown or slowly varying parameters. Adaptive controllers, whether developed for linear or nonlinear systems are inherently nonlinear. For nonlinear systems, adaptive control can be viewed as an alternative to robust nonlinear control.

Robust nonlinear control techniques have proven very effective in a variety of practical control problems, [Healey 1993, Marco 1996, Yoeger 1991, Young 1996]. The controller is designed based on consideration of both the nominal model, and some characterization of the uncertainties associated with the model. Sliding Mode Control provides a systematic approach to the problem of maintaining stability and performance in the presence of modeling inprecisions.

Gain scheduling is an attempt to apply linear control methods to the control of nonlinear systems. It was originally developed by the aircraft industry for the control of high precision aircraft. The idea is to select a number of typical operating points which cover the systems range of operation. The plant is then linearized and a controller designed for each of these points. Between operating points, the gains of the compensator are scheduled resulting in a global controller. The main problems with gain

scheduling is that it has only limited stability guarantees for nonlinear operations, and the computational burden of computing many linear controllers.

D. CASE STUDIES IN DISTURBANCE REJECTION

This section will present and discuss three distinct cases of disturbance rejection for three different disturbance inputs. The performance of each of the control designs will be evaluated by using the nonlinear EOM, Equation 2.94, in simulation studies. During the simulations, each control design will be subjected to a simple harmonic disturbance input, a PM spectrum based disturbance input and real disturbance data obtained from Monterey Bay. Sample data records for each of these disturbance inputs are shown in Figure 5.6.

The three cases are summarized below:

- Case I: High Gain LQR Control. Equation 2.94 will be linearized around a nominal operating point. Based on this linearized model the control gains for a full state feedback controller are calculated using a LQR method.

- Case II: LQR Control With Estimated Disturbance Feedforward. Employing the linearized model from Case I, the system is augmented with an AR model representing the disturbance dynamics. The augmented system is used to calculate the control gains, and the AR model is used as a basis for a disturbance estimator. This controller uses full state feedback, with estimated disturbance state feedforward in the control calculation.

- Case III: Sliding Mode Control (SMC) With Measured Disturbance Feedforward. A model based sliding mode controller will be developed which embeds the disturbance in the control formulation. This controller relies on full state feedback with measured disturbance feedforward.

1. Case I. High Gain LQR Control

Using the 1 DOF surge EOM as a model, it is necessary to linearize this system of equations in order to use linear techniques in the controller design. Linearization can be performed a with a variety of approaches, stochastic [Leira 1987], harmonic [Heyns 1995] or nominal operating, pointwise linearization, condition [Riedel 1998a], but for this design, since the control law will attempt to allow an AUV to hold position

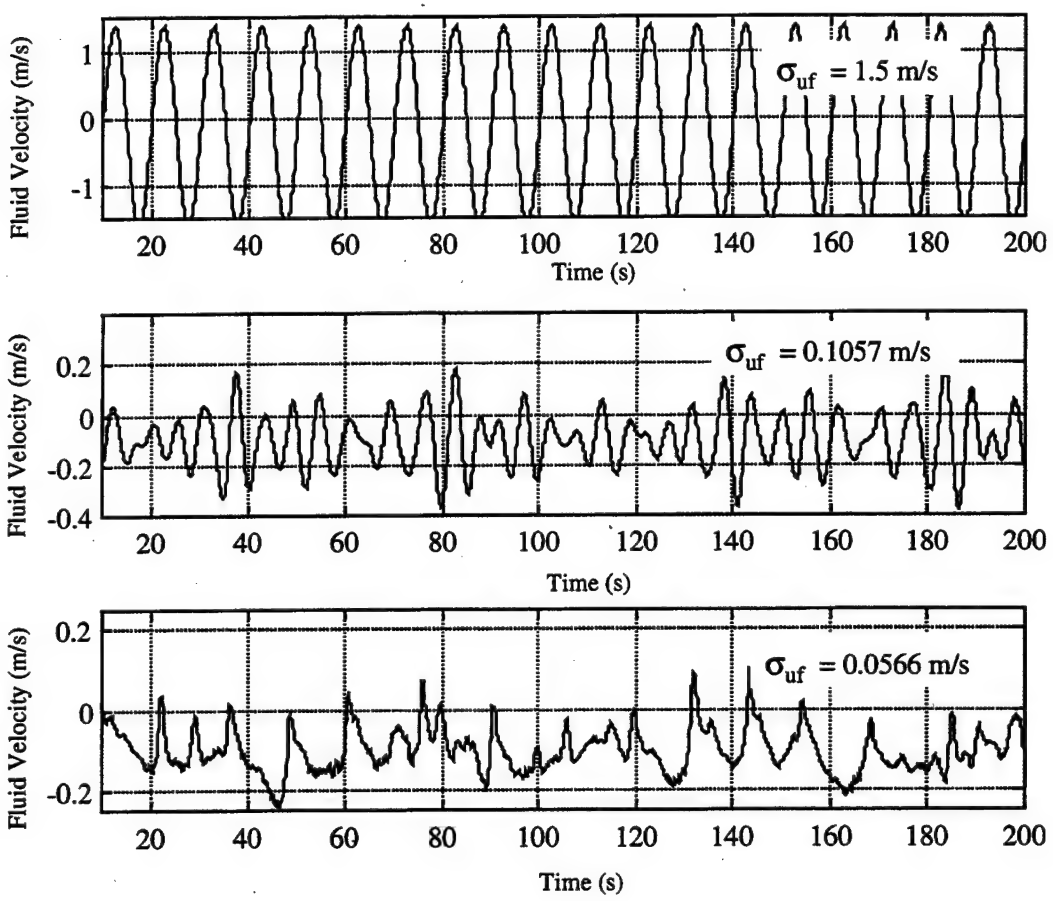

Figure 5.6 Sample Disturbance Input Time Series

with zero ground velocity, the system is linearized about the steady state solution to Equation 2.94 while in the presence of a steady current. Performing this steady state analysis yields,

$$u_{r,o} = -U_{cx}$$

$$F_{prop,o} = \alpha U_{cx}^2 \qquad , \qquad (5.14)$$

$$n_o = \begin{cases} \dfrac{-\dfrac{\gamma}{\beta}u_o \pm \sqrt{\left(\dfrac{\gamma}{\beta}u_o\right)^2 - 4\left(\dfrac{-F_o}{\beta}\right)}}{2} & u_0, n_o > 0 \\ \dfrac{-\dfrac{\gamma}{\beta}u_o \pm \sqrt{\left(\dfrac{\gamma}{\beta}u_o\right)^2 - 4\left(\dfrac{F_o}{\beta}\right)}}{2} & u_0, n_o < 0 \end{cases}$$

as the nominal operating point, where n_o must be real and the same sign as $u_{r,o}$. Using a standard Taylor series linearization, the linearized system of equations, in state space from, can then be written as

$$\begin{bmatrix} \dot{x} \\ \dot{u}_r \\ \dot{F} \end{bmatrix} = \begin{bmatrix} 0 & 1 & 0 \\ 0 & 2\alpha \operatorname{sgn}(u_{r,o})u_{r,o} & 1 \\ 0 & \frac{\gamma}{\tau}|n_o| & \frac{-1}{\tau} \end{bmatrix} \begin{bmatrix} x \\ u_r \\ F \end{bmatrix} + \begin{bmatrix} 0 \\ 0 \\ \frac{\gamma}{\tau}u_{r,o}sign(n_o) + 2\frac{\beta}{\tau}\operatorname{sgn}(n_o)n_o \end{bmatrix} n + \begin{bmatrix} 1 \\ 0 \\ 0 \end{bmatrix} u_f$$

$$y = \begin{bmatrix} 1 & 0 & 0 \\ 0 & 1 & 0 \\ 0 & 0 & 1 \end{bmatrix} \begin{bmatrix} x \\ u_r \\ F \end{bmatrix} \tag{5.15}$$

If it is assumed that the vehicle will be operating in a -0.1 m/s steady current, and the parameters α, β, γ and τ are available then Equation 5.15 can be evaluated numerically.

Since the parameters identified in Chapter IV were obtained from a discrete filter, and it is desired to implement the to be developed control law in a digital computer, the state space equations must be converted into a discrete form. Using a standard Euler discretization, Equation 5.15 can be represented in discrete form as

$$\begin{bmatrix} x(k+1) \\ u_r(k+1) \\ F(k+1) \end{bmatrix} = \begin{bmatrix} 0 & dt & 0 \\ 0 & 1-2\alpha \operatorname{sgn}(u_{r,o})u_{r,o}dt & dt \\ 0 & \frac{\gamma}{\tau}|n_o|dt & 1-\frac{-1}{\tau}dt \end{bmatrix} \begin{bmatrix} x(k) \\ u_r(k) \\ F(k) \end{bmatrix} + \ldots$$

$$\begin{bmatrix} 0 \\ 0 \\ (\frac{\gamma}{\tau}u_{r,o}sign(n_o) + 2\frac{\beta}{\tau}\operatorname{sgn}(n_o)n_o)dt \end{bmatrix} n(k) + \begin{bmatrix} dt \\ 0 \\ 0 \end{bmatrix} u_f(k). \tag{5.16}$$

$$y(k) = \begin{bmatrix} 1 & 0 & 0 \\ 0 & 1 & 0 \\ 0 & 0 & 1 \end{bmatrix} \begin{bmatrix} x(k) \\ u_r(k) \\ F(k) \end{bmatrix}$$

Using standard optimal control techniques the solution for the optimal (LQR) controller can be found as

$$n = -\boldsymbol{R}^{-1}\boldsymbol{B}^{T}\boldsymbol{S}\boldsymbol{x} \tag{5.17}$$

where $\boldsymbol{S}$ is found by solving the steady state algebraic Riccati equation (ARE)

$$\boldsymbol{A}^{T}\boldsymbol{S} + \boldsymbol{S}\boldsymbol{A} - \boldsymbol{S}\boldsymbol{B}\boldsymbol{R}^{-1}\boldsymbol{B}^{T}\boldsymbol{S} + \boldsymbol{Q} = \boldsymbol{0}\,, \tag{5.18}$$

for the positive definite matrix $\boldsymbol{S}$. In Equation 5.26, $\boldsymbol{Q}$ is the weighting matrix on the state error, and R is the weighting scalar, since this is a single input system, that invokes a penalty against the control effort. The LQR approach will always yield a stable system, as long as the Riccati equation provides a positive definite solution matrix $\boldsymbol{S}$, for which the system must be controllable and full state feedback available.

The following sections will show the simulated performance of the LQR controller when subjected to various disturbance inputs. The purpose of the simulations in these sub-cases is to provide a baseline by which to compare the performance the controllers developed in Cases II and III.

a) Monochromatic Disturbance Input (Case Ia)

Using the sine wave disturbance input depicted in Figure 5.6, the LQR controller was formulated and simulated for various control weighting values (R). A plot of the position response for one of these simulations is shown is Figure 5.7. This response, the "best" of the many simulations, is the result of a high gain controller. As can be seen, the oscillations about the commanded position (0 meters) are significant and poor disturbance rejection is obtained. In addition, there is an obvious offset caused by the mean disturbance. This offset can be corrected by incorporating integral control into the LQR design, however, integral control will not correct the severe positional oscillations.

During these simulations, the propellers were not limited, i.e., no saturation. The control input necessary to obtain the positioning shown in Figure 5.7 is displayed in Figure 5.8. As shown is this figure, the propeller oscillations are extreme considering that the model and parameters used in the simulations are based on the NPS Phoenix AUV which has a maximum propeller revolution of 800 rpm. Once again, it must be pointed out that the purpose of the studies in Case I is to obtain a baseline for comparison.

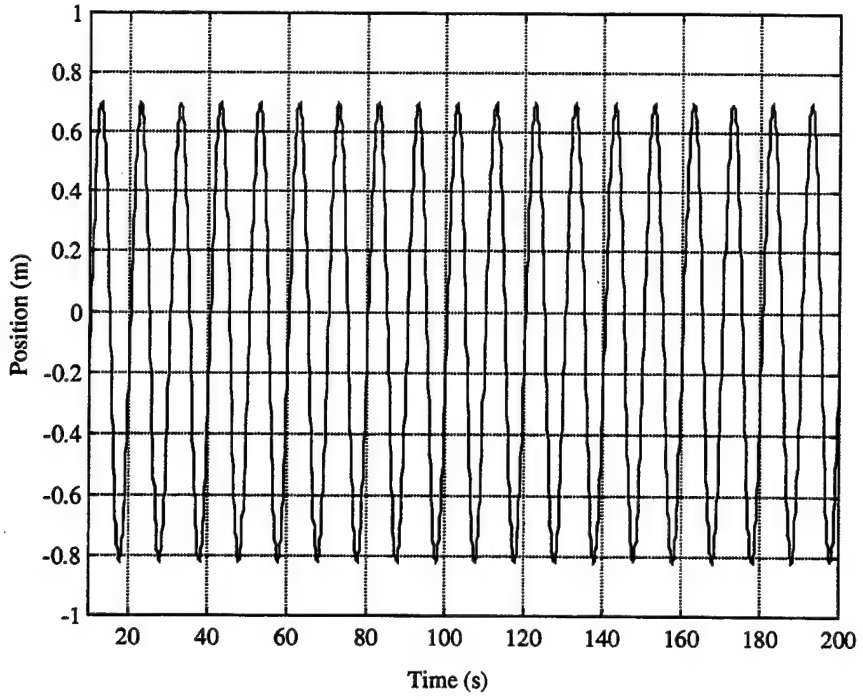

Figure 5.7 Position Response for Case Ia with Monochromatic Disturbance Input

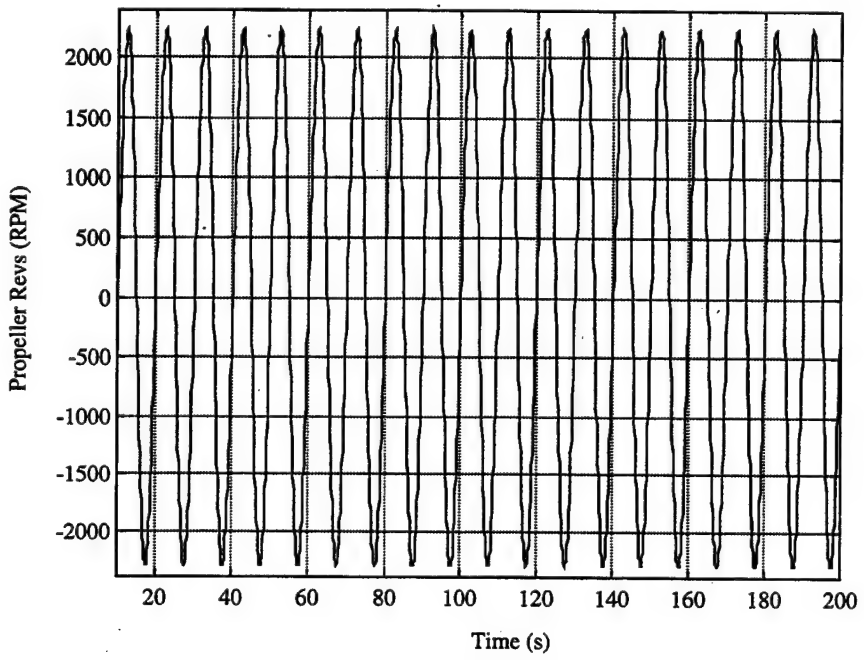

Figure 5.8 Propeller Response for Case Ia with Monochromatic Disturbance Input

b) PM Spectrum Based Disturbance Input

Using the same three state model as with Case Ia, simulation studies using a PM spectrum based disturbance input were conducted. The input disturbance was based on a significant wave height of 1 meter in a water depth of 45 meters. The vehicle was assumed to be operating at a 25 meter depth. The goal of this simulation study was to determine the control performance based on a disturbance input which contained a range of frequencies which the vehicle may encounter.

Using the controller design resulting in the responses displayed in Figures 5.7 and 5.8, a simulation was conducted resulting in the position response shown in Figure 5.9. In this particular simulation, the standard deviation of the position response is significantly reduced due to the magnitude of the disturbance input. Comparing disturbance inputs between Cases Ia and Ib, it can be seen that the magnitude of the PM

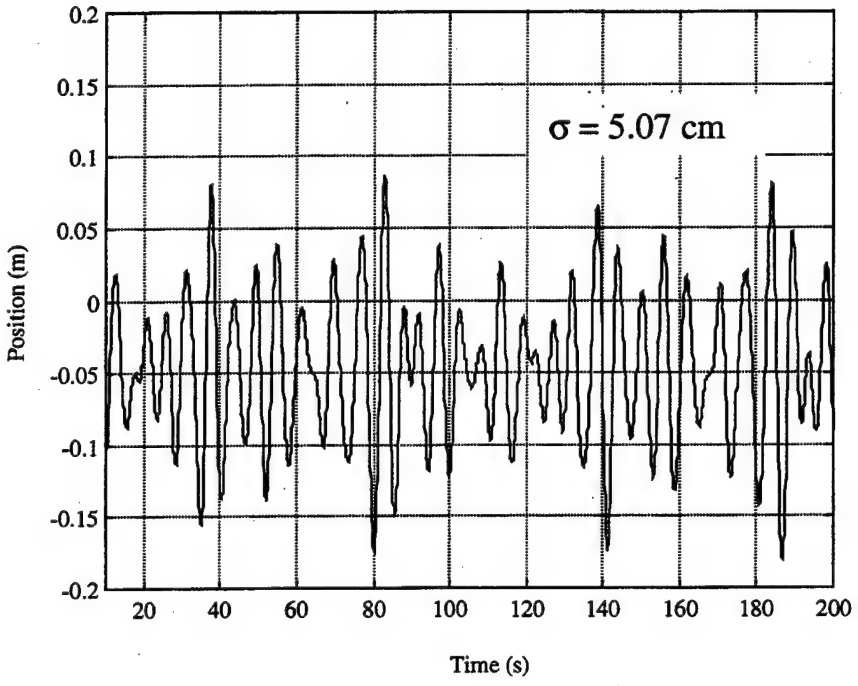

Figure 5.9 Position Response for Case Ib with PM Spectrum Based Disturbance Input

based disturbance is 15 times less than that of the monochromatic disturbance. This reduction in oscillation magnitude is also reflected when comparing position responses.

The propeller input response shown in Figure 5.10, is also significantly less, but still exceeds the maximum propulsion system input of 800 rpm.

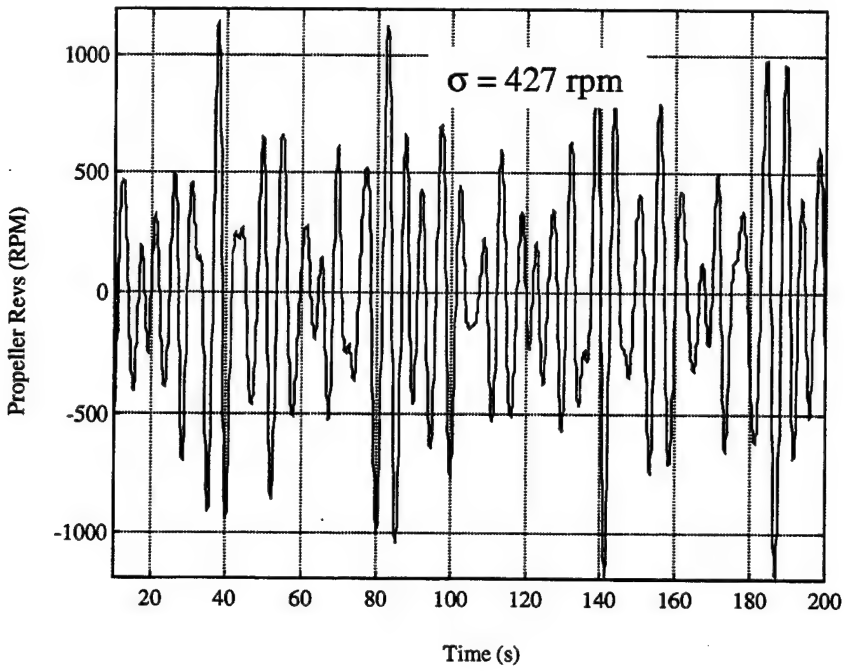

Figure 5.10 Propeller Response for Case Ib with PM Based Disturbance Input

c) Monterey Bay Disturbance Input

Using the control design that resulted in the responses displayed in Figures 5.7-5.10, a third set of simulations was conducted. In this set of simulations, transformed wave buoy data obtained in Monterey Bay, CA was used as the disturbance input. This data was obtained from a Datawell® Waverider Buoy deployed April 9, 1998, from the research vessel R/V POINT SUR, during an NPS oceanography class (OC4610) cruise, under the direction of Prof. Thomas Herbers.

The wave buoy, according to Defense Mapping Agency navigation charts, was deployed in approximately 45 meters of water. The wave elevation data obtained from the buoy was transformed to a subsurface velocity record, at a depth of 25 meters, using the procedure outlined in Chapter IV. A sample of the resulting time series, with a -0.1 m/s steady current superimposed, was displayed in Figure 5.6

The position response using this input disturbance is shown in Figure 5.11. The standard deviation of this response is approximately one-half of the response obtained from the PM based disturbance input with the same control design. Once again, this is due to the fact that the standard deviation of the Monterey Bay input disturbance is about one-half the PM disturbance.

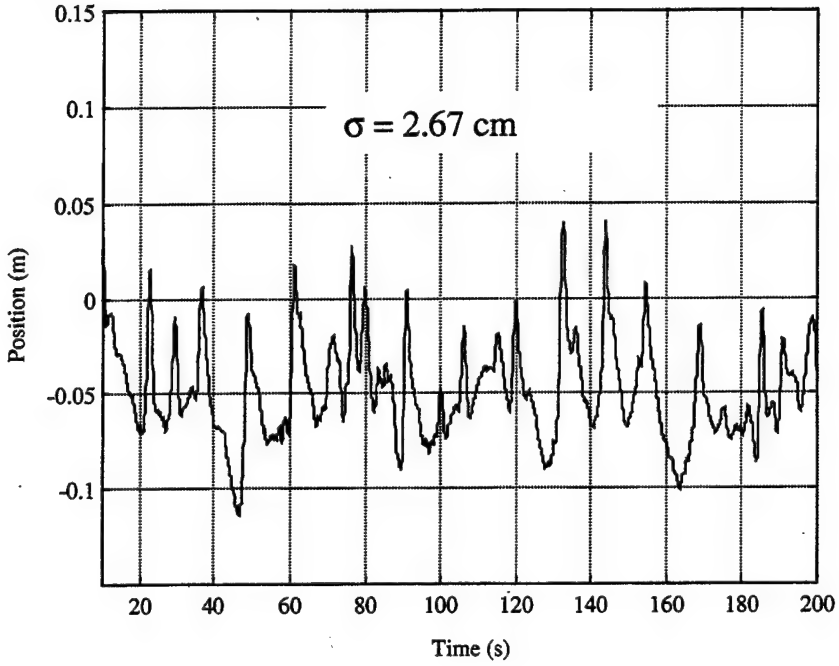

Figure 5.11 Position Response for Case Ic with Monterey Bay Disturbance Input

It is interesting to note, that although the position response reduced by a factor of two, when compared to the PM based case, the propeller input response did not, see Figure 5.12. This is due to the fact that the frequency content of the input disturbances is much different. This is evident by referring back to Figure 5.6. The Bay data contains more high frequency components causing the propulsion system to respond much more.

Since the propulsion system response is still in excess of maximum output, tuning of the controller gains must be performed to bring the propeller rpms within limits. By adjusting the input weighting scalar R, and reducing the controller gains the maximum commanded propeller revolutions can be reduced as well as reducing the sensitivity of the controller to high frequency "noise." This reduction of propeller input is at the

expense of increased position error. These results are shown in Figures 5.13 and 5.14. As shown in Figure 5.13, the standard deviation has increased by a factor of two in order to keep the propeller revolutions within propulsion system limits.

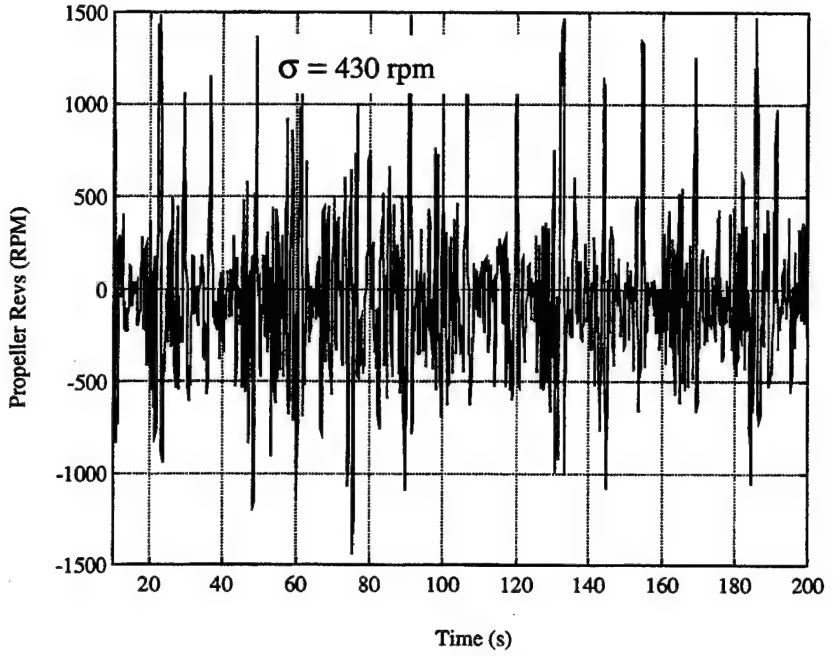

Figure 5.12 Propeller Response for Case Ic, Monterey Bay Disturbance Input

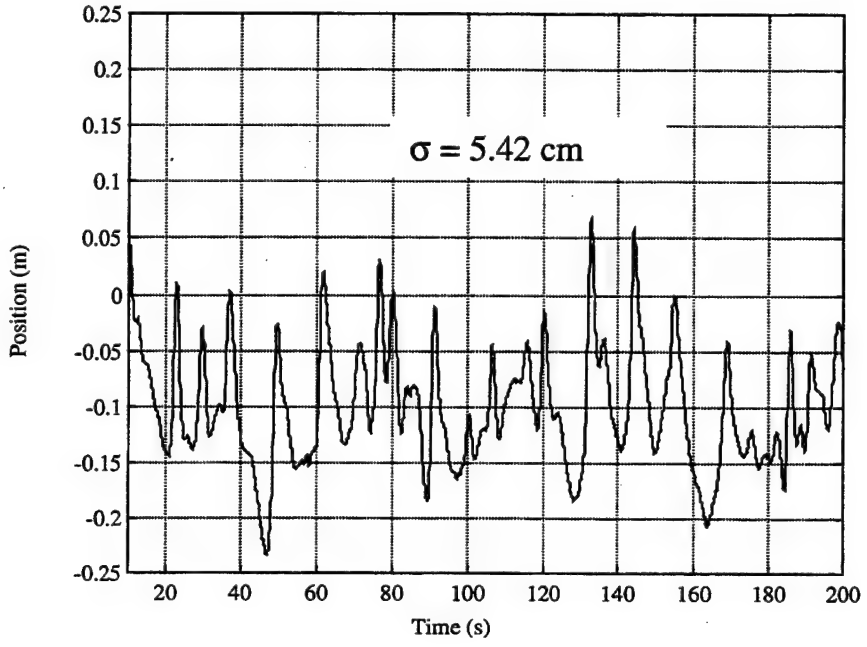

Figure 5.13 Position Response for Case Ic, Monterey Bay Disturbance Input

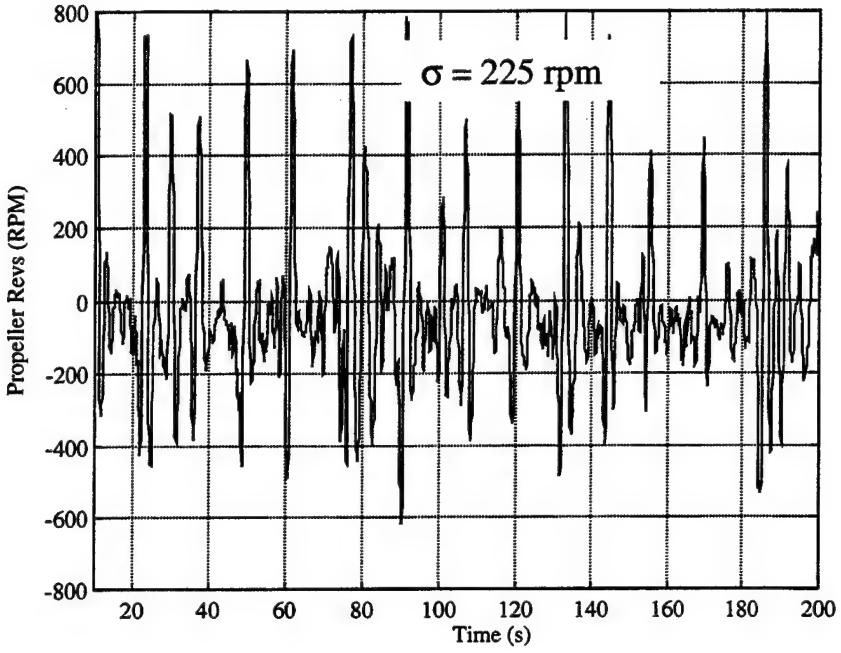

Figure 5.14 Propeller Response for Case Ic, Monterey Bay Disturbance Input, rpms Within Design Limits

Figure 5.15 shows graphically the relationship between the level of control input and the level of disturbance rejection for the standard LQR solution subjected to real wave data from Monterey Bay. The position covariance is normalized by the covariance of the "free floating" or uncontrolled response of the vehicle, and the input covariance is normalized by the maximum rpm available from the propellers. This analysis can give a "feel" for how tight a control law must be provided to achieve a reasonable disturbance rejection.

2. Case II. LQR Control with Disturbance Estimation Feedforward

The problem that now must be addressed is how to achieve better performance. It has been shown , that by embedding an estimator of the disturbance into the control system design, improved performance may be obtained [Grimble 1995, Riedel 1998a].

As outlined in Chapter III, an AR model of the wave disturbance may be written in state space form as

$$\begin{aligned} X_w(k+1) &= A_w X_w(k) + B_w v(k) \\ y_w(k) &= u_f(k) = C_w X_w(k) \end{aligned} \tag{5.19}$$

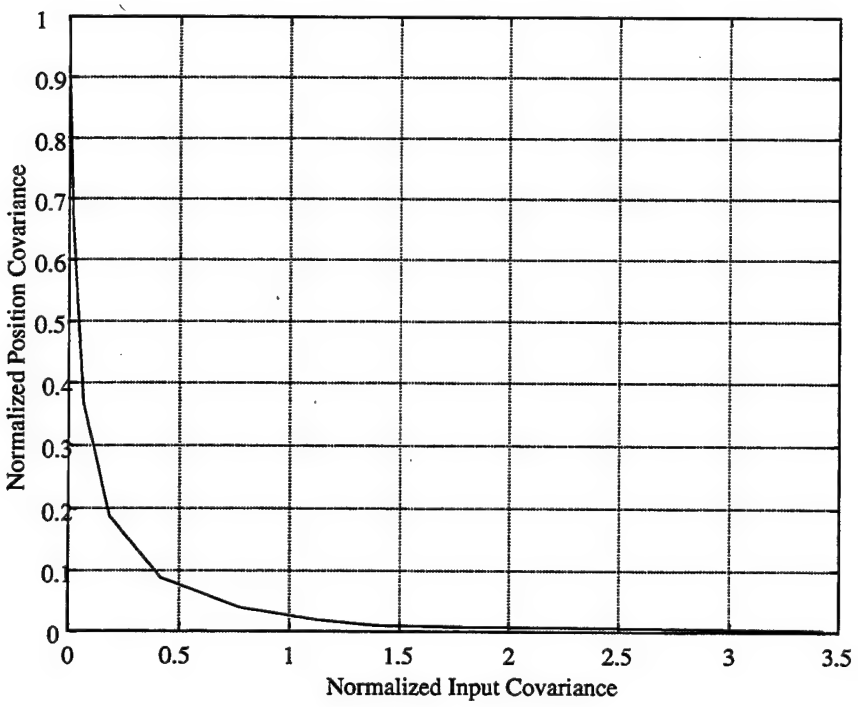

Figure 5.15 Comparison Of Control Input Covariance To Normalized Vehicle Position Covariance, Monterey Bay Wave Data

Augmenting the vehicle state equations with the disturbance state equations, a new control law may be developed using the estimated disturbance states. Defining the new state vector as

$$X_{aug} = \begin{bmatrix} X_{vehicle} \\ X_w \end{bmatrix}, \tag{5.20}$$

where the disturbance states are given as

$$X_w = [X_w(k+N-1),\ldots,X_w(k+1)]^T , \tag{5.21}$$

the new control law may be designed, using the separation principle, assuming all states are measurable. As in the previous optimal control discussion (Case I), the ARE is solved to obtain the appropriate gains for the augmented system. This augmented system is represented by

$$X_{aug}(k+1) = \begin{bmatrix} A_{vehicle} & FC_w \\ 0 & A_w \end{bmatrix} X_{aug}(k) + \begin{bmatrix} B_{vehicle} \\ 0 \end{bmatrix} n(k) + \begin{bmatrix} 0 \\ B_w \end{bmatrix} v(k) . \tag{5.22}$$

With the control law determined, the estimator must be designed. Using optimal estimation theory, an estimator of the form

$$\hat{X}_w(k+1) = (A_w - LC_w)\hat{X}_w(k) + Lu_f(k), \tag{5.23}$$

where $u_f(k)$ is the current disturbance measurement, is developed. This estimator is used in conjunction with the control law developed, and its implementation, in block diagram form, is represented by Figure 5.5.

a) Monochromatic Disturbance Input

To display how well this design procedure can work if an accurate model of the disturbance is available, consider the case of the monochromatic input disturbance. Since the precise model of this disturbance is known, when this model is embedded in the control system design, perfect cancellation of the wave disturbance effects on vehicle positioning may be obtained. These results are displayed in Figures 5.16 and 5.17. Now these results are for demonstration purposes only, and perfect cancellation of the wave disturbances will not be possible since an exact model of the random sea is not available.

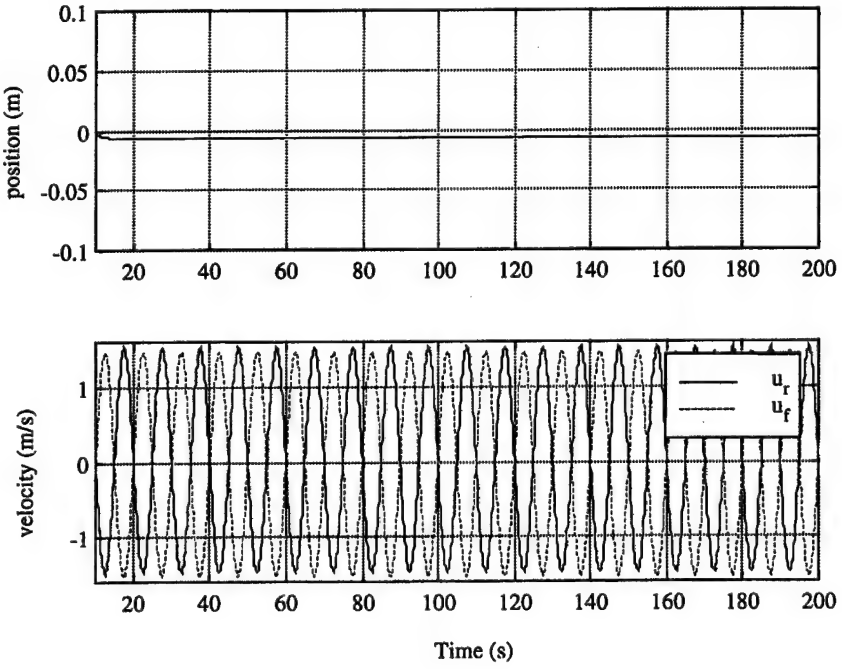

Figure 5.16 Position Response for Case IIa, Monochromatic Disturbance Input

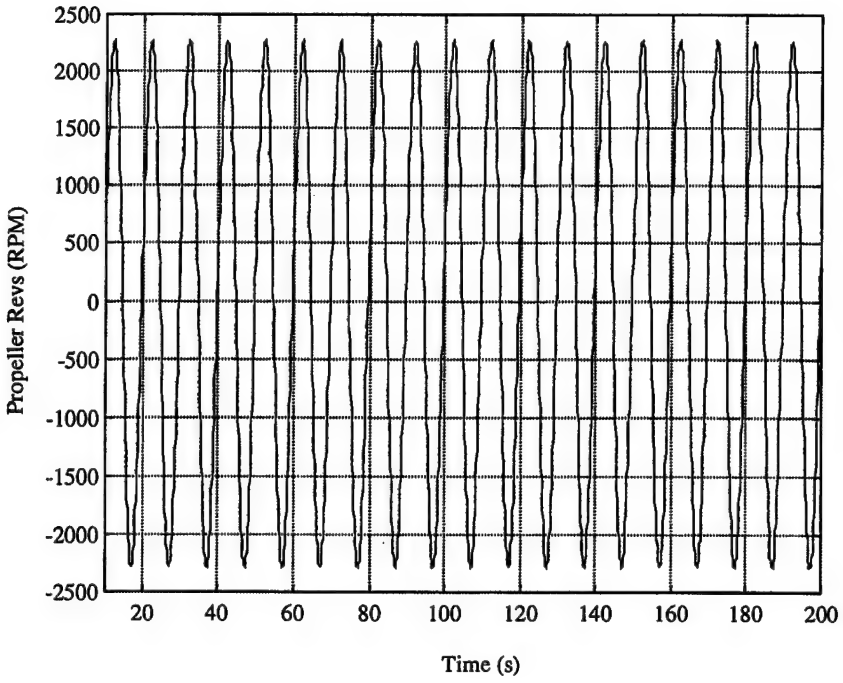

Figure 5.17 Propeller Response Case IIa, Monochromatic Disturbance Input

Although the propeller response is almost identical to the results displayed in Case Ia (Figure 5.8), by having an estimate of the disturbance states to feedforward the propeller input is properly phased to cancel the disturbance.

b) PM Spectrum Based Disturbance Input

Using this approach of a model based disturbance estimator with a LQR controller appears to be an excellent method of canceling the disturbances acting on an underwater vehicle, that is if the model of the disturbance is known. If the exact model of the disturbance is not known, the question is; Is improved disturbance rejection with this method possible?

Adopting the AR modeling techniques presented in Chapter IV, a sixth order AR model for the PM based disturbance was developed. Using this linear model of the disturbance dynamics and the same input weighting scalar as was used in Case Ib, a combined controller/estimator was developed. Using this developed compensator in simulation, improved performance was observed, see Figure 5.18. The position response with the augmented disturbance model improves by a factor of 1.5.

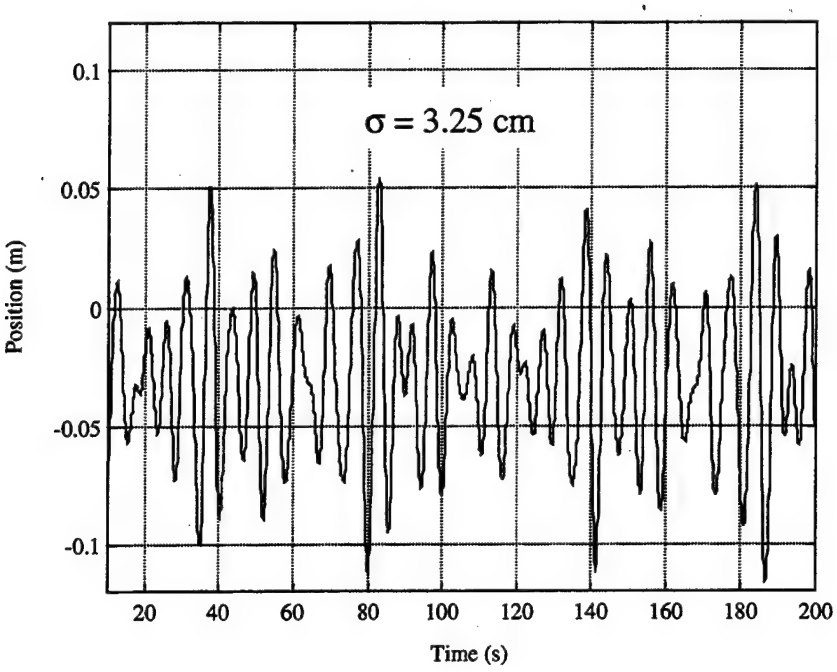

Figure 5.18 Position Response for Case IIb, PM Based Disturbance Input

The improvement in propeller input follows the trend displayed in the comparison between Cases Ia and IIa. The standard deviation of the input response has not changed significantly, as evident in comparisons between Figures 5.19 and 5.10. What has changed is the control input phasing, again due to the disturbance feedforward, thus allowing this design method, even with a low order disturbance model, to obtain improved disturbance rejection.

c) Monterey Bay Disturbance Input

Using identical weighting values that went into the design of the control laws used in the simulations presented in Case Ic, Figures 5.11-5.14, and a sixth-order AR model representing the Monterey Bay disturbance, improved performance was again realized. As can be seen in Figure 5.20, there is a 150% improvement in station keeping as compared Case Ic, and the control input requirements are significantly less, see Figure 5.21. Although the standard deviation of the commanded control input is well within the maximum revolutions able to be provided by the propulsion system, there are some inputs which exceed the limit of 800 rpm. In order to bring the commanded control input within limits, as before, the control gain must be reduced.

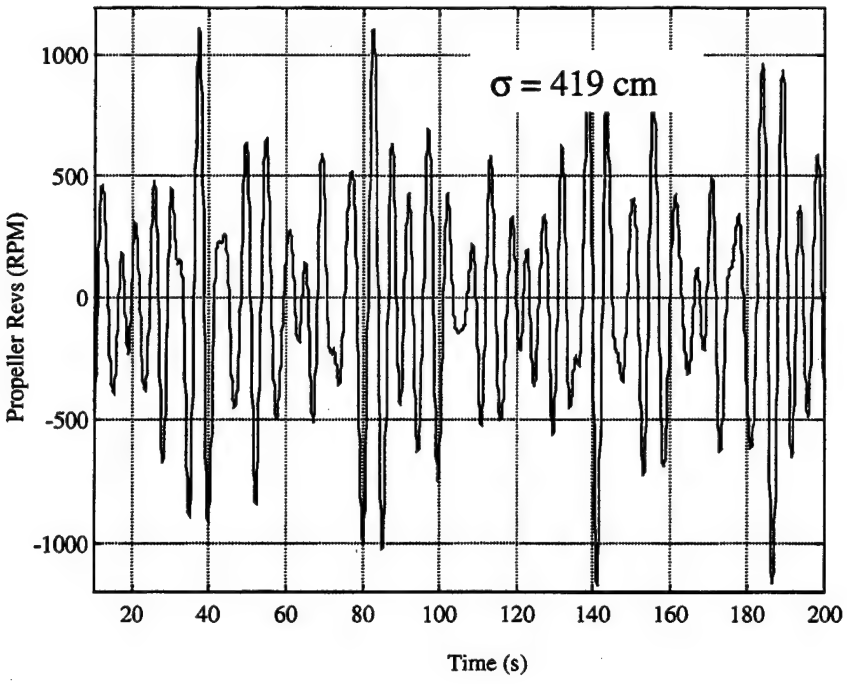

Figure 5.19 Propeller Response for Case IIb, PM Based Disturbance Input

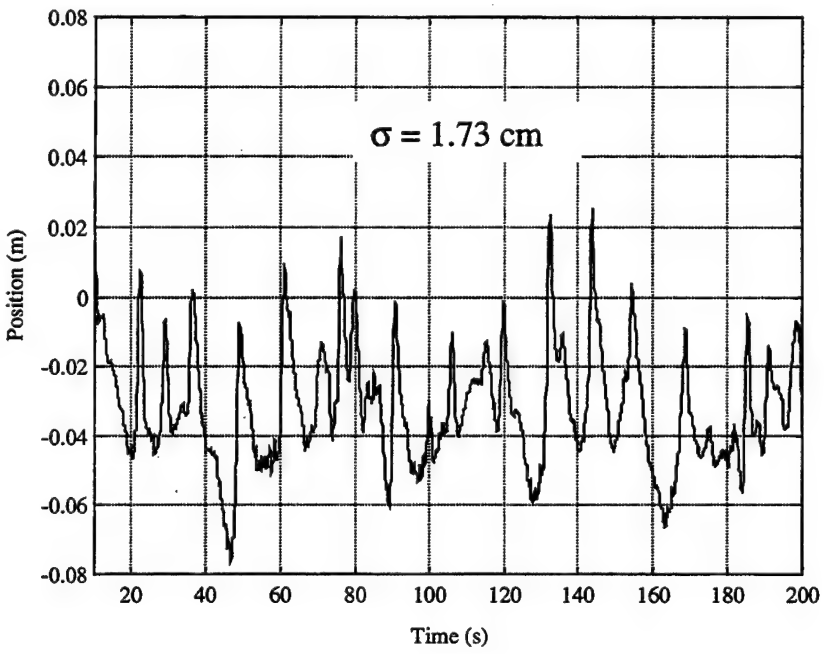

Figure 5.20 Position Response for Case IIc, Monterey Bay Disturbance Input

With the control gains adjusted so that the commanded control input remained within propulsion system limits, the positional error increased by a factor of two, while

the control input reduced by a factor of three The results of this tuning are shown in Figures 5.22 and 5.23. This reduction in control effort is particularly important given the fact that power consumption is the downfall of AUVs.

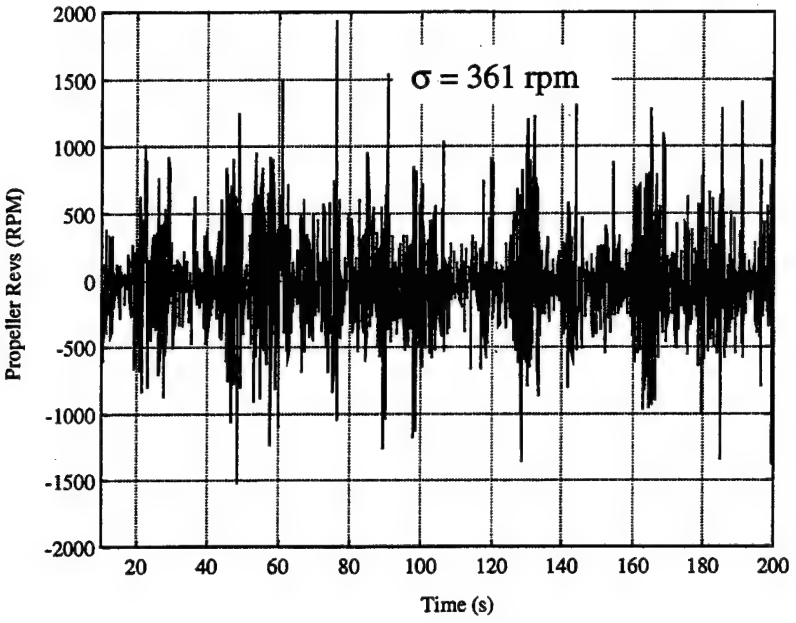

Figure 5.21 Propeller Response for Case IIc, Monterey Bay Disturbance Input

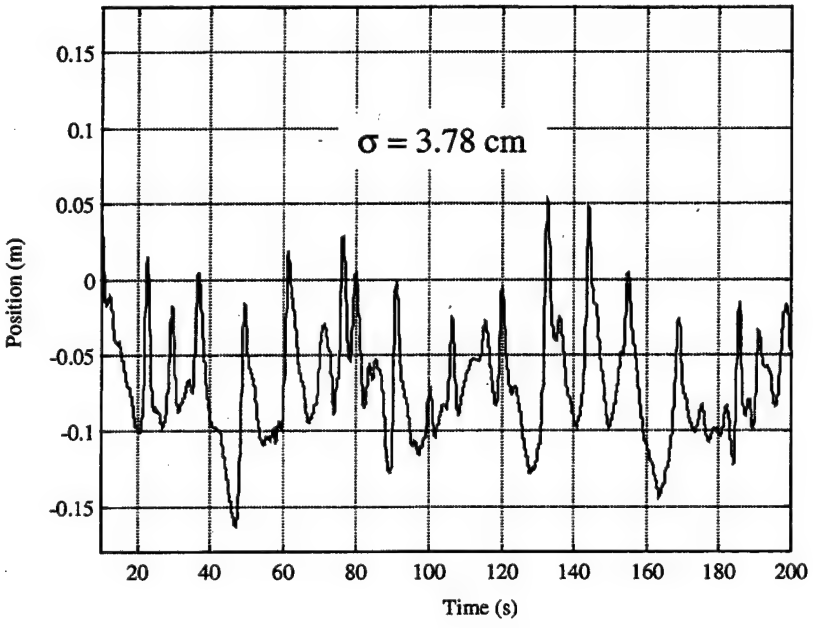

Figure 5.22 Position Response for Case IIc, Monterey Bay Disturbance Input, rpms Within Design Limits

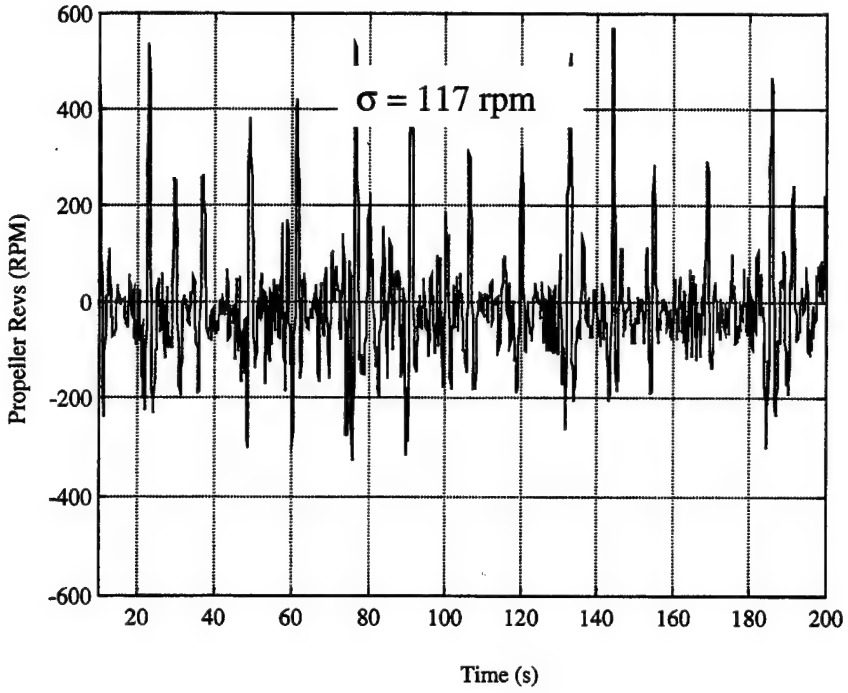

Figure 5.23 Propeller Response for Case IIc, Monterey Bay Disturbance Input, rpms Within Design Limits

3. Case III. Sliding Mode Control with Measured Disturbance Feedforward

Beginning with Equation 2.94, a sliding mode controller was formulated using standard SMC techniques, [Slotine 1991]. The sliding surface σ was defined as a function of the position error,

$$\sigma = \left(\frac{d}{dt} + \lambda\right)^2 (x - x_{com}), \tag{5.24}$$

and the time derivative of σ was defined as

$$\dot{\sigma} = -\eta sat(\sigma / \phi). \tag{5.25}$$

By defining the sliding surface in this manner, stability is guaranteed, based on Lyapunov analysis, since

$$\sigma\dot{\sigma} < 0, \quad \forall\, t \geq 0. \tag{5.26}$$

Taking the time derivative of Equation 5.24 and equating it to Equation 5.25, the control input may be determined.

$$n|n| = \frac{\tau}{\beta}\begin{bmatrix} \dot{\sigma} - 2\alpha u_r sign(u_r)\left[\alpha u_r|u_r| + \gamma u_r|n| + F\right] - \ldots \\ \gamma sign(n)\left[u_r\dot{n} + \left[\alpha u_r|u_r| + \gamma u_r|n| + F\right]n\right] + \ldots \\ \frac{F}{\tau} - \ddot{u}_f + \ddot{x}_{com} - 2\lambda(\alpha u_r|u_r| + \gamma u_r|n| + \ldots \\ F + \dot{u}_f - \ddot{x}_{com}) - \lambda^2(u_r + u_f - \dot{x}_{com}) \end{bmatrix} \tag{5.27}$$

Using the signed square root of Equation 5.27, the commanded control input is found. A detailed description of this controller design approach may be found in [Riedel 1998b].

As seen in Equation 5.27, the commanded control input is a function of the system states, the fluid velocity (including the first and second derivative), the command inputs, and the "to-be computed" control input, due to the fact the system represented by Equation 2.94 is non-affine. To compute the required control input requires solving a difference equation in *n*, as well as measurements of the fluid velocity and its first and second derivative, making this control law extremely complex and possibly difficult to implement in real-time. To overcome these difficulties, some simplifications need to be made.

a) Monochromatic Disturbance Input

If the thrust reduction term is ignored and treated as an unmodeled disturbance, Equation 5.27 reduces to,

$$n|n| = \frac{\tau}{\beta}\begin{bmatrix} \dot{\sigma} - 2\alpha u_r\left[\alpha u_r|u_r| + F\right]sign(u_r) + \ldots \\ \frac{F}{\tau} - \ddot{u}_f + \ddot{x}_{com} - 2\lambda(\alpha u_r|u_r| + F + \ldots \\ \dot{u}_f - \ddot{x}_{com}) - \lambda^2(u_r + u_f - \dot{x}_{com}) \end{bmatrix}, \tag{5.28}$$

which requires only system states, fluid disturbance measurements and command inputs. To display how well this controller is capable of performing, again, consider the case of a monochromatic sine wave disturbance input, where the disturbance and its first and second derivative are known. When direct feedforward of the measured wave disturbance is embedded in the control system design, perfect cancellation of the wave disturbance effects on station keeping may be obtained. The simulated response of the PHOENIX, initially at five meters and closing to a commanded range of 0.5 meters, is displayed in

Figure 5.24. Again, the results in Figure 5.24 are for demonstration purposes only, as a comparison with Case IIa. Perfect cancellation of the wave disturbances is not expected, since exact measurement of each wave disturbance component, i.e., $u_f, \dot{u}_f$ *and* $\ddot{u}_f$, is not possible. The interesting point in this case is the propeller response.

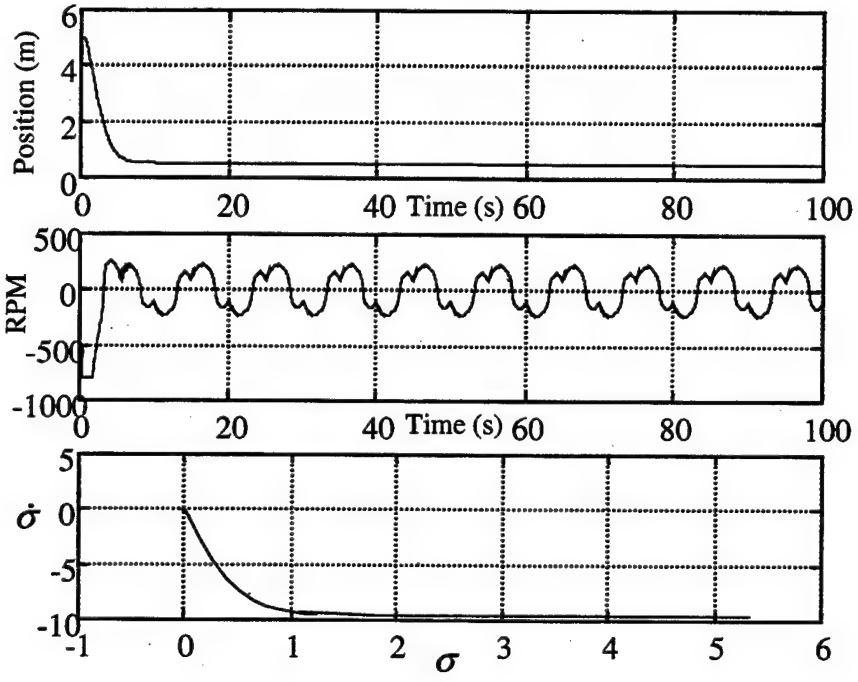

Figure 5.24 Disturbance Cancellation Case IIIa, top to bottom respectively, position vs. time, propeller RPM vs. time, and a phase plane plot of the sliding surface

When comparing the propeller response between the three cases that used a sine wave disturbance input, it can be seen that the SMC (Case IIIa) by far out performs the other designs. The position response is as desired, perfect cancellation, and the propulsion system is well within limits. This result is due to the fact that the system attempting to be controlled is highly nonlinear, requiring a nonlinear controller.

b) PM Spectrum Based Disturbance Input

Prior to continuing with any simulations to determine positioning performance, several simulations were conducted to determine the performance that could be obtained from the controller with and without all disturbance components available. Since the PM based disturbance input was generated using the techniques in

Chapter IV, the derivatives and phasing were known. Based on this, comparative simulations were conducted between controllers which used all the disturbance states and ones which used only the measurable fluid velocity state for disturbance rejection. Comparative results of one simulation are shown in Figure 5.25.

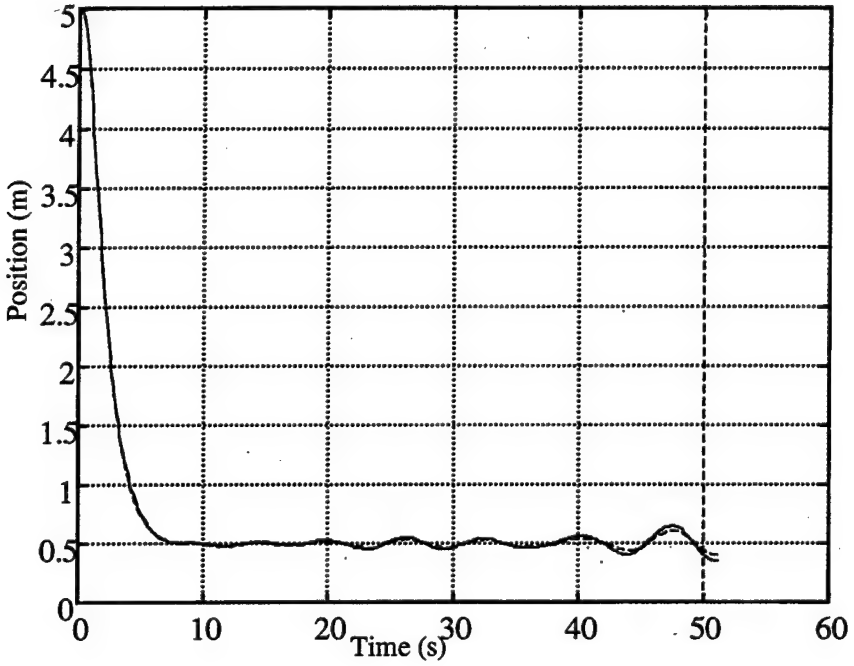

Figure 5.25 Controller Performance Comparison, For A Controller That Uses All The Disturbance Components (Dashed Line), And A Controller That Uses Only Fluid Velocity For Disturbance Cancellation (Solid Line)

As can be seen in Figure 5.25, the station-keeping improvements associated with including all components as opposed to including only the fluid velocity component is very small. In each case, the propulsion system response was within the vehicle's capability. As a result of the comparisons, it was determined that by using only the fluid velocity measurements, significant improvement with regard to positioning may be achieved. Based on this, the SMC takes the form

$$n|n| = \frac{\tau}{\beta}\begin{bmatrix} \dot{\sigma} - 2\alpha u_r\left[\alpha u_r|u_r| + F\right]sign(u_r) + \ldots \\ \frac{F}{\tau} + \ddot{x}_{com} - 2\lambda(\alpha u_r|u_r| + F - \ldots \\ \ddot{x}_{com}) - \lambda^2(u_r + u_f - \dot{x}_{com}) \end{bmatrix}, \qquad (5.29)$$

which will be used for all remaining simulations.

Using the PM based disturbance input allowed the SMC to be tuned to so that the controller would meet bandwidth requirements, limit propulsion system oscillations and avoid chattering. Controller parameters which provided a balanced design consisted of $\eta = 100$, $\lambda = 1.0$, and $\phi = 0.5$. The simulated position response of the Phoenix conducted with this SMC design is shown in Figure 5.26.

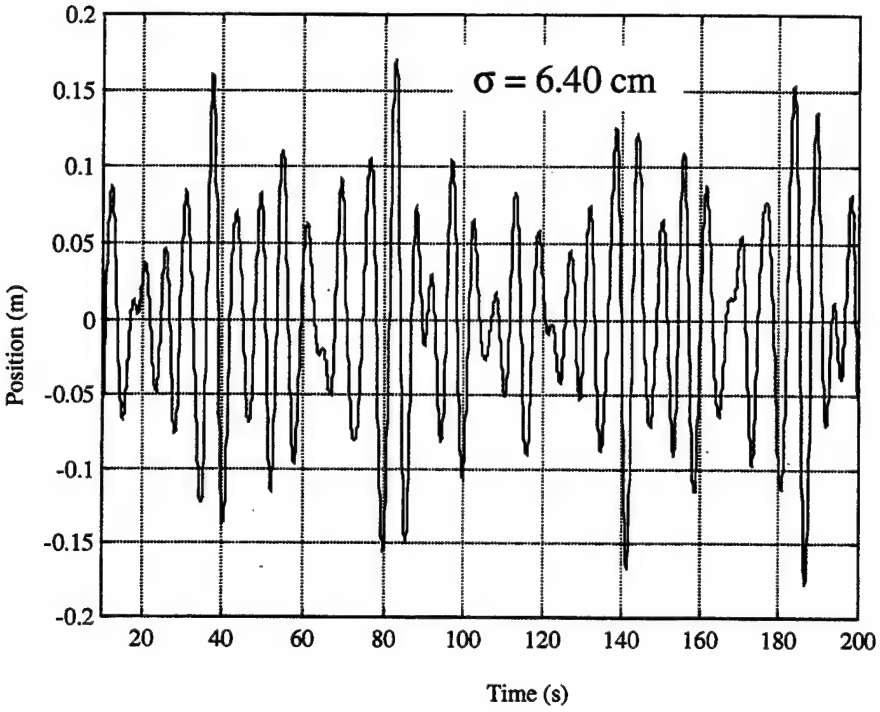

Figure 5.26 Position Response for Case IIIb, PM Based Disturbance Input

The position response shown in Figure 5.26 has a standard deviation of 6.4 cm. This is twice as much as Case IIb, Figure 5.18, however, the standard deviation of the propeller input for the SMC design is one-half a large as the LQR with disturbance estimator design, and is always within propulsion system limits. This can be seen in Figure 5.27. In addition, when comparing the two propeller responses, it appears that the SMC has a smoother output which will extend the life of the propulsion system.

c) Monterey Bay Disturbance Input

Using the same design parameters that allowed the controller to achieve the performance depicted in Figure 5.27, the system was simulated with the disturbance input obtained from Monterey Bay. Since the disturbance magnitude of the Monterey Bay data is less than the PM based input, it is expected that the position response would also be less. By referring to Figure 5.28, it can be seen that this is in fact the case.

The standard deviation of the position response has improved over the LQR based controller (Case IIc) by a factor of 1.4 with only a slight increase in propeller rpms (5% compared to a maximum of 800). These results are shown in Figure 5.29.

4. Disturbance Rejection Case Comparison

After conducting the simulations for each of the cases with the various disturbance inputs, it was apparent that Case III, the SMC with measured disturbance feedforward, out performed the other two cases and to most this is no surprise. What is interesting is the amount by which it out performed the other cases.

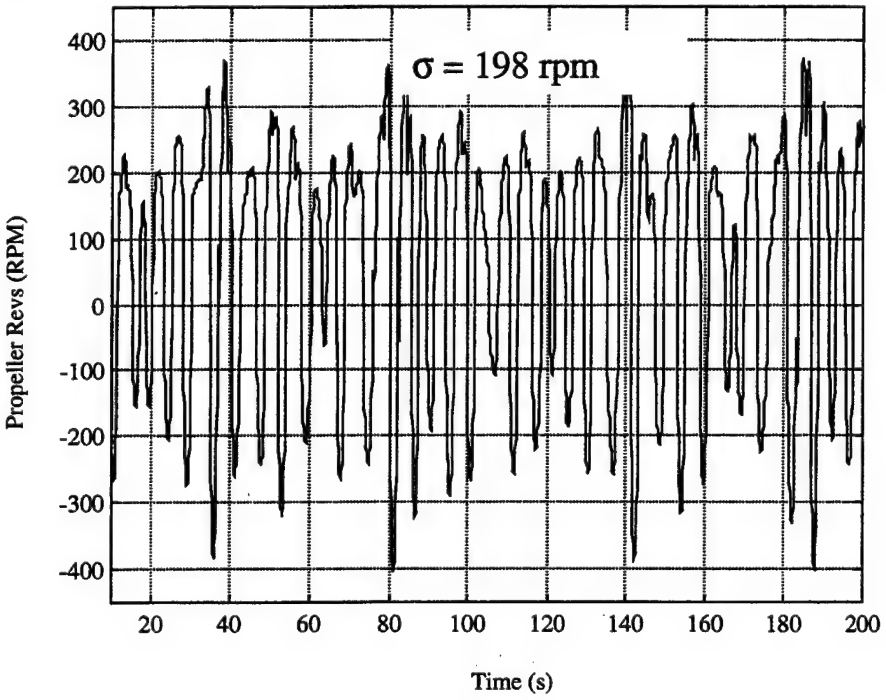

Figure 5.27 Propeller Response for Case IIIb, PM Based Disturbance Input

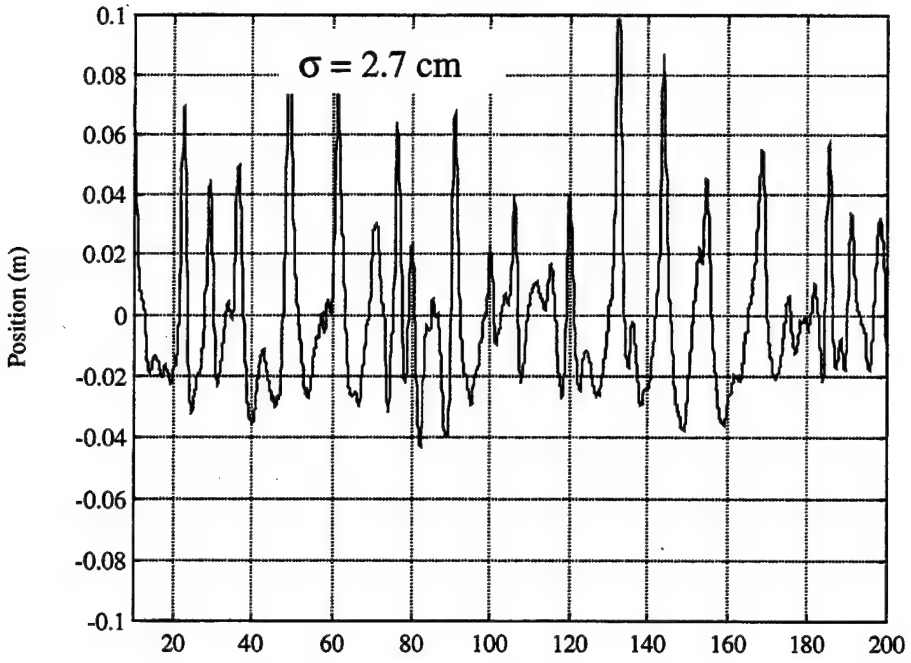

Figure 5.28 Position Response for Case IIIc, Monterey Bay Disturbance Input

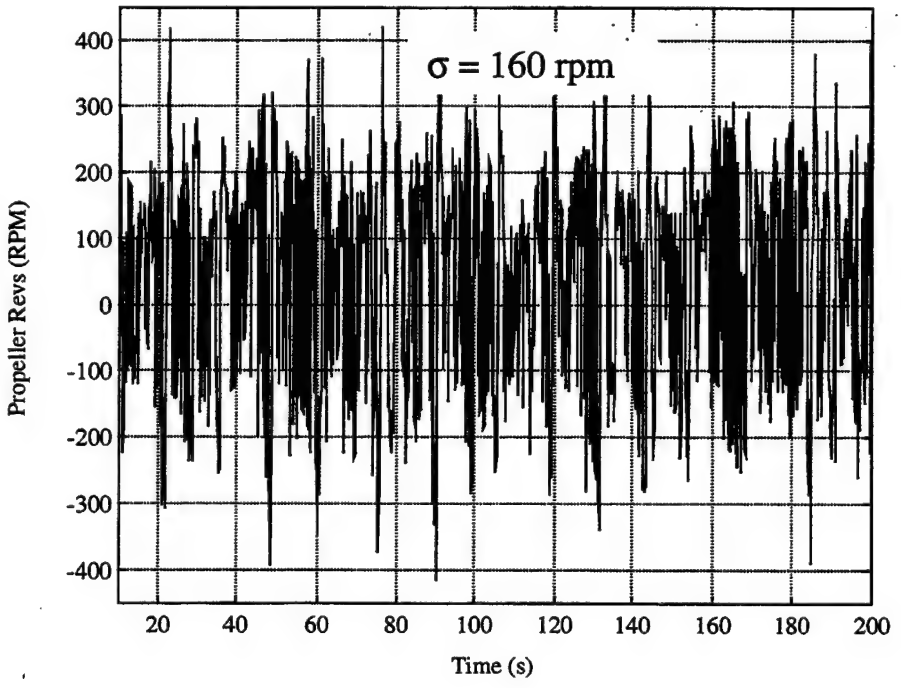

Figure 5.29 Propeller Response for Case IIIc, Monterey Bay Disturbance Input

Using the PM based disturbance input, simulations were conducted for each of the three case previously analyzed, LQR, LQR with disturbance estimator, and SMC with

disturbance measurement feedforward, with gains ranging from high to low. The attempt was to reproduce the "optimality" curve, Figure 5.15, for each controller to study the performance of each control solution.

Conducting this study led to some very interesting results which are shown in Figure 5.30. As seen in this plot, the curves for each controller do not have the traditional optimal curve shape, i.e., as control input increases position error decreases. In fact, the curves indicate that for control designs ranging from low to medium gains, regardless of controller type, it would be better to have no control at all.

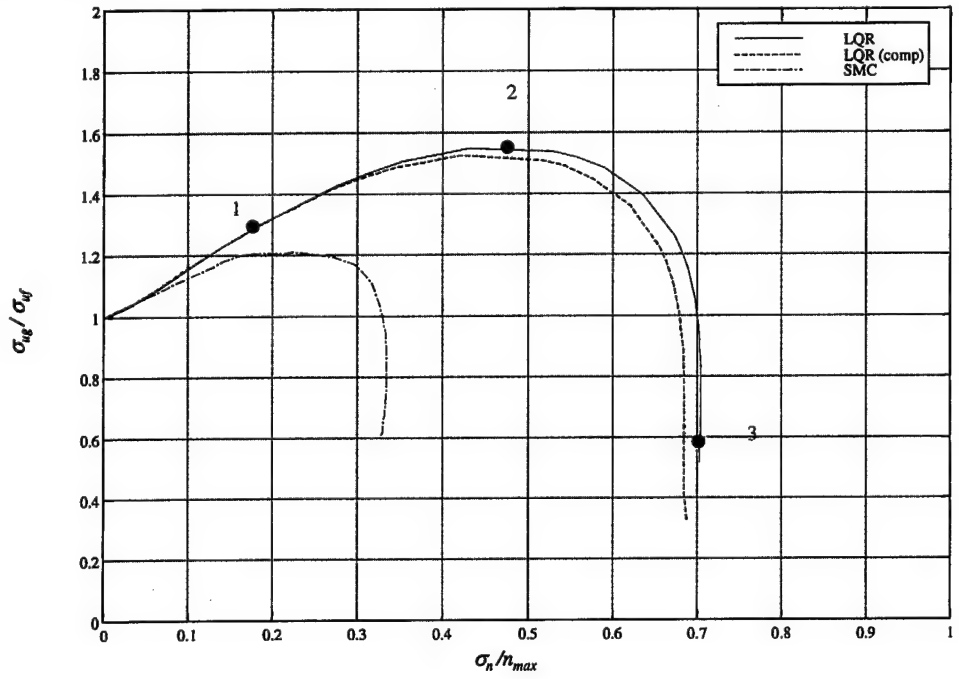

Figure 5.30 Comparison Of Controllers For Various Gains, PM Based Disturbance Input

The explanation for this can be seen in Figure 5.31. which superimposes the closed-loop vehicle frequency response, disturbance input to vehicle position output, over the disturbance spectrum for three different control gains, namely low medium and high. In Figures 5.30 and 5.31, point/curve "1" corresponds to a low gain, point/curve "2" to a medium gain solution and point/curve "3" is high gain control.

As Figure 5.31 displays, the low and medium gain solutions, with this particular disturbance, actually excites the vehicle, and not until a high gain solution is implemented does the vehicle actually reject the disturbance. Using this as an analysis

tool, the range of acceptable gains, for a particular disturbance input may be determined. In addition, it was quite evident that by feeding forward the measured disturbance using the SMC solution, that significant disturbance rejection was capable with much less power consumption.

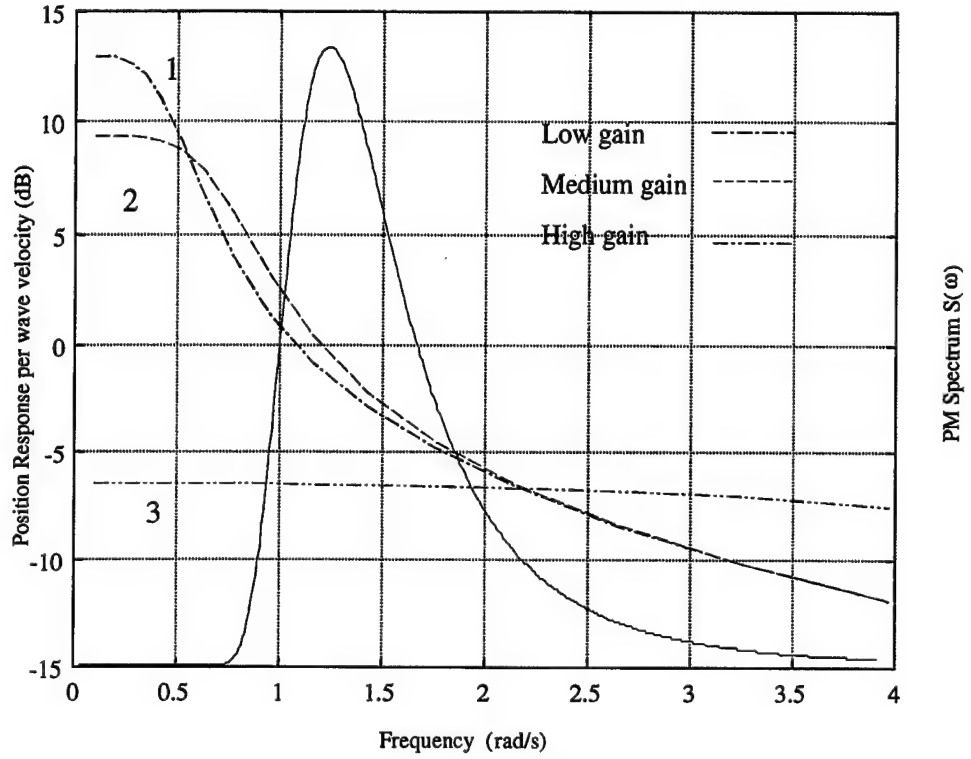

Figure 5.31 Vehicle Frequency Response, (Disturbance Input To Position Output), Superimposed Over The PM Based Disturbance Input

E. SUMMARY

This chapter has outlined the various disturbance rejection techniques available to the control engineer. It has provided a summary of classical, modern and nonlinear control methodologies. Three case studies, which represent the basic design methods used to reject disturbances, were conducted and discussed for three different disturbance inputs. These studies showed that the SMC with measured disturbance feedforward is a far superior design approach for this particular class of problem, and provides significant

disturbance rejection performance for the same input power. Finally, an analysis approach that may be used to study gain selection and performance estimates has been presented.

VI. DISTURBANCE COMPENSATION CONTROLLER (DCC)

A. INTRODUCTION

This chapter will discuss the development of the real-time disturbance compensation controller (DCC) which will allow an AUV to dynamically position itself in the presence of waves. The chapter will begin with an overview of the DCC, followed by a discussion of an asynchronous Extended Kalman Filter for state and disturbance estimation. This nonlinear estimator is critical to the DCC performance since the SMC requires full state feedback, and not all states are measurable. In addition, the EKF provides the controller with a smoothed estimate of the unmeasured fluid velocity which is used to compensate for the wave induced disturbance.

Next, through the design and implementation of an asynchronous simulator, which realistically models the vehicle dynamics, the sensors including noise and the sensor processes, the DCC is tuned and the achievable performance is demonstrated.

Lastly, it is shown that by properly weighting the noise covariance in the estimator the DCC reduces the transmission of sensor noise into the propulsion system while still maintaining the ability of the vehicle to hold position.

B. DCC OVERVIEW

The design of the disturbance compensation controller can be looked at as an optimization problem since there are competing goals. First, since the design requirement is to minimize position error in the presence of disturbances, a high gain control, as Chapter V discussed, is desirable. Using high gain control, the system becomes sensitive to measurement noise and uncertainty, thereby requiring the gain to be reduced to maintain stability.

The estimator is needed to provide the unmeasurable states to the controller, and to filter the sensor noise thereby improving the systems performance. Here, the requirement is to accurately track the signal, again requiring a high filter gain, while smoothing the noise, (a low gain). As with the controller, trade-offs must be made.

The overall goal is to develop a combined controller/estimator which, when implemented, will enable the vehicle to maintain position while using noisy sensor information. The output of this system is a commanded voltage that is sent from the DCC process to the real-time execution computer, without excessive lags to ensure stability. A mathematical description to the above problem is given below, with a block diagram of the DCC in provided in Figure 6.1.

$$
\begin{aligned}
&\textit{State:} && \mathbf{x}^T = [X, u_r, F]; && d = u_f \\
&\textit{System:} && \dot{\mathbf{x}} = f(x,n,d); && \mathbf{y}^T = [x, u_r, u_g,] = \mathbf{C}\mathbf{x} + \mathbf{D}d \\
&\textit{Disturbance:} && \dot{\mathbf{x}}_f = \mathbf{A}\mathbf{x}_f + \boldsymbol{\nu} && u_f = \mathbf{C}x_f \\
&\textit{Control law:} && n = smc(\hat{\mathbf{x}}, \hat{\mathbf{u}}_f, \mathbf{x}_{com}) \\
&\textit{Estimator:} && [\hat{\mathbf{x}}, \hat{\mathbf{u}}_f] = EKF(f(\hat{x},n,\hat{d}), \mathbf{A}, \mathbf{y}, n)
\end{aligned}
\qquad (6.1)
$$

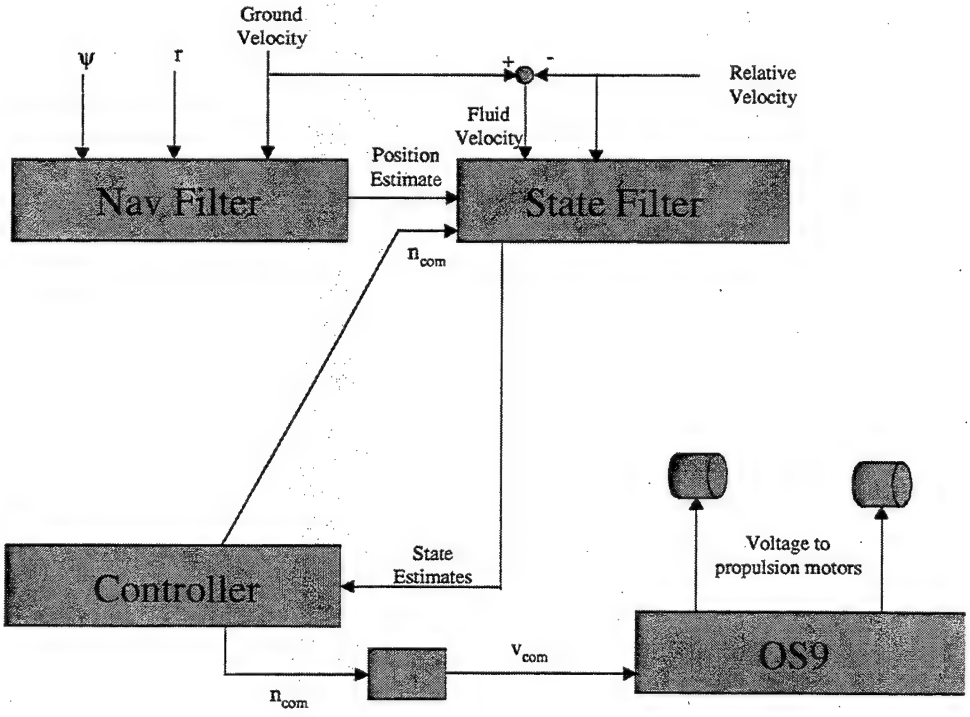

Figure 6.1 Block Diagram of Disturbance Compensation Controller (DCC)

C. STATE AND DISTURBANCE ESTIMATION

There are many methods available to estimate states and disturbances in practice today. A few of these include the Luenberger Observer [Ogata 1990] and the Kalman

Filter [Gelb 1974] for linear systems, and the Sliding Mode Observer [Canudas De Wit 1991], the "Rajamani" Observer [Rajamani 1998] and the Extended Kalman Filter for nonlinear systems. Each method has both pros and cons depending on the application. For this work, an Extended Kalman Filter was chosen since a relatively accurate vehicle model is available, and the stochastic nature of the disturbance.

Kalman filtering is the process of recursively updating an estimate of systems states based upon measurements corrupted by noise. The system state is a collection of variables that describe the dynamics of a system, and in this case they are position, relative velocity and propeller thrust, of which only relative velocity is measurable.

System states are updated with knowledge of system dynamics (vehicle model), measurement dynamics (measurement model), system noise (modeling uncertainty) and measurement noise (measurement errors). The system model is not perfect in describing the dynamics of the vehicle and will contain a certain amount of uncertainty, called system noise. There is also some uncertainty associated with each measurement taken. This uncertainty can be composed of both random white noise and a bias. Measurements which cannot be directly obtained, such as fluid velocity, are related to measurements which are directly obtainable, such as relative velocity and ground velocity, in the measurement model. Recursively updating means the Kalman filter does not need to keep record of all past measurements, only the most recent ones.

1. Model and Filter Development

Using the three state surge model developed in Chapter II, and a four state AR model for the wave dynamics, an augment state and disturbance model was formed, and used as the basis of an EKF. This model allows the disturbance to be treated as an additional state, where the vehicle states and disturbance estimates are filter outputs. The augmented vehicle and disturbance model is given by,

$$
\begin{aligned}
\dot{x} &= u_r + u_f \\
\dot{u}_r &= \alpha u_r |u_r| + F \\
\dot{F} &= \frac{-1}{\tau} F + \frac{\gamma}{\tau} u_r |n| + \frac{\beta}{\tau} n|n| \\
\dot{x}_{w,1} &= x_{w,2} = u_f \\
\dot{x}_{w,2} &= \dot{u}_f = x_{w,3} \\
\dot{x}_{w,3} &= a_1 x_{w,1} + a_2 u_f + a_3 x_{w,3} + a_4 x_{w,4} \\
\dot{x}_{w,4} &= \nu \\
\mathbf{y} &= [x, u_r, u_g]^T
\end{aligned}
\quad , \qquad (6.2)
$$

where the AR coefficients are found using the procedure outline in Chapter V.

2. Kalman Filter Algorithm

Using standard design techniques [Gelb 1974], the filter was developed and implemented using the following algorithm. First, the system model matrix $\boldsymbol{A}$, system noise matrix $\boldsymbol{Q}$, measurement matrix $\boldsymbol{C}$, measurement noise matrix $\boldsymbol{R}$, and the error covariance matrix $\boldsymbol{P}$ are initialized to appropriate values. The error covariance matrix can be thought of as a level of uncertainty in the state vector. Then the state vector, error covariance and measurement vector are propagated one time step using the model.

When the new measurement is received, the innovation is calculated based on the difference between the measured values and the estimated values. Using the propagated error covariance, measurement noise matrix and measurement matrix, a gain is determined for the state vector and error covariance update. This process of propagating and updating is repeated through out the length of the vehicle mission. This recursive algorithm, in discrete form is given by,

$$
\begin{aligned}
&\boldsymbol{\Phi}_{k/k-1} = \exp(AT); \qquad \mathbf{A} = \left. \frac{\partial \mathbf{f}(\mathbf{x}_{aug}, n)}{\partial \mathbf{x}_{aug}} \right|_{\hat{\mathbf{x}}_{k-1/k-1}} \\
&\hat{\mathbf{x}}_{k/k-1} = \boldsymbol{\Phi}_{k/k-1} \hat{\mathbf{x}}_{k-1/k-1} \\
&\mathbf{P}_{k/k-1} = \boldsymbol{\Phi}_{k/k-1} \mathbf{P}_{k-1/k-1} \boldsymbol{\Phi}^T_{k/k-1} + \mathbf{Q} \\
&\mathbf{G}_k = \mathbf{P}_{k/k-1} \mathbf{h}_k^T / \mathbf{h}_k \mathbf{P}_{k/k-1} \mathbf{h}_k^T + \mathbf{R}]^{-1} \\
&\hat{\mathbf{x}}_{k/k} = \hat{\mathbf{x}}_{k/k-1} + \mathbf{G}_k [\mathbf{y}_k - \mathbf{h}_k \hat{\mathbf{x}}_{k/k-1}] \\
&\mathbf{P}_{k/k} = [\mathbf{I} - \mathbf{G}_k \mathbf{h}_k] \mathbf{P}_{k/k-1}
\end{aligned}
\quad , \qquad (6.2)
$$

where Φ represents the linearized system dynamics matrix, and $h=C$ since the measurements are linear in the state. The continuous linearized matrices for this particular design are given as,

$$\mathbf{A}=\begin{bmatrix} 0 & 1 & 0 & 0 & 1 & 0 & 0 \\ 0 & 2\alpha\hat{u}_r sign(\hat{u}_r) & 1 & 0 & 0 & 0 & 0 \\ 0 & \frac{\beta}{\tau}|n_{com}| & \frac{-1}{\tau} & 1 & 0 & 0 & 0 \\ 0 & 0 & 0 & 0 & 1 & 0 & 0 \\ 0 & 0 & 0 & 0 & 0 & 1 & 0 \\ 0 & 0 & 0 & -1 & -4 & -6 & -4 \\ 0 & 0 & 0 & 0 & 0 & 0 & 0 \end{bmatrix} \tag{6.3}$$

$$\boldsymbol{C}=\begin{bmatrix} 1 & 0 & 0 & 0 & 0 & 0 & 0 \\ 0 & 1 & 0 & 0 & 0 & 0 & 0 \\ 0 & 0 & 0 & 0 & 1 & 0 & 0 \end{bmatrix}$$

3. Asynchronous Data Processing

In the preceding discussion, the data contained in the measurements was assumed to be received at the same time with equal intervals through out the mission. In reality, all measurements are not received at the same rate, therefore, the EKF design must allow for this asynchronous sampling rate. In the Phoenix AUV, the vehicle control loop currently runs at 8 Hz, while the RDI DVL runs at 2 Hz, and the SonTek ADV at 6 Hz. (See Appendix B for a more through description of sensor operations). The main data acquisition process samples the sensor processes at the same frequency as the control loop, however, if the sensor has not yet updated, the data acquisition process records the value of the previous time step. The filter allows for the varying measurement rates by using a dynamic switching of the measurement matrix, C, [Healey 1998]. The measurement matrix basically uses a zero-order hold on the measurement channel that has not been updated, and propagates the state using the previous measurement.

D. ASYNCHRONOUS SIMULATOR DEVELOPMENT

Using the filter design from the previous section, and the sliding mode controller developed in Chapter V, Equation 5.37, an asynchronous simulator was developed for

design validation. The simulator contains the non-linear vehicle dynamics, Equation 2.94, asynchronous sensor models with measurement noise, seaway dynamics and the DCC. Using this simulator as a design tool allowed the DCC's control and estimation parameters to be adjusted prior to real-time implementation. Figure 6.2 shows a sample of the sensor outputs, during one of the simulation runs. As seen, the position output, which is a product of a navigation filter, is at 8 Hz. The relative velocity, u_r, which is measured by the ADV, is at 6 Hz, and the ground velocity, u_g, from the RDI is recorded at 2 Hz. In addition, the ADV output has noise imposed on the signal representative of the vendor advertised levels.

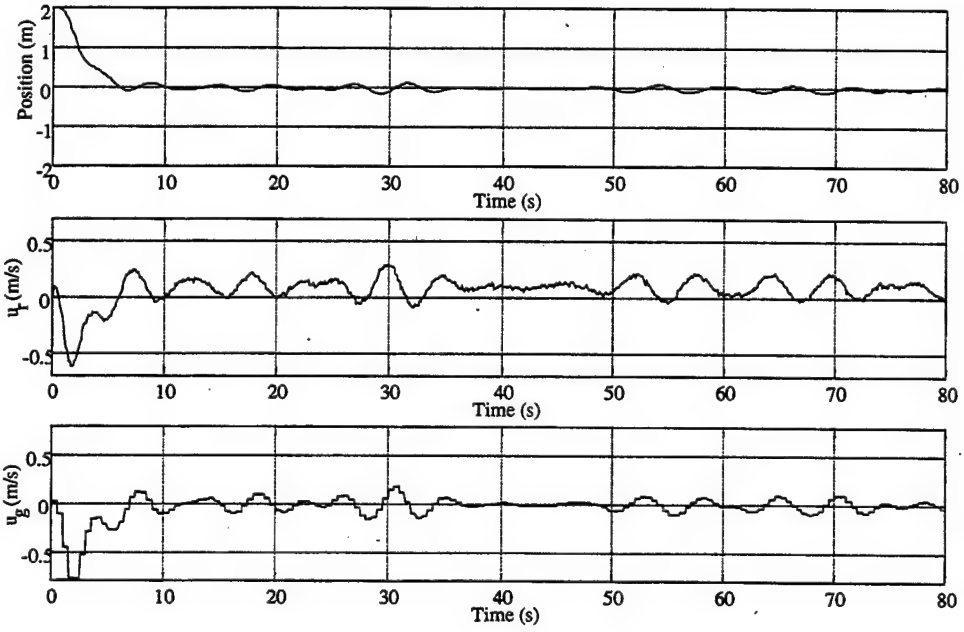

Figure 6.2 Asynchronous simulation with realistic noise models - Disturbance from PM Spectrum, H_s= 1 meter, operating depth 10 meters

Using this developed simulator, the DCC was adjusted to achieve an optimum design. The gains in both the controller and filter were adjusted so that performance requirements discussed earlier were met. Sample results showing the performance of final design are given in Figures 6.3 and 6.4. As can be seen, the estimates of both position and thrust track the actual values, and the position response is maintained within a standard deviation of 8 cm. This performance is extremely good, recalling that the

same controller, with the same disturbance input was able to achieve a standard deviation in position of 6.5 cm, without noise and using full state feedback, see Figure 5.31.

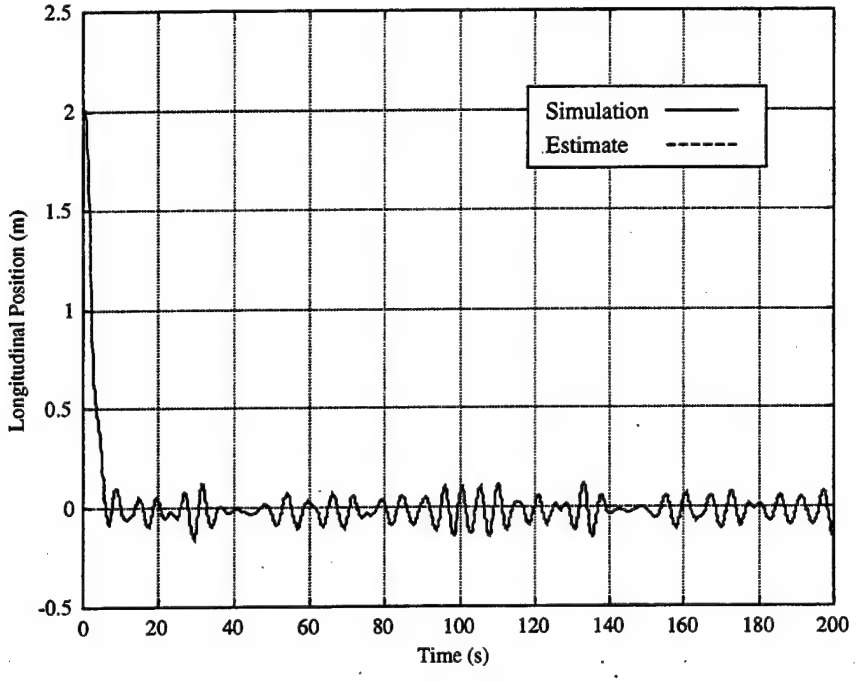

Figure 6.3 Simulated and Estimated Position Response, Using Final DCC Design

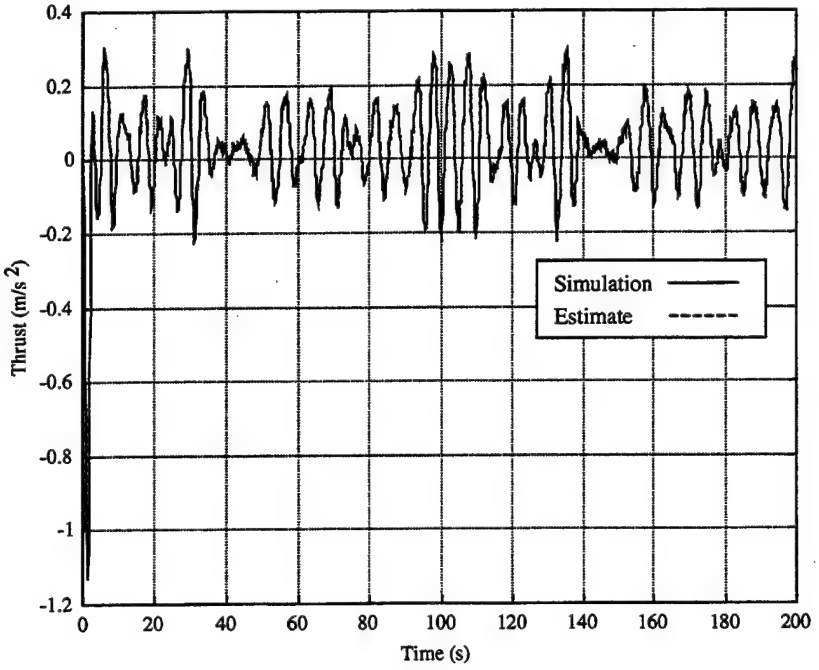

Figure 6.4 Simulated and Estimated Thrust Response, Using Final DCC Design

The stability performance of the estimator is shown through simulation, see Figure 6.5, since there are no formal proofs to determine the stability of combined nonlinear estimators and controllers. As seen, the error covariance levels all converge indicating a stable nonlinear filter design. Some of the covariance levels may appear to be "too high" giving the feeling that the filter is not properly designed, however, design decisions must be made to ensure that the filter lags are not too excessive, and that the estimator tracks well.

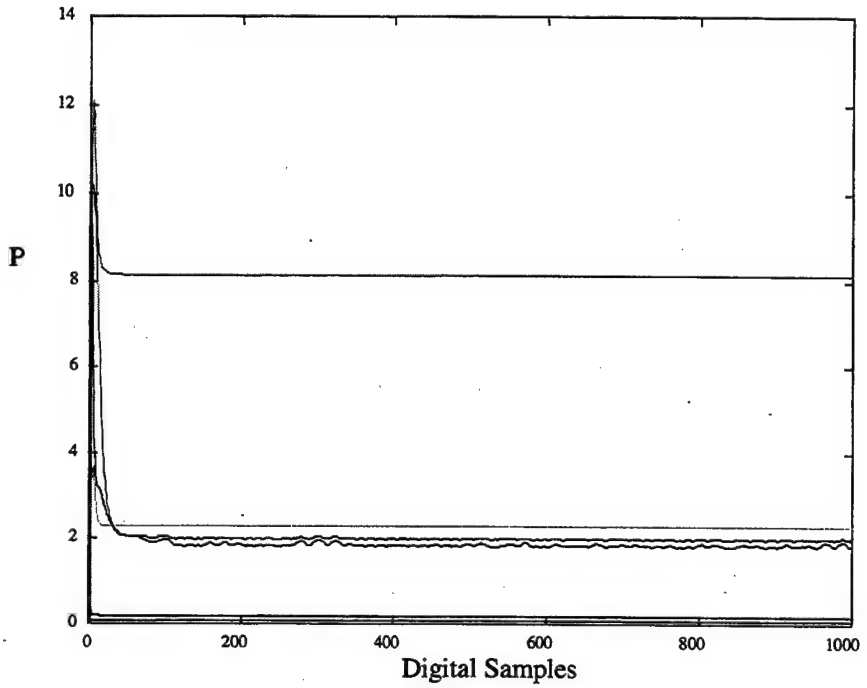

Figure 6.5 DCC Error Covariance Evolution

E. INITIAL IN-WATER TESTING

Using short missions, that DCC was adjusted to achieve acceptable performance. These runs were performed on March 25, 1999, in Monterey Harbor. Of concern, was the amount of noise that was resident on the ADV sensor. This noise was far beyond the level which the vendor advertised. Using the design results from the simulations, the DCC was implemented in the Phoenix AUV. Figures 6.6-6.10 display initial results. As seen, the filter tracks the signals extremely well, including the noise.

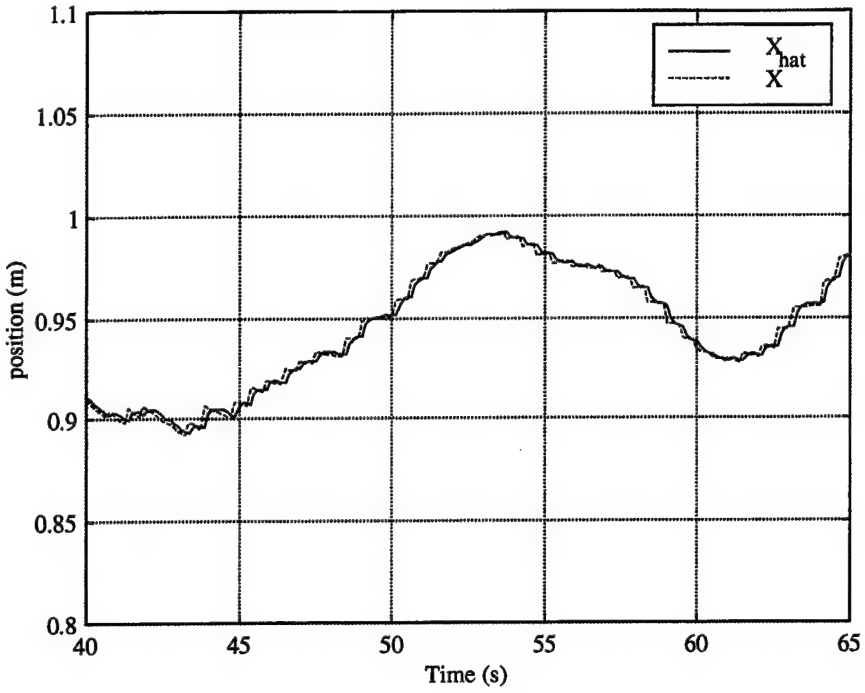

Figure 6.6 Short Segment In-Water Results, Position for R_{ADV}=10

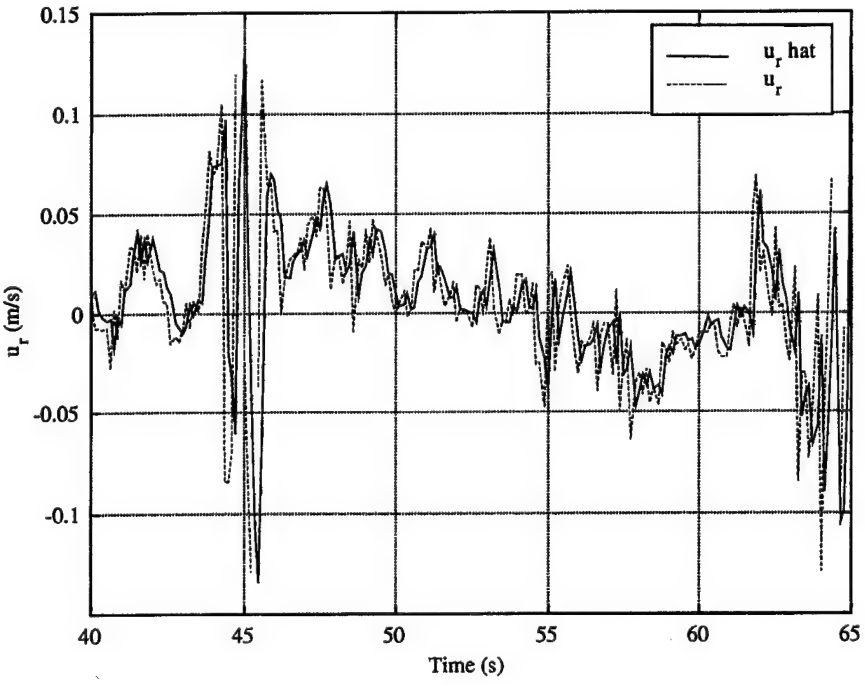

Figure 6.7 Short Segment In-Water Results, Relative Velocity for R_{ADV}=10

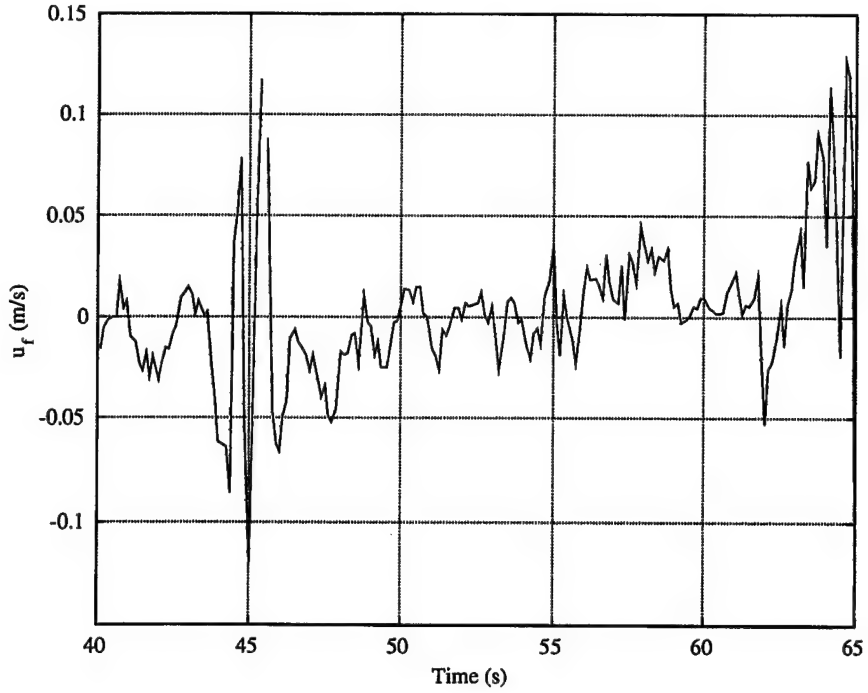

Figure 6.8 Short Segment In-Water Results, Fluid Velocity Estimate for R_{ADV}=10

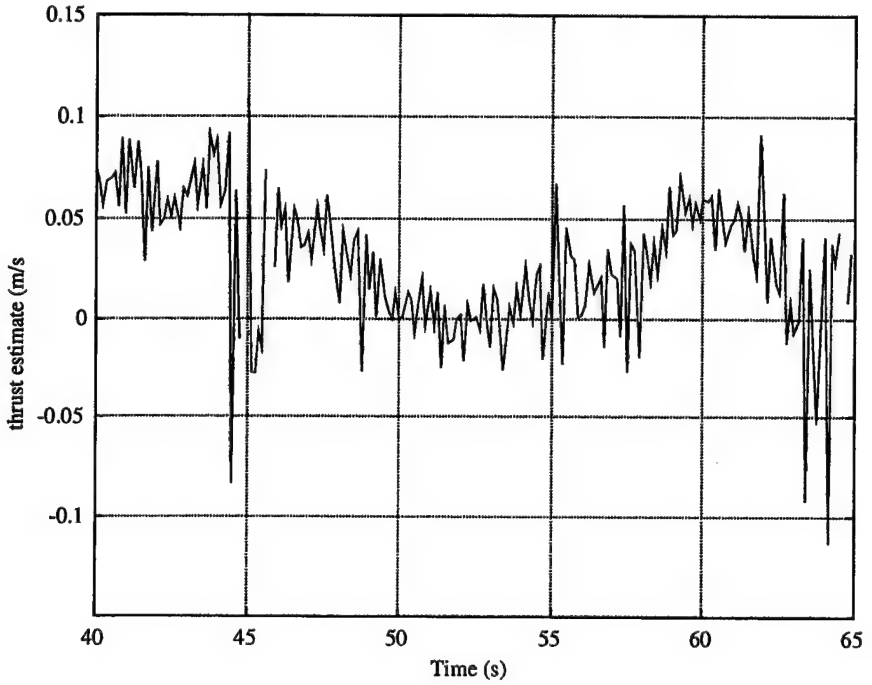

Figure 6.9 Short Segment In-Water Results, Thrust Estimate for R_{ADV}=10

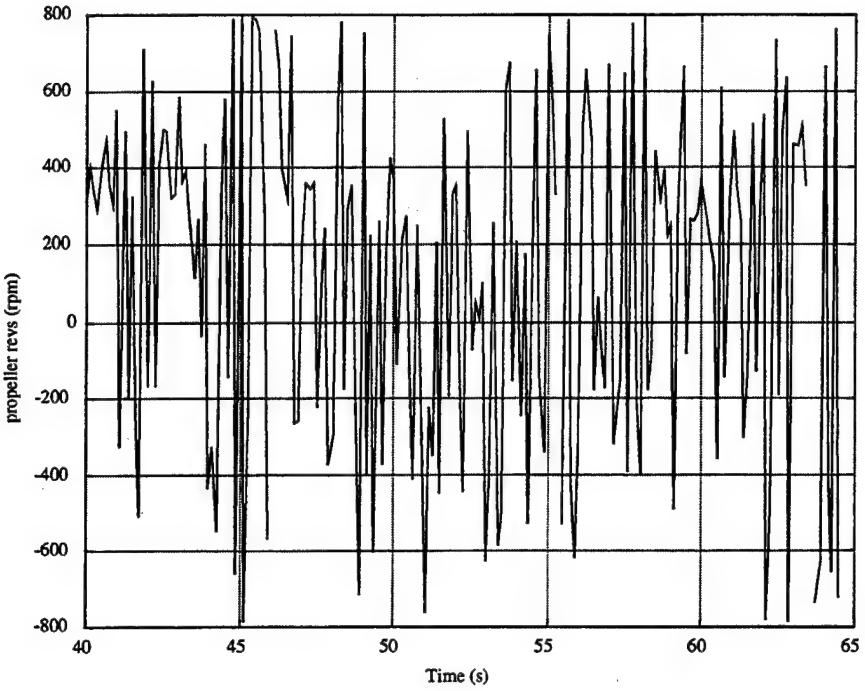

Figure 6.10 Short Segment In-Water Results, Propeller RPMs for R_{ADV}=10

This tracking of the noise has significant detrimental effects to the propulsion system as seen in Figure 6.10. The noise had been transmitted into the controller resulting in severe oscillation in the propeller response. These oscillations eventually lead to mechanical failure of the propulsion system shafting due to the shearing of connecting pins.

Using the information obtain during this set of runs allowed the filter gains to be adjusted to eliminate the transmission of sensor noise into the controller. Using linear design techniques, the combined controller filter transfer function from ADV input to propeller output was formed. By adjusting the level of the measurement noise parameters, attenuation of the noise into the control system was accomplished. These results are shown in Figures 6.11 and 6.12. As the Figures shown, for the smaller noise estimate (R_{ADV}=10), the noise transmission is amplified over most of the range of the controller, while for the higher noise estimate (R_{ADV}=100), the input to the controller in attenuated. This improvement in frequency response will reduce the propeller

oscillations, thereby minimizing the chance of mechanical failure of the propulsion system.

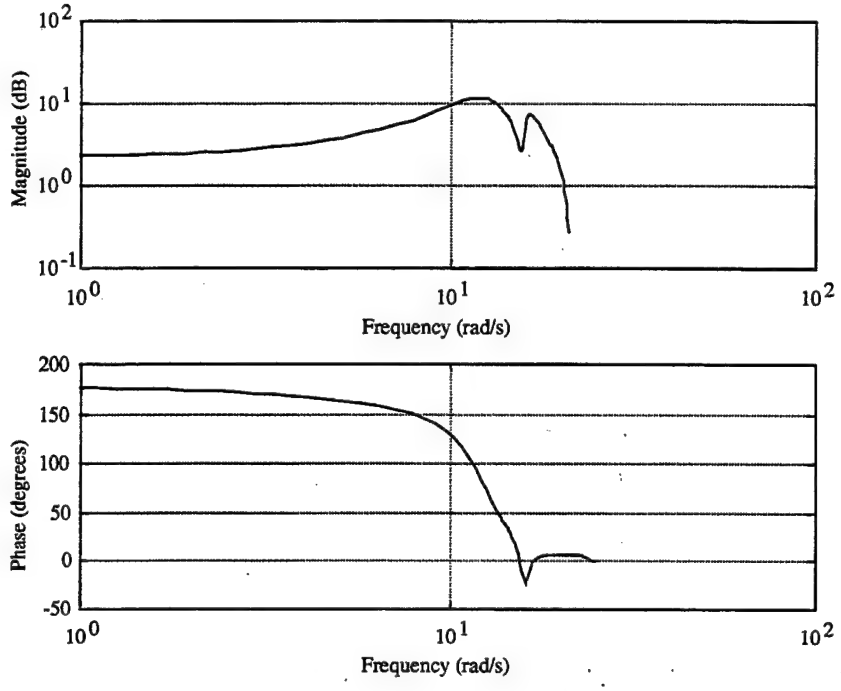

Figure 6.11 DCC Frequency Response, ADV Input to Propeller Output , R_{ADV}=10

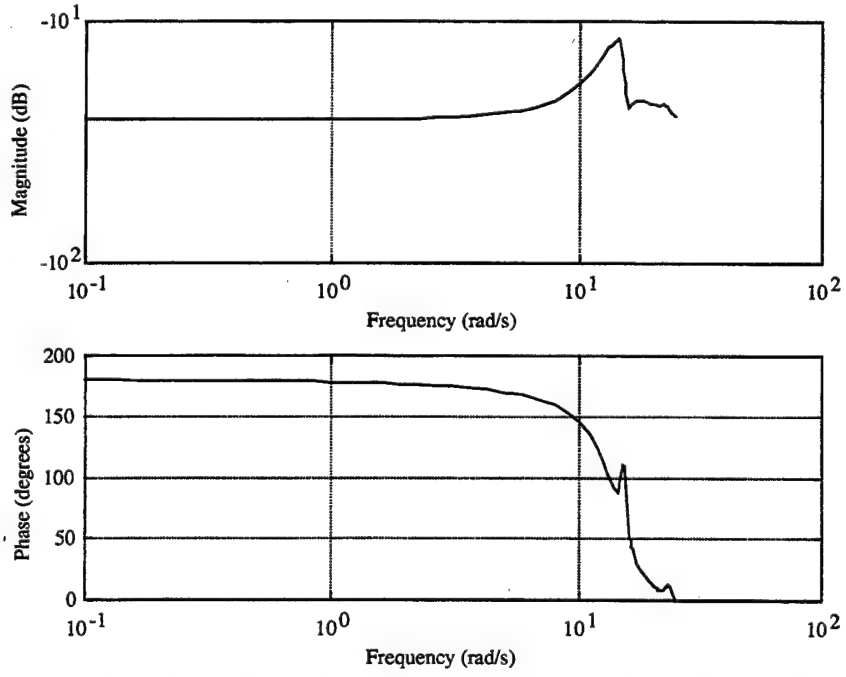

Figure 6.12 DCC Frequency Response, ADV Input to Propeller Output , R_{ADV}=100

Using the new design values, the DCC was again tested in Monterey Harbor. The results of this testing are shown in Figures 6.13-6.17.

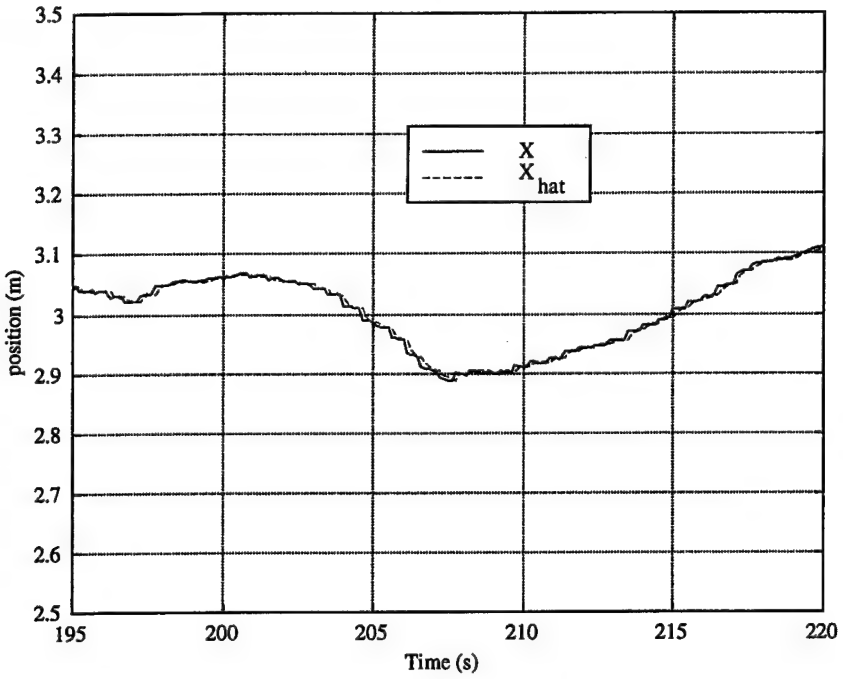

Figure 6.13 Short Segment In-Water Results, Position for R_{ADV}=100

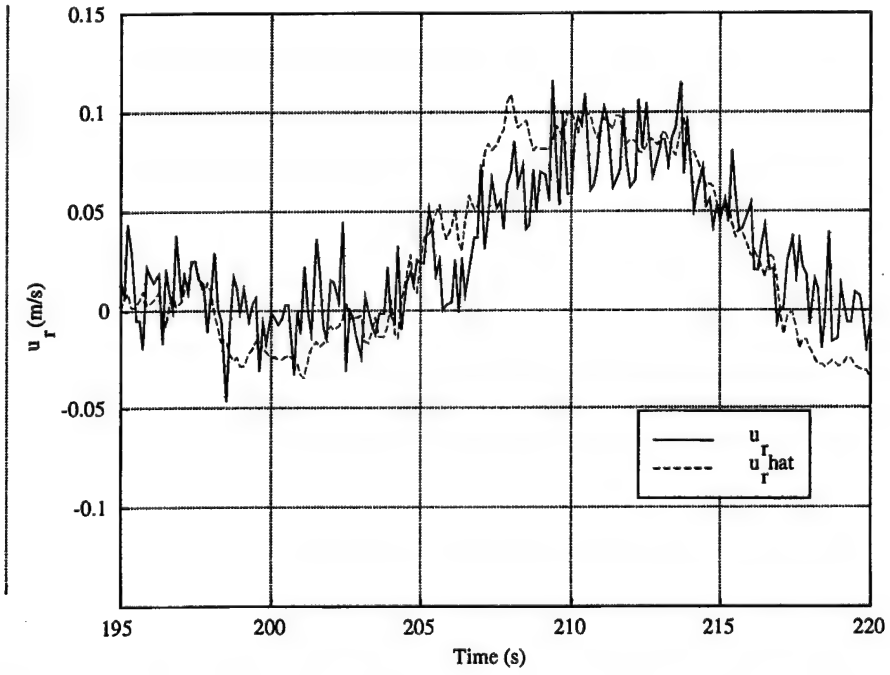

Figure 6.14 Short Segment In-Water Results, Relative Velocity for R_{ADV}=100

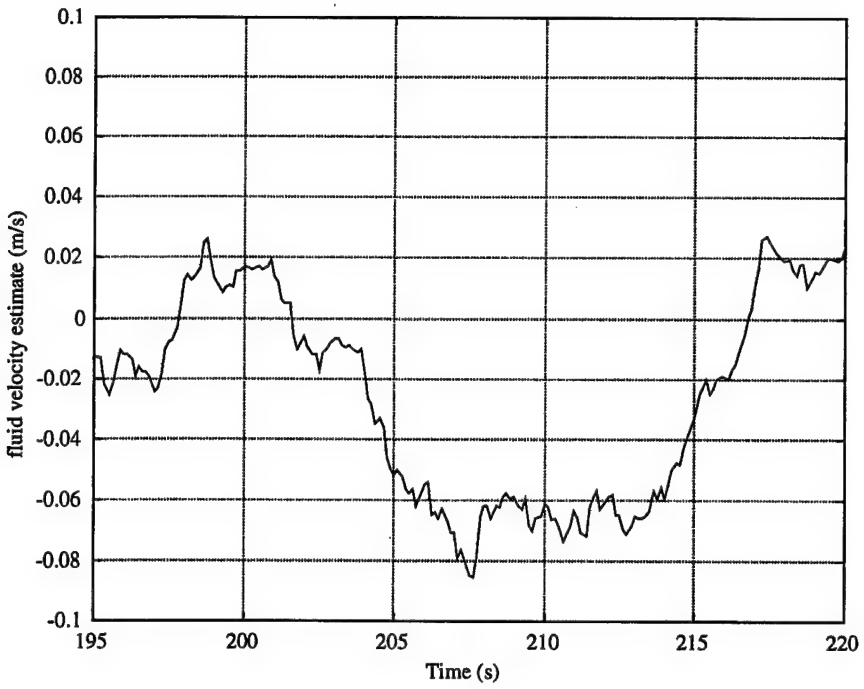

Figure 6.15 Short Segment In-Water Results, Fluid Velocity Estimate for R_{ADV}=100

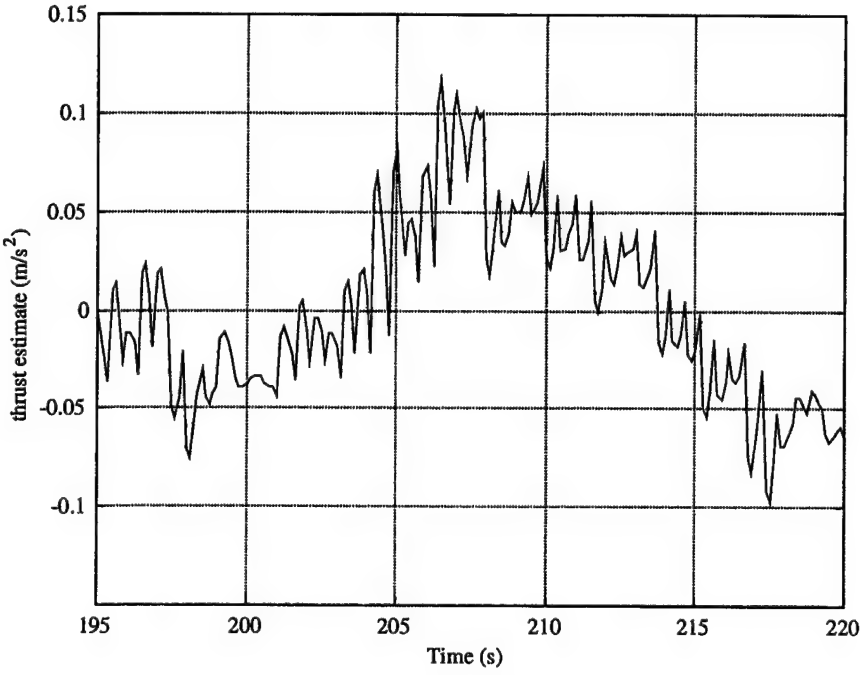

Figure 6.16 Short Segment In-Water Results, Thrust Estimate for R_{ADV}=100

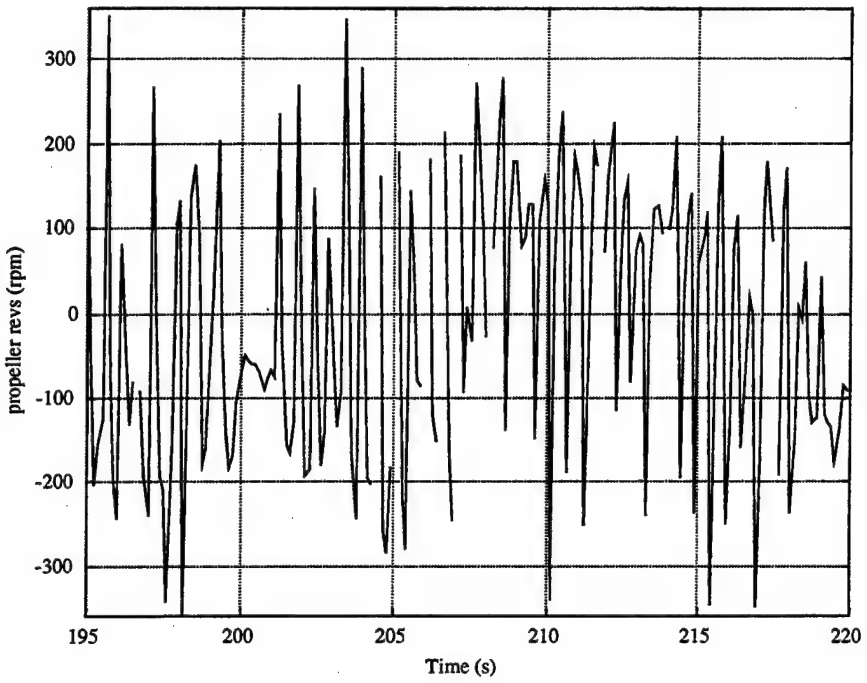

Figure 6.17 Short Segment In-Water Results, Propeller RPMs for R_{ADV}=100

As the result of the tuning of the DCC, the performance has improved dramatically. As before, the DCC maintains position extremely well, with a much reduced propeller response. Comparing the magnitude of the estimated fluid velocities between the two designs, Figures 6.8 and 6.15, it can be seen that for the same magnitude of input disturbance, position response has remained unchanged, but propeller response has reduced increasing the life of the propulsion system.

F. SUMMARY

The design and implementation of a new Disturbance Compensation Controller (DCC) has been presented. The results indicate that by using a properly tuned system, the ability of a tetherless underwater vehicle to dynamically position itself with minimal input is possible. Although no formal proof for stability is available, asynchronous simulations have demonstrated that the DCC is stable and provides acceptable tracking and estimation of state and disturbance inputs.

VII. ESTIMATION OF WAVE DIRECTIONALITY FROM A MOVING PLATFORM

A. INTRODUCTION

This chapter will outline the underlying principles used in identification of wave directions from standard wave following buoys. It will present the mathematical formulas used in determining the wave direction as a function of frequency. Extension of these algorithms to subsurface velocity sensors will be made, where, through the use of the Doppler equation, a moving AUV can be used to determine wave directions. Lastly, it will be shown how a control command can be obtained from the frequency dependent wave direction estimates.

The information in this chapter is not new, only the application to which this method is applied. For more detailed descriptions of the mathematical formulations presented in this chapter, the reader is referred to [O'Reilly 1996} and the references therein.

B. WAVE SPECTRA AND DIRECTIONAL ESTIMATES

As discussed in Chapter II, a wave record, $\eta(t)$, measured at a fixed location can be represented as a linear superposition of waves of different frequencies. Wave components with different frequencies are usually assumed to be statistically independent because they are generated by random wind forces at different locations. From the central limit theorem it follows that the probability distribution of $\eta(t)$ is approximately Gaussian, consistent with many observations, [Soong 1993].

The procedure presently employed by many of the operational data buoys in based on Fourier analysis. In Fourier analysis it is convenient to work with complex exponentials rather than sine and cosine functions, there fore using the relation

$$\cos(\omega t+\phi)=\frac{\exp(i(\omega t+\phi))+\exp(-i(\omega t+\phi))}{2} \tag{7.1}$$

the expression for the surface elevation can be written as

$$\eta(t)=\sum_{\omega} A_{\omega}\exp(i\omega t)\,, \tag{7.2}$$

where

$$A_\omega = \frac{1}{2} a_\omega \exp(i\phi_\omega) \tag{7.3}$$

and the summation is over both positive and negative frequencies.

As discussed in Chapter III, the energy spectrum $E(\omega)$, is defined as

$$E(\omega) = \frac{\left\langle |A_\omega|^2 \right\rangle}{\Delta\omega} \tag{7.4}$$

where $\langle\ \rangle$ indicates an average over many data records and $\Delta\omega$ is the spacing of the frequency bands. The spectrum is closely related to the energy of the waves, and represents the distribution of wave energy as a function of frequency.

To describe the spatial and temporal characteristics of the sea surface linear superposition of wave components is used. In exponential terms this can be represented as

$$\eta(x, y, t) = \sum_\omega \sum_\theta A_{\omega,\theta} \exp(i(k(x\cos\theta + y\sin\theta) - wt)) \tag{7.5}$$

where x, y are the horizontal spatial coordinates, and ω and k obey the dispersion relation. The frequency directional wave spectrum is defined as

$$E(\omega) = \frac{\left\langle |A_{\omega,\theta}|^2 \right\rangle}{\Delta\omega\,\Delta\theta} \tag{7.6}$$

and describes the distribution of energy as a function of frequency and direction.

C. WAVE BUOYS

The most commonly used instrument for measuring waves in deep water is the "heave, pitch and roll buoy" that measures the surface height and slope in two orthogonal directions. The newer Datawell® Directional Waverider measures 3-component accelerations of the buoy which are integrated to yield the horizontal and vertical displacements of the buoy. The hull and mooring were designed to give the buoy good wave following characteristics, thereby allowing the buoy displacements to approximate the displacements of an actual water particle at the sea surface.

For a wave train propagating in the positive x-direction, the fluid particle motion is given by Equation 2.49. For the more general case of a wave train propagating at some angle relative to the x-axis, it can be shown that the flow field is given by

$$\begin{aligned} u(x,y,t) &= a\omega\cos\theta\exp(kZ)\cos(k(x\cos\theta+y\sin\theta)-\omega t) \\ v(x,y,t) &= a\omega\sin\theta\exp(kZ)\cos(k(x\cos\theta+y\sin\theta)-\omega t) \\ w(x,y,t) &= a\omega\exp(kZ)\sin(k(x\cos\theta+y\sin\theta)-\omega t) \end{aligned} \tag{7.7}$$

Let the average position of the buoy be given by x=y=z=0. For small amplitude waves, the expected buoy displacements are small compared to the surface wavelength, therefore the buoy motion can be approximated by the fluid velocity at x=y=z=0.

For a full spectrum of waves, the buoy displacements can be expressed using complex notation as

$$\begin{aligned} X(t) &= \sum_{\omega}\sum_{\theta} -iA_{\omega,\theta}\cos\theta\exp(iwt) \\ Y(t) &= \sum_{\omega}\sum_{\theta} -iA_{\omega,\theta}\sin\theta\exp(iwt) \\ Z(t) &= \sum_{\omega}\sum_{\theta} -A_{\omega,\theta}\exp(iwt) \end{aligned} \tag{7.8}$$

where the $-i$ is due to the 90° phase difference between the vertical and horizontal displacements. The expressions in Equation 7.8 can be written using Fourier transforms as

$$\begin{aligned} X(t) &= \sum_{\omega} X(\omega)\exp(iwt) \\ Y(t) &= \sum_{\omega} Y(\omega)\exp(iwt) \\ Z(t) &= \sum_{\omega} Z(\omega)\exp(iwt) \end{aligned} \quad , \tag{7.9}$$

where the Fourier transforms are given by

$$\begin{aligned} X(\omega) &= \sum_{\theta} -iA_{\omega,\theta}\cos\theta \\ Y(\omega) &= \sum_{\theta} -iA_{\omega,\theta}\sin\theta \\ Z(\omega) &= \sum_{\theta} A_{\omega,\theta} \end{aligned} \quad . \tag{7.10}$$

To derive the relationships between the measured time series and the unknown frequency-directional wave spectrum the cross spectrum must be considered. In general,

the cross spectrum between two time series $X(t)$ and $Y(t)$ with Fourier transforms $X(\omega)$ and $Y(\omega)$ is defined as

$$C_{XY}(\omega) = \frac{\langle X(\omega)Y^*(\omega)\rangle}{\Delta\omega} \tag{7.11}$$

where * indicates the complex conjugate, [Soong 1993]. Substitution of Equation 7.10 into Equation 7.11 yields

$$C_{XY}(\omega) = \sum_{\theta} \cos\theta \sin\theta E(\omega,\theta) \tag{7.12}$$

where it is assumed that the wave components propagating in different directions are statistically independent. The cross spectrum C_{XY} can be expressed in continuous form as

$$C_{XY}(\omega) = \int_0^{2\pi} \cos\theta \sin\theta E(\omega,\theta) d\theta\,. \tag{7.13}$$

Cross-spectra of the other time series pairs can be obtained in a similar manner. The full set of relations for buoy cross-spectra can be found in [Dean 1984].

It is convenient to define a normalized directional distribution of energy at a frequency ω as

$$S(\theta;\omega) = \frac{E(\omega,\theta)}{E(\omega)} \tag{7.14}$$

with unit integral

$$\int_0^{2\pi} S(\theta;\omega) d\theta = \frac{\int_0^{2\pi} E(\omega,\theta) d\theta}{E(\omega)} = \frac{E(\omega)}{E(\omega)} = 1\,. \tag{7.15}$$

With this definition, Equation 7.13 and the other referenced spectral relations can be combined and expressed in terms of $S(\theta;\omega)$. Dropping the frequency dependence these relations can be expresses as

$$
\begin{aligned}
\frac{\mathrm{Im}(C_{XZ})}{((C_{XX}+C_{YY})C_{ZZ})^{1/2}} &= \int_0^{2\pi}\cos\theta S(\theta)d\theta \equiv a_1 \\
\frac{\mathrm{Im}(C_{YZ})}{((C_{XX}+C_{YY})C_{ZZ})^{1/2}} &= \int_0^{2\pi}\sin\theta S(\theta)d\theta \equiv b_1 \\
\frac{C_{XX}-C_{YY}}{C_{XX}+C_{YY}} &= \int_0^{2\pi}\cos 2\theta S(\theta)d\theta \equiv a_2 \\
\frac{2\,\mathrm{Re}(C_{XY})}{C_{XX}+C_{YY}} &= \int_0^{2\pi}\sin 2\theta S(\theta)d\theta \equiv b_2
\end{aligned}
\tag{7.16}
$$

These four relations between the cross-spectra of the buoy measurements and the directional distribution of wave energy, derived by [Long 1980], form the basis for most of the buoy analysis techniques currently used.

D. EXTENSION TO SUBSURFACE SENSORS

As discussed in the previous section, the motion of a wave buoy is directly related to the fluid velocity, therefore, the cross-spectra of a tri-directional current meter yields the same low resolution directional wave information obtained from buoy measurements. Substituting the normalized spectra of the vertical (Z) velocity component w, and the horizontal (X, Y) velocity components u and v into Equation 7.16, the lowest four Fourier moments of the directional distribution of wave energy can be obtained and are given by

$$a_1(\omega) = \frac{\mathrm{Im}(C_{wu}(\omega))}{[C_{ww}(\omega)[C_{uu}(\omega)+C_{vv}(\omega)]]^{1/2}}, \tag{7.17}$$

$$b_1(\omega) = \frac{\mathrm{Im}(C_{wv}(\omega))}{[C_{ww}(\omega)[C_{uu}(\omega)+C_{vv}(\omega)]]^{1/2}}, \tag{7.18}$$

$$a_2(\omega) = \frac{C_{uu}(\omega)-C_{vv}(\omega)}{C_{uu}(\omega)+C_{vv}(\omega)}, \tag{7.19}$$

$$b_2(\omega) = \frac{2\,\mathrm{Re}(C_{uv}(\omega))}{C_{uu}(\omega)+C_{vv}(\omega)}, \tag{7.20}$$

where $C(\omega)$ is the spectral matrix of the velocity components u, v, w. Since the wave direction, θ, is referenced to the navigation frame (N-E-D), vehicle borne sensor measurements must be transformed prior to use. It is interesting to note that the estimates

of these directional moments are insensitive to errors, so long as the errors are the same on all measurement axes of the sensors, which is typical with oceanographic sensors installed on AUVs.

The objective of the data analysis is to infer the directional distribution $S(\theta)$, from the four measured moments a_1, b_1, a_2, and b_2. The most widely used techniques are described below.

a) The Cosine Power Distribution

[Longuet-Higgins 1963] introduced a simple cosine-power distribution,

$$S(\theta) = A\cos^{2s}\left(\frac{\theta - \theta_{mean}}{2}\right) \tag{7.21}$$

with θ_{mean} the mean propagation direction, s a parameter that controls the width of the distribution and A, a normalization coefficient. The parameters θ_{mean} and s are determined by fitting Equation 7.21 to the relations given in Equations 7.17-7.20.

The main drawback to this simple method is that Equation 7.21, with only two free parameters can describe only unimodal distributions, and thus fails in situations with a bimodal sea state (e.g., multi-directional seas during a wind veering event or swell arriving from two different sources).

b) The Maximum Entropy Method

[Lygre and Krogstad 1986] introduced the maximum entropy or MEM estimate of $S(\theta)$. Unlike Equation 7.21, this approach can describe both unimodal and bimodal distributions and exactly fits the relations given in Equations 7.17-7.20. This directional spectrum is given by

$$S(\theta) = \frac{1}{2\pi}\frac{1 - \phi_1 c_1^* - \phi_2 c_2^*}{\left(1 - \phi_1 e^{-i\theta} - \phi_2 e^{-2i\theta}\right)^2} \tag{7.22}$$

with

$$
\begin{aligned}
c_1 &\equiv a_1 + ib_1 \\
c_2 &\equiv a_2 + ib_2 \\
\phi_1 &\equiv \frac{c_1 - c_2 c_1^*}{1 - |c_1|^2} \\
\phi_2 &\equiv c_2 - c_1 \phi_1
\end{aligned}
\tag{7.23}
$$

Still, the directional distribution is poorly constrained by only four moments and the estimates require careful interpretation, [Krogstad 1991].

c) Mean Direction and Directional Spread

An alternative approach that avoids the pitfalls of $S(\theta)$ estimation, is to describe the directionality of waves by a few simple parameters. For narrow $S(\theta)$, a mean propagation direction θ_m and a root-mean-square measure of the directional spreading energy σ_θ can be defined in terms of the first-order and second-order Fourier moments a_1, b_1, a_2 and b_2 [Kuik 1988], given by,

$$\theta_m = \tan^{-1}\left(\frac{b_1}{a_1}\right) \tag{7.21}$$

$$\sigma_\theta^2 = 2[1 - [a_1 \cos(\theta_m) + b_1 \sin(\theta_m)]] \tag{7.22}$$

$$\theta_m = \frac{1}{2}\tan^{-1}\left(\frac{b_2}{a_2}\right) \tag{7.23}$$

$$\sigma_\theta^2 = \frac{1}{2}[1 - [a_2 \cos(2\theta_m) + b_2 \sin(2\theta_m)]]. \tag{7.24}$$

Again, this method fails to identify bimodal distributions but it is useful to determine a base direction so that a control command could be determined. More on this approach will be discussed later in this chapter.

E. CORRECTION FOR A MOVING PLATFORM (THE DOPPLER EQUATION)

The equations for the wave directionality estimations presented in the previous section is valid for a non-moving sensor. However, when information is obtained from an AUV, corrections must be made to account for the vehicle motion. As discussed in

Chapter III, the wave frequency which the vehicle encounters while moving through the wave field has been shifted. This shift can be determined by using the well known Doppler equation, Equations 2.56 or 4.25.

Using the techniques outlined in the previous section will give the wave directional distribution as a function of vehicle encounter frequency. If these estimations are used in conjunction with the Doppler equation in a recursive manner, the estimation of $S(\theta)$ can be found as a function of true frequency.

The method by which this is performed is outlined below;

- Determine the three components of the fluid velocity in vehicle body fixed coordinates.
- Transform the fluid velocities into the global navigation frame using Equation 2.8.
- Compute the auto- and cross-spectra of the fluid velocity components.
- Determine the Fourier moments using Equations 7.17-7.20.
- Convert the Fourier moments into Krogstad notation and use the MEM to determine the directional distribution $S(\theta)$.
- Using the vehicles mean velocity, and the mean direction obtained from Equation 7.21 or 7.23, apply the Doppler equation to determine the frequency shift.
- Return to 3 and complete the process until frequencies converge.

The corrections to the estimation of $S(\theta)$ using the Doppler equation are quite small for slow moving vehicles. Considering, for example, the NPS Phoenix AUV which has a maximum forward velocity of 1.5 m/s, the error associated with not using the Doppler equation are approximately $\pm$ 1 sec in identification of wave periods between 4 and 40 seconds. Similarly, the error in direction estimation is approximately 5-7 degrees. When an AUV goes into a station keeping mode, where vehicle velocities are significantly reduced, the modifications required due to the Doppler shift are negligible.

F. DETERMINATION OF CONTROL COMMANDS

The resulting directions and variances, from Equations 7.21-7.24, are for each frequency component of the wave field. To use this information in determining a heading command, single direction must be found. Bulk Fourier moments, weighted by the energy density of the wave field,

$$\begin{bmatrix} a_1^b \\ b_1^b \\ a_2^b \\ b_2^b \end{bmatrix} = \frac{1}{E^b} \int_{f_l}^{f_u} E(f) \begin{bmatrix} a_1(\omega) \\ b_1(\omega) \\ a_2(\omega) \\ b_2(\omega) \end{bmatrix} d\omega \qquad (7.2\#)$$

with E^b the swell variance given by,

$$E^b = \int_{f_l}^{f_u} E(\omega) d\omega, \qquad (7.2\#)$$

may be substituted into Equations 7.21-7.24 to yield a bulk fluid direction and variance. It is this bulk fluid direction that is used in generation the heading command dependent on the mission requirements.

G. SUMMARY

This chapter has presented the techniques currently employed for the determination of wave directional estimations from standard wave following buoys. It has extended this analysis for use in determining directional estimates from data gathered by an Autonomous Underwater Vehicle. Using this data gathered, an approach was presented which will allow the deployed vehicle to obtain information about the directionality of its working environment thereby allowing the vehicle to have information available to make decisions regarding mission execution.

VIII. EXPERIMENTAL RESULTS

A. INTRODUCTION

With the theoretical presentation of this dissertation complete, the primary focus of this chapter will be on the experimental validation of the Disturbance Compensation Controller (DCC). In addition, results from the ONR sponsored AUVFEST '98 will prove the concept of wave direction estimation from a moving platform presented in Chapter VII.

This chapter will begin with a discussion of the real-time implementation of the DCC in the NPS Phoenix AUV. It will follow with a presentation of the experimental results, conducted in Monterey Harbor, which displays the achievable performance of the DCC. Comparison between theoretical and experimental results will be made. Lastly, directional energy and spectral plots obtained by Phoenix, while operating in the Gulf of Mexico, south of Gulfport, MS, will be shown.

B. SOFTWARE IMPLEMENTATION

The implementation of this control process is unique since it is split between the two CPUs installed in Phoenix. The NPS AUV uses a Pentium based PC-104 running QNX and a GESPAC Card Cage running OS9 for mission control and execution. The DCC requires information from both processors, connected by Ethernet sockets, to compute and pass the commanded propeller RPMs to the execution level.

The control architecture presently running in Phoenix is based on shared memory processes. The PC-104 computer runs a "main" process that controls the synchronization of the data sharing, while the GESPAC clock controls the real-time control features. The two-processors use the shared memory as the common data buffer, controlled by semaphores to ensure the information transfer is consistent with the clock speed. A graphical representation of this description is shown in Figure 8.1. As seen in the graphic, for the DCC implementation, all needed processes are run in the PC-104 with the main purpose of the GESPAC is to provide the commanded voltages to the propulsion motors.

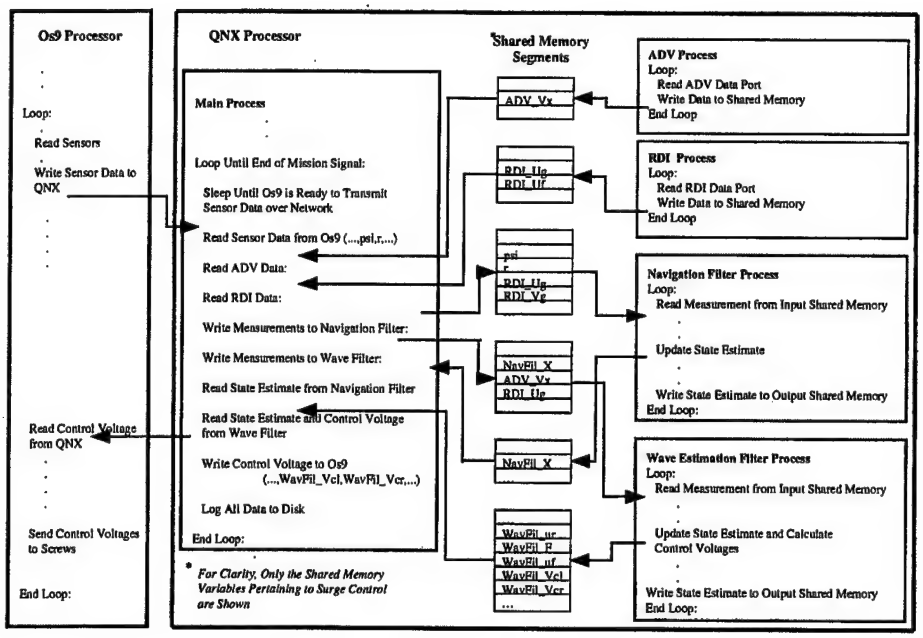

Figure 8.1 Software Implementation of DCC

A block diagram of the DCC implementation in the Phoenix AUV was given in Chapter VI, Figure 6.1. It is redisplayed as Figure 8.1 for easy reference. This diagram represents the melding of the software and the hardware in the vehicle. The ground velocity is from the RDI, the relative velocity from the ADV and ψ, r from the directional gyro.

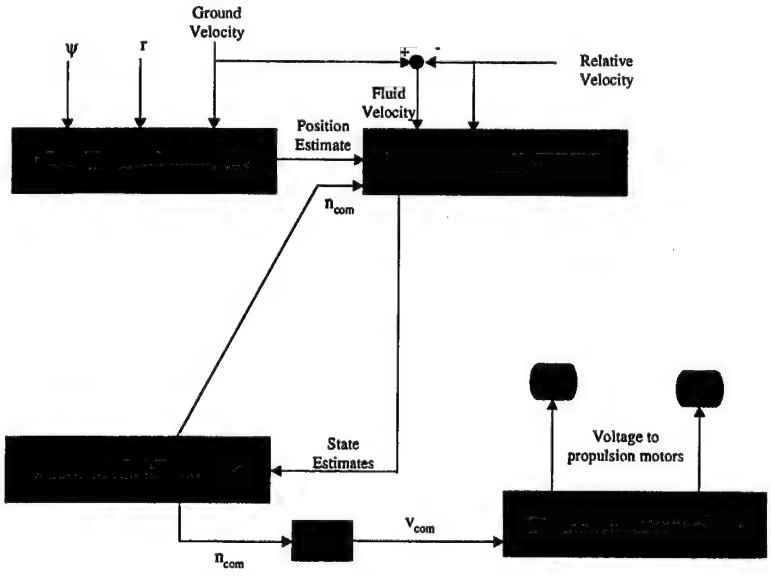

Figure 8.2 Block Diagram of DCC Implementation

C. EXPERIMENTAL VALIDATION OF THE DCC

The DCC was tested in Monterey Harbor between the months of March and May 1999. During this time, the Phoenix was held under surge control for over 90 minutes, during various runs, without a drive off. Table 8.1 provides a sample of the runs conducted during the validation of the controller.

Date	Run#	Length	*DRR*	σ_n / n_{max}	comments
4/2/99	4	4 min	0.3624	2.96	high gain, short run
	5	4 min	0.6324	3.08	high gain, short run, vehicle physical disturbed
	6	4 min	0.4312	0.265	high gain, short run
	8	4 min	0.5090	0.285	high gain, short run
4/22/99	3	10 min	0.5508	0.108	high gain, single shaft
5/25/99	6	10 min	0.3620	0.192	medium-high gain, ADV noise problem
	8	10 min	0.3978	0.126	medium-low gain, ADV noise problem
	9	10 min	0.4957	0.083	low gain, ADV noise problem
	11	10 min	0.3587	0.202	medium-high gain, ADV noise problem
	12	10 min	0.4276	0.144	medium-low gain, ADV noise problem

Table 8.1 Sample Summary of DCC Validation Runs

Defining a measure of performance, the disturbance rejection ratio (*DRR*), as the ratio of standard deviation of the vehicle ground velocity to the standard deviation of the fluid velocity, the ability of an AUV to reject disturbances for different conditions and control designs can be compared. Referring to the DRR definition, for perfect disturbance cancellation the DRR will be equal to zero, while for designs where the control input excites the vehicle, as was shown in Chapter V, the DRR will be greater than one. For each operating point, the standard deviation of the propeller response is normalized by the maximum propeller revolutions, n_{max}.

Table 8.1 indicates that excellent disturbance rejection was achieved, even for the short runs where only limited statistical information was recorded. The tests showed that even when the vehicle was disturbed by a source other than the fluid velocity, it was able to return to the commanded position in a stable fashion.

A series a plots, Figures 8.3-8.8, show the results of one of the validation runs. This run was conducted on April 22, 1999 in Monterey Harbor. The Phoenix was commanded to a navigational position of 0 meters in the longitudinal direction. As the results indicate, the vehicle behaved as expected. The standard deviation of the

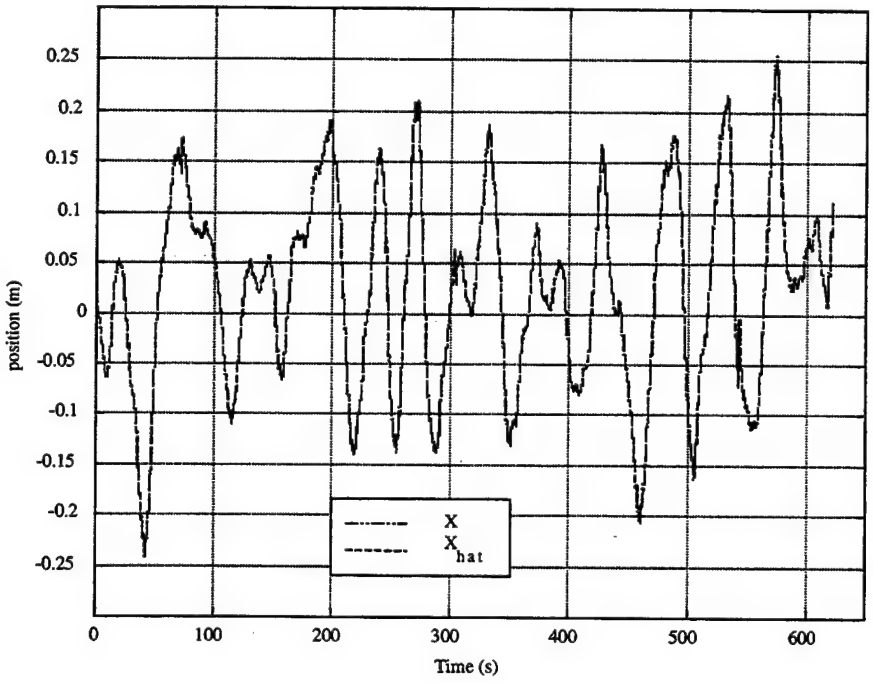

Figure 8.3 Comparison of Measured and Estimated Position, April 22, 1999, Run#3

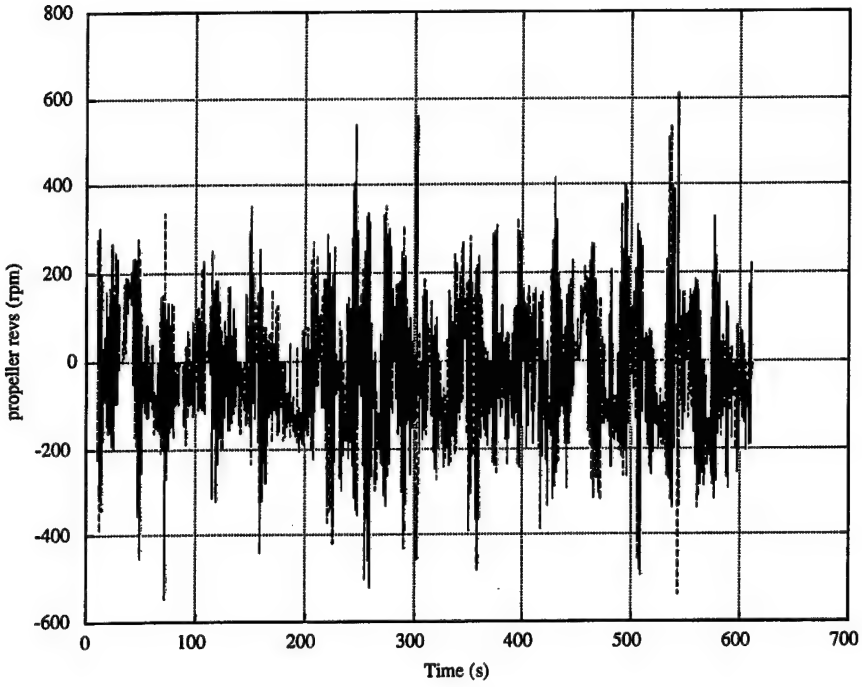

Figure 8.4 Propeller Response, April 22, 1999, Run#3

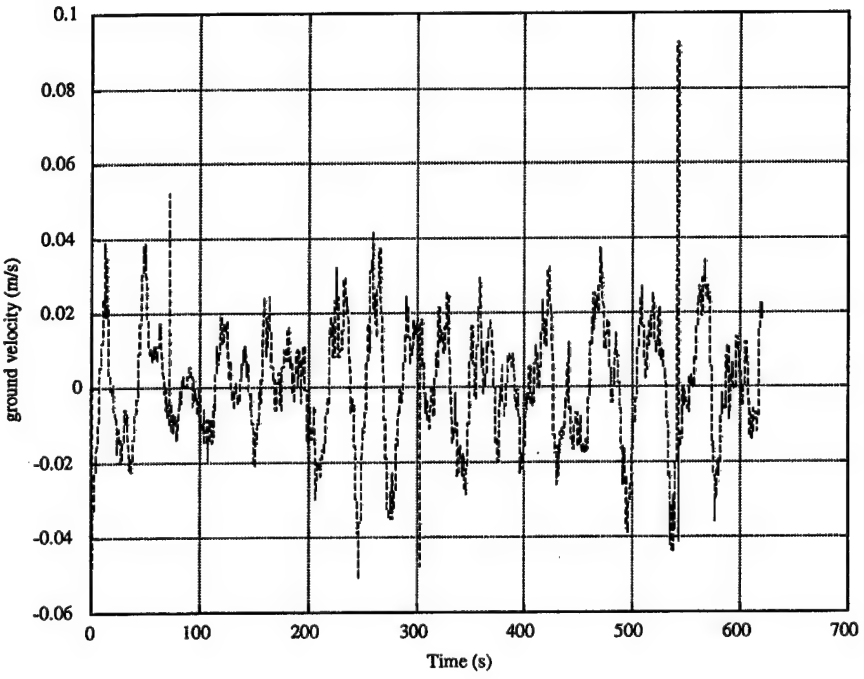

Figure 8.5 Measured Ground Velocity, April 22, 1999, Run#3

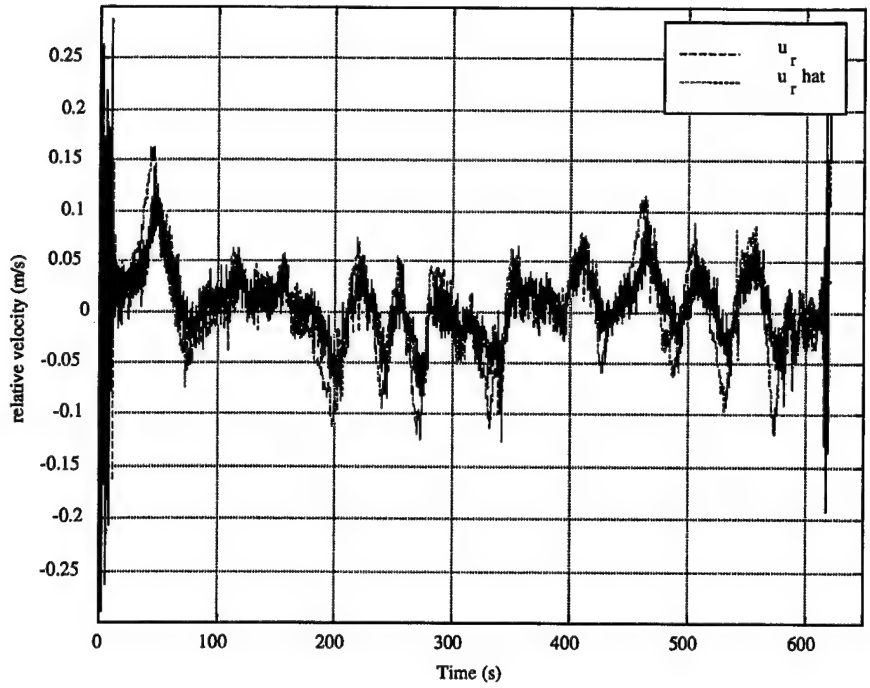

Figure 8.6 Comparison of Measured and Estimated Relative Velocity, April 22, 1999, Run#3

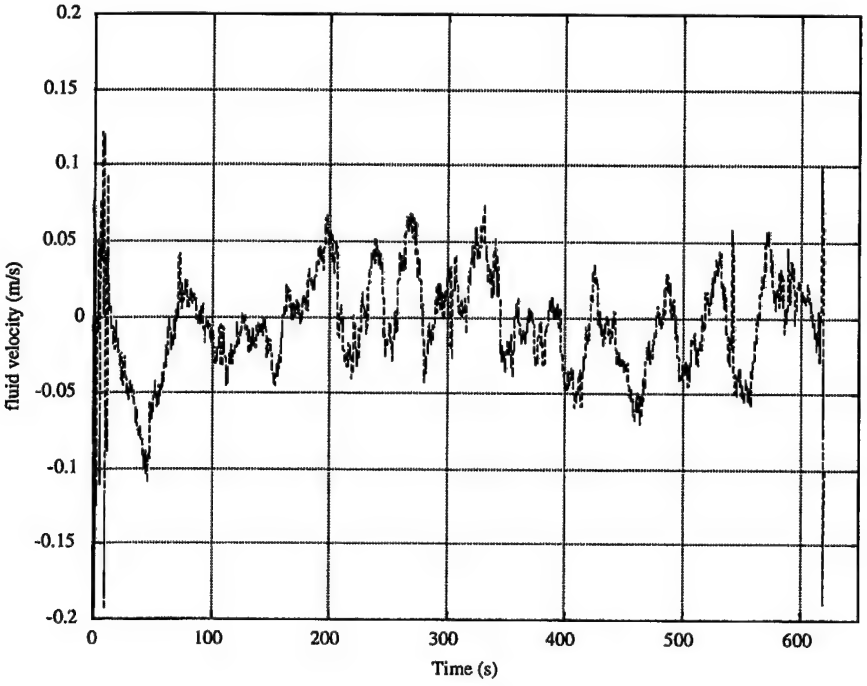

Figure 8.7 Fluid Velocity Estimate, April 22, 1999, Run#3

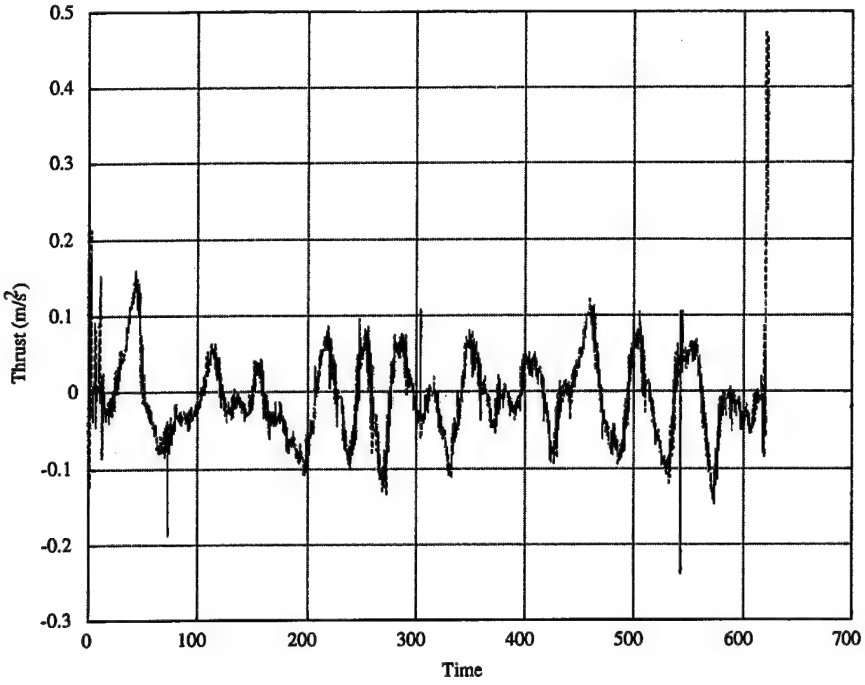

Figure 8.8 Estimated Thrust, April 22, 1999, Run#3

positional error was 9.6 cm with ground velocity standard deviation of 1.5 cm/s.

This run was the most interesting of the validation runs conducted. At the beginning of this run, it was noticed that the starboard shaft was not turning. Even with this propulsion system casualty, the vehicle was able to hold position and the controller did not go unstable. With only one shaft turning the effective input gain for the vehicle was reduced by 50%. Operations of this nature indicate a very robust design. It can be seen in Figure 8.4, that there is a small increase in propeller revolutions around the 50 second point of the run. Data analysis indicated that this was approximately when the starboard shaft failed. Investigation into the cause of the shaft failure determined that a universal joint in that shafting had worked loose.

As a graphical representation of the performance expected for the DCC a various simulations ware conducted, using the asynchronous simulator discussed in the Chapter VI, with the estimated fluid velocity obtained during this run (April 22, 1999, run# 3) as the disturbance. The gains on the DCC were varied to produce a position response verses propeller response curve. The actual experimental results, presented in Table 8.1, were superimposed on the theoretical curve obtained from simulation. These results are shown

in Figure 8.9. As seen, the experimental and theoretical results are very close indicating a physically realistic simulator.

The comparisons displayed in Figure 8.9, contrast data analyzed from experimental results together with computer predicted results with the same disturbance, and yield insight into the achievable performance of the DCC. It indicates that there is a limit to the amount of disturbance rejection that is physically realizable. This limit is controlled by ability of the propulsion system to produce the needed input to maintain position without excessive oscillations. The excessive oscillations have a detrimental effect of the life of the propulsion system.

As a note, the short runs, displayed in Figure 8.9, were conducted with a controller gain parameter of η = 100, a high gain. If the length of these runs were extended, these points would move closer to the curve as with the other runs displayed.

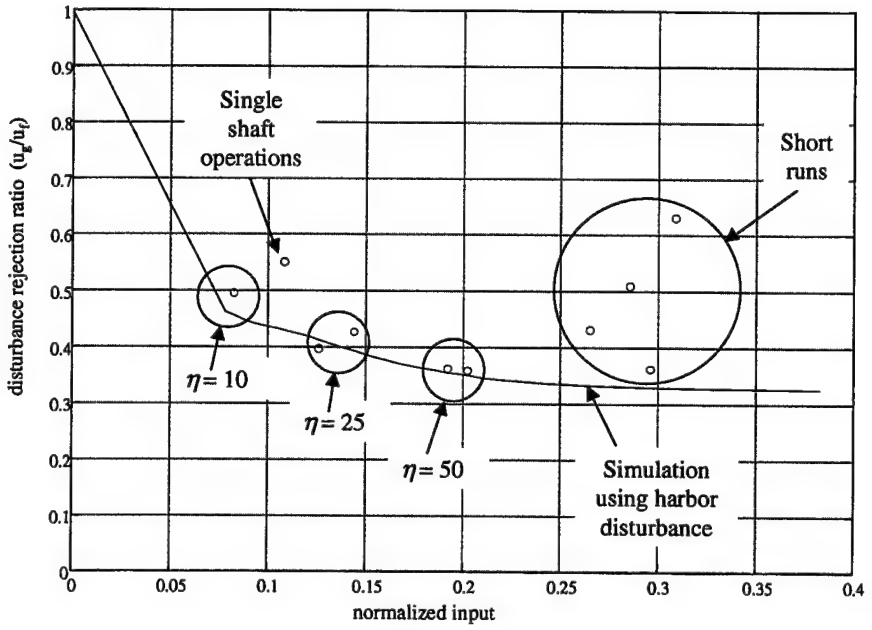

Figure 8.9 Comparison of DCC Performance, Simulation and Experimental

Up to this point, the only results presented are for the Phoenix maintaining position to the origin, the point which the run was initiated. Questions arise as to how effective the controller is in dealing with transients. This question may be answered by referring to Figure 8.10. This figure depicts the transient response of the Phoenix for the

various DCC gains presented in Figure 8.9. As the figure indicates, the controller deals with transients extremely well.

The responses displayed in Figure 8.10 are for the regulator solution. What is meant by this, recalling that the SMC formulation requires kinematically consistent position, velocity and acceleration, is that no command inputs, other that position were used. In doing this, it is expected that the vehicle will over shoot and oscillate around the commanded position consistent with some settling time.

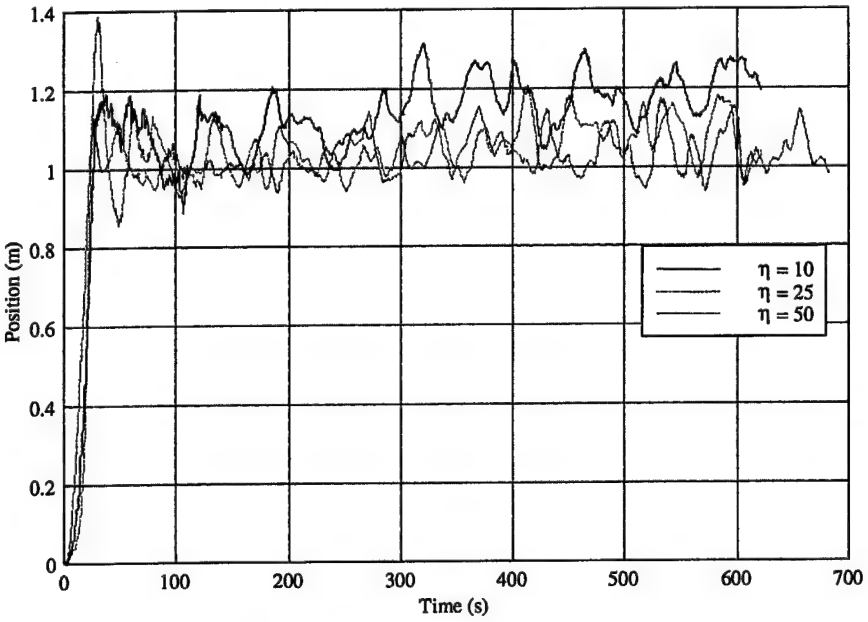

Figure 8.10 Comparison of Transient Response for Various Control Gains

With these transient responses come some issues with regard to operational implementation. If the goal is to position the vehicle close to, but with out touching, an object, some means of predicting the transient must be available. A resulting question that needs to be answered is; Does the developed simulator, which, based on the comparison in Figure 8.9, accurately predict the transient response? By comparing the results of the experimental runs and the simulated results, for the same disturbance input and DCC design, see Figure 8.11, the question can be answered, "yes."

As seen in this plot, the simulated results accurately reflects the measured transient response of the Phoenix. The steady state response, however, does not match exactly. The reason for this is two-fold. First, the Phoenix, for recovery reasons, is

maintained approximately two-pounds buoyant. This weight and buoyancy mismatch, as discussed in Chapter II, cause additional excitation forces resulting from the wave induced fluid accelerations. Since the fluid acceleration cannot be measured, this additional excitation force is difficult to replicate in simulation yielding errors between the real and simulated response. Second, the experimental results are measured from a 6DOF rigid body, where as the simulator results come from a 1DOF surge model. The coupling effects from the surge-pitch dynamics will effect the comparison.

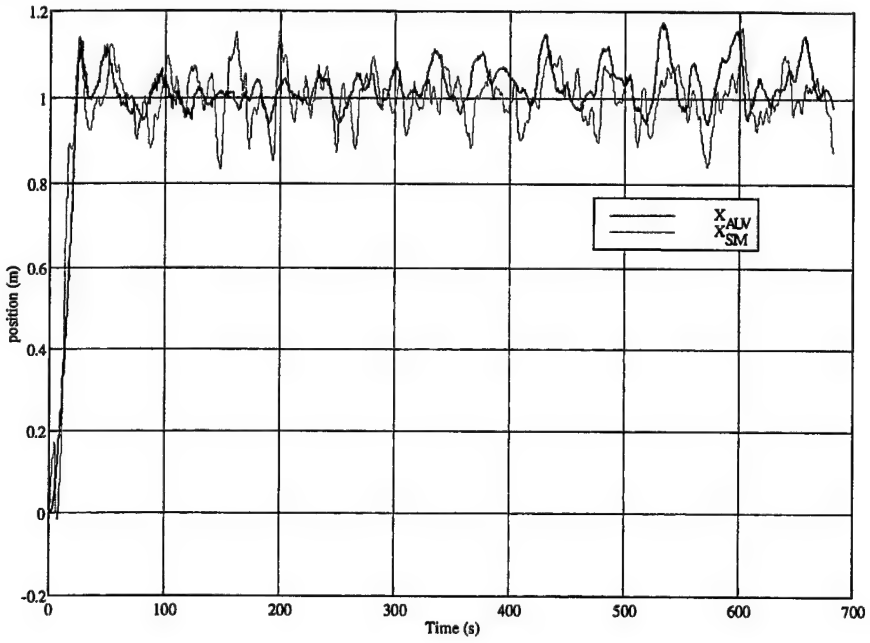

Figure 8.11 Transient Response Prediction of the DCC

D. WAVE DIRECTIONAL ESTIMATION USING THE NPS PHOENIX AUV

During November 1998, the NPS Center for AUV Research, under the direction of Professor Anthony Healey, participated in the ONR sponsored AUVFEST '98. This AUV technology demonstrator was held in the Gulf of Mexico, south of Gulfport, MS. A complete description of the exercise can be found in Appendix D.

The Phoenix AUV was used during this exercise as a mobile sensor to gather oceanographic data. Using the concepts presented in Chapter VII, the vehicle conducted 27 short-term sampling missions. The products that were obtained included directional energy plots, directional spectrum plots and mean current estimations.

The key to the ability of Phoenix to obtain data capable of producing this information is the combined ADV/RDI/MotionPak/Directional Gyro sensor suite. With these sensors, accurate three dimensional fluid velocities, expressed in global quantities, were capable of being obtained in post-processing. Since the RDI/ADV sensors are collocated, little vehicle induced motion remains after processing the data.

The data obtained validated the concept of obtaining tactical oceanographic data from an underwater vehicle. During the collection of the data, remnants of Hurricane Mitch were still present in the Gulf, providing an excellent source of ground swell. In addition, there was a significant wind generated wave component in a different direction than the swell component, resulting in a multi-modal spectrum.

The results presented in Figures 8.12-8.14 provide a sample of the oceanographic data obtained during this offshore exercise. As seen in Figure 8.12, the bi-modal properties of the seaway are captured, as well as an estimate of the significant wave height. The ability to estimate the dual directions is due to the use of the MEM algorithm presented in Chapter VII. Figure 8.13 presents the associated spectrum plots for this energy estimate. The ability of an AUV to estimate currents is shown in Figure 8.14. Using a triangular, time based run, the current can be determined using set and drift calculations from the error in final position as well as the heading error on each leg. This information can be feed directly into the vehicle's navigation process to account for the offset due to current thereby increasing navigation accuracy. Short term averages from each of the three legs are in general agreement with the overall average determined from the navigational drift.

E. SUMMARY

This chapter has presented the experimental results associated with this dissertation. The results validate the theory and show that it is possible for a small AUV to reject wave induced disturbances making it capable of performing positioning tasks in shallow water. In addition, the robustness of the design to sensor noise and propulsion faults has been demonstrated.

Phoenix Survey Data

Significant Wave Height (m): 0.351
Peak Frequency(Hz)/Period(sec): 0.25 / 4
Peak Direction: 90degrees

Max. Energy: 0.005203cm^2/Hz

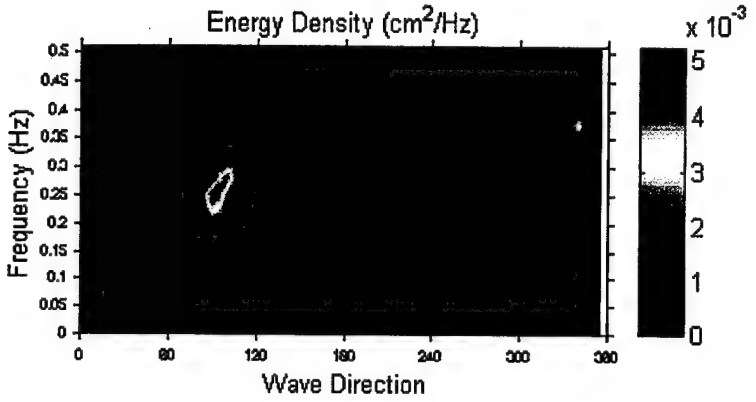

Figure 8.12 Sample Direction Energy Plot From Phoenix Data, Nov. 4, 1998 (Run# 9), Gulf of Mexico

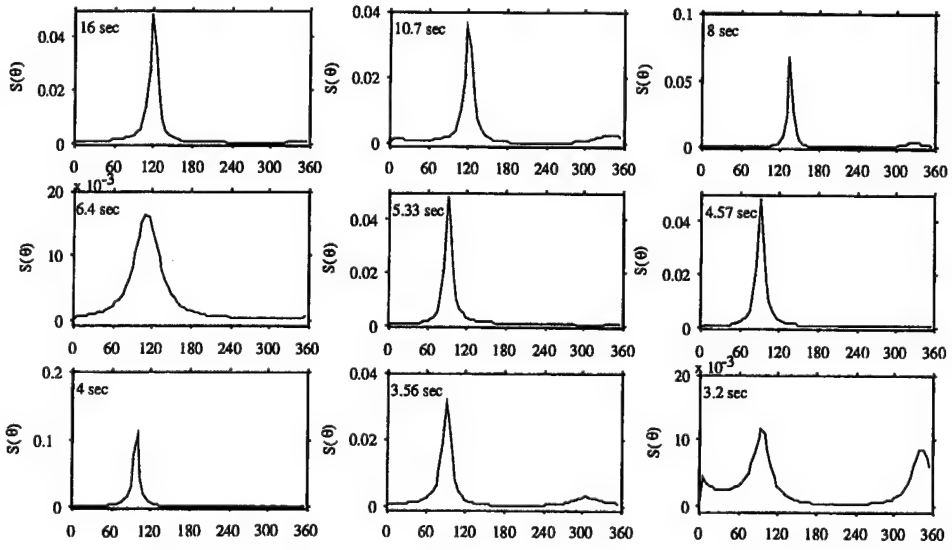

Figure 8.13 Sample Direction Spectrum Plots From Phoenix Data, Nov. 4, 1998 (Run# 9), Gulf of Mexico

As a supplement, due to the sensor suite available, it was shown that tactical oceanographic data is obtainable from a moving AUV. The vehicle in this manner becomes an intelligent, mobile off-board sensor, thus presenting the argument for AUV deployment with operational fleet units.

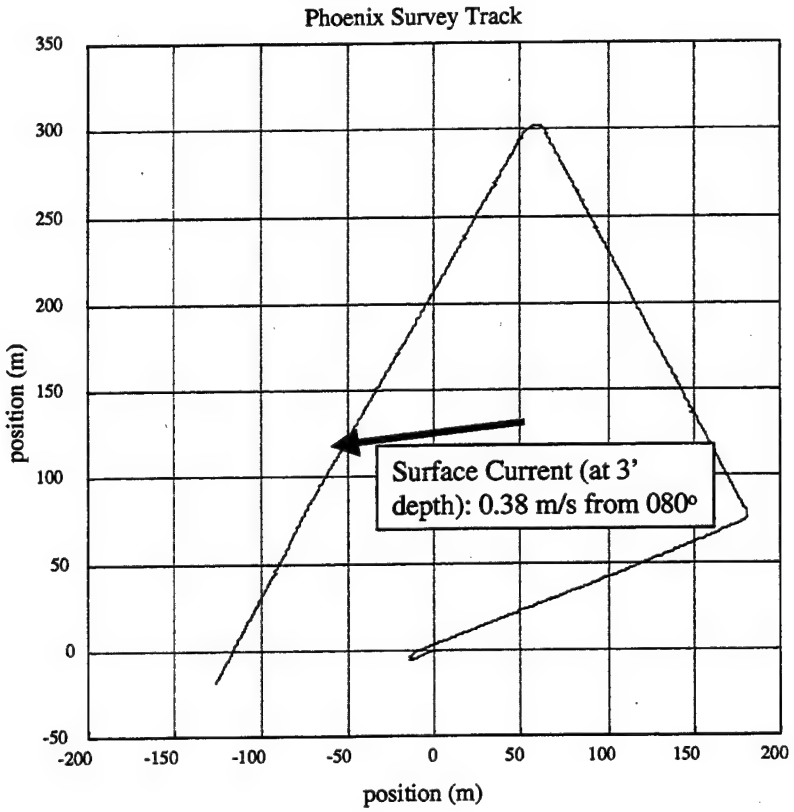

Figure 8.14 Short-term Current Estimation from Phoenix, November 8, 1999, (Run# 2), Gulf of Mexico

IX. CONCLUSIONS AND RECOMMENDATIONS

A. CONCLUSIONS

This research has shown through modeling, simulation and experimental validation that intervention tasks performed by intelligent underwater robots are improved by their ability to gather, learn and use information about their working environment. The development, implementation and verification of a real-time embedded Disturbance Compensation Controller (DCC) for small AUVs, has provided a new technology showing that it is possible to use underwater vehicles for station-keeping tasks in shallow water.

The work conducted in support of the dissertation objectives has provided three specific contributions to the field of tetherless underwater robotics. First, a new generalized approach to the modeling of small underwater vehicles subject to shallow water wave and current effects was developed. Using appropriate modeling formulations, the fluid disturbance effects are incorporated directly into the equations of motion leading to model based control laws for disturbance compensation. In addition, this formulation provides the ability to construct a generalized distributed simulation capability for the evaluation of underwater vehicle systems in shallow water, which is particularly useful to U.S. Navy tactical decision making.

Secondly, it is proven using asynchronous simulations and in-ocean experimental validations, that substantial compensation of wave induced disturbances may be achieved from direct on-line measurements of the water column velocities. This technique eliminates the need to develop and incorporate sophisticated predictive disturbance models in the control system design.

Thirdly, it is shown how small underwater vehicles, using direct fluid measurements, can obtain short-term wave magnitude and direction, as well as current estimates, thereby providing useful information in the area of tactical oceanography. It is also shown how a general seaway direction may be obtained from this information for use in mission planning and control.

In addition to the general contributions listed above, several specific conclusions may be drawn from this research. In particular,

- The input requirements associated with the DCC are vehicle position, relative velocity, propulsion force, and water column velocity. The attractive nature of the DCC is that these quantities may be measured or estimated from a hull mounted sensor suite. With these the full benefits of DCC can be realized.

- The DCC proved to be very robust to sensor noise and propulsion system faults. Stable vehicle performance was maintained in the presence of the loss of a propulsion shaft.

- The design of the propulsion system must allow for a rapid, oscillatory response to the call for propeller speed commands. In addition, considerations for fault tolerant operations are recommended.

- For the application of dynamic station-keeping, propulsion system lags and associated thrust reduction terms must be identified and taken into account.

- Identified parameters of the nonlinear model provided stable and easily tunable controllers, as verified by in-water experiments. Excellent agreement was achieved between experimental and simulated results.

- Seaway models developed using AR representations require high order to effectively achieve spectral matching. However, lower order models (four or six) can be used adequately for estimation and control.

- Extended Kalman filtering methods for seaway estimation appear to be satisfactory.

B. RECOMMENDATIONS FOR FUTURE RESEARCH

As a result of the work performed in this dissertation several research areas have arisen requiring further investigation. These include:

- The validation of the 6DOF model for other control modes with field data is recommended. This is particularly interesting in flight control where motion minimization is critical to improve side-scan imagery.

- Application of the disturbance compensation techniques presented herein to other control modes used in shallow water positioning needs inquiry. By achieving compensation in all three planes, small AUVs may be employed in a number of positioning tasks, including mine neutralization.

- A sensitivity study as to the required degree and accuracy of the disturbance model, with regard to disturbance compensation, is warranted. It is believed that improved disturbance dynamics models may increase DCC robustness.

- While this work has used EKF methods for the identification of seaway dynamics, other techniques, such as neural networks and MUSIC, may have advantages that could be explored.

- The DCC formulation does allow for prediction of future water column velocities. This added information may possibly provide additional benefits not explored here, although, this study has indicated that the DCC is not highly sensitive to future information.

APPENDIX A. EQUATIONS OF MOTION AND PARAMETERS FOR THE NPS PHOENIX

The equations of motion, parameter description and parameter values used to simulate the dynamic behavior of the NPS Phoenix AUV is given in this Appendix.

PHYSICAL PARAMETERS

Parameter	Description	Value
W	Weight	1934.9 N (435 lbs)
m	mass	197.2 kg (13.52 lb-sec^2-ft^{-1})
B	Buoyancy	1934.9 N (435 lbs)
l	Characteristic Length	2.225 m (7.302 ft)
I_{xx}	Mass Moment of Inertia about x-axis	3.66 N-m-sec^2 (2.7 ft-lb-sec^2)
I_{yy}	Mass Moment of Inertia about y-axis	56.94 N-m-sec^2 (42. ft-lb-sec^2)
I_{zz}	Mass Moment of Inertia about z-axis	61.01 N-m-sec^2 (42.0 ft-lb-sec^2)
I_{xy}	Cross Product of Inertia about xy-axes	0.0 N-m-sec^2 (0.0 ft-lb-sec^2)
I_{yz}	Cross Product of Inertia about yz-axes	0.0 N-m-sec^2 (0.0 ft-lb-sec^2)
I_{xz}	Cross Product of Inertia about xz-axes	0.0 N-m-sec^2 (0.0 ft-lb-sec^2)

x_G	x Coordinate of *CG* From Body Fixed Origin	0.003 m (0.01 ft)
y_G	y Coordinate of *CG* From Body Fixed Origin	0.003 m (0.01 ft)
z_G	z Coordinate of *CG* From Body Fixed Origin	0.0128 m (0.042 ft)
x_B	x Coordinate of *CB* From Body Fixed Origin	0.003 m (0.01 ft)
y_B	y Coordinate of *CB* From Body Fixed Origin	0.00 m (0.0 ft)
z_B	z Coordinate of *CB* From Body Fixed Origin	0.00 m (0.0 ft)
x_{bvt}	Location of Bow Vertical Thruster from *CG*	0.432 m (1.420 ft)
x_{svt}	Location of Stern Vertical Thruster from *CG*	-0.432 m (-1.420 ft)
x_{blt}	Location of Bow Lateral Thruster from *CG*	0.585 m (1.920 ft)
x_{slt}	Location of Stern Lateral Thruster from *CG*	-0.585 m (-1.920 ft)
y_{ls}	Location of Left Propeller from *CG*	-0.10 m (-0.33 ft)
y_{rs}	Location of Left Propeller from *CG*	0.10 m (0.33 ft)

CONTROL INPUTS

Parameter	Description	Value
F_{ls}	Left Propeller Force	±44.45 N (± 10 lbs)
F_{rs}	Right Propeller Force	±44.45 N (± 10 lbs)
F_{blt}	Bow Lateral Thruster Force	± 22.25 N (± 5 lbs)
F_{slt}	Stern Lateral Thruster Force	± 22.25 N (± 5 lbs)
F_{bvt}	Bow Vertical Thruster Force	± 22.25 N (± 5 lbs)
F_{svt}	Bow Vertical Thruster Force	± 22.25 N (± 5 lbs)
δ_{br}	Bow Rudder Deflection	± 0.4 rad
δ_{sr}	Stern Rudder Deflection	± 0.4 rad
δ_{bp}	Bow Plane Deflection	± 0.4 rad
δ_{sp}	Stern Plane Deflection	± 0.4 rad

NON-DIMENSIONAL HYDRODYNAMIC COEFFICIENTS

Surge Hydrodynamic Coefficients:

X'_{pp}=0.0	X'_{pr}=0.0	X'_{vp}=0.0	$X'_{q\delta_{sp}}$=0.0
X'_{vv}=-0.01743	X'_{qq}=0.0	$X'_{\dot{u}}$= -0.00282	X'_{vr}=0.0
$X'_{r\delta_{br}}$=0.0	X'_{ww}=0.0	X'_{rr}=-0.00753	X'_{wq}=0.0
$X'_{q\delta_{bp}}$=0.0	$X'_{r\delta_{sr}}$=0.0	$X'_{\delta_r\delta_r}$= -0.01018	$X'_{\delta_{sp}\delta_{sp}}$=-0.01018
$X'_{\delta_{bp}\delta_{bp}}$=-0.01018	X_{res}=-0.4024	$X'_{q\delta_{sp}}$=0.0	

Sway Hydrodynamic Coefficients:

$Y'_{\dot{p}}$=0.0	$Y'_{\dot{v}}$=-0.03430	Y'_{wp}=0.0	$Y'_{\delta sr}$=0.01241
$Y'_{\dot{r}}$=-0.00178	Y'_{p}=0.0	Y'_{wr}=0.0	$Y'_{\delta br}$=0.01241
Y'_{pq}=0.0	Y'_{r}=0.01187	Y'_{v}=-0.10700	Y'_{qr}=0.0
Y'_{vq}=0.0	Y'_{vw}=0.0		

Heave Hydrodynamic Coefficients:

$Z'_{\dot{q}}$=-0.00253	$Z'_{\dot{w}}$=-0.09340	Z'_{w}=-0.78440	Z'_{pp}=0.0
Z'_{vp}=0.0	Z'_{q}=-0.07013	Z'_{vv}=0.0	Z'_{pr}=0.0
$Z'_{\delta sp}$=-0.02110	Z'_{rr}=0.0	Z'_{vr}=0.0	$Z'_{\delta bp}$=-0.02110

Roll Hydrodynamic Coefficients:

$K'_{\dot{p}}$=-0.00024	$K'_{\dot{v}}$=0.0	K'_{wp}=0.0	$K'_{\dot{r}}$=0.0
K'_{p}=-0.00540	K'_{wr}=0.0	K'_{pq}=0.0	K'_{r}=0.0
K'_{v}=0.0	K'_{qr}=0.0	K'_{vq}=0.0	K'_{vw}=0.0

Pitch Hydrodynamic Coefficients:

$M'_{\dot{q}}$=-0.00625	$M'_{\dot{w}}$=-0.00253	M'_{w}=0.05122	M'_{pp}=0.0
M'_{q}=-0.01530	M'_{vv}=0.0	M'_{pr}=0.0	M'_{vp}=0.0
$M'_{\delta sp}$=-1.7664	M'_{rr}=0.0	M'_{vr}=0.0	$M'_{\delta bp}$=1.3260

Yaw Hydrodynamic Coefficients:

$N'_{\dot{p}}$=0.0	$N'_{\dot{v}}$=-0.00178	N'_{wp}=0.0	$N'_{\delta r}$=-1.7663
$N'_{\dot{r}}$=-0.00047	N'_{p}=0.0	N'_{wr}=0.0	$N'_{\delta r}$=1.3259
N'_{pq}=0.0	N'_{r}=-0.00390	N'_{v}=-0.00769	N'_{vw}=0.0
N'_{qr}=0.0	N'_{vq}=0.0		

EQUATIONS OF MOTION

The equations of motion for the NPS Phoenix AUV are presented in this section of the Appendix. These equations are based on the vector-matrix equation given in equation 2.87. The expanded equations use the assumption that Phoenix possesses both horizontal and vertical plane symmetry.

Mass Matrix:

$$M = \begin{bmatrix} m - X_{\dot{u}} & 0 & 0 & 0 & mz_G & -my_G \\ 0 & m - Y_{\dot{v}} & 0 & -(mz_G + Y_{\dot{p}}) & 0 & mx_G - Y_{\dot{r}} \\ 0 & 0 & m - Z_{\dot{w}} & my_G & -(mx_G + Z_{\dot{q}}) & 0 \\ 0 & -(mz_G + K_{\dot{v}}) & my_G & I_{xx} - K_{\dot{p}} & -I_{xy} & -(I_{xz} + K_{\dot{r}}) \\ mz_G & 0 & -(mx_G + M_{\dot{w}}) & -I_{xy} & I_{yy} - M_{\dot{q}} & -I_{yz} \\ -my_G & mx_G - N_{\dot{v}} & 0 & -(I_{xz} + N_{\dot{p}}) & -I_{yz} & I_{zz} - N_{\dot{r}} \end{bmatrix}$$

Centrifugal/Coriolis Matrix:

$C(x) =$

$$\begin{bmatrix} 0 & -mr & mq & m(y_G q + z_G r) & -mx_G q - Z_{\dot{w}} w & -mx_G r + Y_{\dot{v}} v \\ mr & 0 & -mp & -my_G p + Z_{\dot{w}} w & m(z_G r + x_G p) & -my_G r - X_{\dot{u}} u \\ -mq & mp & 0 & -mz_G p - Y_{\dot{v}} v & -mz_G q + X_{\dot{u}} u & m(x_G p + y_G q) \\ -m(y_G q + z_G r) & my_G p - Z_{\dot{w}} w & mz_G p + Y_{\dot{v}} v & 0 & -I_{yz} q - I_{xz} p + I_z r - N_{\dot{r}} r & I_{yz} r + I_{xy} p - I_y q + M_{\dot{q}} q \\ mx_G q + Z_{\dot{w}} w & -m(z_G r + x_G p) & mz_G q - X_{\dot{u}} u & I_{yz} q + I_{xz} p - I_z r + N_{\dot{r}} r & 0 & -I_{zz} r - I_{xy} q + I_x p - K_{\dot{p}} p \\ mx_G r - Y_{\dot{v}} v & my_G r + X_{\dot{u}} u & -m(x_G p + y_G q) & -I_{yz} r - I_{xy} p + I_y q - M_{\dot{q}} q & I_{zz} r + I_{xy} q - I_x p + K_{\dot{p}} p & 0 \end{bmatrix}$$

Control Allocation Matrix:

$B(x) =$

$$\begin{bmatrix} urX_{r\delta_{br}} + u|u|X_{\delta_r \delta_r} \delta_{br} & uqX_{q\delta_{bp}} + u|u|X_{\delta_{bp}\delta_{bp}} \delta_{bp} & urX_{r\delta_{sr}} + u|u|X_{\delta_r \delta_r} \delta_{sr} & uqX_{q\delta_{sp}} + u|u|X_{\delta_{sp}\delta_{sp}} \delta_{sp} & 1 & 1 & 0 & 0 & 0 & 0 \\ u|u|Y_{\delta_{br}} & 0 & u|u|Y_{\delta_{sr}} & 0 & 0 & 0 & 0 & 1 & 0 & 1 \\ 0 & u|u|Z_{\delta_{bp}} & 0 & u|u|Z_{\delta_{sp}} & 0 & 0 & 1 & 0 & 1 & 0 \\ 0 & 0 & 0 & 0 & 0 & 0 & 0 & 0 & 0 & 0 \\ 0 & u|u|M_{\delta_{bp}} & 0 & u|u|M_{\delta_{sp}} & 0 & 0 & -x_{bvt} & 0 & -x_{svt} & 0 \\ u|u|N_{\delta_{br}} & 0 & u|u|N_{\delta_{sr}} & 0 & -y_{ls} & -y_{rs} & 0 & x_{blt} & 0 & x_{slt} \end{bmatrix}$$

Control Input Vector:

$$\boldsymbol{u} = [\delta_{br}, \delta_{bp}, \delta_{sr}, \delta_{sp}, F_{ls}, F_{rs}, F_{bvt}, F_{blt}, F_{svt}, F_{slt}]^T$$

Euler Angle Rates and Global Positions:

$$\dot{X} = U_f + u\cos\psi\cos\theta + v[\cos\psi\sin\theta\sin\phi - \sin\psi\cos\phi] + w[\cos\psi\sin\theta\cos\phi + \sin\psi\sin\phi]$$

$$\dot{Y} = V_f + u\sin\psi\cos\theta + v[\sin\psi\sin\theta\sin\phi + \cos\psi\cos\phi] + w[\sin\psi\sin\theta\cos\phi - \cos\psi\sin\phi]$$

$$\dot{Z} = W_f - u\sin\theta + v\cos\theta\sin\phi + w\cos\theta\cos\phi$$

$$\dot{\phi} = p + q\sin\phi\tan\theta + r\cos\phi\tan\theta$$

$$\dot{\theta} = q\cos\phi - r\sin\phi$$

$$\dot{\psi} = \frac{(q\sin\phi + r\cos\phi)}{\cos\theta}$$

Rotation Matrix:

This rotation is based on equation 2.86.

$$\boldsymbol{T} = \begin{bmatrix} \boldsymbol{T}_1 & \boldsymbol{0} \\ \boldsymbol{0} & \boldsymbol{T}_2 \end{bmatrix}$$

$$\boldsymbol{T}_1 = \begin{bmatrix} \cos\psi\cos\theta & \sin\psi c\theta & -\sin\theta \\ \cos\psi\sin\theta\sin\phi - \sin\psi\cos\phi & \sin\psi\sin\theta\sin\phi + \cos\psi\cos\phi & \cos\theta\sin\phi \\ \cos\psi\sin\theta\cos\phi + \sin\psi\sin\phi & \sin\psi\sin\theta\cos\phi - \cos\psi\sin\phi & \cos\theta\cos\phi \end{bmatrix}$$

$$\boldsymbol{T}_2 = \begin{bmatrix} 1 & 0 & -\sin\theta \\ 0 & \cos\theta & \sin\theta \\ 0 & -\sin\phi & \cos\theta\cos\phi \end{bmatrix}$$

Surge Motion Equation:

$$m[\dot{u} - vr + wq - x_G(q^2 + r^2) + y_G(pq - \dot{r}) + z_G(pr + \dot{q})] - Z_{\dot{w}}wq + Y_{\dot{v}}vr$$

$$= X_{pp}p^2 + X_{qq}q^2 + X_{rr}r^2 + X_{pr}pr + X_{\dot{u}}\dot{u} + X_{wq}wq + X_{vp}vp + X_{vr}vr$$

$$+ uq(X_{q\delta_{bp}}\delta_{bp} + X_{q\delta_{sp}}\delta_{sp}) + ur(X_{r\delta_{br}}\delta_{br} + X_{r\delta_{sr}}\delta_{sr})$$

$$+ X_{vv}v^2 + X_{ww}w^2 + u|u|(X_{\delta_r\delta_r}(\delta_{sr}^2 + \delta_{br}^2) + X_{\delta_{sp}\delta_{sp}}\delta_{sp}^2 + X_{\delta_{bp}\delta_{bp}}\delta_{bp}^2)$$

$$-(W - B)sin\theta + F_{ls} + F_{rs} - X_{res}u|u|)$$

$$-\left(\frac{W-B}{g}\right)[\dot{T}_{11}U_f + \dot{T}_{12}V_f + \dot{T}_{13}W_f + T_{11}\dot{U}_f + T_{12}\dot{V}_f + T_{13}\dot{W}_f]$$

Sway Motion Equation:

$$m[\dot{v}+ur-wp+x_G(pq+\dot{r})-y_G(p^2+r^2)+z_G(qr-\dot{p})]+Z_{\dot{w}}wp+X_{\dot{u}}ur$$

$$=Y_{\dot{p}}\dot{p}+Y_{\dot{r}}\dot{r}+Y_{pq}pq+Y_{qr}qr+Y_{\dot{v}}\dot{v}+Y_{p}up+Y_{r}ur+Y_{vq}vq+Y_{wp}wp+Y_{wr}wr$$

$$+Y_{v}uv+Y_{vw}vw+u|u|(Y_{\delta sr}\delta_{sr}+Y_{\delta br}\delta_{br})$$

$$-\frac{\rho}{2}\int_{tail}^{nose}[C_{dy}h(x)|(v+xr)|(v+xr)]\,dx$$

$$+(W-B)\cos\theta\sin\phi+F_{blt}+F_{slt}$$

$$-\left(\frac{W-B}{g}\right)[\dot{T}_{21}U_f+\dot{T}_{22}V_f+\dot{T}_{23}W_f+T_{21}\dot{U}_f+T_{22}\dot{V}_f+T_{23}\dot{W}_f]$$

Heave Motion Equation:

$$m[\dot{w}-uq+vp+x_G(pr-\dot{q})+y_G(qr+\dot{p})-z_G(p^2+q^2)]-Y_{\dot{v}}vp+X_{\dot{u}}ur$$

$$=Z_{\dot{q}}\dot{q}+Z_{pp}p^2+Z_{pr}pr+Z_{rr}r^2+Z_{\dot{w}}\dot{w}+Z_{q}uq+Z_{vp}vp+Z_{vr}vr$$

$$+Z_{vv}v^2+Z_{w}uw+u|u|(Z_{\delta sp}\delta_{sp}+Z_{\delta bp}\delta_{bp})$$

$$-\frac{\rho}{2}\int_{tail}^{nose}[C_{dz}b(x)|(w-xq)|(w-xq)]\,dx$$

$$+(W-B)\cos\phi\cos\theta+F_{bvt}+F_{svt}$$

$$-\left(\frac{W-B}{g}\right)[\dot{T}_{31}U_f+\dot{T}_{32}V_f+\dot{T}_{33}W_f+T_{31}\dot{U}_f+T_{32}\dot{V}_f+T_{33}\dot{W}_f]$$

Roll Motion Equation:

$$I_x\dot{p}+(I_z-I_y)qr+I_{xy}(pr-\dot{q})-I_{yz}(q^2-r^2)-I_{xz}(pq+\dot{r})-Z_{\dot{w}}vw+Y_{\dot{v}}vw$$
$$-N_{\dot{r}}qr+M_{\dot{q}}qr+m[y_G(\dot{w}-uq+vp)-z_G(\dot{v}+ur-wp)]$$
$$=K_{\dot{p}}\dot{p}+K_{\dot{r}}\dot{r}+K_{pq}pq+K_{qr}qr$$
$$+K_{\dot{v}}\dot{v}+K_pup+K_rur+K_{vq}vq+K_{wp}wp+K_{wr}wr+K_vuv+K_{vw}vw$$
$$+(y_GW-y_BB)\cos\phi\cos\theta-(z_GW-z_BB)\cos\theta\sin\phi$$
$$+\left(\frac{Wz_G-Bz_B}{g}\right)\left[\dot{T}_{21}U_f+\dot{T}_{22}V_f+\dot{T}_{23}W_f+T_{21}\dot{U}_f+T_{22}\dot{V}_f+T_{23}\dot{W}_f\right]$$
$$-\left(\frac{Wy_G-By_B}{g}\right)\left[\dot{T}_{31}U_f+\dot{T}_{32}V_f+\dot{T}_{33}W_f+T_{31}\dot{U}_f+T_{32}\dot{V}_f+T_{33}\dot{W}_f\right]$$

Pitch Motion Equation:

$$I_y\dot{q}+(I_x-I_z)pr-I_{xy}(qr+\dot{p})+I_{yz}(pq-\dot{r})+I_{xz}(p^2-r^2)$$
$$-m[x_G(\dot{w}-uq+vp)-z_G(\dot{u}-vr+wq)]+Z_{\dot{w}}uw-X_{\dot{u}}uw+N_{\dot{r}}pr-K_{\dot{p}}pr$$
$$=M_{\dot{q}}\dot{q}+M_{pp}p^2+M_{pr}pr+M_{rr}r^2+M_{\dot{w}}\dot{w}+M_quq+M_{vp}vp+M_{vr}vr$$
$$+M_{vv}v^2+M_wuw+u|u|(M_{\delta sp}\delta_{sp}+M_{\delta bp}\delta_{bp})$$
$$+\frac{\rho}{2}\int_{tail}^{nose}\left[C_{dz}b(x)|(w-xq)|(w-xq)x\right]dx$$
$$-(x_GW-x_BB)\cos\phi\cos\theta-(z_GW-z_BB)\sin\theta-x_{bvt}F_{bvt}-x_{svt}F_{svt}$$
$$-\left(\frac{Wz_G-Bz_B}{g}\right)\left[\dot{T}_{11}U_f+\dot{T}_{12}V_f+\dot{T}_{13}W_f+T_{11}\dot{U}_f+T_{12}\dot{V}_f+T_{13}\dot{W}_f\right]$$
$$+\left(\frac{Wx_G-Bx_B}{g}\right)\left[\dot{T}_{31}U_f+\dot{T}_{32}V_f+\dot{T}_{33}W_f+T_{31}\dot{U}_f+T_{32}\dot{V}_f+T_{33}\dot{W}_f\right]$$

Yaw Motion Equation:

$$I_z\dot{r}+(I_y-I_x)pq-I_{xy}(p^2-q^2)-I_{yz}(pr+\dot{q})+I_{xz}(qr-\dot{p})$$

$$+\ m[x_G(\dot{v}+ur-wp)-y_G(\dot{u}-vr+wq)]-Y_{\dot{v}}uv+X_{\dot{u}}uv-M_{\dot{q}}pq+K_{\dot{p}}pq$$

$$=N_{\dot{p}}\dot{p}+N_{\dot{r}}\dot{r}+N_{pq}pq+N_{qr}qr+N_{\dot{v}}\dot{v}+N_pup+N_rur+N_{vq}vq+N_{wp}wp+N_{wr}wr$$

$$+N_vuv+N_{vw}vw+u|u|(N_{\delta sr}\delta_{sr}+N_{\delta br}\delta_{br})$$

$$-\frac{\rho}{2}\int_{tail}^{nose}\left[C_{dy}h(x)|(v+xr)|(v+xr)x\right]dx$$

$$+(x_GW-x_BB)\sin\phi\cos\theta+(y_GW-y_BB)\sin\theta$$

$$+x_{blt}F_{blt}+x_{slt}F_{slt}-y_{ls}F_{ls}-y_{rs}F_{rs}$$

$$+\left(\frac{Wy_G-By_B}{g}\right)\left[\dot{T}_{11}U_f+\dot{T}_{12}V_f+\dot{T}_{13}W_f+T_{11}\dot{U}_f+T_{12}\dot{V}_f+T_{13}\dot{W}_f\right]$$

$$-\left(\frac{Wx_G-Bx_B}{g}\right)\left[\dot{T}_{21}U_f+\dot{T}_{22}V_f+\dot{T}_{23}W_f+T_{21}\dot{U}_f+T_{22}\dot{V}_f+T_{23}\dot{W}_f\right]$$

APPENDIX B. DOPPLER SENSORS

This Appendix provides an overview of the two Doppler sensors used for control implementation in this dissertation; namely the SonTek® ADV Ocean and the RDI® Navigator DVL.

THE SONTEK ADVOCEAN

The SonTek ADVOcean (Acoustic Doppler Velocimeter Ocean Probe) is a versatile, high-precision instrument used to measure 3D water velocity in the most challenging applications, Figure B.1. The ADVOcean is designed for a wide range of environments including the surf zone, open ocean, rivers, lakes, and estuaries.

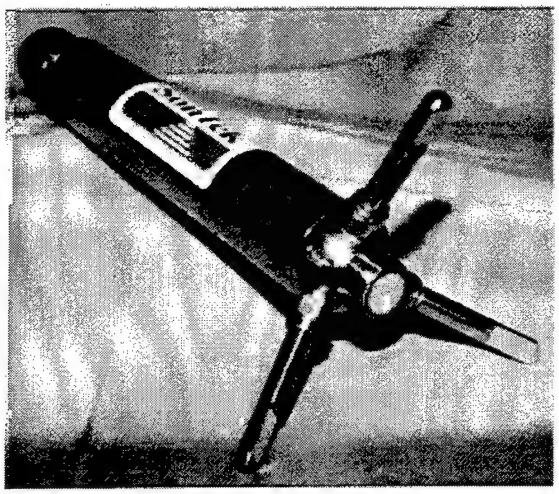

Figure B.1 ADVOcean Probe

The ADVOcean uses acoustic Doppler technology to measure 3D flow in a small sampling volume located a fixed distance (18-cm) from the probe, Figure B.2. The velocity range is programmable from ±5 to ±500 cm/s. Data can be acquired at sampling rates up to 25 Hz.

With no zero offset, the ADVOcean can be used to measure flow velocities from less than 1 mm/s to over 5 m/s. The remote sampling volume, stability, and rapid response of the ADVOcean make it perfect for al l types of flow measurement: mean currents, waves, and turbulent flow parameters.

The ADVOcean consists of two elements: a probe and processor. The probe includes the acoustic sensors, receiver, and optional sensors in a submersible housing. It is connected to the processor using a custom shielded cable.

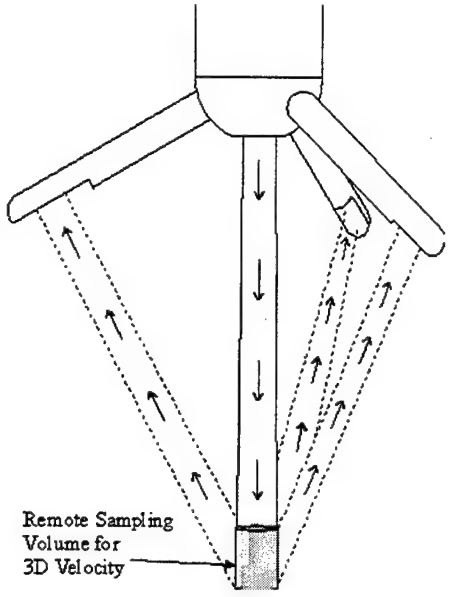

Figure B.2 ADV Sampling Volume

The ADVOcean processor operates from external DC power and outputs data using serial communication or a set of analog voltages. The processor can be operated from any PC-compatible computer or can be integrated with a variety of data acquisition systems.

STANDARD ADVOCEAN

The standard ADVOcean probe, Figure B.3, is designed for long-term deployments in hostile environments. The entire probe is constructed from 316 stainless steel, and protected from corrosion by a sacrificial zinc anode. With no moving parts, the ADVOcean has excellent resistance to biological fouling. For added protection, the entire probe, including the transducers, can be coated with anti-fouling paint. The probe is connected to the processor using an underwater mateable connector.

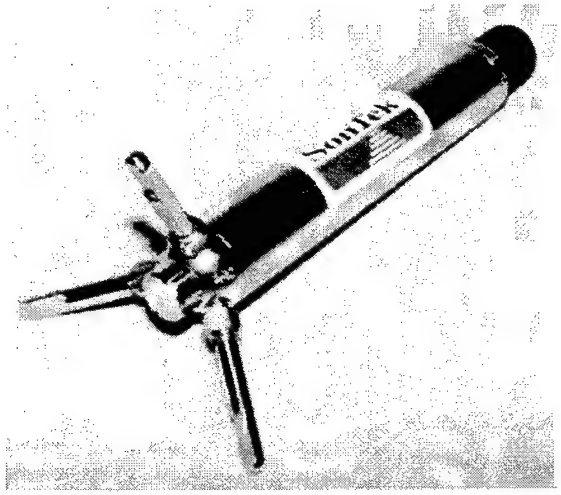

Figure B.3 Standard ADVOcean Probe

For deep-water deployments, the ADVOcean can be rated for depths up to 2000 m (the standard depth rating is 400 m). Deep-water ADVOcean systems are commonly used on autonomous underwater vehicles (AUVs) and remotely operated vehicles (ROVs) for detailed microstructure measurements.

In any configuration, the ADVOcean probe is immune to zero drift and has no inherent minimum detectable velocity. The probe calibration can only change with physical damage to the system. No regular maintenance or re-calibration is needed.

ADVOCEAN WITH OPTIONAL SENSORS

The ADVOcean probe can include a number of optional sensors to greatly expand its measurement capabilities. These include a compass and 2-axis tilt sensor allowing the ADVOcean to report velocity data in Earth (East-North-Up) coordinates; a pressure sensor for wave height estimation (PUVW) and surface-level measurements; and a temperature sensor for automatic sound speed compensation.

ADVOcean probes with optional sensors use an expanded housing, Figure B.4, constructed from acetyl (Delrin), and have the same reliability and performance as the standard ADVOcean probe.

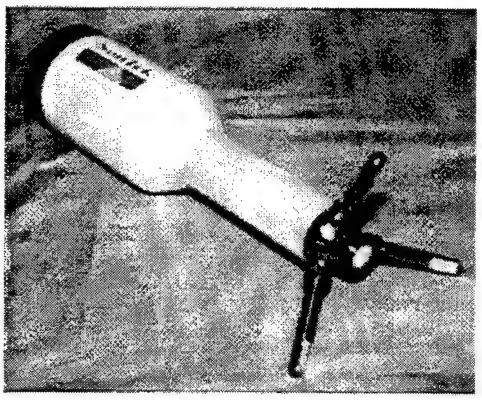

Figure B.4 ADVOcean Probe with Optional Sensors Housing

ADVOCEAN PROCESSOR

The ADVOcean processor can be housed in two different ways depending upon whether the processor will need to be submerged. The ADVOcean processor operates from DC power and is typically connected to a portable computer running SonTek's powerful data acquisition software. It can also be integrated with a variety of data acquisition systems using serial communication or the analog output voltages.

STANDARD FEATURES

ADVOcean systems include the following standard features listed in Table B.1.

ADVOcean Probe	ADVOcean Processor
• Factory Calibration (can only change with physical damage to the probe) • Programmable velocity range from ±5 to ±500 cm/s • Submersible to 400 m • 10-m cable to processor (50-m max.)	• Dual serial communication (RS-232 standard, RS-422 for cable lengths to 1500 m) • Four analog output voltages (3 velocity, 1 signal strength) for integration with analog data acquisition systems • Hardware synchronization with external sensors using sync input and output

Table B.1 Standard ADVOcean Features

OPTIONS

Several options are available for use with ADVOcean systems. The most common are the compass, pressure and temperature sensors. The compass and 2-axis tilt sensors allow the ADVOcean to report velocity data in Earth (East-North-Up) coordinates. The sensor has a built-in calibration feature to compensate for magnetic distortion. The user can easily re-orient the compass for up, down, or side-looking operation. Any ADVOcean with compass/tilt or pressure sensor includes a temperature sensor to compensate for changes in sound speed. Sound speed is used to convert Doppler-shift to water velocity.

ADVOCEAN PERFORMANCE SPECIFICATIONS

The performance specifications of the ADVOcean are listed in Table B.2. More information may be found at the SonTek web site http://www.sontek.com.

Performance Specifications	
General Operation • Acoustic frequency: 5 MHz • Sampling rate: Programmable from 0.1 to 25 Hz • Sampling volume size: 2.0 cm3 • Distance to sampling volume: 18 cm • Minimum water depth: 20 cm • Input power : 12-24 VDC **Velocity Data** • Range: Programmable to ±5, 20, 50, 200 or 500 cm/s • Resolution: 0.01 cm/s • Accuracy: ±1 percent of measured velocity, ±0.25 cm/s • Random noise: Approximately 1 % of velocity range at 25 Hz;	**Compass/Tilt Sensor** • Resolution (heading, pitch, roll): 0.1° • Accuracy (heading): ±2° Accuracy (pitch, roll): ±1° **Temperature Sensor** • Resolution: 0.01°C • Accuracy: ±0.1°C **Pressure Sensor** • Available full-scale ranges: 10, 20, 50, 100, 200, and 500 m • Resolution: 0.00025 x (full scale) • Accuracy: ±0.5 percent full scale **Environmental** • Operating temperature: -5° to 40°C • Storage temperature: -10° to 50°C **Dimensions** • See Figure B.5

Table B.2 ADVOcean Performance Specifications

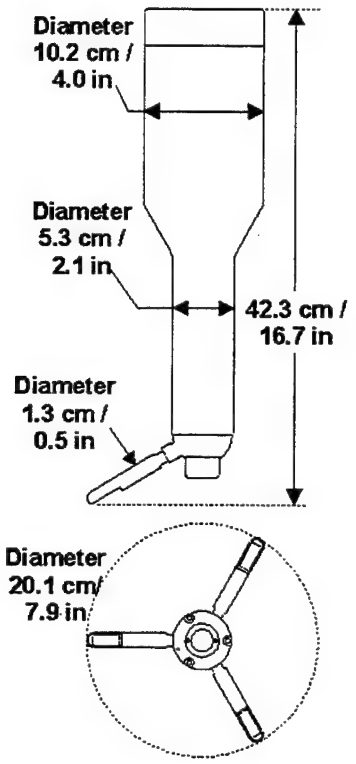

Figure B.5 ADVOcean Dimensions

THE RDI NAVIGATOR DVL

The WORKHORSE NAVIGATOR DVL is designed to provide rapid, precise velocity updates. Its small size, high accuracy, and low power consumption make it well suited to applications such as station keeping and sea bed surveys from underwater vehicles. The NAVIGATOR can be integrated with existing navigational systems (USBL, LBL and/or inertial). Its high-resolution velocity data provides a better focused picture of your vehicle's location and altitude. The NAVIGATOR is less than half the length and weight of standard broadband DVLs. Average power consumption of the WHN-1200 is only 8 watts. The NAVIGATOR is about 60 % of the price of standard broadband DVLs. The NAVIGATOR uses the patented Broadband technology. The WHN-1200 kHz has velocity accuracy of +/-0.2% +/- 0.2 cm/s. The NAVIGATOR measures velocity, altitude, heading, pitch/roll, and temperature. For a description of the operations of this sensor refer to [Gordon 1996]

WHN-1200 SPECIFICATIONS

The specification for the 1.2 MHz Navigator are presented in Table B.3. Further specifications can be found at the RDI web site http://www.rdinstruments.com.

Transducer and Pressure Case	
Actual Frequency	1229 kHz
Beamwidth	1.2°
Beam Angle (from vertical)	30°
Configuration	4-beam-convex
Housing & Transducer Material	6061 aluminum
External Connector	7-pin low-profile
Weight (in air)	6.4 kg
Weight (in water)	4.2 kg
Altitude	
Minimum	0.3 m
Maximum	30 m
Bottom Velocity	
Short Term Error (V = 1.0 m/s)	0.3 cm/s
Long term Error	±0.2% ±0.2 cm/s
Ping Rate	1-10 Hz

Table B.3 Navigator DVL Specifications

APPENDIX C. THE NPS PHOENIX AUV

The physical layout of the NPS Phoenix AUV is shown in Figure C.1. Detailed description of the vehicle can be found in [Marco 1996] and [Brutzman 1997]. In addition an online description can be found on the NPS center for AUV Research web site at http://www.cs.nps.navy.mil/research/auv/auvstats.

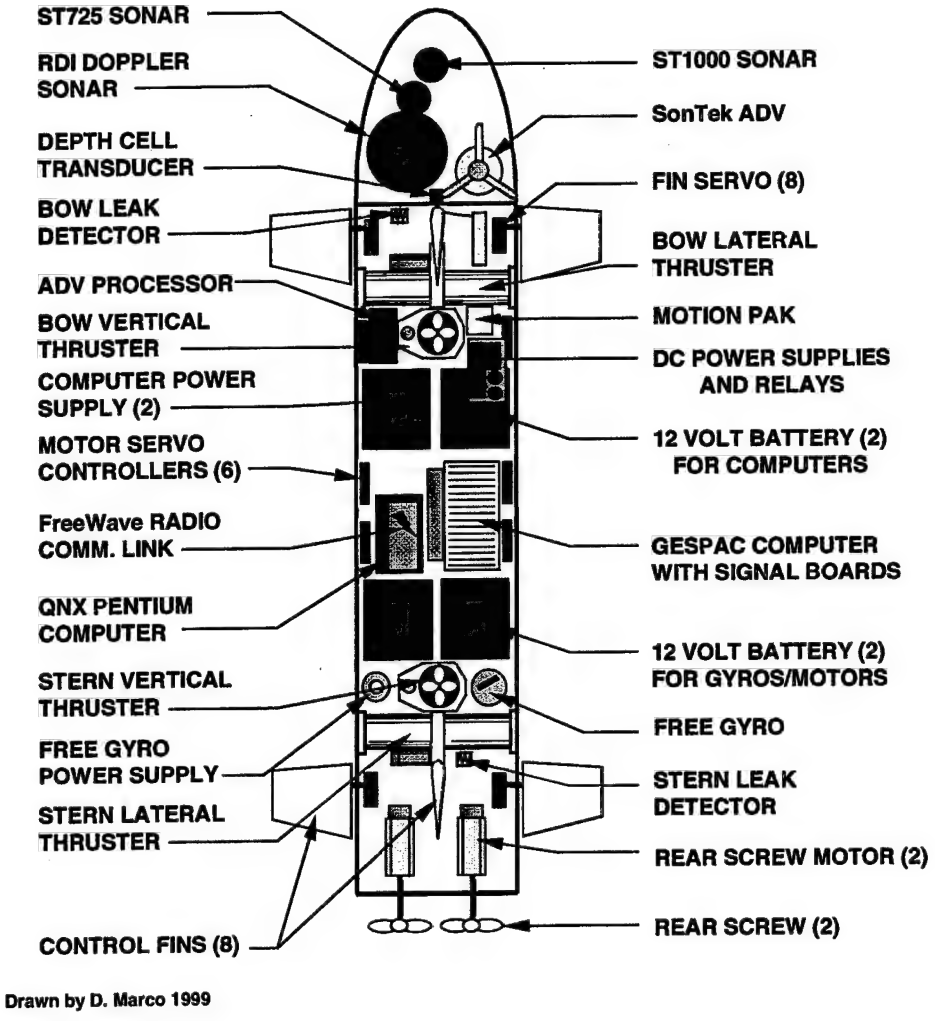

Figure C.1 Physical Layout of Phoenix AUV

Prior to September 1996, Phoenix was used extensively as a test tank research vehicle. To transition the vehicle and the center to an ocean going operational unit required some significant upgrades in vehicle capabilities and center acquisitions. Table C.1 summarizes the upgrades and acquisitions that were performed to allow Phoenix to

become deployable in the ocean. It also highlights the design features of the new vehicle, Figures C.1a and C.1b, presently being outfitted at the center.

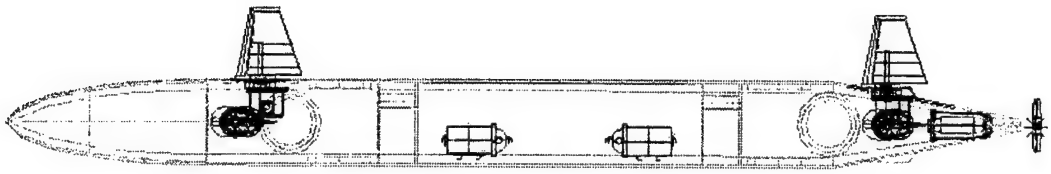

Figure C.1a Wire Frame Diagram of New NPS AUV

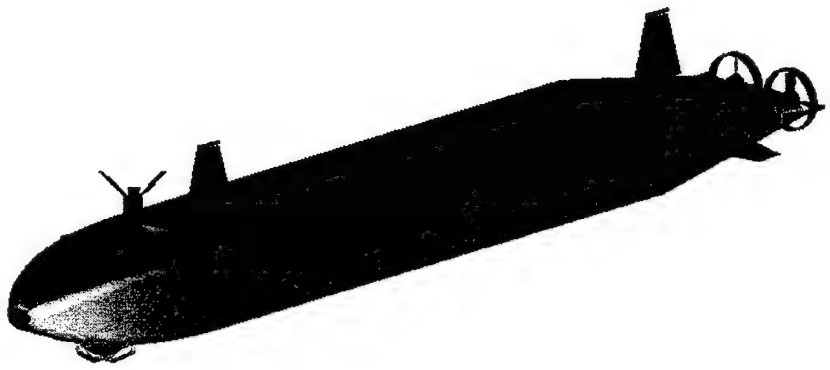

Figure C.1b Solid Model of New NPS AUV

	Pre-July 1996	Present	New Vehicle
Propulsion Motors	two 24v brushed DC	two 1/4 hp, 24v brushless DC (see figure C.2)	two 48v DC, 1/4 hp, brushless
Propellers	3.5 in model submarine propellers (see figure C.3)	7 in ducted propellers (in house designed) (see figure C.4)	7 in ducted propellers (in house designed)
Control Actuators	eight control surfaces, (two fwd rudders, two aft rudders, and a pair of bow and stern planes), four 3 .5 in thrusters (two vertical fore and aft and two horizontal fore and aft) (see figure C.5)	seven control surfaces, (one lower fwd rudders, two aft rudders, and a pair of bow and stern planes), four 3 .5 in thrusters (see figure C.4a(two vertical fore and aft and two horizontal fore and aft) (see figure C.5)	seven control surfaces, (one lower fwd rudders, two aft rudders, and a pair of bow and stern planes), four 6 in thrusters (two vertical fore and aft and two horizontal fore and aft)
Vehicle Control Computer	GESPAC Computer System running OS-9 real-time operating system	GESPAC Computer System running OS-9 real-time operating system	PC-104 with a Pentium chip (166 MHz) running QNX (see figure C.6)
Mission Control Computer	Sun Solaris	PC-104 with a Pentium chip (90 MHz) running QNX (see figure C.6)	PC-104 with a Pentium chip (166 MHz) running QNX (see figure C.6)
Electrical Power System	two independent 24v lead acid battery systems	two independent 24v lead acid battery systems	single 48v Absorbed Glass Mat (AGM) battery system
Ballast System	manual lead ballast	manual lead ballast with syntactic foam for minor	Variable ballast system
Communication System	Ethernet cable while in test tank	Ethernet cable while in test tank, 900 MHz spread spectrum modem during missions (see figure C.7)	Ethernet cable while in test tank, 900 MHz spread spectrum modem and u/w acoustics during missions
Navigation System	DR using water speed and vehicle heading	EKF fusing Doppler and vehicle motion	EKF fusing Doppler, GPS, LBL and vehicle motion
Attitude Sensor	three axis Mechanical Rate Gyro's and a vertical gyro	6DOF Solid State inertial sensing system (see figure C.8)	6DOF Solid State inertial sensing system

Table C.1 Vehicle Upgrades and Acquisitions

Heading Reference	Directional Gyro	Directional Gyro with a PrecisionNav electronic compass backup (see figure C.9)	Directional Gyro (possible a Honeywell ring laser gyro) with a PrecisionNav electronic compass backup
Speed Reference	turbo probe	RDI DVL and SonTek ADV (see figures C.10 and C.11)	RDI DVL and SonTek ADV
Sensor Suite	ST-725 Scanning Sonar, ST-1000 Imaging Sonar (see figure C.12)	ST-725 Scanning Sonar, ST-1000 Imaging Sonar, RDI DVL, SonTek ADV	ST-725 Scanning Sonar, ST-1000 Imaging Sonar, RDI DVL, SonTek ADV, Altimeter , video camera
Support equipment	Transport cart (see figure C.13)	Wells Cargo® Travel trailer outfitted with a mobile lab, 12' inflatable boat and trailer, portable generator and computer workstation, vehicle shipping containers LXT acoustic tracking system (see figures C.14, C.15, C.16 and C.17)	Wells Cargo® Travel trailer outfitted with a mobile lab, 12' inflatable boat and trailer, portable generator and computer workstation, vehicle shipping containers

Table C.1 Vehicle Upgrades and Acquisitions (Cont.)

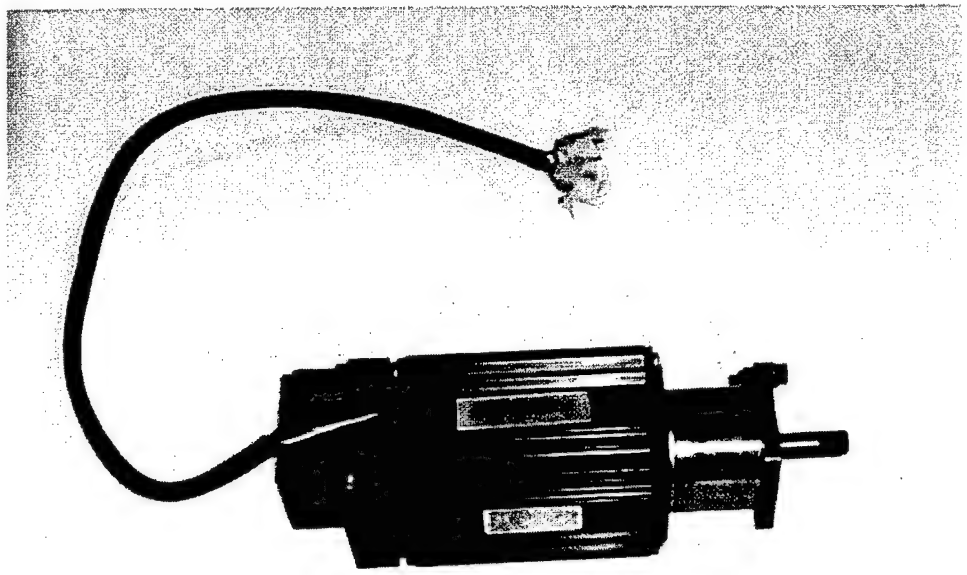

Figure C.2 Brushless DC Motors

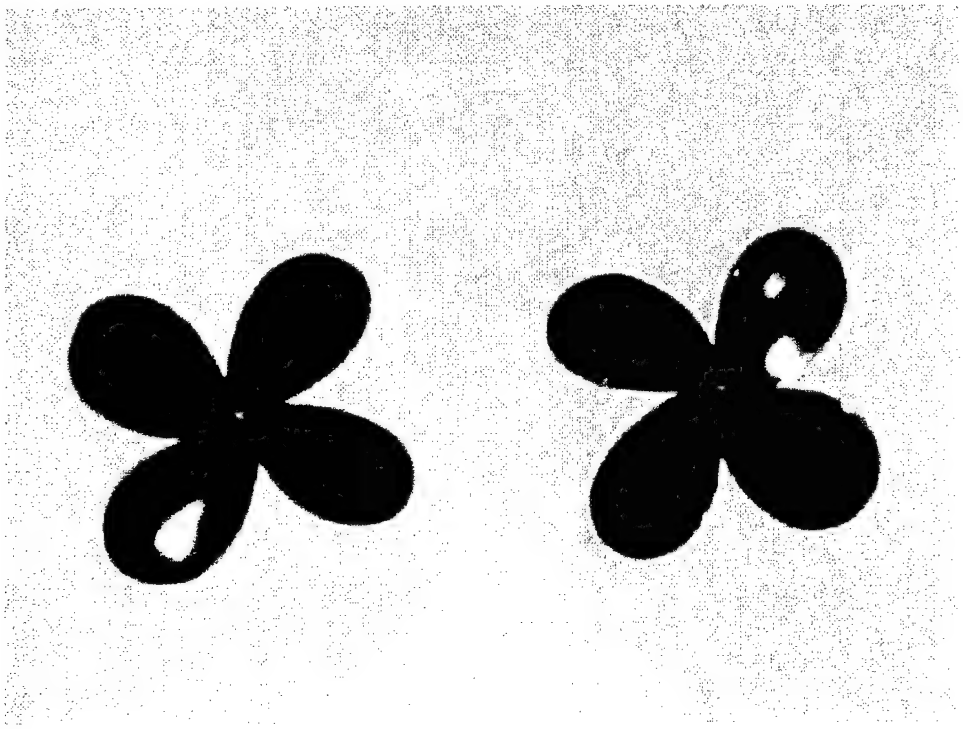

Figure C.3 Old 3-in. Props

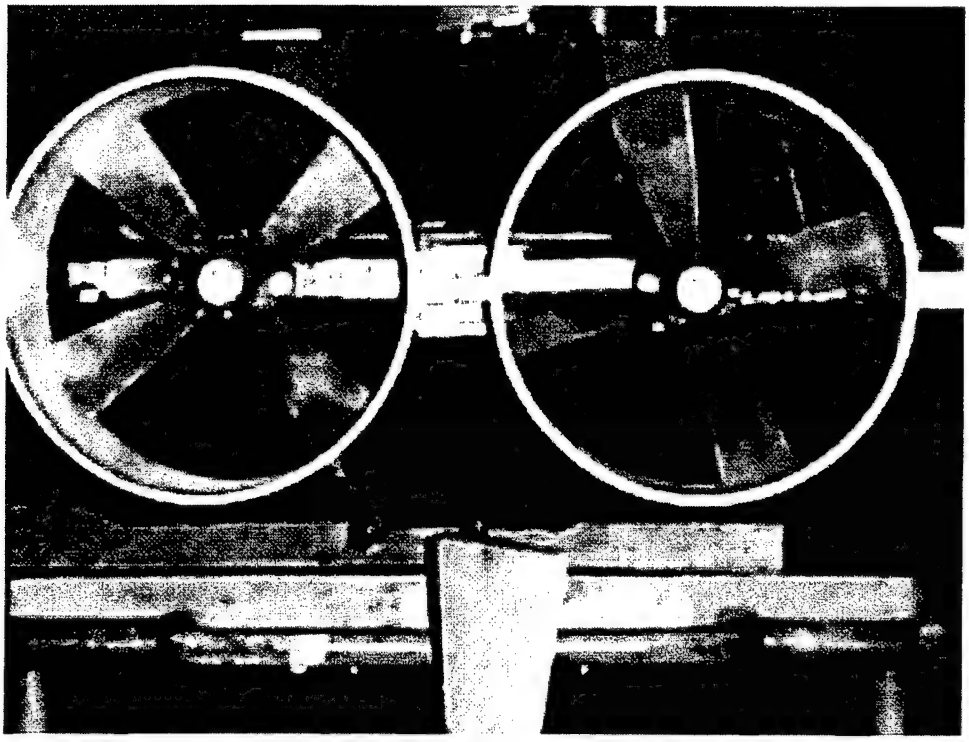

Figure C.4 Present 7-in Ducted Props

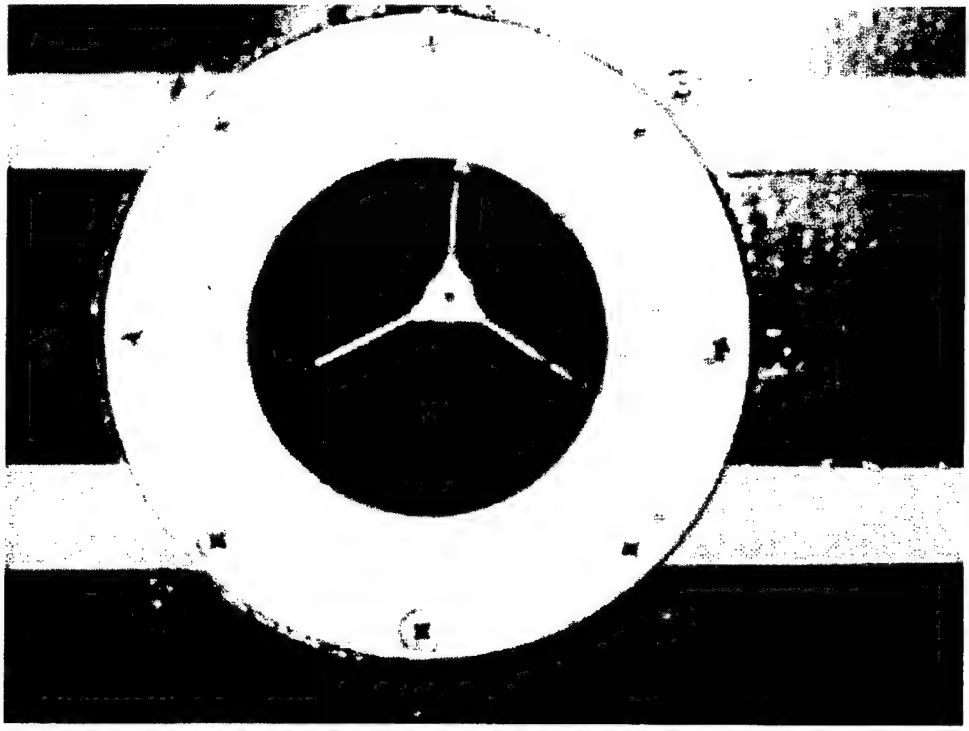

Figure C.4a Present 3.5-in Thrusters

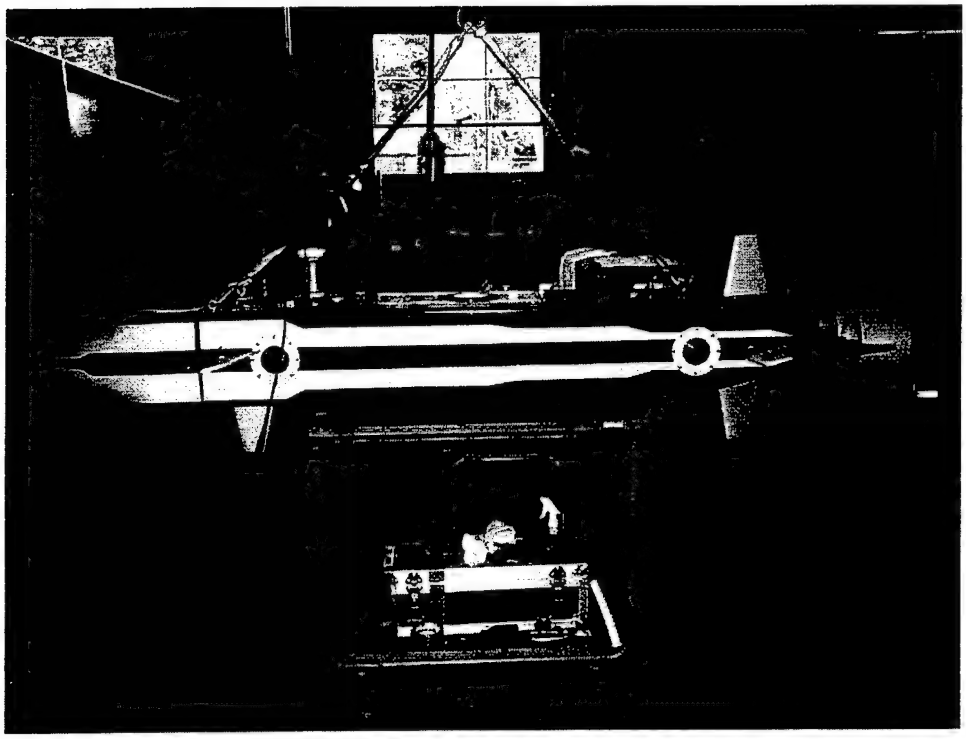

Figure C.5 Phoenix Control Actuators

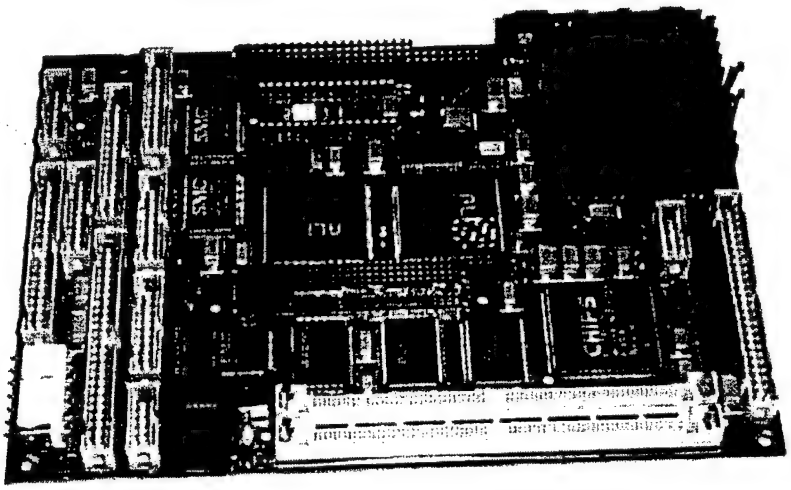

Figure C.6 Mission Control Computer

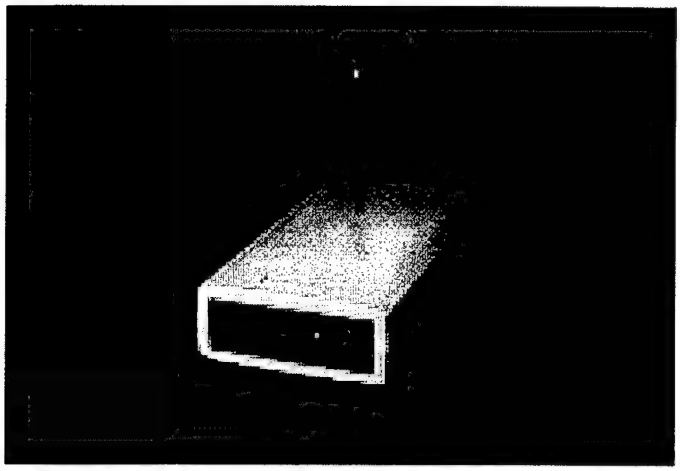

Figure C.7 FreeWave Modem

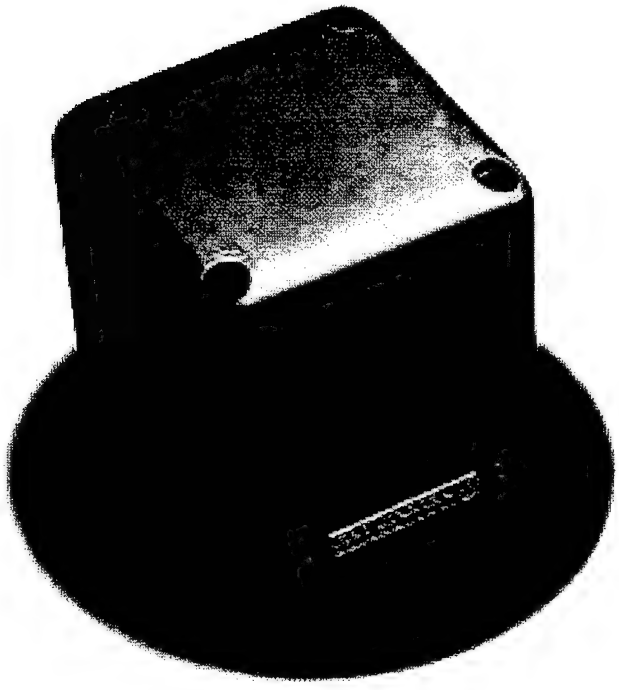

Figure C.8 Systron Donner MotionPak

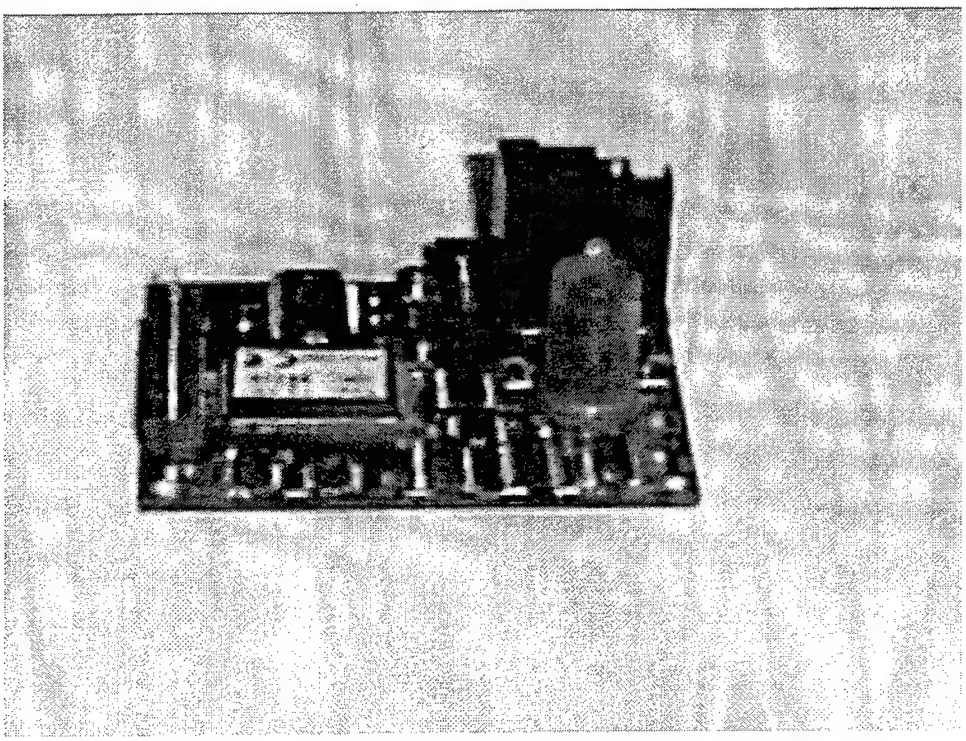

Figure C.9 PrecisionNav TCM2 Compass

Figure C.10 RDI Navigator DVL

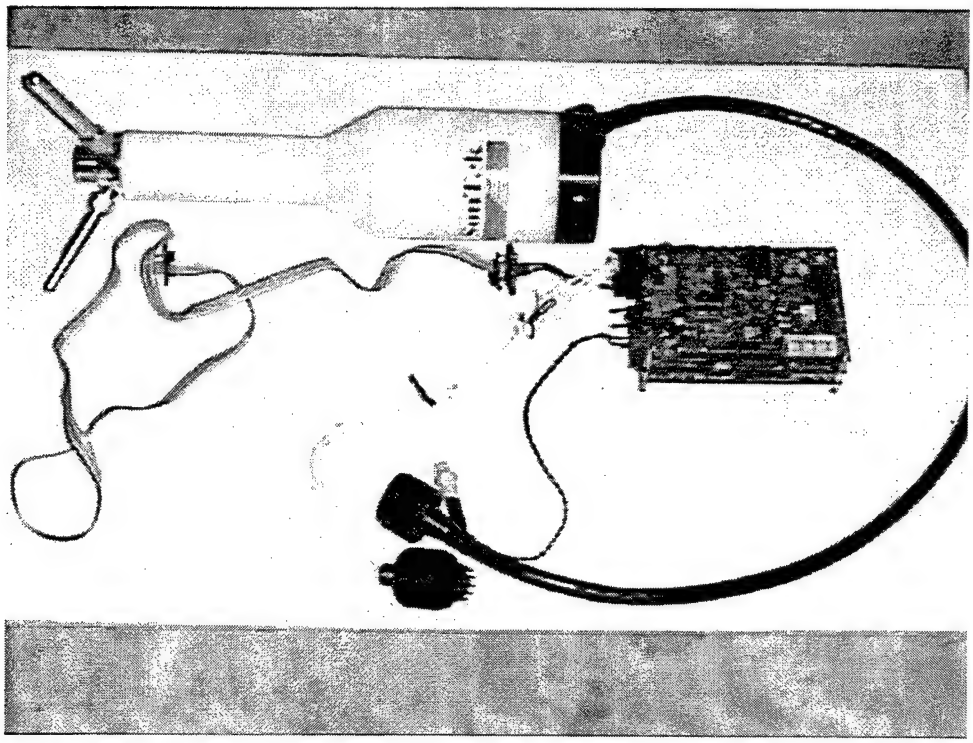

Figure C.11 ADVOcean Acoustic Doppler Velocimeter

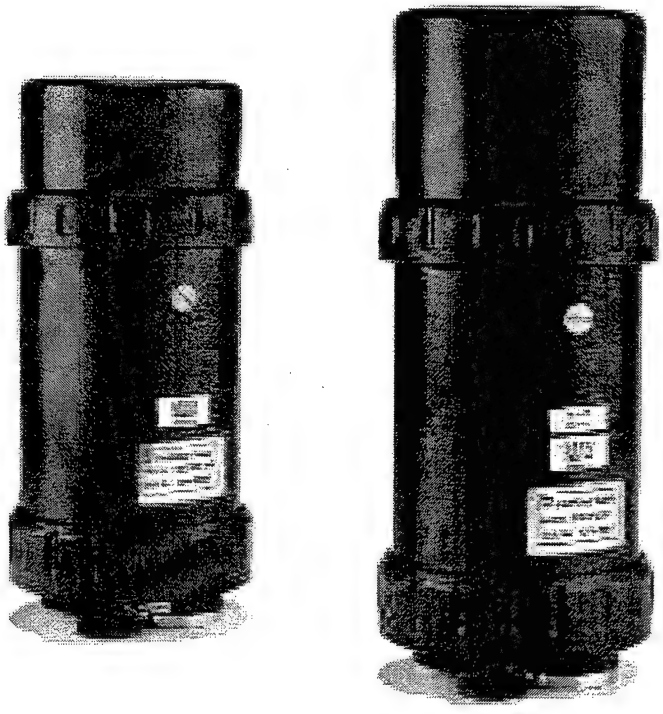

Figure C.12 ST-725 and ST-1000 Sonars

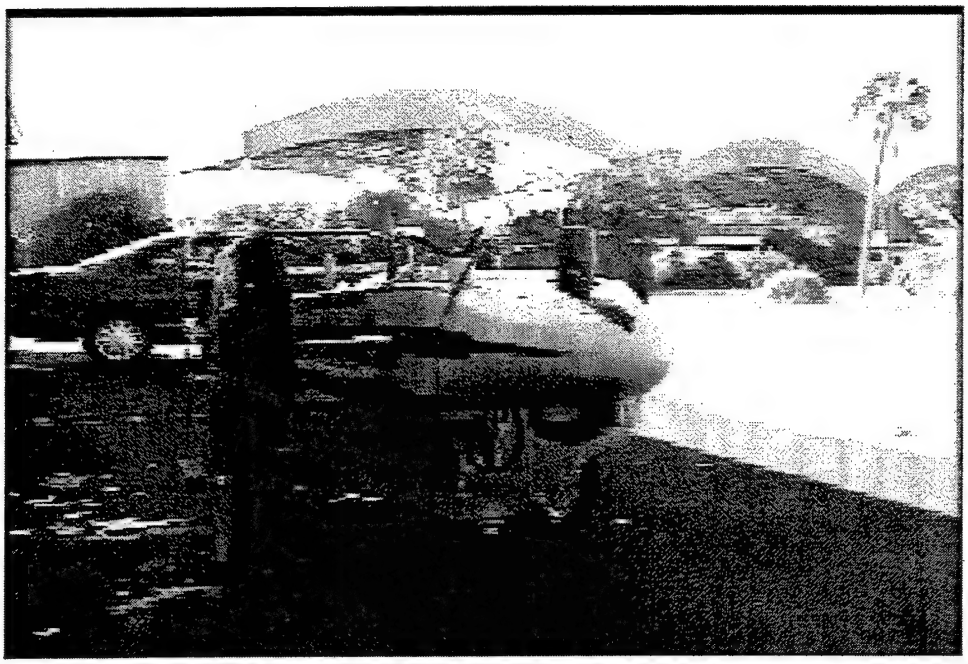

Figure C.13 Transport Cart

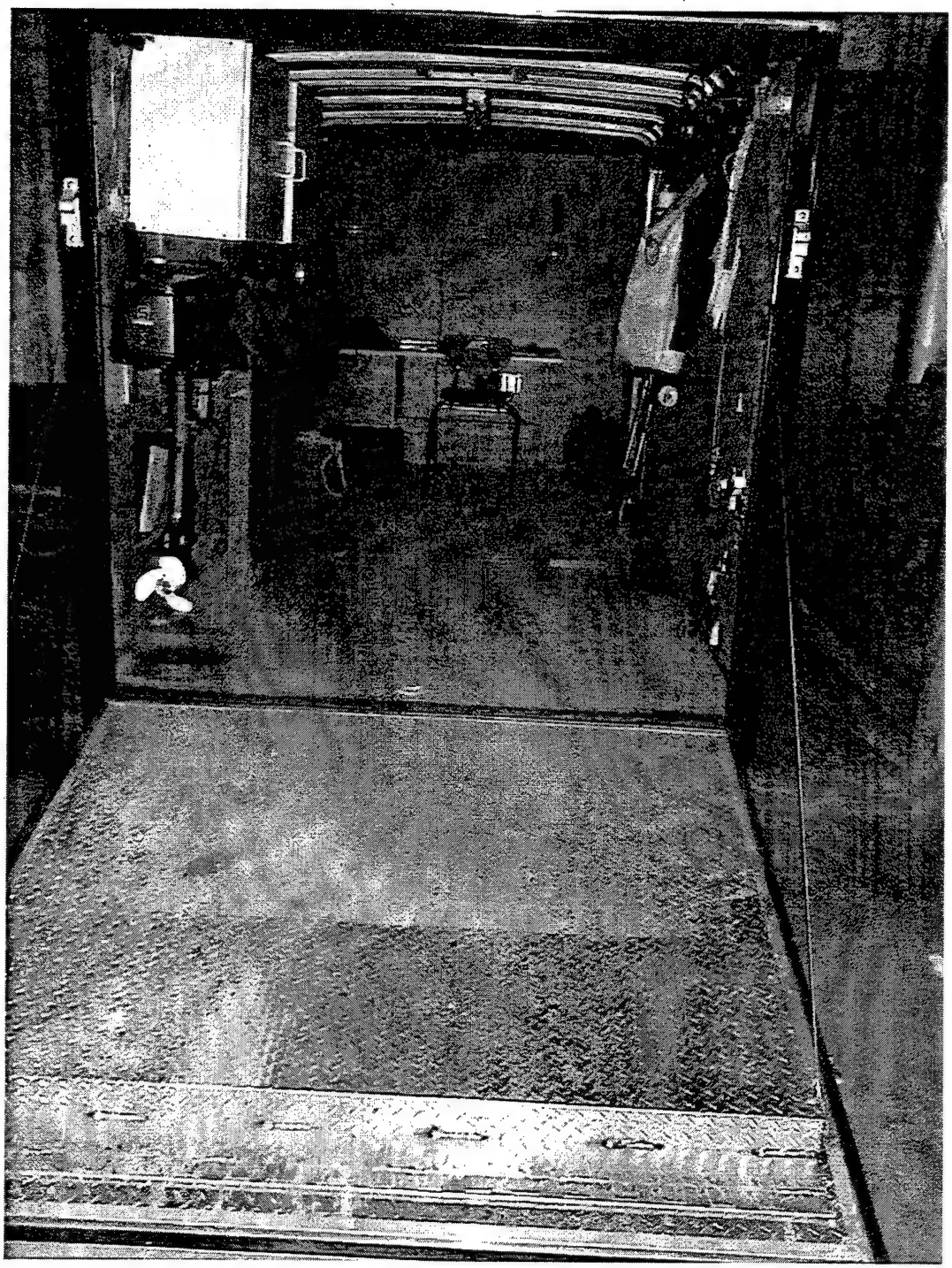

Figure C.14 Mobile Lab Internals

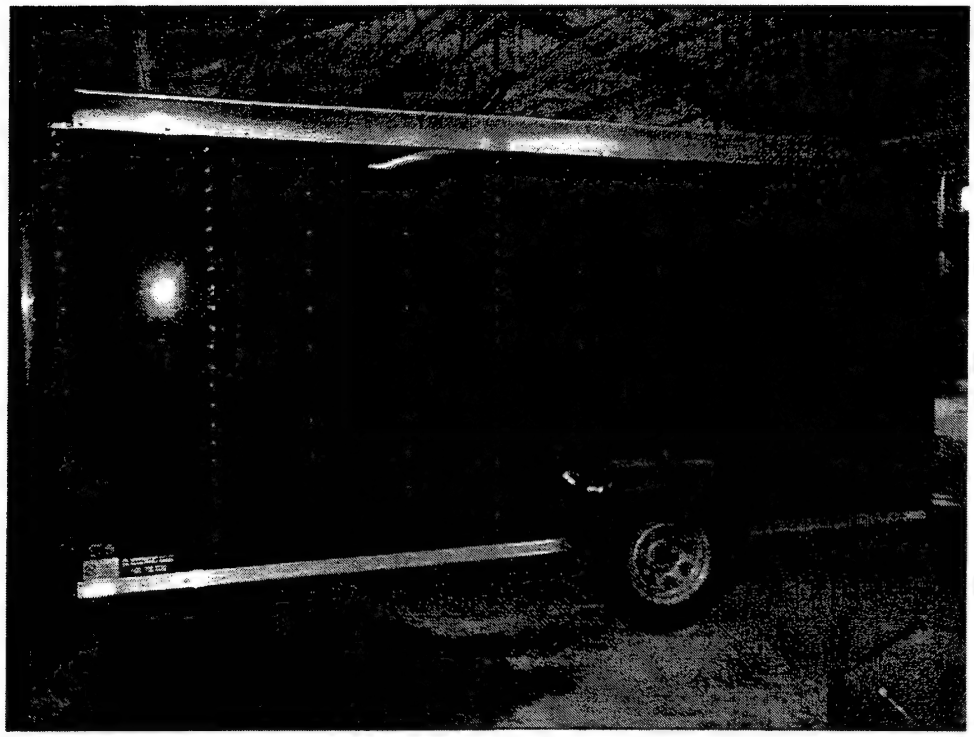

Figure C.15 Mobile Lab

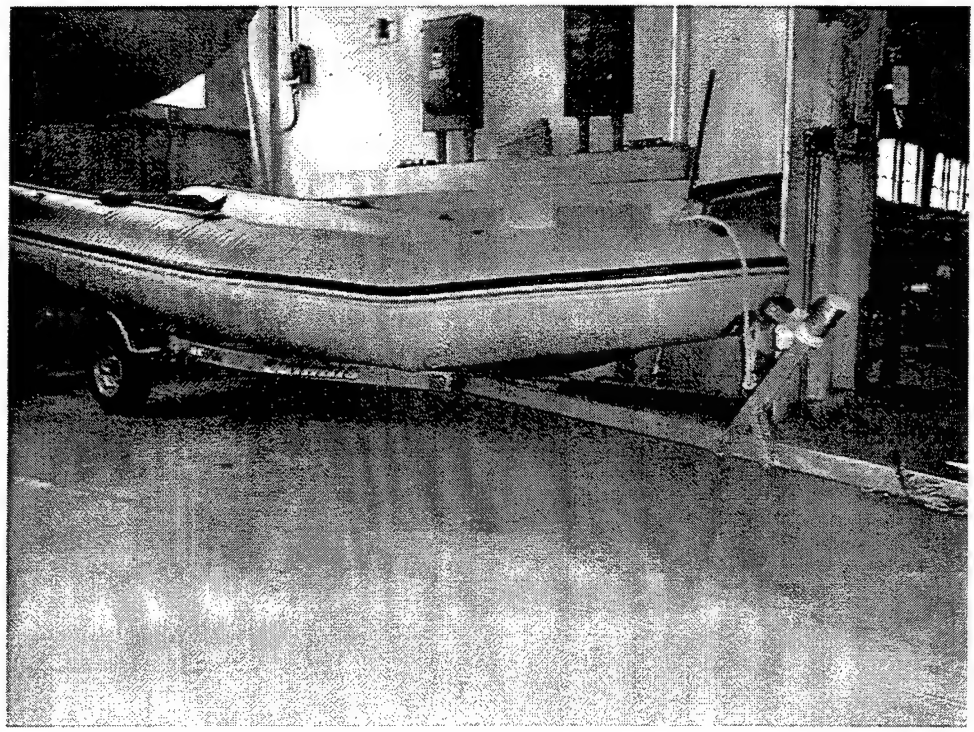

Figure C.16 Support Craft

Figure C.17 LXT Acoustic Tracking System

APPENDIX D. AUVFEST '98

OVERVIEW

The Naval Postgraduate School (NPS) participated in the NAVO sponsored AUVFEST for the first time, [Bunce 1998]. The lessons learned from this exercise were extremely valuable for future operational planning and vehicle development. First, the NPS Phoenix vehicle, a research platform, had never been deployed offshore from a research ship before. This task provided challenges that the four-man team failed to recognize beforehand, but was able to overcome. Like all other participants, the vehicle and support equipment had to be transported from their base of operations to Gulfport, MS. This movement of equipment was new to the Center for AUV Research (www.cs.nps.navy.mil/research/auv), but enlightened the Center on the logistics involved with offshore operations.

During the work-ups for this exercise, two significant hardware problems occurred. First, the Doppler unit originally integrated into Phoenix failed the week just prior to departure for Gulfport. This sensor was beyond repair, and a new Doppler needed to be purchased. A RDI Navigator DVL, a $25K unit, was purchased, through the Naval Supply System, and delivered to the Center in five days. The purchase of this unit in this time period was remarkable considering the government regulations that must be followed for a major purchase of this type. The vehicle, the support equipment, the new Doppler and all other sensors were shipped to Gulfport, installed, integrated into the vehicle control system and tested without faults in three days, a major accomplishment for a group that had never performed missions away from their base of operation.

Secondly, during the weekend prior to shipboard load out, after the vehicle had been reassembled and all systems had been successfully tested and verified as performing, the SonTek Acoustic Doppler Velocimeter (ADV) was physically damaged. The damage to the ADV was not recognized until the after the vehicle had been loaded aboard the R/V GURE, and vessel was underway. The Center was able to contact the vendor and have a new unit shipped overnight to Gulfport where immediate configuration and installation was accomplished without error, affording Phoenix the ability to remain operational.

The objectives of the Center during AUVFEST '98 were two-fold. First, NPS planned to use the sensors suite installed on Phoenix to demonstrate the ability of a moving platform to characterize the seaway. The theory and results from this section have been presented in Chapter VII and VIII, respectively. The second goal was to use the Phoenix's forward-looking, sector-scanning sonar (Tritech ST725), to image water column targets and demonstrate the Phoenix's onboard target identification algorithm. Navigation of Phoenix was accomplished using the RDI DVL together with a directional gyro heading reference in a deadreckoning filter. Details with regard to the above goals and vehicle missions are presented in the following sections.

LOGISTICS

The Phoenix AUV and all its associated support equipment was air freighted from Monterey, CA to Gulfport, MS via FedEx. This was a challenge for the Center since this was the first operational deployment. Custom shipping containers were purchased from Hardigg Industries, see Figure D.1, to hold the hull and nose fairing. These containers performed extremely well and protected the vehicle. The NPS shipping department provided packaging of the centers support equipment, see Figure D.2. Again due to the professional nature of the NPS employees, not a single item was damaged or turned up missing.

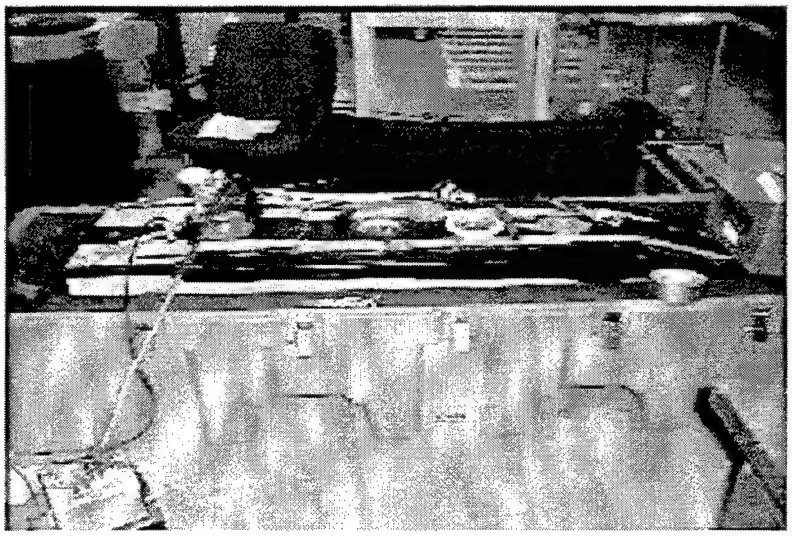

Figure D.1 Phoenix Shipping Containers'

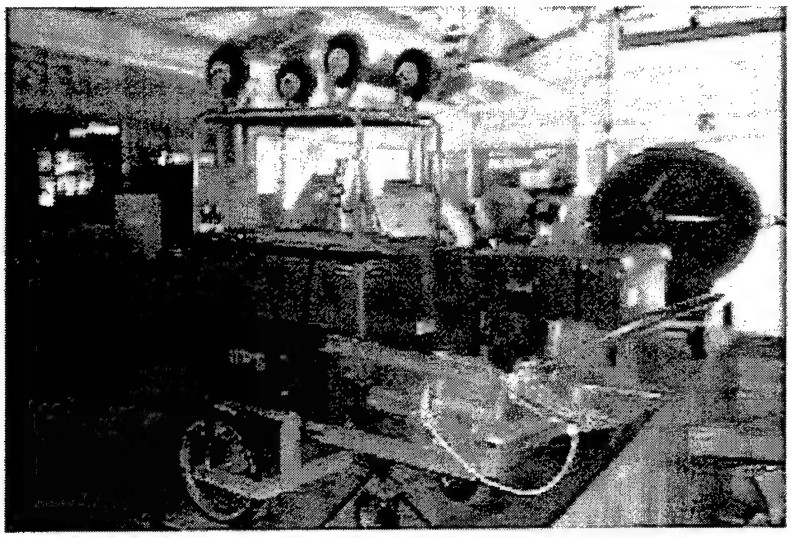

Figure D.2 Packaging of Support Equipment

Upon arrival in Gulfport, the Center set-up shop in the NAVO BOATDET office, see Figure D.3. The vehicle was reassembled, including the newly purchased Doppler, bench tested and water tested, without any system degradations in two days.

Figure D.3 Gulfport Temporary Work Space

SHIPBOARD OPERATIONS

The Phoenix, with its support equipment, was loaded aboard the Texas A&M University research ship, R/V *GYRE*, see Figure D.4. In addition to NPS, there were participants from Florida Atlantic University (FAU), Woods Hole Oceanographic

Institute (WHOI) and Massachusetts Institute of Technology (MIT) taking part in the demonstrations.

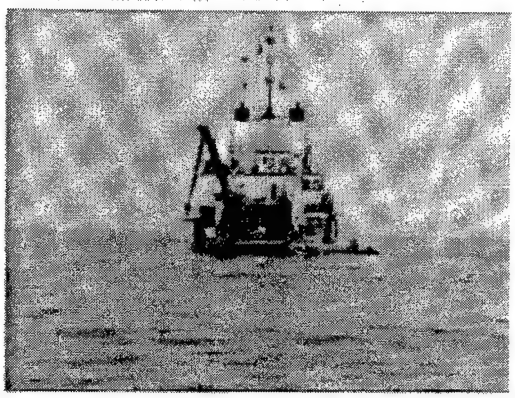

Figure D.4 R/V Gyre at Anchor

During the seven day exercise, the Phoenix conducted 27 separate open ocean runs, see Table D.1 for a sample. This was a significant accomplishment seeing that the Phoenix was designed for tank testing some 10 years earlier.

Operations from the ship were challenging. This was the first time Center personnel launched Phoenix from a crane, see Figure D.5. By the end of the second day of operations, the Phoenix crew was acting as if this was "old hat."

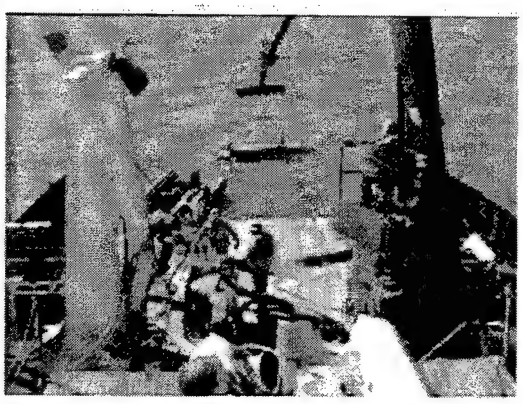

Figure D.5 Phoenix Being Launched from the Gyre

The exercise was conducted in the Gulf of Mexico, south of Gulfport, MS. Figure D.6 displays the operating area. In this operating area, there were three different mission boxes. Each box had separate features so that the vehicles from the various participants could demonstrate their capabilities.

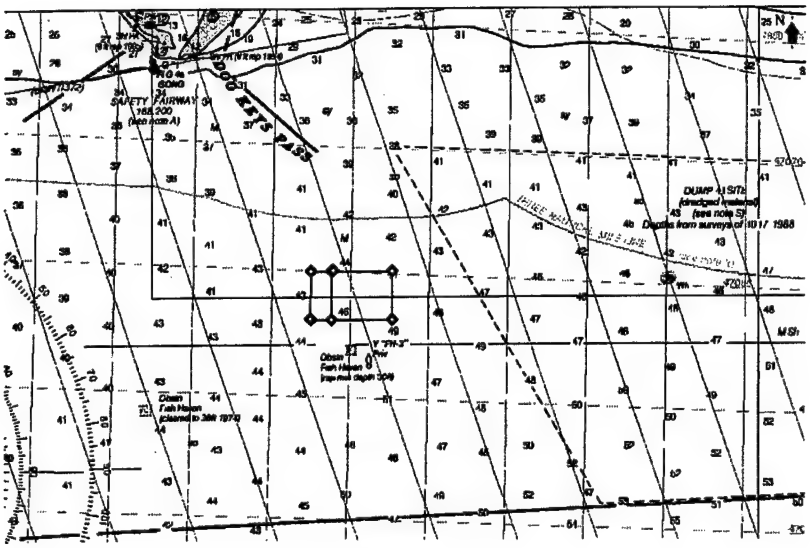

Figure D.6 AUVFEST Operations Area

DIRECTIONAL WAVE INFORMATION

Directional wave information was obtained during the AUVFEST missions. See Chapters VII and VIII for more information.

AUTOMATIC SONAR TARGET RECOGNITION EXPERIMENTS

One of the objectives of the AUVFEST experiments involved testing a recently developed sonar target recognition software module. The software is designed to process the sonar returns in real time and provide a reduced data set from the large amounts of data gathered. From the data, the centers of concentrations of high intensity sonar returns are identified and their locations stored during mission time, which requires no post processing. The location information can be then be used for post mission analysis or path re-planning to return to these areas for further study during the same mission. High intensity concentrations suggest underwater objects or structures, while areas of low intensity do not. Since the majority of the open ocean is clear, only a small amount of the data gathered is meaningful, and this approach greatly reduces the data storage requirements of the onboard computer system. The following will give a brief description of the sonar used, the identification algorithm, and finally the results from one of the missions.

Day/Data file name	Run Number	comments on Run	Problems/ Fixes	Sea State comments	General info
DAY 1					
1103_01	1	Set up/balancing/vehicle was heavy by nose, ~2lbs light. Time base run 4 mins (2 min out, 2 in back) at 3' depth.	added buoyancy in nose / tow float/reset fins/	light (1 foot seas, multi-directional, wind ~10 mph)	salinity 29.5 ppt at surface to 34.0 ppt at bottom. Water temp ~74 degrees.
DAY 2					
1104_02	1	TB run. At 090 true to go to GB. Initialize dg to ships head. Went to command but 180 off expected course. Mag compass 330 degrees.	Fix sign error in DG offset calc. Due to sign error, we ended up with twice the ship's heading, which was 100 degrees, error.	sea state 1-2 (2-3 feet, 4 foot swells). Seas from multi-directions. Swells from 115 true. Wind driven from 025 true. Wind 10-15 mph	Taking ships heading/go to Gyre do a small WP run, a large WP run, then a run to area 2 buoy
1104_03	2	repeat of first run. no changes to script. Same results as first run.	Fix sign error in DG offset calc		
1104_04	3	Same run as first. Changed DG offset by 2*pi. Results were no different than first run	Fix sign error in DG offset calc		
1104_05	4	Same run as first. Attempted to give a 270 heading command. Results were no different than first run	Fix sign error in DG offset calc		
1104_06	5	Reinitialized vehicle headed at Gyre. New zero for DG. (~085 true) Time based run for 2 minutes with a commanded heading of 000.	Behaved as commanded. Run was successful.		
1104_07	6	Same run as previous. No reinitialization.	Behaved as commanded. Run was successful.		
1104_08	7	Time based run at -090 for five minutes. Heading away from Gyre.	Behaved as commanded. Run was successful.		Checked battery (24.5v) and computer (22.8v) voltages when mission was complete. Leak detectors at 1.09.
1104_09	8	Time based run at 045 for seven minutes. Heading towards Gyre.	Behaved as commanded. Run was successful.		Comments from the chase boat was that we were doing ~2.5 mph.
1104_10	9	Time based run at 045 for two minutes. Heading towards the Gyre.	Behaved as commanded. Run was successful.		
1104_11	10	small waypoint run for 90 seconds heading away from the Gyre. Way points were (0,40,30), (-40,80,3), (-70,110,0) relative to initialized heading	Behaved as commanded. Run was successful.		
1104_12	11	long waypoint run. Attempted to start at (0,0) and returned to (0,0). Vehicle timed out trying to get to (100,-85) due to turning the long way.	Run was moderately successful.		Waypoints were (0,0), (50,0), (100,0), (150, -10), (190,-40), (200, -60), (180,-80), (140,-90), (100,-85), (50,-65), (20,-30), (0,0). With 6-meter diameter watch circle.
1104_13	12	long waypoint run. Attempted to start at (0,0) and returned to (0,0). Vehicle timed out trying to get to (100,-85) due to turning the long way. Attempted to increase watch circle.	Run was moderately successful. Fix is to correct the heading command with an if statement to ensure that the vehicle always turns the shortest direction.		Waypoints were (0,0), (50,0), (100,0), (150, -10), (190,-40), (200, -60), (180,-80), (140,-90), (100,-85), (50,-65), (20,-30), (0,0). With 10-meter diameter watch circle

Table D.1 Sample Phoenix Missions

SONAR HEAD GENERAL DESCRIPTION

The NPS Phoenix is equipped with two mechanically scannable high frequency sonar heads built by Tritech Corp. One is a ST725 scanning sonar and the other is a ST1000 profiler sonar. Each head can be scanned continuously through 360 degrees of rotation or swept through any defined angular sector around the central axis of the unit. During normal operation, the head will ping, wait for return echoes to process, and then rotate a specified angular width and repeat. Step widths of 0.9 °, 1.8 °, and 3.6 ° are computer selectable.

All missions performed at AUVFEST '98 used the ST725 which operates at a frequency of 725 kilohertz and emits an acoustic beam 2.5 ° wide in the horizontal plane by 24° wide in the vertical plane. This device is described as a scanning sonar due to the nature of the range and intensity information returned for each ping. A scanning sonar operates by placing the intensities of the echoes from each ping into discrete segments of range called range bins. For this sonar, the number of range bins is nominally 128, but for operating ranges of 10 meters or less, the number of range bins is reduced to 64. The maximum operating range of the ST725 is 100 meters with a minimum operating range of 6 meters, and provides a resolution of (Maximum Range)/128 or (Maximum Range)/64, depending on the range setting used. The range setting used in the Gulf was 20 meters, which gave a resolution of approximately 15 cm.

In order to more clearly analyze the returns, the data can be thresholded to analyze only returns above a certain intensity level so that significant objects/structures can be seen, while other less significant entities (e. g. suspended particles in the water column, weak multi-path echoes, noise, etc.), are excluded. Combining thresholding with an appropriate power setting for the transducer, high quality results can be achieved.

SONAR CLUSTER IDENTIFICATION PROGRAM

The identification algorithm is designed to recognize areas of contiguous high intensity sonar returns. Below is a section of a test case showing sonar scanlines that have been thresholded to record intensities above 10.

```
00000000000000000000000000000000000
00000000000000000000000000000000000
00000000000000000000000000000000000
00000000000000000000000000000000000
00000000000000000000000000000000000
00000000000000000000000000000000000
00000000 11 11 0000000000000000000000
00000000 11 13 12 11 0000000000000000000
00000000 11 13 15 13 12 11 00000000000000000
00000012 11 0 14 13 12 12 11 000000000000000
00000000 12 13 14 14 13 12 12 11 000000000 11 000
00000000000000000000000000000000000
00000000 13 13 14 15 14 12 11 000000000000000
00000000 13 13 0 15 15 11 00000000000000000
00000000 12 13 14 13 0000000000000000000
00000000011 0000000000000000000000
00000000000000000000000000000000000
00000000000000000000000000000000000
00000000000000000000000000000000000
00000 14 0000000000000000000000000000
000000 13 000000000000000000000000000
00000000000000000000000000000000000
00000000000000000000000000000000000
00000000000000000000000000000000000
00000000000000000000000000000000000
00000000 13 2 11 0000000000000000000000
00000000 12 13 14 13 14 13 0000000000000000
00000000 13 13 1 15 15 11 12 12 12 12 00000000000
00000000 12 13 14 13 14 0000000000000000000
00000000011 11 0000000000000000000000
00000000 12 12 0000000000000000000000
00000000 13 13 0000000000000000000000
00000000 14 14 0000000000000000000000
00000000 11 11 0000000000000000000000
00000000 12 12 0000000000000000000000
```

The algorithm records the centroid (X, Y pairs) of each cluster of high intensity returns, while ignoring noise or small concentrations such as the 14, 13 group shown above. Several parameters are selectable to tune the algorithm for target identification such as maximum cluster width, breadth, number of non-contiguous contacts, etc. The following presents the results of the identification algorithm from a run at AUVFEST.

SONAR RESULTS FROM AUVFEST

Since there were no submerged targets in the area where the Phoenix operated, the chase boat served as a suitable target. Figure D.7 shows the targets identified (chase boat) with the centroid of each marked with a cross-hair. The trajectory of the Phoenix is shown with a solid line while the sonar returns with an intensity above 10 are shown with asterisks. Figure D.8 shows the lower right target cluster with the centroid clearly identified by the algorithm. Since the AUVFEST results were very positive, further experiments will be conducted in Monterey Bay in the early summer of 1999.

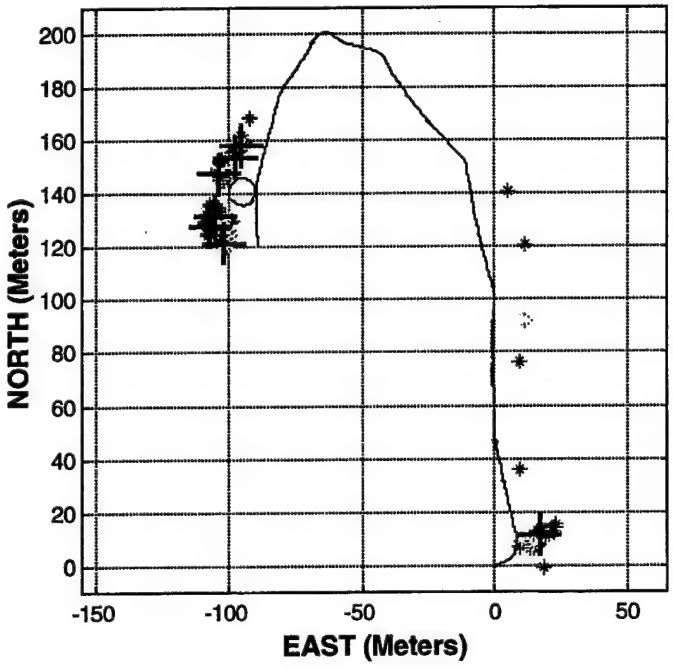

Figure D.7 Clusters Identified.

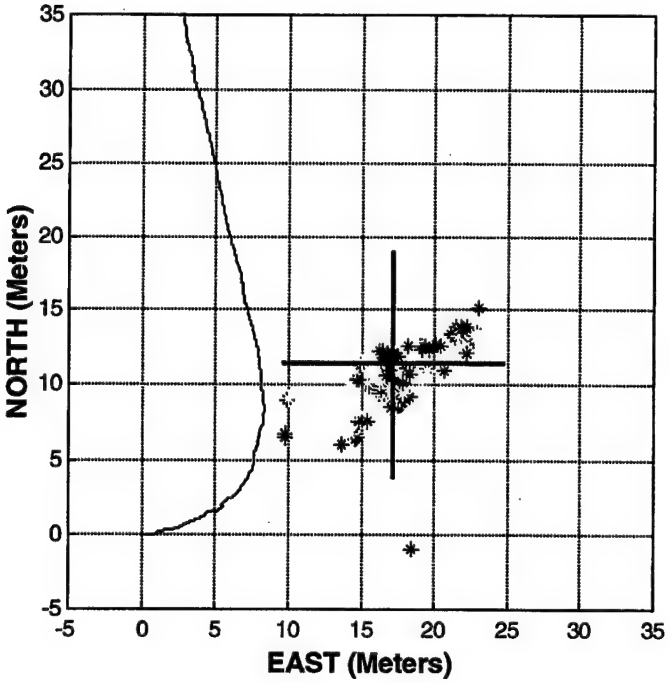

Figure D.8 Lower right cluster with centroid.

REFERENCES

Ackermann, J., *Sampled Data Systems*, Springer-Verlag, 1985.

An, P.E., Leavitt, G., Smith, S.M., and Dunn, S.E.,"A Quantitative Measure Of Sea-State Effect On Small Autonomous Underwater Vehicle Motion In Shallow Water," *Proceedings of Oceanology International 96*, Brighton, UK, March 1996, pp. 211-233.

Astrom, K. J.; "Theory And Applications Of Adaptive Control - A Survey," *Automatica*, v 19, n 5 September 1983.

Astrom, K.J. and Wittenmark, B., *Adaptive Control*, Addison-Wesley, 1989.

Bachmayer, R., Whitcomb, L.L., and Grosenbaugh, M.A., "A Four Quadrant Finite Dimensional Thruster Model," *IEEE Proceedings of the Conference on Oceans '98*, Nice, FR, October 1998, pp. 660-666.

Balchen, J.G., et al., "Dynamic Positioning Using Kalman Filtering and Optimal Control Theory," *Proceedings of the IFAC/IFIP Symposium on Automation in Offshore Oil Field Operation*, Holland, Amsterdam, September 1976, pp. 183-186.

Berteaux, H.O., *Buoy Engineering*, John Wiley & Sons, 1976.

Brutzman, D., Healey, T., Marco, D., and McGhee, B., "The Phoenix Autonomous Underwater Vehicle," *AI-Based Mobile Robots*, MIT/AAFI Press, 1997.

Bunce, J., Boatman, J., and Wadell, J., "Unmanned Underwater Vehicles: Technology Demonstration 2," *Sea Technology*, December 1998, pp. 25-28.

Byrnes, R. B.; et al., "Rational Behavior Software Architecture For Intelligent Ships," *Naval Engineers Journal*, v 108, n 2 March 1996, p 43-55.

Canudas de Wit, C. and Slotine, J.-J.E., "Sliding Observers for Robot Manipulators," *Automatica*, v. 27, n. 5, 1991, pp. 859-864.

Chance, T.S., "AUV Needs in the Gulf Coast Region," *Proceedings of the First International Workshop on Autonomous Underwater Vehicles for Shallow Waters and Coastal Environments (IARP '98)*, Lafayette, LA, 17-19 February 1998.

Craig, J.J., *Adaptive Control of Mechanical Manipulators*, Addison-Wesley, 1989.

Curtin, T.B., et al., "Autonomous Oceanographic Sampling Networks," *Oceanography*, v 6, n 3, December 1993, pp. 86-94.

Dean, R.G. and Dalrymple, R.A., *Water Wave Mechanics for Engineers and Scientists*, Prentice-Hall, 1984.

Faltinsen, O.M., *Sea Loads on Ships and Offshore Structures*, Cambridge University Press, 1990.

Feldman, J., "Revised Standard Submarine Equations of Motion," *Technical Report DTNSRDC-SPD-0393-09*, Naval Ship Research and Development Center, Washington, DC, 1979.

Fossen, T.I. and Balchen, J. G. "The NEROV Autonomous Underwater Vehicle," *IEEE Proceedings of OCEANS '91 Conference*, Honolulu, HI, October 1991.

Fossen, T.I., *Guidance and Control of Ocean Vehicles*, John Wiley & Sons, Chichester, England, 1994.

Fossen, T.I., Sagatun, S.I., and Sørensen, A.J., "Identification of Dynamically Positioned Ships," *Proceedings of the 3rd IFAC Workshop on Control Applications in Marine Systems (CAMS'95)*, Trondheim, Norway, May 1995, pp. 362-369.

Fowler, T. B., "Application of Stochastic Control Techniques to Chaotic Nonlinear Systems," *IEEE Transactions on Automation and Control*, v 34, n 2, February 1989, pp. 201-205.

Fryxell, D., et al., "Integrated Approach to The Design and Analysis of Navigation, Guidance And Control Systems For Autonomous Underwater Vehicles," *IEE Computing and Control Division Colloquium on Control and Guidance of Remotely Operated Vehicles*, London, UK, June 1995.

Fung, P.T-K. and Grimble, M.J., "Dynamic Ship Positioning Using a Self-tuning Kalman Filter," *IEEE Transactions on Automatic Control*, v AC-28, n 3, March 1983, pp. 339-349.

Gelb, A., *Applied Optimal Estimation*, MIT Press, Cambridge, MA, 1974.

Gertler, M. and Hagen, G.R., "Standard Equations of Motion for Submarine Simulations," *Naval Ship Research and Development Report 2510*, 1967.

Gordon, R. L., *Acoustic Doppler Current Profiler Principles of Operation, A Practical Primer*, RD Instruments, San Diego, CA, 1996.

Greenwood, D.T., *Principles of Dynamics*, second edition, Prentice Hall, Englewood Cliffs, NJ, 1988.

Grimble, M.J., "State-Space Approach to LQG Multivariable Predictive and Feedforward Optimal Control," *Transactions of the ASME*, v 116, December 1995, pp. 610-617.

Hartley P. and Butler, B., "AUV Fiber Optic Cable Laying - From Concept to Reality," *Proceedings of the Seventh International Symposium on Unmanned Untethered Submersible Technology*, Autonomous Undersea Systems Institute, Durham, NH, September 1991.

Hasselmann, K., et al., "Measurements of Wind-wave Growth and Swell Decay During the Joint North Sea Wave Project (JONSWAP)," *Dt. hydrogr. Z.*, A12, 95, 1973.

Healey, A.J., "Dynamics of Marine Vehicles," course notes for ME4823, Naval Postgraduate School, Monterey, CA, Fall 1992.

Healey, A.J., "Model-Based Maneuvering Controls for Autonomous Underwater Vehicles," *Journal of Dynamic Systems, Measurement and Control*, v 114, n 4, December 1992, pp. 614-622.

Healey, A.J. and Lienard, D., "Multivariable Sliding Mode Control for Autonomous Diving and Steering of Unmanned Underwater Vehicles," *IEEE Journal of Oceanic Engineering*, vol. 18 no. 3, July 1993, pp. 327-339.

Healey, A.J., et al., "Toward an Improved Understanding of Thruster Dynamics for Underwater Vehicles," *Proceedings of the IEEE Symposium on Autonomous Underwater Vehicle Technology (AUV' 94)*, Cambridge, MA, July 1994, pp. 340-352.

Healey, A. J., Marco, R.B., and McGhee, R.B., "Autonomous Underwater Vehicle Control Coordination Using a Tri-Level Hybrid Software Architecture," *Proceedings of the IEEE Robotics and Automation Conference*, Minneapolis, MN, April 1996, pp. 2149-2159.

Healey, A.J.; An, E.P.; and Marco, D.B.; "On Line Compensation of Heading Sensor Bias for Low Cost AUVs," *Proceedings of the IEEE Symposium on Autonomous Underwater Vehicle Technology*, Cambridge, MA, August 1998.

Heyns, L.J. and Kruger, J.J., "Describing-Function Based Criterion for a Route to Chaos in Autonomous Nonlinear Systems," *International Journal of Control*, v 61, n 1, January 1995, pp. 211-228

Hoerner, S.F., *Fluid-Dynamic Drag*, Hoerner Fluid Dynamics, Brick Town, NJ, 1965.

Hoerner, S.F. and Borst, H.V., *Fluid-Dynamic Lift*, Hoerner Fluid Dynamics, Brick Town, NJ, 1975.

Honegger, B., editor., *Proceedings Of The Technology And The Mine Problem Symposium*, Naval Postgraduate School, Monterey, CA, November 1996.

Huang, N.E., et al., "A Unified Two-parameter Wave Spectral Model for a General Sea State," *Journal of Fluid Mechanics*, v 112, 1981, pp. 203-244.

Humphreys, D.E. and Watkinson, K.W., "Prediction of the Acceleration Hydrodynamic Coefficients for Underwater Vehicles from Geometric Parameters," *Technical Report NCSL-TR-327-78*, Naval Coastal Systems Center, Panama City, FL, 1978.

Humphreys, D.E. and Watkinson, K.W., "Hydrodynamic Stability and Control Analysis of the UNH-EAVE Autonomous Underwater Vehicle," *Technical Report A.R.P.A. Tech. Memo. No. 82-2*, University of New Hampshire, Marine Systems Engineering Lab, Durham, NH, 1982.

Humphreys, D.E. Smith, N.E. and Watkinson, K.W., *Hydrodynamic Coefficients and Six Degree of Freedom Model for the NUWC UUV*, Vehicle Control Technologies, Inc., Burke, VA, 1994.

Jenssen, N.A., *Estimation and Control in Dynamic Positioning of Vessels*, Ph.D. Dissertation, Norwegian Institute of Technology, Trondheim, Norway, December 1980.

Kallstrom, C.G., *Identification and Adaptive Control Applied to Ship Steering*, Ph.D. Dissertation, Lund Institute of Technology, Lund, Sweden, September 1979.

Kalske, S., "Motion Dynamics of Subsea Vehicles," *Technical Report SF-02150*, Technical Research Center of Finland, Espoo, Finland, January 1989.

Kato, N, et al., "Optimization of Configuration Of Autonomous Underwater Vehicle for Inspection of Underwater Cables," *Proceedings of the IEEE International Conference on Robotics and Automation*, Leuven, Belgium, May 1998, pp. 1045-1050.

Kuik, A.J., van Vledder, G. Ph., and Holthuijsen, L.H., "A Method for Routine Analysis of Pitch-and-Roll Buoy Data," *Journal of Physical Oceanography*, v 18, 1988.

Lamb, H., *Hydrodynamics*, Cambridge University Press, New York, 1932.

Leira, B.J., "Multidimensional Stochastic Linearization of Drag Forces," *Journal of Applied Ocean Research*, v 9, n 3, July 1987, pp. 150-162.

Lewis, E.V., editor, *Principles of Naval Architecture*, second revision, Society of Naval Architects and Marine Engineers (SNAME), Jersey City, NJ, 1988.

Liu, P.C., "Representing Frequency Spectra for Shallow Water Waves," *Ocean Engineering*, v 12, n 2, 1985, pp. 151-160.

Ljung, L., *System Identification-Theory for the User*, Prentice-Hall, 1987.

Long, R.B., "The Statistical Evaluation of Directional Spectrum Estimates Derived From Pitch/Roll Buoy Data," *Journal of Physical Oceanography*, v 10, 1980.

Longuet-Higgins, M.S., "On the Statistical Distribution of the Heights of Sea Waves," *Journal of Marine Research*, v 11, p. 245, 1953.

Longuet-Higgins, M.S., Cartwright, D.E., and Smith, N.D., *Ocean Wave Spectra*, Prentice Hall, 1963.

Marco, D.B., Healey, A.J., McGhee, R.B., and Brutzman, D.P., "Control Systems Architecture, Navigation, and Communication Research Using the NPS Phoenix Underwater Vehicle" *Proceedings of the 6th International Advanced Robotics Program Workshop on Underwater Robotics*, Toulon, France, March 27-29, 1996.

Marco, D.B., Healey, A.J., and McGhee, R.B., "Autonomous Underwater Vehicles: Hybrid Control of Mission and Motion," *Autonomous Robots 3*, Kluwer Academic Publishers, 1996.

Marco, D.B., *Autonomous Control of Underwater Vehicles and Local Area Maneuvering*, Ph.D. Dissertation, Naval Postgraduate School, Monterey, CA, September 1996.

Marco, D.B. and Healey, A.J., "Local Area Navigation Using Sonar Feature Extraction and Model-Based Predictive Control," *International Journal of Systems Science*, v 29, n 10, 1998, pp. 1123-1133.

Marco, D., Martins, A., and Healey, A.J., "Surge Motion Parameter Identification for the NPS Phoenix AUV,'' First International Workshop on Autonomous Underwater Vehicles for Shallow Waters and Coastal Environments (IARP '98), Lafayette LA, 17-19 February 1998.

Marquest, "ROV Dynamic Positioning ROV-DP," *Sales Brochure*, Marquest Group, Inc., Bourne, MA, 1991.

Morison, J.R., et al., "The Force Exerted by Surface Waves on Piles," *Pet. Trans*, PT-189, 1950, pp. 149-154.

Milne-Thomson, L.M., *Theoretical Hydrodynamics*, MacMillan Education Ltd., 1968.

Newman, J.N., *Marine Hydrodynamics*, MIT Press, 1977.

O'Reilly, W.C., Herbers, T.H.C., Seymour, R.J., and Guza, R.T., "A Comparison of Directional Buoy and Fixed Platform Measurements of Pacific Swell," *Journal of Atmospheric and Oceanic Technology*, v 13, n 1, February 1996, pp. 231-238.

Ogata, K., *Modern Control Engineering*, Prentice-Hall, 1990.

ONR, "VSW BAA," http://www.onr.navy.mil/02/baa/baa98008.htm, February 1998.

Pereira, F.L., et al., "AUV System Requirements for Coastal Oceanography," *Proceedings of the Symposium on Autonomous Underwater Vehicle Technology (AUV '96)*, Monterey, CA, June 1996, pp. 399-406.

Rahman, M., editor, *Ocean Waves Engineering*, Computational Mechanics Publications, 1994.

Rajamani, R., "Observers for Lipschitz Nonlinear Systems," *IEEE Transactions on Automatic Control*, v 43, n 3, March 1998, pp. 397-401.

Riedel, J.S. and Healey, A.J., "A Discrete Filter For The Forward Prediction Of Sea Wave Effects on AUV Motions," *Proceedings of the Tenth International Symposium on Unmanned Untethered Submersible Technology*, Autonomous Undersea Systems Institute, Durham, NH, September 1997.

Riedel, J.S. and Healey, A.J., "Model Based Predictive Control of AUVs for Station Keeping in a Shallow Water Wave Environment," *Proceedings of the First International Workshop on Autonomous Underwater Vehicles for Shallow Waters and Coastal Environments (IARP '98)*, Lafayette, LA, 17-19 February 1998.

Riedel, J.S. and Healey, A.J., "Shallow Water Station Keeping of AUVs Using Multi-Sensor Fusion for Wave Disturbance Prediction and Compensation," *IEEE Proceedings of Oceans '98*, Nice, France, September 1998.

Saelid, S. and Jenssen, N.A., "Adaptive Ship Autopilot with Wave Filter," *Modeling, Identification and Control*, v MIC-4, n 1, August 1983, pp. 33-46.

Santos, A., et al., "Dealing in Real Time with A Priori Unknown Environment on Autonomous Underwater Vehicles (AUVs)," *Proceedings of the International Conference on Robotics and Automation*, Nagoya, Japan, May 1995, pp. 1579-1584.

Saridis, G.N., "Intelligent Robotic Control," *IEEE Transactions on Automatic Control*, v AC-28, n 5 May 1983, pp. 547-557.

Sarpkaya, T., "Forces on Cylinders and Spheres in a Sinusoidally Oscillating Fluid," *Journal of Applied Mechanics*, v 42, March 1975, pp. 32-47.

Sarpkaya, T. and Isaacson, M., *Mechanics of Wave Forces on Offshore Structures*, Van Nostrand Rienhold Company Inc., 1981.

Silvestre, C., Pascoal, A., Kaminer, I., and Healey, A.J., "Plant/Controller Optimization with Applications to Integrated Surface Sizing and Feedback Controller Design for Autonomous Underwater Vehicles (AUVs)," *Proceedings of the American Controls Conference '98*, Philadelphia, PA, June 1998.

Silvestre, C., Pascoal, A., and Healey, A.J., "AUV Control Under Wave Disturbances: An Application of Mixed H_2/H_∞ Design Methods," *Proceedings of CONTROLO '98 (3rd Portuguese Conference on Automatic Control)*, Coimbra, Portugal, September 1998, pp. 423-429.

Slotine, J.-J.E. and Li, W., *Applied Nonlinear Control*, Prentice Hall, 1991.

Smith, S.M. and Dunn, S., "The Ocean Voyager II: An AUV Designed for Coastal Oceanography," *Proceedings of the IEEE Oceanic Engineering Society Conference on Autonomous Underwater Vehicles (AUV '94)*, Cambridge, MA, July 1994, pp. 139-148.

SNAME (The Society of Naval Architects and Marine Engineers), "Nomenclature for Treating the Motion of a Submerged Body Through a Fluid," *Technical Research Bulletin 1-5*, Jersey City, NJ, 1950.

Soong, T.T. and Grigoriu, M., *Random Vibration of Mechanical and Structural Systems*, Prentice Hall, 1993.

Sørensen, A.J., Sagatun S.I., and Fossen, T. I., "Design of a Dynamic Positioning System Using Model Based Control," *Journal of Control Engineering Practice*, v CEP-4, n 3, June 1996, pp. 359-368.

Spanos, P-T.D. and Hansen, J.E., "Linear Prediction Theory for Digital Simulation of Sea Waves," *ASME Journal of Energy Resources Technology*, v 103, n 1, Sep. 1981, pp. 243-249.

Triantafyllou, M.S., et al., "Real Time Estimation of Ship Motions Using Kalman Filtering Techniques," *IEEE Journal of Ocean Engineering*, v OE-8, n 1, 1983, pp. 9-20

Wendel, K., "Hydrodynamic Masses and Hydrodynamic Moments of Inertia," *TMB Translation 260*, July 1956.

Whitcomb, L.L. and Yoeger, D.R., "Comparitive Experiments in the Dynamics and Model-Based Control of Marine Thrusters," *IEEE Proceedings of the Conference on Oceans '95*, San Diego, CA, October 1995, pp. 1019-1028.

White, F.M., *Fluid Mechanics*, McGraw Hill, 1986.

Williams, G.N., Lagace, G.E., and Woodfin, A., "A Collision Avoidance Controller For Autonomous Underwater Vehicles," *IEEE Proceedings of the Symposium on Autonomous Underwater Vehicle Technology - AUV '90*, June 1990, pp. 206-212.

Yavnai, A, "Architecture for an Autonomous Reconfigurable Intelligent Control System (ARICS)," *Proceedings of the IEEE Symposium on Autonomous Underwater Vehicle Technology*, Monterey, CA, June 1996.

Yaz, E. and Azemi, A., "Variable Structure Observer With a Boundary-Layer For Correlated Noise/Disturbance Models and Disturbance Minimization," *International Journal of Control*, v. 57, n. 5, 1993, pp. 1191-1206.

Yoeger, D.R and Slotine, J.-J.E., "Adaptive Sliding Control of an Experimental Underwater Vehicle," *Proceedings of the IEEE Conference on Robotics and Automation*, Sacramento, CA, April 1991, pp.2746-2751.

Yoeger, D.R., Cooke, J.G., and Slotine, J.-J.E., "The Influence of Thruster Dynamics on Underwater Vehicle Behavior and Their Incorporation Into Control System Design," *Journal of Oceanic Engineering*, v. 15, n. 3, 1991, pp. 167-178.

Yuh, J, "Modeling and Control of Underwater Vehicles," *IEEE Transactions of Systems, Man, and Cybernetics*, v 20, November-December 1990, pp.1475-1483.

BIBLIOGRAPHY

Abkowitz, M., *Stability and Motion Control of Ocean Vehicles*, MIT Press, 1969.

Abreu, M., Larraza, A., and Thornton, E., "Nonlinear Transformation of Directional Wave Spectra in Shallow Water," *Journal of Geophysical Research*, v 97, n C10, October 1992, pp. 15,579-15,589.

Ackermann, J., *Sampled Data Systems*, Springer-Verlag, 1985.

Allmendinger, E.E. editor, *Submersible Vehicle Systems Design*, The Society of Naval Architects and Marine Engineers, 1990.

An, P.E., Leavitt, G., Smith, S.M., and Dunn, S.E.,"A Quantitative Measure of Sea-State Effect on Small Autonomous Underwater Vehicle Motion in Shallow Water," *Proceedings of Oceanology International 96*, Brighton, UK, March 1996, pp. 211-233.

An, P.E. and Smith, S.M., "Experimental Self-Motion Study of the Ocean Explorer AUV in Controlled Sea States," *IEEE Journal of Oceanic Engineering*, v 23, n 3, July 1998, pp. 274-284.

Anderson, B.D.O. and Moore, J.B., *Optimal Control: Linear Quadratic Methods*, Prentice-Hall, 1990.

Appleby, B., Bonnice, W., and Bedrossian, N., "Robustness Analysis Methods for Underwater Vehicle Control Systems," *IEEE Proceedings of the Symposium on Autonomous Underwater Vehicle Technology (AUV '90)*, Washington, D.C., June 1990, pp. 74-80.

Astrom, K. J.; "Theory and Applications of Adaptive Control - A Survey," *Automatica*, v 19, n 5 September 1983.

Astrom, K.J. and Wittenmark, B., *Computer Controlled Systems Theory and Design*, Prentice-Hall, 1984.

Astrom, K.J. and Wittenmark, B., *Adaptive Control*, Addison-Wesley, 1989.

Athans, M. and Falb, P.L., *Optimal Control*, McGraw-Hill, 1966.

Bachmayer, R., Whitcomb, L.L., and Grosenbaugh, M.A., "A Four Quadrant Finite Dimensional Thruster Model," *IEEE Proceedings of the Conference on Oceans '98*, Nice, FR, October 1998, pp. 660-666.

Baiardi, P., et al., "Dynamic Simulation of Underwater Vehicles," *Fourth International Advanced Robotics Programme (IARP) Workshop on Underwater Robotics*, Genoa, Italy, November 1992.

Balchen, J.G., et al., "Dynamic Positioning Using Kalman Filtering and Optimal Control Theory," *Proceedings of the IFAC/IFIP Symposium on Automation in Offshore Oil Field Operation*, Holland, Amsterdam, September 1976, pp. 183-186.

Barke, F.G., *On-Line Identification Of The Speed, Steering And Diving Response Parameters Of An Autonomous Underwater Vehicle From Experimental Data*, Master's Thesis, Naval Postgraduate School, Monterey, CA, 1992.

Bellingham, J., et al., "A Second Generation Survey AUV," *Proceedings of the IEEE Oceanic Engineering Society Conference on Autonomous Underwater Vehicles (AUV '94)*, Cambridge, MA, July 1994, pp. 148-155.

Belmont, M.R. and Morris, E.L., "Adaptive Measurement and Signal Processing Strategies Associated with Deterministic Sea Wave Prediction," *IEE Proceedings of the 6th International Conference on Electronic Engineering in Oceanography*, Cambridge, U.K., July 1994, pp. 181-188.

Bendat, J.S. and Piersol, A.G., *Random Data: Analysis and Measurement Procedures*, Wiley Interscience, 1971.

Berteaux, H.O., *Buoy Engineering*, John Wiley & Sons, 1976.

Bonasso, R.P., "Coordinating Perception and Action with an Underwater Robot in a Shallow Water Environment," *Proceedings of SPIE-Sensor Fusion IV*, v 1611, Boston, MA, November 1991, pp. 320-330.

Boncal, R.J., *A Study Of Model Based Maneuvering Controls For Autonomous Underwater Vehicles*, Master's Thesis, Naval Postgraduate School, Monterey, CA, December 1987.

Bowden, J.A. and White, R.A., "Measurements of The Orbital Velocities of Sea Waves and Their Use in Determining the Directional Spectrum," *Geophys. J. Roy. Astron. Soc.*, v 12, 1996.

Brown, J., *Four Quadrant Dynamic Model of the AUV II Thruster*, Master's Thesis, Naval Postgraduate School, Monterey, CA, September 1993.

Brutzman, D., Healey, T., Marco, D., and McGhee, B., "The Phoenix Autonomous Underwater Vehicle," *AI-Based Mobile Robots*, MIT/AAFI Press, 1997.

Bryson, A.E. and Ho, Y-C., *Applied Optimal Control*, John Wiley & Sons, 1975.

Bunce, J., Boatman, J., and Wadell, J., "Unmanned Underwater Vehicles: Technology Demonstration 2," *Sea Technology*, December 1998, pp. 25-28.

Byrnes, C.I., Priscoli, F.D., and Isidori, A., *Output Regulation of Uncertain Nonlinear Systems*, Edwards Brothers, 1997.

Byrnes, R. B.; et al., "Rational Behavior Software Architecture for Intelligent Ships," *Naval Engineers Journal*, v 108, n 2 March 1996, p 43-55.

Canudas de Wit, C. and Slotine, J.-J.E., "Sliding Observers for Robot Manipulators," *Automatica*, v. 27, n. 5, 1991, pp. 859-864.

Chan, C.Y. and Sirisena, H.R., "Stochastic Adaptive Control of a Class of Non-Minimum-Phase Systems," *Optimal Control Applications and Methods*, v 10, n 3, July-September 1989, pp. 267-274.

Chance, T.S., "AUV Needs in the Gulf Coast Region," *Proceedings of the First International Workshop on Autonomous Underwater Vehicles for Shallow Waters and Coastal Environments (IARP '98)*, Lafayette, LA, 17-19 February 1998.

Chen, G. and Chung, S-H, "Depth Control of a Submersible Vehicle Under a Seaway Using a Noise Estimator," *IEE Proceedings on Electronic Engineering in Oceanography*, n 394, July 1994, pp. 30-34.

Chen, H-F. and Guo, L., "Robust Stochastic Adaptive Controller," *IEEE Transactions on Automation and Control*, v 33, n 11, November 1988, pp. 1035-1043.

Chen, X., et al., "6 DOF Nonlinear AUV Simulation Toolbox," *IEEE Proceedings of Oceans 97*, Halifax, NS, October 1997.

Chinn, N.L. and Roberts, G.N., "Simulating Wave Disturbances Using Directional Energy Sea Spectra for Spatial Wave Profiles in Time," *Proceedings of the 1993 American Control Conference*, San Francisco, CA, June 1993, pp. 2601-2604.

Chryssostomidis, C. and Oakes, M.C., "Selection of Wave Spectra for use in Ship Design," *Proceedings of the International Symposium on Ocean Wave Measurement and Analysis*, New Orleans, LA, September 1974, pp. 217-234.

Chung, J.C., Bien, Z., and Kim, Y.S., "A Note on Ship-Motion Prediction Based on Wave-Excitation Input Estimation," *IEEE Journal of Oceanic Engineering*, v 15, n 3, July 1990, pp. 244-250.

Close, C. and Frederick; D.K., *Modeling and Analysis of Dynamic Systems*, John Wiley & Sons, 1993.

Cody, S.E., *An Experimental Study of the Response of Small Tunnel Thrusters to Triangular and Square Wave Inputs*, Master's Thesis, Naval Postgraduate School, Monterey, CA, December 1992.

Cooper, G.R. and McGillem; C.D., *Probabilistic Methods of Signal and System Analysis*, Holt, Rinehart and Winston, CBS College Publishing, 1986.

Craig, J.J., *Adaptive Control of Mechanical Manipulators*, Addison-Wesley, 1989.

Cristi, R. and Healey, A.J., "Adaptive Identification and Control of an Autonomous Underwater Vehicle," *Sixth International Symposium on Unmanned Untethered Submersible Technology (UUST)*, University of New Hampshire (UNH) Marine Systems Engineering Laboratory (MSEL), Durham, NH, June 1989, pp. 563-572.

Cristi, R., Papoulias, F.A., and Healey, A.J., "Adaptive Sliding Mode Control of Autonomous Underwater Vehicles in the Dive Plane," *Journal of Oceanic Engineering*, v 15, n 3, July 1990, pp. 152-160.

Cristi, R., Caccia, M., Veruggio, G., and Healey, A. J., "A Sonar Based Approach to AUV Localization," *Proceedings of CAMS '95*, Trondheim, Norway, May 1995.

Crook, T.P., *An Initial Assessment Of Free Surface Effects On Submerged Bodies*, Master's Thesis, Naval Postgraduate School, Monterey, CA, September 1994.

Curtin, T.B., et al., "Autonomous Oceanographic Sampling Networks," *Oceanography*, v 6, n 3, December 1993, pp. 86-94.

Dean, R.G. and Dalrymple, R.A., *Water Wave Mechanics for Engineers and Scientists*, Prentice-Hall, 1984.

DeCarlo, R.A., Zak, S.H., and Matthews, G.P., "Variable Structure Control of Nonlinear Multivariable Systems: a Tutorial," *IEEE Proceedings*, v 76, March 1988, pp. 212-232.

Dhanak, M.R. and Holappa, K., "AUV Platform Requirements For Ambient Turbulence Measurement," *Proceedings of the International Offshore and Polar Engineering Conference*, v 2, Honolulu, HI, May 1997, pp. 89-92.

Doyle, J.C. and Stein, G., "Robustness With Observers," *IEEE Transactions on Automatic Control*, v AC-24, August 1979, pp. 607-611.

Dunn, S.E., Smith, S.M., Betzer, P., and Hopkins, T., "Integrated Sensors and UUV Technologies for Coastal Ocean Applications," COSU '95, Yokohama, Japan, May 1995.

Faltinsen, O.M., *Sea Loads on Ships and Offshore Structures*, Cambridge University Press, 1990.

Feldman, J., "Revised Standard Submarine Equations of Motion," *Technical Report DTNSRDC-SPD-0393-09*, Naval Ship Research and Development Center, Washington, DC, 1979.

Feuer, A. and Goodwin; G.C., *Sampling in Digital Processing and Control*, Birkhauser Publishing, 1996.

Fossen, T.I, and Balchen, J. G. "The NEROV Autonomous Underwater Vehicle," *IEEE Proceedings of OCEANS '91 Conference*, Honolulu, HI, October 1991.

Fossen, T.I., *Guidance and Control of Ocean Vehicles*, John Wiley & Sons, Chichester, England, 1994.

Fossen, T.I. and Fjellstad, O-E, "Nonlinear Modelling of Marine Vehicles in 6 Degrees of Freedom," *Journal of Mathematical Modeling of Systems*, v 1, n 1, 1995.

Fossen, T.I., Sagatun, S.I., and Sørensen, A.J., "Identification of Dynamically Positioned Ships," *Proceedings of the 3rd IFAC Workshop on Control Applications in Marine Systems (CAMS'95)*, Trondheim, Norway, May 1995, pp. 362-369.

Fowler, T. B., "Application of Stochastic Control Techniques to Chaotic Nonlinear Systems," *IEEE Transactions on Automation and Control*, v 34, n 2, February 1989, pp. 201-205.

Freeman, R.A. and Kokotovic; P.V., *Robust Nonlinear Control Design: State-space and Lyapunov Technique*, Birkhauser, 1996.

Friedland, B., *Control System Design*, McGraw-Hill, 1986.

Friedland; B., *Advanced Control System Design*, Prentice-Hall, 1996.

Fryxell, D., et al., "Integrated Approach to the Design and Analysis of Navigation, Guidance and Control Systems for Autonomous Underwater Vehicles," *IEE Computing and Control Division Colloquium on Control and Guidance of Remotely Operated Vehicles*, London, UK, June 1995.

Fu, H-S., *Optimal Stochastic Sliding Mode Control Of Replenishment In A Random Sea*, Master's Thesis, Naval Postgraduate School, Monterey, CA, December 1991.

Fung, P.T-K. and Grimble, M.J., "Dynamic Ship Positioning Using a Self-tuning Kalman Filter," *IEEE Transactions on Automatic Control*, v AC-28, n 3, March 1983, pp. 339-349.

Gelb, A. and Vander Velde, W.E., *Multiple-Input Describing Functions and Nonlinear System Design*, McGraw-Hill, 1968.

Gelb, A., *Applied Optimal Estimation*, MIT Press, Cambridge, MA, 1974.

Gertler, M. and Hagen, G.R., "Standard Equations of Motion for Submarine Simulations," *Naval Ship Research and Development Report 2510*, 1967.

Goodwin, G.C. and Sin, K.S., *Adaptive Filtering Prediction and Control*, Prentice-Hall, 1984.

Gordon, R. L., *Acoustic Doppler Current Profiler Principles of Operation, A Practical Primer*, RD Instruments, San Diego, CA, 1996.

Greenwood, D.T., *Principles of Dynamics*, second edition, Prentice Hall, Englewood Cliffs, NJ, 1988.

Grimble, M.J., "LQG Predictive Optimal Controller for Continuous-Time Systems," *IEE Proceedings-D*, v 140, n 3, May 1993, pp. 181-190.

Grimble, M.J., "Two-degree-of-freedom Linear Quadratic Gaussian Predictive Control," *IEE Proceedings on Control Theory Applications*, v 142, n 4, July 1995, pp. 295-306.

Grimble, M.J., "State-Space Approach to LQG Multivariable Predictive and Feedforward Optimal Control," *Transactions of the ASME*, v 116, December 1995, pp. 610-617.

Gustafasson, F., Gunnarsson, S., and Ljung, L., "On Time-Frequency Resolution of Signal Properties Using Parametric Techniques," *IEEE Proceedings of the 33rd Conference on Decision and Control*, Lake Buena Vista, FL, December 1994, pp. 2259-2264.

Hajosy, M.F., *Six Degree of Freedom Vehicle Controller Design for the Operation of an Unmanned Underwater Vehicle in a Shallow Water Environment*, Engineer's Thesis, Massachusetts Institute of Technology, Cambridge, MA, September 1994.

Hartley P. and Butler, B., "AUV Fiber Optic Cable Laying - From Concept to Reality," *Proceedings of the Seventh International Symposium on Unmanned Untethered Submersible Technology*, Autonomous Undersea Systems Institute, Durham, NH, September 1991.

Hartley, T.T., Beale, G.O., and Chicatelli, S.P., *Digital Simulation of Dynamic Systems: A Control Theory Approach*, Prentice Hall, 1994.

Haskind, M.D., "On Wave Motions of a Heavy Fluid," *Prikl. Mat. Mekh.*, PMM-18, 1954.

Hasselmann, K., et al., "Measurements of Wind-wave Growth and Swell Decay During the Joint North Sea Wave Project (JONSWAP)," *Dt. hydrogr. Z.*, A12, 95, 1973.

Hawkinson, T.D., *Multiple Input Sliding Mode Control for Autonomous Diving and Steering of Underwater Vehicles*, Master's Thesis, Naval Postgraduate School, Monterey, CA, December 1990.

Hayes, J., "Ocean Current-Wave Interaction Study," *Journal of Geophysical Research*, v 85, n C9, September 1980, pp. 5025-5031.

Healey, A.J., Papoulias, F.A., and Cristi, R., "Design and Experimental Verification of a Model-Based Compensator for Rapid AUV Depth Control," *Sixth International Symposium on Unmanned Untethered Submersible Technology (UUST)*, University of New Hampshire (UNH) Marine Systems Engineering Laboratory (MSEL), Durham, NH, June 1989, pp. 458-474.

Healey, A.J., et al., "Research on Autonomous Underwater Vehicles at the Naval Postgraduate School," *Naval Research Reviews*, Office of Naval Research, Washington, D.C., v XLIV, n 1, Spring 1992.

Healey, A.J., "Dynamics of Marine Vehicles," course notes for ME4823, Naval Postgraduate School, Monterey, CA, Fall 1992.

Healey, A.J., "Model-Based Maneuvering Controls for Autonomous Underwater Vehicles," *Journal of Dynamic Systems, Measurement and Control*, v 114, n 4, December 1992, pp. 614-622.

Healey, A.J. and Lienard, D., "Multivariable Sliding Mode Control for Autonomous Diving and Steering of Unmanned Underwater Vehicles," *IEEE Journal of Oceanic Engineering*, vol. 18 no. 3, July 1993, pp. 327-339.

Healey et al.., "Coordination of the Hovering Behaviors of the NPS AUV II using Onboard Sonar Servoing," *Proceedings of the 1994 NSF IARP Workshop on Mobile Robots for Subsea Environments*, MBARI, Pacific Grove, CA. May 1994.

Healey, A.J., et al., "Tactical/Execution Level Coordination for Hover Control of the NPS AUV II using Onboard Sonar Servoing," *Proceedings of the IEEE Oceanic Engineering Society Conference on Autonomous Underwater Vehicles (AUV '94)*, Cambridge, MA, July 1994, pp. 129-138.

Healey, A.J., et al., "Toward an Improved Understanding of Thruster Dynamics for Underwater Vehicles," *Proceedings of the IEEE Symposium on Autonomous Underwater Vehicle Technology (AUV' 94)*, Cambridge, MA, July 1994, pp. 340-352.

Healey, A.J., Pascoal, A.M., and Pereira, F.L., "Autonomous Underwater Vehicles: An Application of Intelligent Control Technology," *Proceedings of the American Control Conference*, Seattle, WA, June 1995, pp. 2943-2949.

Healey, A.J., Marco, R.B., and McGhee, R.B., "Autonomous Underwater Vehicle Control Coordination Using a Tri-Level Hybrid Software Architecture," *Proceedings of the IEEE Robotics and Automation Conference*, Minneapolis, MN, April 1996, pp. 2149-2159.

Healey, A.J.; An, E.P.; and Marco, D.B.; "On Line Compensation f Heading Sensor Bias for Low Cost AUVS," *Proceedings of the IEEE Symposium on Autonomous Underwater Vehicle Technology*, Cambridge, MA, August 1998.

Herbers, T.H.C., Elgar, S., and Guza, R.T., "Directional Spreading of Waves in the Nearshore," submitted December 1997 to the *Journal of Geophysical Research.*

Herbers, T.H.C. and Guza, R.T., "Wind-Wave Nonlinearity Observed at the Sea Floor. Part I: Forced-Wave Energy," *Journal of Physical Oceanography*, v 21, n 12, December 1991, pp. 1740-1761.

Heyns, L.J. and Kruger, J.J., "Describing-Function Based Criterion for a Route to Chaos in Autonomous Nonlinear Systems," *International Journal of Control*, v 61, n 1, January 1995, pp. 211-228

Hjalmarsson, H. and Ljung, L., "A Discussion of 'Unknown-but-Bounded' Disturbances in System Identification," *IEEE Proceedings of the 32nd Conference on Decision and Control*, San Antonio, TX, December 1993, pp. 535-536.

Hoerner, S.F., *Fluid-Dynamic Drag*, Hoerner Fluid Dynamics, Brick Town, NJ, 1965.

Hoerner, S.F. and Borst, H.V., *Fluid-Dynamic Lift*, Hoerner Fluid Dynamics, Brick Town, NJ, 1975.

Holappa, K., Dhanak, M., Smith, S.M., and An, P.E., "Ocean Flow Measurement Using an Autonomous Underwater Vehicle," *Proceedings of the Symposium on Autonomous Underwater Vehicle Technology (AUV '96)*, Monterey, CA, June, 1996, pp.424-429.

Honegger, B., editor., *Proceedings Of The Technology And The Mine Problem Symposium*, Naval Postgraduate School, Monterey, CA, November 1996.

Huang, N.E., et al., "A Unified Two-parameter Wave Spectral Model for a General Sea State," *Journal of Fluid Mechanics*, v 112, 1981, pp. 203-244.

Hudspeth, R.T. and Borgman, L.E., "Efficient FFT Simulation of Digital Time Sequences," *Proceedings of the American Society of Civil Engineers*, v 105, n EM2, April 1977, pp. 223-235.

Hudspeth, R.T. and Chen, M-C., "Digital Simulation of Nonlinear Random Waves," *Proceedings of the American Society of Civil Engineers*, v 105, n WW1, February 1978, pp. 67-85.

Humphreys, D.E. and Watkinson, K.W., "Prediction of the Acceleration Hydrodynamic Coefficients for Underwater Vehicles From Geometric Parameters," *Technical Report NCSL-TR-327-78*, Naval Coastal Systems Center, Panama City, FL, 1978.

Humphreys, D.E. and Watkinson, K.W., "Hydrodynamic Stability and Control Analysis of the UNH-EAVE Autonomous Underwater Vehicle," *Technical Report A.R.P.A. Tech. Memo. No. 82-2*, University of New Hampshire, Marine Systems Engineering Lab, Durham, NH, 1982.

Humphreys, D.E., Smith, N.E., and Watkinson, K.W., *Hydrodynamic Coefficients and Six Degree of Freedom Model for the NUWC UUV*, Vehicle Control Technologies, Inc., Burke, VA, 1994.

Imlay, F.H., "The Complete Expression for Added Mass of a Rigid Body Moving in an Ideal Fluid," *Technical Report DTMB 1528*, David Taylor Model Basin, Washington, DC, 1961.

Ioannou, P.A. and Sun, J., *Robust Adaptive Control*, Prentice Hall, 1996.

Isidori, A., *Nonlinear Control Systems*, Springer-Verlag, 1995.

Jenssen, N.A., *Estimation and Control in Dynamic Positioning of Vessels*, Ph.D. Dissertation, Norwegian Institute of Technology, Trondheim, Norway, December 1980.

Jurewicz, T.A., *A Real Time Autonomous Underwater Vehicle Dynamic Simulator*, Master's Thesis, Naval Postgraduate School, Monterey, CA, December 1990.

Kallstrom, C.G., *Identification and Adaptive Control Applied to Ship Steering*, Ph.D. Dissertation, Lund Institute of Technology, Lund, Sweden, September 1979.

Kalske, S., "Motion Dynamics of Subsea Vehicles," *Technical Report SF-02150*, Technical Research Center of Finland, Espoo, Finland, January 1989.

Kam, M., Zhu, X., and Kalata, P., "Sensor Fusion for Mobile Robot Navigation," *Proceedings of the IEEE*, v 85, n 1, January 1997, pp. 108-119.

Karmen, E.W., *Introduction to Signals and Systems*, Macmillan Publishing Company, 1990.

Katebi, M.R., Grimble, M.J., and Zhang, Y., "H_∞ Robust Control Design for Dynamic Ship Positioning," *IEE Proceedings in Control Theory Applications*, v 144, n 2, March 1997, pp. 110-120.

Kato, N, et al., "Optimization of Configuration of Autonomous Underwater Vehicle for Inspection of Underwater Cables," *Proceedings of the IEEE International Conference on Robotics and Automation*, Leuven, Belgium, May 1998, pp. 1045-1050.

Kinsman, B., *Wind Waves, Their Generation and Propagation on the Ocean Surface*, Prentice-Hall, 1965.

Kolk, W.R. and Lerman, R.A., *Nonlinear System Dynamics*, Van Nostrand Reinhold, 1992.

Komo, J.J., *Random Signal Analysis in Engineering Systems*, Academic Press, Inc., 1987.

Krogstad, H.E., Gordon R.L., and Miller M.C., "High-Resolution Directional Wave Spectra From Horizontally-Mounted Acoustic Doppler Current Meters," *Journal of Atmospheric and Oceanic Technology*, v 5, pp. 340-352.

Kuik, A.J., van Vledder, G. Ph., and Holthuijsen, L.H., "A Method for Routine Analysis of Pitch-and-Roll Buoy Data," *Journal of Physical Oceanography*, v 18, 1988.

Kulkarni, S.R. and Posner, S.E., "Universal Prediction of Nonlinear Systems," *IEEE Proceedings of the 34th Conference on Decision & Control*, New Orleans, LA, December 1995, pp. 4024-4029.

Lamb, H., *Hydrodynamics*, Cambridge University Press, New York, 1932.

Lee, C.H. and Newman, J.H., "First- and Second-Order Wave Effects on a Submerged Spheroid," *Journal of Ship Research*, v 35, n 3, September 1991, pp. 183-190.

Leira, B.J., "Multidimensional Stochastic Linearization of Drag Forces," *Journal of Applied Ocean Research*, v 9, n 3, July 1987, pp. 150-162.

Leonard, J.J. and Smith, C.M., "Sensor Data Fusion in Marine Robotics," *Proceedings of the Seventh (1997) International Offshore and Polar Engineering Conference*, Honolulu, HI, May 1997, pp. 100-106.

Levesque, B. and Richard, M.J., "Simplified Dynamics and Stochastic Controller for Underwater Robots," *IEEE Proceedings of the Conference on Oceans '93*, October 1993, pp. 317-320.

Lewis, E.V., editor, *Principles of Naval Architecture*, v II, second revision, Society of Naval Architects and Marine Engineers (SNAME), Jersey City, NJ, 1988.

Li, C.K. and Leigh, J.R., "S-Domain Realization of Sea Spectrum," *Electronic Letters*, v 19, n 5, 1983, pp. 186-187.

Liu, P.C., "Representing Frequency Spectra for Shallow Water Waves," *Ocean Engineering*, v 12, n 2, 1985, pp. 151-160.

Ljung, L. and Söderström, T., *Theory and Practice of Recursive Identification*, MIT Press, 1983.

Ljung, L., *System Identification-Theory for the User*, Prentice-Hall, 1987.

Ljung, L., "Some Results on Identifying Linear Systems Using Frequency Domain Data," *IEEE Proceedings of the 32nd Conference on Decision and Control*, San Antonio, TX, December 1993, pp. 3534-3538.

Ljung, L., "Building Models From Frequency Domain Data," *Adaptive Control, Filtering and Signal Processing*, Springer-Verlag, 1995, pp. 229-240.

Long, C.E., "A Mathematical Basis for Wave Directional Estimation," notes from a short course on Field Wave Gauging Methods, Coastal Engineering Research Center Field Research Facility, Duck, North Carolina, May 1991.

Long, C.E., "Notes on a Derivation of the Maximum Likelihood Estimator for Ocean Wind Wave Directional Spectra," Coastal Engineering Research Center Field Research Facility, Duck, North Carolina, October 1997.

Long, R.B., "The Statistical Evaluation of Directional Spectrum Estimates Derived From Pitch/Roll Buoy Data," *Journal of Physical Oceanography*, v 10, 1980.

Longuet-Higgins, M.S., "On the Statistical Distribution of the Heights of Sea Waves," *Journal of Marine Research*, v 11, p. 245, 1953.

Longuet-Higgins, M.S., Cartwright, D.E., and Smith, N.D., *Ocean Wave Spectra*, Prentice Hall, 1963.

Lublin, L. and Athans, M., "Disturbance Source Identification for Multivariable Control," *Proceedings of the American Control Conference*, Seattle, WA, June 1995, pp. 4055-4059.

Makhoul, J., "Linear Prediction: A Tutorial Review," *Proceedings of the IEEE*, v 63, April 1975, pp. 561-580.

Marco, D. B. and Healey, A.J., "Sliding Mode Acoustic Servoing for an Autonomous Underwater Vehicle from Simulations and Experiments," *Proceedings of the 1992 Offshore Technology Conference*, Houston Tx, 1992.

Marco, D.B., Healey, A.J., McGhee, R.B., and Brutzman, D.P., "Control Systems Architecture, Navigation, and Communication Research Using the NPS Phoenix Underwater Vehicle" 6th International Advanced Robotics Program Workshop on Underwater Robotics, Toulon, France, March 27-29, 1996.

Marco, D.B., *Autonomous Control of Underwater Vehicles and Local Area Maneuvering*, Ph.D. Dissertation, Naval Postgraduate School, Monterey, CA, September 1996.

Marco, D.B., Healey, A.J., and McGhee, R.B., "Autonomous Underwater Vehicles: Hybrid Control of Mission and Motion," *Autonomous Robots 3*, Kluwer Academic Publishers, 1996.

Marco, D., Martins, A., and Healey, A.J., "Surge Motion Parameter Identification for the NPS Phoenix AUV," First International Workshop on Autonomous Underwater Vehicles for Shallow Waters and Coastal Environments (IARP '98), Lafayette LA, 17-19 February 1998.

Marco, D.B. and Healey, A.J., "Local Area Navigation Using Sonar Feature Extraction and Model-Based Predictive Control," *International Journal of Systems Science*, v 29, n 10, 1998, pp. 1123-1133.

Marquest, "ROV Dynamic Positioning ROV-DP," *Sales Brochure*, Marquest Group, Inc., Bourne, MA, 1991.

McCormick, M.E., *Ocean Engineering Wave Mechanics*, Wiley, New York, 1973.

McGhee, R.B., et al., "An Experimental Study of an Integrated GPS/INS System for Shallow-Water AUV Navigation (SANS)," *Proceedings of the Ninth International Symposium on Unmanned Untethered Submersible Technology*, Autonomous Undersea Systems Institute, Durham, NH, September 1997.

Miller, C.A., *An Application of Extended Kalman Filtering to a Model-Based, Short-Range Navigator for an AUV*, Master's Thesis, Naval Postgraduate School, Monterey, CA, December 1991.

Milne-Thomson, L.M., *Theoretical Hydrodynamics*, MacMillan Education Ltd., 1968.

Morison, J.R., et al., "The Force Exerted by Surface Waves on Piles," *Pet. Trans*, PT-189, 1950, pp. 149-154.

Musker, A.J., Loader, P.R., and Butcher, M.C., "Simulation of a Submarine Under Waves," *International Shipbuilding Programme*, v 35, n 404, 1988, pp. 389-410.

Newman, J.N., *Marine Hydrodynamics*, MIT Press, 1977.

Ni, S.Y., Zhang, L., and Dai, Y.S., "Hydrodynamic Forces on a Moving Submerged Body in Waves," *International Shipbuilding Progress*, v 41, pp. 95-111, 1994.

O'Reilly, W.C., Herbers, T.H.C., Seymour, R.J., and Guza, R.T., "A Comparison of Directional Buoy and Fixed Platform Measurements of Pacific Swell," *Journal of Atmospheric and Oceanic Technology*, v 13, n 1, February 1996, pp. 231-238.

Ogata, K., *Modern Control Engineering*, Prentice-Hall, 1990.

Ogata, K., *Discrete-Time Control Systems*, Prentice-Hall, 1995.

Ohshima, M., et al., "Model Predictive Control With Adaptive Disturbance Prediction and Its Application to Fatty Acid Column Control," *Journal of Process Control*, v 5, n 1, 1995, pp. 41-48.

ONR, "VSW BAA," http://www.onr.navy.mil/02/baa/baa98008.htm, February 1998.

Oppenheim, A.V. and Schafer, R.W., *Discrete Time Signal Processing*, Prentice Hall, 1989.

Oretga, R. and Spong, M.W., "Adaptive Motion Control of Rigid Robots: A Tutorial," *IEEE Conference on Decision and Control*, Austin, TX, 1988.

Papageorgiou, M. and Bauschert, T., "Stochastic Optimal Control of Moving Vehicles in a Dynamic Environment," *International Journal of Robotics Research*, v 13, n 4, August 1994, pp. 343-353.

Papoulias, F.A., Cristi, R., Marco, D., and Healey, A.J., "Modeling, Sliding Mode Control Design, and Visual Simulation of AUV Dive Plane Dynamic Response," *Sixth International Symposium on Unmanned Untethered Submersible Technology (UUST)*, University of New Hampshire (UNH) Marine Systems Engineering Laboratory (MSEL), Durham, NH, June 1989, pp. 536-547.

Papoulis; A, *Probability Random Variables, and Stochastic Processes*, McGraw-Hill, 1991.

Patton, K.T., "Table of Hydrodynamic Mass Factors for Translational Motion," *Proceedings of the ASME Annual Conference*, Winter, 1965.

Pawka, S. S., "Island Shadows In Wave Directional Spectra," *Journal of Geophysical Research*, v 88, 1983, 2579-2591.

Pereira, F.L., et al., "AUV System Requirements for Coastal Oceanography," *Proceedings of the Symposium on Autonomous Underwater Vehicle Technology (AUV '96)*, Monterey, CA, June 1996, pp. 399-406.

Peterson, R.S., Nguyen, T.C., and Rodriguez, R.R., "Motion Minimization of AUV's for Improved Imaging Sensor Performance Beneath a Seaway," *Proceedings of the IEEE Oceanic Engineering Society Conference on Autonomous Underwater Vehicles (AUV '94)*, Cambridge, MA, July 1994, pp. 247-254.

Price, W.G. and Bishop, R.E.D., *Probabilistic Theory of Ship Dynamics*, Chapman and Hall, 1974.

Rahman, M., editor, *Ocean Waves Engineering*, Computational Mechanics Publications, 1994.

Rajamani, R., "Observers for Lipschitz Nonlinear Systems," *IEEE Transactions on Automatic Control*, v 43, n 3, March 1998, pp. 397-401.

Richards, R.J. and Stoten, D.P., "Depth Control of a Submersible Vehicle," *Shipbuilding and Marine Engineering International*, v 28, n 318, February 1981, pp. 30-39.

Riedel, J.S., *Pitchfork Bifurcations and Dive Plane Reversal of Submarines at Low Speeds*, Master's Thesis, Naval Postgraduate School, Monterey, CA, June 1993.

Riedel, J.S. and Healey, A.J., "A Discrete Filter for the Forward Prediction of Sea Wave Effects on AUV Motions," *Proceedings of the Tenth International Symposium on Unmanned Untethered Submersible Technology*, Autonomous Undersea Systems Institute, Durham, NH, September 1997.

Riedel, J.S. and Healey, A.J., "Model Based Predictive Control of AUVs for Station Keeping in a Shallow Water Wave Environment," *Proceedings of the First International Workshop on Autonomous Underwater Vehicles for Shallow Waters and Coastal Environments (IARP '98)*, Lafayette, LA, 17-19 February 1998.

Riedel, J.S. and Healey, A.J., "Shallow Water Station Keeping of AUVs Using Multi-Sensor Fusion for Wave Disturbance Prediction and Compensation," *IEEE Proceedings of Oceans '98*, Nice, France, September 1998.

Rodrigues, L., Tavares, P., and Prado, M., "Sliding Mode Control of an AUV in the Diving and Steering Planes," *IEEE Proceedings of Oceans '96*, Fort Lauderdale, FL, September 1996, pp. 576-583.

Saelid, S. and Jenssen, N.A., "Adaptive Ship Autopilot with Wave Filter," *Modeling, Identification and Control*, v MIC-4, n 1, August 1983, pp. 33-46.

Safonov, M.G. and Athans, M., "Robustness and Computational Aspects of Nonlinear stochastic Estimators and Regulators," *IEEE Transactions on Automatic Control*, v AC-23, n 4, August 1978, pp. 717-725.

Santos, A., et al., "Dealing in Real Time with A Priori Unknown Environment on Autonomous Underwater Vehicles (AUVs)," *Proceedings of the International Conference on Robotics and Automation*, Nagoya, Japan, May 1995, pp. 1579-1584.

Saridis, G.N., "Intelligent Robotic Control," *IEEE Transactions on Automatic Control*, v AC-28, n 5 May 1983, pp. 547-557.

Sarpkaya, T., "Forces on Cylinders and Spheres in a Sinusoidally Oscillating Fluid," *Journal of Applied Mechanics*, v 42, March 1975, pp. 32-47.

Sarpkaya, T. and Isaacson, M., *Mechanics of Wave Forces on Offshore Structures*, Van Nostrand Rienhold Company Inc., 1981.

Shearer, J.L., Kulakowski, B.T., and Gardner, J.F., *Dynamic Modeling and Control of Engineering Systems*, Prentice Hall, 1997.

Sidar, M.M. and Doolin, B.F., "On the Feasibility of Real-Time Prediction of Aircraft Carrier Motion at Sea," *IEEE Transactions on Automatic Control*, v AC-28, n 3, March 1983, pp. 350-356.

Silvestre, C., Pascoal, A., Kaminer, I., and Healey, A.J., "Plant/Controller Optimization with Applications to Integrated Surface Sizing and Feedback Controller Design for Autonomous Underwater Vehicles (AUVs)," *Proceedings of the American Controls Conference '98*, Philadelphia, PA, June 1998.

Silvestre, C., Pascoal, A., and Healey, A.J., "AUV Control Under Wave Disturbances: An Application of Mixed H_2/H_∞ Design Methods," *Proceedings of CONTROLO '98 (3rd Portuguese Conference on Automatic Control)*, Coimbra, Portugal, September 1998, pp. 423-429.

Slotine, J.-J.E. and Li, W., *Applied Nonlinear Control*, Prentice Hall, 1991.

Slotine, J.-J.E., Hedrick, J.K., and Misawa, E.A., "Sliding Observers for Nonlinear Systems," *Journal of Dynamic Systems, Measurement and Control*, v. 109, 1987, pp. 245-252.

Smith, J.M., *Mathematical Modeling and Digital Simulation for Engineers and Scientists*, John Wiley & Sons, 1987.

Smith, S.M. and Dunn, S., "The Ocean Voyager II: An AUV Designed for Coastal Oceanography," *Proceedings of the IEEE Oceanic Engineering Society Conference on Autonomous Underwater Vehicles (AUV '94)*, Cambridge, MA, July 1994, pp. 139-148.

Smith, S.M., Dunn, S.E., and An, P.E., "Data Collection with Multiple AUVs for Coastal Oceanography," Oceanology International 96, Brighton, U.K, March, 1996, pp.263-279.

SNAME (The Society of Naval Architects and Marine Engineers), "Nomenclature for Treating the Motion of a Submerged Body Through a Fluid," *Technical Research Bulletin 1-5*, Jersey City, NJ, 1950.

Song, G., et al., "Integrated Sliding-Mode Adaptive-Robust Control," *Proceedings of the International Conference on Control Applications*, Dearborn, MI, September 1996.

Soong, T.T. and Grigoriu, M., *Random Vibration of Mechanical and Structural Systems*, Prentice Hall, 1993.

Sørensen, A.J., Sagatun S.I., and Fossen, T. I., "Design of a Dynamic Positioning System Using Model Based Control," *Journal of Control Engineering Practice*, v CEP-4, n 3, June 1996, pp. 359-368.

Spanos, P-T.D. and Hansen, J.E., "Linear Prediction Theory for Digital Simulation of Sea Waves," *ASME Journal of Energy Resources Technology*, v 103, n 1, Sep. 1981, pp. 243-249.

Spanos, P.D., "Filter Approaches to Wave Kinematics Approximation," *Applied Ocean Research*, v 8, n 1, 1986, pp. 2-7.

Spanos, P.D., "ARMA Algorithms for Ocean Wave Modeling," ASME *Journal of Energy Resources Technology*, v 105, September 1983, pp. 300-309.

Spanos, P.D. and Mignolet, M.P., "Z-Transform Modeling of P-M Wave Spectrum," *Journal of Engineering Mechanics*, v 112, n 8, August 1986, pp. 745-759.

Steele, K.E. and Earle, M.D., "Directional Ocean Wave Spectra Using Buoy Azimuth, Pitch and Roll Derived from Magnetic Components," *IEEE Journal of Oceanic Engineering*, v 16, n 4, October 1991, pp. 427-433.

Terray, E. A., et al., "Measuring Wave Direction Using Upward-Looking Doppler Sonar," *Proceedings of the Fourth Working Conference on Current Measurement*, IEEE, New York (IEEE Catalog n 90CH2861-3), pp. 252-257.

Thornton, E.B. and Kraphol, R.F., "Water Particle Velocities Measured Under Ocean Waves," *Journal of Geophysical Research*, v 79, n C6,1974.

Thornton, E., "Nearshore and Wave Processes," course notes for OC4213, Naval Postgraduate School, Monterey, CA, Winter 1996.

Tolliver, J.V., "*Studies on Submarine Control for Periscope Depth Operations*," Engineer's Thesis, Naval Postgraduate School, September 1996.

Tomizuka, M., "Optimal Continuous Finite Preview Problem," *IEEE Transactions on Automatic Control*, June 1975, pp. 362-365.

Tomizuka, M. and Whitney, D.E., "Optimal Discrete Finite Preview Problems (Why and How is Future Information Important)," *Journal of Dynamic Systems, Measurement, and Control*, December 1975, pp. 319-325.

Tomizuka, M., "Model Based Prediction, Preview and Robust Controls in Motion Control Systems," *Proceedings of the 1996 4th International Workshop on Advanced Motion Control (AMC'96)*, Tsu, Japan, March 1996, pp. 1-6.

Toprak, U., *Assessment of Shallow Water Near Surface Response of Submersible Vehicles*, Master's Thesis, Naval Postgraduate School, Monterey, CA, June 1996.

Trevorrow, M. V. and Booth, I. J., "Extraction of Ocean Wave Directional Spectra Using Steerable Doppler Side-Scan Sonars," *Journal of Atmospheric and Oceanic Technology*, v 12, 1995, pp. 1087-1100.

Triantafyllou, M.S., et al., "Real Time Estimation of Ship Motions Using Kalman Filtering Techniques," *IEEE Journal of Ocean Engineering*, v OE-8, n 1, 1983, pp. 9-20

Triantafyllou, M.S. and Grosenbaugh, M.A., "Robust Control for Underwater Vehicle Systems with Time Delay," *Journal of Oceanic Engineering*, v 16, n 1, 1991, pp. 146-152.

Tugnait, J.K., "Identification Of Multivariable Stochastic Linear Systems Via Spectral Analysis Given," *IEEE Transactions on Signal Processing*, v 46, n 5, May 1998, pp. 1458-1463.

VanDerKamp, M.M., *Modeling and Classification of Biological Signals*, Master's Thesis, Naval Postgraduate School, Monterey, CA, December 1992.

Veruggio, G., et al., "Variable Configuration UUVs for Marine Science Applications," *Proceedings of The First International Workshop on Autonomous Underwater Vehicles for Shallow Waters and Coastal Environments*, Lafayette, LA, 17-19 February 1998.

Visbeck, M. and Fischer, J., "Sea Surface Conditions Remotely Sensed By Upward-Looking ADCPS," *Journal of Atmospheric and Oceanic Technology*, v 12, 1995, pp. 141-149.

Von Alt, C., et al., "Remote Environmental Measuring Units," *Proceedings of the IEEE Oceanic Engineering Society Conference on Autonomous Underwater Vehicles (AUV '94)*, Cambridge, MA, July 1994, pp. 13-20.

Wendel, K., "Hydrodynamic Masses and Hydrodynamic Moments of Inertia," *TMB Translation 260*, July 1956.

Whitcomb, L.L. and Yoeger, D.R., "Comparative Experiments in the Dynamics and Model-Based Control of Marine Thrusters," *IEEE Proceedings of the Conference on Oceans '95*, San Diego, CA, October 1995, pp. 1019-1028.

White, F.M., *Fluid Mechanics*, McGraw Hill, 1986.

Willey, C.J., *Attitude Control of an Underwater Vehicle Subjected to Waves*, Engineer's Thesis, Massachusetts Institute of Technology, Cambridge, MA, September 1994.

Williams, G.N., Lagace, G.E., and Woodfin, A., "A Collision Avoidance Controller For Autonomous Underwater Vehicles," *IEEE Proceedings of the Symposium on Autonomous Underwater Vehicle Technology - AUV '90*, June 1990, pp. 206-212.

Wolovich, W., *Automatic Control Systems*, Saunders College Publishing, 1994.

Yun, X., et al., "Integrated GPS/INS Navigation System For Small AUVs Using An Asynchronous Kalman Filter," *Proceedings of the IEEE Symposium on Autonomous Underwater Vehicle Technology*, Cambridge, MA, August 1998.

Yamomoto, T., Nath, J., and Sloka, L., "Wave Forces on Horizontal Submerged Cylinders," *Bulletin n 47*,Oregon State University, Corvallis, Oregon, 1973.

Yavnai, A, "Architecture for an Autonomous Reconfigurable Intelligent Control System (ARICS)," *Proceedings of the IEEE Symposium on Autonomous Underwater Vehicle Technology*, Monterey, CA, June 1996.

Yaz, E., "Robust Design of Stochastic Controllers for Nonlinear Systems," *IEEE Transactions on Automation and Control*, v 34, n 3, March 1989, pp. 349-353.

Yaz, E. and Azemi, A., "Variable Structure Observer With a Boundary-Layer for Correlated Noise/Disturbance Models And Disturbance Minimization," *International Journal of Control*, v. 57, n. 5, 1993, pp. 1191-1206.

Yoeger, D.R and Slotine, J.-J.E., "Adaptive Sliding Control of an Experimental Underwater Vehicle," *Proceedings of the IEEE Conference on Robotics and Automation*, Sacramento, CA, April 1991, pp.2746-2751.

Yoeger, D.R., Cooke, J.G., and Slotine, J.-J.E., "The Influence of Thruster Dynamics on Underwater Vehicle Behavior and Their Incorporation Into Control System Design," *Journal of Oceanic Engineering*, v. 15, n. 3, 1991, pp. 167-178.

Yong, I.R. "A Shallow Water Spectral Wave Model," *Journal of Geophysical Research*, v 93, n C5, May 1988, pp. 5113-5129.

Young, D.K., Utkin, V .I., and Ozguner, U., "A Control Engineer's Guide to Sliding Mode Control," *Proceedings from the IEEE Workshop on Variable Structure Systems*, 1996.

Yuh, J, "Modeling and Control of Underwater Vehicles," *IEEE Transactions of systems, Man, and Cybernetics*, v 20, November-December 1990, pp.1475-1483.

Zedel, L., "Deep Ocean Wave Measurements Using a Vertically Oriented Sonar," *Journal of Atmospheric and Oceanic Technology*, v 11, 1994, pp. 182-191.

Zeitouni, O., "Class of Adaptive Control Problems Solved Via Stochastic Control," *System Control Letters*, v 12, n 1, January 1989, pp. 57-62.

INITIAL DISTRIBUTION LIST

1. Defense Technical Information Center.....2
   8725 John J. Kingman Road, STE 0944
   Ft. Belvoir, VA 22060-6218

2. Dudley Knox Library.....2
   Naval Postgraduate School
   411 Dyer Rd.
   Monterey, CA 93943-5101

3. Dr. A. J. Healey, Code ME/Hy.....2
   Department of Mechanical Engineering
   Naval Postgraduate School
   Monterey, CA 93943

4. Dr. Roberto Cristi, Code EC/Cx.....1
   Department of Electrical and Computer Engineering
   Naval Postgraduate School
   Monterey, CA 93943

5. Dr. Young S. Shin, Code ME/Ys.....1
   Department of Mechanical Engineering
   Naval Postgraduate School
   Monterey, CA 93943

6. Dr. Fotis Papoulias, Code ME/Pa.....1
   Department of Mechanical Engineering
   Naval Postgraduate School
   Monterey, CA 93943

7. Dr. Edward B. Thornton, Code OC/Th.....1
Department of Oceanography
Naval Postgraduate School
Monterey, CA 93943

8. Mr. Norman Caplan.....1
National Science Foundation
4201 Wilson Blvd., Rm. 725
Arlington, VA 22230

9. Dr. Thomas Curtin (Code 32OE).....1
Office of Naval Research (ONR)
800 North Quincy Street
Arlington, VA 22217

10. Dr. Samuel M. Smith.....1
Dept of Ocean Engineering
Florida Atlantic University
500 N.W. 20 Street
Boca Raton, FL 33431-0991

11. Gary Trimble, Program Manager.....1
EODRWP
Lockheed Martin Inc.
Organization 8K-01, Building 586E
1111 Lockheed Way
Sunnyvale, CA 94089-3504

12. Dr. Jim Bellingham 1
MIT Sea Grant Program
MIT
Cambridge, MA 02139

13. Dr. Dana R. Yoerger 1
Woods Hole Oceanographic Institution
Deep Submergence Laboratory
Woods Hole, MA 02543

14. Professor Junku Yuh 1
Department of Mechanical Engineering
2540, Dole Street, Holmes 302
University of Hawaii
Honolulu, Hawaii, 96822

15. Dr. Antonio Pascoal 1
Institute Superior Tecnico
Av. Rovisco Pals,
1096 Lisboa Codex, PORTUGAL

16. Dr. David Lane 1
Senior Lecturer
Ocean Systems Laboratory
Dept. of Computing & Electrical Engineering
Heriot-Watt University
Riccarton, Edinburgh, SCOTLAND

17. Richard Blidberg 1
Autonomous Undersea Systems Institute
86 Old Concord Turnpike
Lee, NH 03824

18. Dr. Jerome Milgram 1
Ocean Engineering Department
MIT
Cambridge, MA 02139

19. Joel Charles 1
Centre Technique Systemes Navals
BP 28 - 83800 Toulon-Naval, FRANCE

20. Dr. Tamaki Ura 1
Institute of Industrial Science,
University of Tokyo
7-22-1 Roppongi, Minato-ku
Tokyo 106 JAPAN

21. Gianmarco Verrugio 1
Istituto per l'Automazione Navale
Via De Marini, 6 Torre di Francia
16149 Genova, ITALY

22. Thor I. Fossen 1
Professor of Guidance, Navigation and Control
Department of Engineering Cybernetics
Norwegian University of Science and Technology, NTNU
N-7054 Trondheim, NORWAY

23. Naomi Leonard 1
Dept. of Mechanical and Aerospace Engineering
Princeton University, Princeton, NJ 08544

24. Dr. John Leonard 1
MIT Sea Grant Program
MIT
Cambridge, MA 02139

25. Dr. David Marco, Code Me/Ma 1
Naval Postgraduate School
Monterey, CA 93943-5101

26. Dr. Donald Brutzman, Code UW/Br 1
Undersea Warfare Academic Group
Naval Postgraduate School
Monterey, CA 93943

27. LCDR Jeffery S. Riedel, USN 3
80 Boot Pond Rd
Plymouth, MA 02360

28. Naval Engineering Curricular Office, Code 34 1
Naval Postgraduate School
Monterey, CA 93943-5101

29. Chairman, Department of Mechanical Engineering 1
Naval Postgraduate School
Monterey, CA 93943-5101

30. Dr. Thomas Swean 1
Office of Naval Research (ONR)
800 North Quincy Street
Arlington, VA 22217

31. Chris von Alt 1
Woods Hole Oceanographic Institution
Ocean Systems Lab
Woods Hole, MA 02543

32. Massimo Caccia 1
Istituto Automazione Navale
Consiglio Nazionale delle Ricerche
Via De Marni 6,16149 Genoa, Italy